Impact of Improved Sorbents on the Performance of the Carbonate Looping Process

Ben Schüppel

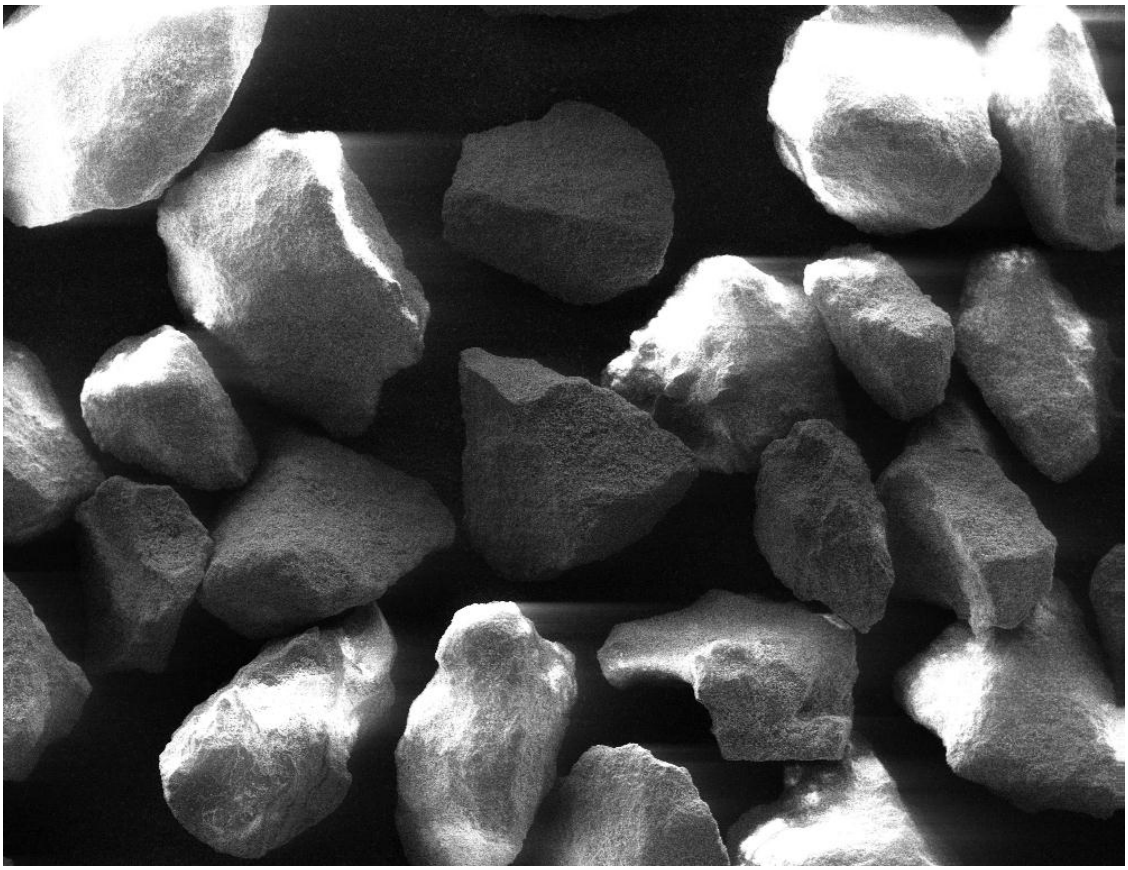

Declaration

I hereby declare that this submission is my own work and that, to the best of my knowledge and belief, it contains no material previously published or written by another person nor material which to a substantial extent has been accepted for the award of any other degree or diploma of the university or other institute of higher learning, except where due acknowledgment has been made in the text.

_____

Ben Schüppel

E-MAIL: BEN.SCHUEPPEL@WG-28.DE

BEN SCHÜPPEL

EDUCATION

School

Jun 2003: A-levels, Franziskaneum Meißen, Saxony

Special learning achievement[1] done
"Bau eines geschlossenen, reversible Brennstoffzellensystems und der Nachweis der Funktionalität"
Topic: Fuel cell accumulator – construction and erection

University

° Oct 2004 – Apr 2009: Studies in Chemistry, Technical University Dresden

Diploma Thesis
"Entwicklung von Modellen zur Optimierung der Sanierung saurer Tagebaufolgeseen und Validierung im Labormaßstab"
Topic: Remediation of acidified lakes

° May 2009 – Oct 2012: PhD, Technical University Darmstadt

"Impact of Improved Sorbents on the Performance of the Carbonate Looping Process"

Language Skills:

° German (native speaker)

° English (CEFR class: C1)

° Russian (CEFR class: A2), Swedish and French (CEFR class: A1)

[1] A special learning achievement is a scientific work similar to a diploma thesis which is created in the 11th and 12th class at school besides the usual learning programme.

For Katja and my little star Laura.

Impact of Improved Sorbents on the Performance of the Carbonate Looping Process

Department of Mechanical Engineering
Technical University Darmstadt
(D17)

Dissertation

A Thesis Submitted for the Degree of
Doctor rerum naturalium

Created by
Dipl.-Chem. Ben Schüppel
Born in Schlema

Advisor: Prof. Dr.-Ing. Bernd Epple
Co-Advisor: Prof. Dr.-Ing Herbert Vogel
Date of Submission: 20.04.2012
Date of Viva: 11.07.2012
Darmstadt 2012

Table of Contents

Preface

This work was created between 2008 and 2011 as an industrial thesis at Rheinkalk GmbH. All results were achieved through a close cooperation with the Research and Development centre of the Lhoist Group in Nivelles, Belgium, the Department of Energy Systems and Technology Darmstadt (EST), the Imperial College London, the Centre for Solar and Hydrogen Research Stuttgart (ZSW), the "Ingenieurbüro Berger" and the Fisia Babcock GmbH.

I would like to express my special thanks to Prof. Dr.-Ing. Bernd Epple for giving me the chance to realise my PhD thesis at the worldwide biggest carbonate looping test facility. As well, I would like to express my special thanks to Prof. Dr.-Ing. Herbert Vogel for becoming my co-advisor.

Christopher Pust, my superior at Rheinkalk GmbH, supported me not only in an excellent way in technical questions but taught me patience and to see things from various perspectives.

Special thanks also go to Wolfgang König who started the carbonate looping project several years ago at Rheinkalk. He did his very best that I was assigned to this topic.

As well, I wanted to thank Thierry Chopin, head of the Lhoist Research and Development centre, for his support of my work.

My special thanks go to Guillaume Criniere, Robert Gärtner, Marion Lorgoulioux and Marc Pelletier for all critical questions that made such a deep understanding of the process possible as it was achieved.

I also wish to thank the scientific co-workers of the EST, namely Alexander Galloy, Johannes Kremer, Mathias Orth, Stefan Plötz, Markus Junk and Jochen Ströhle for the excellent collaboration.

Special thank also goes to Ulrich Priesmeier who always found the time to discuss detailed questions on the topic of the carbonate looping process.

And last but not least, I want to thank my beloved family for their support during the partially hard time of this thesis.

Used Symbols

Symbol	Description	Unit
α	Structure and mechanism dependent pre-factor	---
δ	Additional energy demand due to the CL process	%
$\Delta_V H$	Specific vaporisation enthalpy of water	$\frac{kJ}{mol}$
ε^{LLCR}	Energy loss within the CL-Process	%
ϕ	Binding factor for ionic interactions	---
λ	Oxygen excess	---
υ	Atomic vibration frequency	Hz
π	Specific energy consumption for each ton of CO_2 separated	$\frac{GJ}{t_{CO_2}}$
Ψ_{CO_2}	Benchmark number for the costs of produced CO_2	$\frac{€}{t_{CO_2}}$
$\Psi_{MWh_{el}}$	Benchmark number for the difference between specific production costs of a power plant with and without the CL process – negative numbers indicate economic advantages offered by the CL process	$\frac{€}{MWh}$
$\rho^{Flue\,gas}$	Density of flue gas	$\frac{t}{m^3}$
χ	Additional CO_2 produced by CL for 1 mol CO_2 separated	%
σ	Free surface energy	$\frac{kJ}{mol \cdot m^2}$
$\eta_{CO_2\,treatment}^{Total\,w/o\,compression}$	Overall plant Efficiency without compression	%
$\Delta\eta_{CO_2\,treatment}^{Total\,w/o\,compression}$	Overall change in plant Efficiency without compression	%
$\eta_{CO_2\,treatment}^{Total\,incl.compression}$	Overall plant Efficiency with compression	%
$\Delta\eta_{CO_2\,treatment}^{Total\,incl.compression}$	Overall change in plant efficiency including CO_2 compression	%
$\eta_{TotalSeparation}^{CO_2\ flue\,gas}$	Degree of CO_2-separation	%
$\eta_{Electrical}^{Power\,plant}$	Electrical efficiency of existing power plant	%
$\eta_{CO_2\,treatment}^{FlueGas}$	CO_2 from the treated flue gas (this is determined by thermodynamics and the operation regime of the utility)	%
$\eta_{CO_2\,treatment}^{Sorbent}$	Absorption efficiency regarding CaO	%
$\eta_{Electrical}^{LLCR}$	Electrical Efficiency of CL retrofit utilities	%
$\eta_{Sulphurcapture}^{Carbonator}$	SO_2/SO_3 capture rate in carbonator	%
$\eta_{Sulphurcapture}^{Calciner}$	SO_2/SO_3 capture rate in calciner by sorbent	%
$A_{Treated}^{Flue\,gas}$	Amount of flue gas treated within CL process	%
a_i	Chemical activity of a substance i	---
A	Surface area	m²
a	Lattice parameter	nm
C_{Carbon}^{Fuel}	Content of carbon (based on dry coal)	%
$C_{Sulphur}^{Fuel}$	Content of sulphur	%
C_{Oxygen}^{Air}	Content of oxygen in air	%

$C_{Water}^{Flue\,gas}$	Content of water vapour in the flue gas	%
$c_p^{Flue\,gas}$	Heat capacity of flue gas	$\frac{kJ}{kg\,K}$
$C_{Sulphur}^{Flue\,gas}$	SO_2/SO_3 content of flue gas after FGD [g S/t flue gas]	$\frac{g_{Sulphur}}{t^{Flue\,gas}}$
c_p^{Bleed}	Heat capacity of bleed	$\frac{J}{mol\,K}$
$c_p^{Calcinedsorbent}$	Heat capacity of calcined sorbent	$\frac{J}{mol\,K}$
$c_p^{CaSO_4}$	Heat capacity of $CaSO_4$	$\frac{J}{mol\,K}$
$c_p^{CaCO_3}$	Heat capacity of $CaCO_3$	$\frac{J}{mol\,K}$
c_p^{CaO}	Heat capacity of CaO	$\frac{J}{mol\,K}$
$c_p^{CO_2}$	Heat capacity of CO_2	$\frac{J}{mol\,K}$
c_p^{Makeup}	Heat capacity of $CaCO_3$ or CaO	$\frac{J}{mol\,K}$
c_i	Concentration of substance i	$\frac{mol}{l}$
C_{CaO}	Content of CaO in the sample	mass-%
D_{Oxygen}^{Fuel}	Demand of oxygen for complete combustion of the fuel	$\frac{kg_{O_2}^{\min}}{kg_{Fuel}}$
d^{Sauter}	Sauter diameter	m
$E_{Oxygen}^{Production}$	Energy demand for oxygen production	$\frac{kWh}{t_{O_2}}$
$E_{CO_2}^{Compression}$	Energy demand for CO_2 compression	$\frac{kWh}{t_{O_2}}$
$E_{Auxillaries}^{LLCR}$	Additional energy demand (pumps, fans, cooling etc.)	$\frac{kWh}{t_{O_2}}$
f	Activity constant	---
F_0	Make-up rate	$\frac{t}{h}$
F_R	Mole flow of Ca between the calciner and the carbonator	$\frac{mol}{h}$
Γ	Scaling exponent	-
G	Free enthalpy	$\frac{kJ}{mol}$
H_{Fuel}	Calorific value of the coal	$\frac{kJ}{kg}$
$h_{Carbonisation}$	Reaction enthalpy for carbonisation	$\frac{kJ}{mol}$

$\Delta_R H$	Reaction enthalpy	$\frac{kJ}{mol}$
$\Delta_R H^{\Theta}$	Reaction enthalpy under standard conditions	$\frac{kJ}{mol}$
K_2	Costs for the individual CL equipment in the year of construction	M€
K_{2005}	Costs for the individual CL equipment in the year 2005	M€
Ki_2	Costs index for the individual CL equipment in the year of construction	M€
K_{2005}	Costs index for the individual CL equipment in the year 2005	M€
K	Equilibrium constant	---
k_B	Boltzmann constant	$\frac{eV}{K}$
KS	"Kalkstandard", a value for indicating the amount of SiO_2, Al_2O_3 and Fe_2O_3 in relation to the CaO content	---
$K_{MWh_{el}}^{Power\ plant}$	Specific costs of the production of one MWh electricity in a power plant that has to purchase CO_2 emission allowances	$\frac{€}{MWh}$
$K_{MWh_{el},original}^{Power\ plant}$	Specific costs of the production of one MWh electricity in a power plant without CCS	$\frac{€}{MWh}$
$K_{Certificate}^{CO_2}$	Cost for an emission allowance of CO_2	$\frac{€}{t_{CO_2}}$
$K_{MWh_{el}}^{LLCR}$	Specific costs of the production of one MWh electricity in the CL process	$\frac{€}{MWh}$
k_0	Pre-exponential factor	$\frac{1}{s}$
$k_{AttritionS}$	Attrition rate constant	$\frac{kg}{\min}$
L	Lifetime of CaO	[Theoretical cycles till complete los of sorbent via cyclone/bleed]
$\dot{m}_{beforeLLCR}^{Flue\ gas}$	Flue gas flow after FGD before CL [t/h]	$\frac{t_{Flue\ gas}}{h}$
$\dot{m}_{after\ LLCR}^{Flue\ gas}$	Flue gas flow after FGD treated in CL [t/h]	$\frac{t_{Flue\ gas}}{h}$
$\dot{m}_{Coal}^{Power\ plant}$	Coal flow to power plant	$\frac{t_{Coal}}{h}$
$\dot{m}_{CO_2}^{Power\ plant}$	Produced CO_2 (from power plant)	$\frac{t_{CO_2}}{h}$
$\dot{m}_{CO_2\ separated}^{Power\ plant}$	Separated CO_2	$\frac{t_{CO_2}}{h}$
$\dot{m}_{CO_2}^{LLCR}$	Additional CO_2 through CL	$\frac{t_{CO_2}}{h}$
$\dot{m}_{CO_2}^{Total}$	Total CO_2 separation	$\frac{t_{CO_2}}{h}$
$\dot{m}_{Coal}^{LLCR}$	Additional coal consumption through CL	$\frac{t_{Coal}}{h}$
$\dot{m}_{CaO}^{LLCR}$	Flow of CaO in the CL process	$\frac{t_{CaO}}{h}$

$\dot{m}_{CaO/CaCO_3}^{LLCR}$	Flow of $CaCO_3$/CaO-mixture to calciner	$\frac{t_{CaO/CaCO_3}}{h}$
$m_{Sorbent}^{LLCR}$	Needed CaOvalue in the cycle	t
$m_{CaO/CaSO_4}^{LLCR}$	Real mass of CaO and $CaSO_4$ in the system	t
$\dot{m}_{CaOMakeup}^{LLCR}$	Make-up expressed as CaO	$\frac{t_{CaO}}{h}$
$\dot{m}_{CaOMakeup}^{LLCR}$	Make-up expressed as $CaCO_3$	$\frac{t_{CaCO_3}}{h}$
$\dot{m}_{CaCO_3\,demand}^{FGD}$	Needed $CaCO_3$ for flue gas desulfuration	$\frac{t_{CaCO_3}}{h}$
$\dot{m}_{CaCO_3\,losscalciner}^{LLCR}$	Loss of sorbent expressed as carbonate due to the formation of $CaSO_3$/$CaSO_4$ in the calciner	$\frac{t_{CaCO_3}}{h}$
$\dot{m}_{CaCO_3\,losscarbonator}^{LLCR}$	Loss of sorbent expressed as carbonate due to the formation of $CaSO_3$/$CaSO_4$ in the carbonator	$\frac{t_{CaCO_3}}{h}$
$\dot{m}_{CaCO_3\,losstotal}^{LLCR}$	Loss of sorbent expressed as carbonate due to the formation of $CaSO_3$/$CaSO_4$ all together	$\frac{t_{CaCO_3}}{h}$
$\dot{m}_{Bleed}^{LLCR}$	Mass flow of bleed of the CL process (ash not included)	$\frac{t}{h}$
$\dot{m}_{Bleed,total}^{LLCR}$	Mass flow of bleed of the CL process (ash included)	$\frac{t}{h}$
M_i	Molar mass of the substance i	$\frac{g}{mol}$
$\dot{n}_{Makeup}^{LLCR}$	Moles of make-up introduced into the calciner	$\frac{kmol}{h}$
$\dot{n}_{Sorbent}^{LLCR}$	Moles of lime in carbonator/calciner	$\frac{kmol}{h}$
$\dot{n}_{Bleed}^{LLCR}$	Mole flow of the bleed of the CL process	$\frac{kmol}{h}$
$\dot{n}_{Sulphurin}^{LLCR}$	Mole flow of sulphur in the CL process (due to sulphur in fuel and flue gas)	$\frac{kmol}{h}$
$\dot{n}_{Sulphurout}^{LLCR}$	Mole flow of sulphur out of the CL process	$\frac{kmol}{h}$
$P_{Thermal}^{Q1}$	Q1	MW
$P_{Thermal}^{Q2}$	Q2	MW
$P_{Thermal}^{Q3}$	Q3	MW
$P_{Thermal}^{Q4}$	Q4	MW
$P_{Thermal}^{All\ heatexchangers}$	Q1-Q4	MW
P_{Excess}^{LLCR}	Excess energy	MW
$P_{O_2\,Production}^{LLCR}$	Electrical power for O2 production	MW
$P_{CO_2\,Compression}^{LLCR}$	Electrical power for CO2 compression	MW
$P_{Auxilliar}^{LLCR}$	Power for supporting units of CL process	MW
$P_{Sorbentheating}^{LLCR}$	Energy for first heating of the sorbent	MW

$P_{Sorbentcalcination}^{LLCR}$	Energy for first calcination of the sorbent	MW
$P_{Electrical}^{Totalincl.compression}$	Total electrical energy net production including CO_2compression	MW
$P_{Electrical}^{Totalw/ocompression}$	Total electrical energy net production without compression	MW
$P_{Thermal}^{Power\ plant}$	Thermal output power plant	MW
$P_{ThermalOut}^{LLCR}$	Total thermal output through CL	MW
$P_{ThermalIn}^{LLCR}$	Total thermal Input into CL	MW
$P_{Electrical}^{LLCR}$	Additional el. output through CL	MW
$P_{Electrical}^{Power\ plant}$	Electrical output	MW
$P_{Total}^{Power\ plant}$	Capacity of the boiler	MW
p_{CO2}	Partial pressure of CO_2	% of 1 atm
Q_2	Power/output of the equipment that is going to be erected	-
Q_{2005}	Power/output of the equipment that has been assumed for the CL plant in 2005	-
Q	Activation energy for diffusion	eV or $\frac{J}{mol}$
R	Universal gas constant	$\frac{J}{K\,mol}$
r	Rate constant	---
r_n	Share of particles that have undergone a given number of carbonation calcination cycles	%
$S_{MWh_{el}}^{CO_2}$	Share of emitted CO_2 based on the production of one MWh of electricity	$\frac{t_{CO_2}}{MWh}$
S_0	Specific surface area at the beginning	$\frac{m^2}{g}$
S	Specific surface area	$\frac{m^2}{g}$
S_a	Specific surface area after infinite sintering time	$\frac{m^2}{g}$
T_{Exit}^{FGD}	Temperature of FGD	$°C$
$T_{Entrance}^{Carbonator}$	carbonator temperature entrance	$°C$
$T_{Exit}^{Carbonator}$	carbonator temperature exit	$°C$
$T^{Calciner}$	calciner temperture [°C]	$°C$
T_{Exit}^{Q2}	Exit temperature Q2 [°C]	$°C$
T_{Exit}^{Q3}	Exit temperature Q3 [°C]	$°C$
T_{Exit}^{Q2}	Exit temperatureQ4 [°C]	$°C$
T_S	Melting point	K
t	Time	s
U	Superficial velocity	$\frac{m}{s}$
$\dot{V}_{beforeLLCR}^{Flue\ gas}$	Flue gas flow after FGD before CL [m³/h]	$\frac{m^3}{h}$
$\dot{V}_{after\,LLCR}^{Flue\ gas}$	Flue gas flow after FGD treated in CL [m³/h]	$\frac{m^3}{h}$

$X_{CaSO_3/CaSO_4}^{LLCR}$	Molar conversion of the sorbent ($CaO/CaCO_3$) to $CaSO_3$ or $CaSO_4$	%
$X_{CaCO_3}^{LLCR}$	Average molar conversion of the calcined sorbent ($CaO/CaCO_3$) to $CaCO_3$ after each cycle (the formation of $CaSO_3$ or $CaSO_4$ is included	%
$X_{CaCO_3}^{LLCR,0}$	Average molar conversion of the calcined sorbent ($CaO/CaCO_3$) to $CaCO_3$ after each cycle (theoretical maximum without the presence of impurities)	%
$X_{\text{Production}}^{Power\ plant}$	Contribution of the power plant to the overall electricity production	---
$X_{\text{Production}}^{LLCR}$	Contribution of the CL process to the overall electricity production	---
x_k	Conversion ratio of limestone	---
Z	CaO cycles per hour	$\frac{1}{h}$

Used Abbreviations

AER	Absorption Enhanced Reforming
ASU	Air Separation Unit
BFB	Bubbling Fluidised Bed
CCS	Carbon Capture and Storage
CFB	Circulating fluidised bed
CL	Carbonate looping
EU	European Union
FGD	Flue Gas Desulfuration
HGI	Hard Grove Index
KS	Kalkstandard
LoI	Loss of Ignition
PCC	Precipitated Calcium Carbonate
SD	Superheated Dehydration
TGA	Thermogravimetric Analyzer
VBA	Visual Basic for Applications
ZSW	Centre for Solar Energy and Hydrogen Research

Abstract

One of the most promising future technologies for CO_2 separation is the carbonate looping process. Recent studies ([3], [7], [78]) have shown that the total capture costs for this technology are around 20 €/t CO_2 separated.

The carbonate looping process consists of two coupled fluidised bed reactors that use calcium in the form of calcium oxide (CaO) and calcium carbonate ($CaCO_3$), to separate the CO_2 from the flue gas in the carbonator and release a nearly pure stream of CO_2 in the calciner. Mainly due to the high temperature level, loss of specific surface area of the sorbent particles takes place causing a drop in the CO_2 capture ability and thus higher circulating mass flows or a lower CO_2 separation degree, resulting in a higher efficiency penalty for the power plant.

Besides chemical properties, the mechanical behaviour of the sorbent will affect the process in a critical manner. High attrition rates would require larger dedusting equipment. As well, the bleed would not be controlled by the operator of the CL process but by the material attrition. Moreover, if a lot of material leaves the system a lot of make-up would have to be reintroduced in the loop. This would cause major difficulties in the disposal or utilisation of the bleed and transportation of fresh make-up. Accordingly, the precise definition of sorbent properties is essential for a good design of the process and a focused sorbent research.

This work aims to give an overview over the aspects associated with CL sorbents. After a short introduction and description of the carbonate looping process in **chapter one,** solid state chemistry concepts, the substances involved in the carbonate looping process and lime based know-how is given in the **second chapter**. Particular attention is paid to the discussion of the role of impurities in the CL process that are brought in via the fuel. As well, thermodynamics and kinetics of the decomposition of $CaCO_3$ and the re-carbonation of CaO are discussed. It will be shown that the full calcination of the $CaCO_3$ particles with a diameter of 500µm will take not more than 100 seconds in the calciner.

Chapter three reviews the latest literature results on carbonate looping sorbents. Test protocols are presented and discussed. Results on natural sorbents are shown as well as outcomes on synthetic ones. It will be demonstrated that most of the outstanding outcomes in terms of CO_2 capture ability of synthetic sorbents might only be an effect of randomly beneficial chosen TGA test conditions. Mechanical and chemical reactivation routes are

presented as well. However, only the reactivation process proposed by MATERIC, Superheated Dehydration (SD) seems to have the potential for an industrial application.

The **fourth chapter** is dedicated to a detailed process simulation that will enable the definition of the term "good sorbent". It will outline that optimisations can be done with different emphasis. CO_2 capture costs or overall efficiency penalty could be optimised, for example. Both optima would require different sorbent properties. Accordingly, different optima and the according required sorbent properties will be presented.

The **fifth and sixth chapter** are devoted to experimental work. More than 50 different natural and various advanced and synthetic sorbents were investigated in terms of CO_2 capture ability and hardness. During the research efforts, one general and serious problem became obvious: Ca-based sorbents appear to have some sort of process memory. By this, outcomes and relative rankings of TGA and hardness tests could be altered, in some cases very easily, by changed test conditions. For example, some pre-treated products revealed a constant or decreasing CO_2 capture ability under harsh conditions, while displaying an increasing CO_2 capture ability under mild conditions. The same was also applicable for hardness investigations: Top products in a small BFB were failing completely in a large BFB. However, it will be demonstrated that synthetic sorbents may have no advantages over a very good natural sorbent under harsh TGA test conditions.

The **seventhes chapter** provides an outlook and gives suggestions for further research steps.

.

1 Introduction

"Assessments by the Intergovernmental Panel on Climate Change (IPCC) suggest that the Earth's climate has warmed between 0.6 and 0.9°C over the past century and that this temperature rise is very likely due to the observed increase in anthropogenic greenhouse gas (GHG) concentrations" [69]. Therefore, politicians decided to lower the amount of CO_2 emitted into the atmosphere. To achieve minor CO_2 emissions, the European Union (EU) established a trade system for CO_2 emissions certificates in 2005. Starting in 2013 about 20% of these emission rights are going to be auctioned, by 2025 the target is 100%. On the long-term, the price for one ton of emitted CO_2 is going to be equal with the costs for the sequestration of the same amount of CO_2. Therefore, huge efforts are undertaken to develop new technologies with significantly lower CO_2 capture costs. Amine-based capture systems which "generate" capture costs of more than 50 € per ton of CO_2 separated are a current reference.

Another first generation CO_2 capture system is the oxyfuel process: Pure oxygen is used to burn the fuel, and therefore, to receive a nearly pure stream of CO_2 at the outlet of the boiler. However, this process has the drawback, that a significant amount of electricity is needed to produce the required oxygen from air. By this, the overall efficiency drop of an oxyfuel power plant is considerable. Consequently, second generation technologies are under evaluation to lower the efficiency penalty and the separation costs.

The pre-combustion process Absorption Enhanced Reforming (AER) and the Carbonate Looping (CL) process are two very promising second generation technologies that have been researched intensively during the past years and that use lime at high temperature for the separation of CO_2. Both need special Ca-based sorbents to produce a rather pure stream of CO_2. Following, the processes and chemistry behind will be described in detail.

1.1 Absorption Enhanced Reforming (AER)

The use of lime for the separation of CO_2 "dates back to 1867, when DuMotay and Marechal first patented the use of lime to aid the gasification of carbon by steam (Squires, 1967)" [6]. This old idea was somehow rediscovered in the middle of the 1990's due to the significant price increase of fossil fuels and the political will to become more independent from countries

that own natural gas and oil. Another property of the process became more and more important at the beginning of the 21st century: The in situ separation of carbon in the form of pure CO_2.

Every steam gasification of carbon based substance occurs according to the following reactions:

$$[\text{-C-}] + H_2O \rightarrow H_2 + CO \qquad \Delta_R H = 119 \frac{kJ}{mol} \qquad 1\text{-}1$$

$$CO + H_2O \rightleftharpoons H_2 + CO_2 \qquad \Delta_R H = -42 \frac{kJ}{mol} \qquad 1\text{-}2$$

$$CO_2 + [\text{-C-}] \rightarrow 2\ CO \qquad \Delta_R H = 161 \frac{kJ}{mol} \qquad 1\text{-}3$$

$$CO + 3\ H_2 \rightleftharpoons CH_4 + H_2O \qquad \Delta_R H = -207 \frac{kJ}{mol} \qquad 1\text{-}4$$

$$[\text{-C-}] + 2\ H_2 \rightarrow CH_4 \qquad \Delta_R H = -84 \frac{kJ}{mol} \qquad 1\text{-}5$$

The AER process adds one new chemical reaction to the gasification process.

$$CaO + CO_2 \rightleftharpoons CaCO_3 \qquad \Delta_R H = -178 \frac{kJ}{mol} \qquad 1\text{-}6$$

Summarising eq. 1-1 to 1-6 leads to

$$CaO + [\text{-C-}] + 2\ H_2O \rightarrow CaCO_3 + 2\ H_2 \qquad \Delta_R H = -101 \frac{kJ}{mol} \qquad 1\text{-}7$$

in case of coal and to

$$CaO + CH_4 + 2\ H_2O \rightarrow CaCO_3 + 4\ H_2 \qquad \Delta_R H = -13 \frac{kJ}{mol} \qquad 1\text{-}8$$

in case of the reforming of natural gas.

By examining reactions 1-7 and 1-8 two things become obvious: First, by taking CO_2 out of the whole system (reaction 1-6) the reaction yield regarding H_2 will increase. Second, the whole process could be kept under auto-thermal conditions due to the high reaction enthalpy of the carbonation of quick lime ([84]).

Heavy boiling tar is also likely to form during gasification and it will stick to the sorbent particles. Up to now, it is believed that this tar could be easily burned off in a second reactor ([84]). Operating this second reactor under oxyfuel conditions might produce a pure stream consisting mainly of steam and CO_2. This basic principle is given in Fig. 1-1.

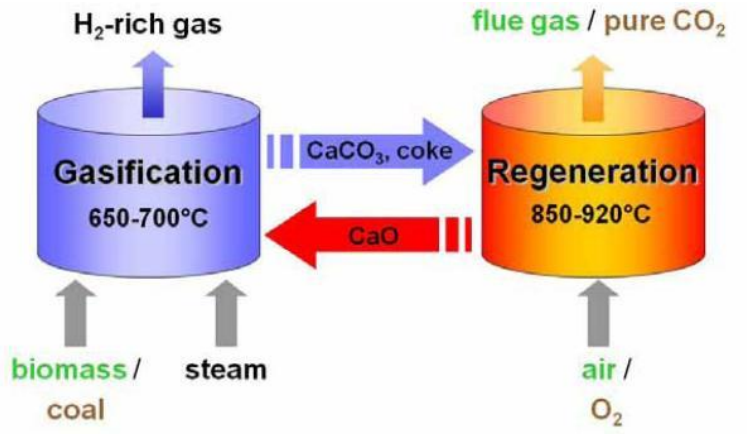

Fig. 1-1: Scheme of the Absorption Enhanced Reforming (AER) process. Figure taken from [112].

The fuel is introduced to a fluidized bed gasification reactor. There, the hot CaO coming from the regenerator and the energy that is set free by the carbonisation (reaction 1-6) delivers the reaction enthalpy for the gasification. At a certain temperature level the reaction between carbon and water vapour to H_2 and other gaseous substances starts. Because cracking of long biomolecules always leads to the formation of tar and other heavy boiling substances ([18], [138]), the $CaO/CaCO_3$ is covered with those substances. The mixture of lime, carbonate and heavy boiling organic compounds is transferred into the regenerator. There, pure oxygen is introduced to the mixture and all the organic compounds are completely burned off the surface of the lime. This delivers the energy for the heating of the $CaCO_3$, the calcinaion and the heating of the CaO. The regenerated hot sorbent is reintroduced into the gasification reactor.

The advantages of the AER process are ([83]):

- high reaction yields regarding H_2,
- relatively clean product gas,
- insitu desulfuration,
- autothermal process,
- utilisation of high moisture fuel,
- low tar content,
- char is used in the regenerator,
- production of pure CO_2 for storage and
- solid purge could be used for cement industry.

Within this process, the sorbent properties (of the used CaO) are very crucial: On the one hand, the sorbent should be as hard as possible to prevent any undesired loss of material due to attrition. High attrition rates would lead to an extensive use of the dedusting systems and to

a very high demand for make-up (fresh sorbent) causing uneconomic high operation costs. On the other hand, the sorbent should be able to capture as much CO_2 as possible to keep the circulation mass flows and the make-up low.

These objectives are applicable to the CL process as well but may be much harder to reach at the same time in the AER process due to impurities (like sodium or potassium) concentrated in the tars that will be released in close contact with the sorbent particles (burning off the tars in the regenerator). Low melting eutectics are very likely to form and to lead to a sticky product with nearly no CO_2 capture ability. However, the intensity of those problems will vary significantly with the composition of the ash and operational parameters ([54]).

The first 10 MW_{th} demonstration plant will be setup in Geislingen-Türkheim, Germany, and is scheduled to go into operation by 2011 ([2]).

1.2 Carbonate Looping (CL)

In contrast to the AER process, the CL is used end of pipe as post combustion CO_2 capture unit. It consists of two reactors: The carbonator that is operated at 650°C and the calciner that is operated between 850 and 950°C ([3], [5], [12]). Fig. 1-2 shows the basic process flow scheme.

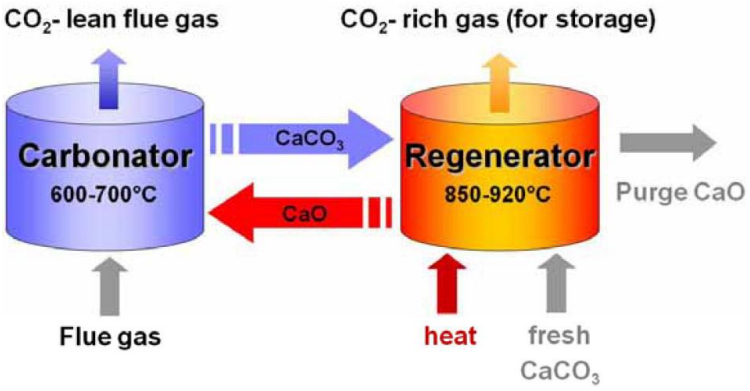

Fig. 1-2: Flow scheme of the CL-process. Figure taken from [112].

Calciner and carbonator are two coupled fluidized bed reactors. Fresh $CaCO_3$ driven into the process is first calcined in the calciner and then transferred into the carbonator. There, CaO reacts with CO_2. This reaction releases huge amounts of heat due to the formation of $CaCO_3$. With the help of heat exchangers this reaction is controlled and the heat can be recovered for the production of steam. Following this step, $CaCO_3$ is transferred into the calciner again where it is burned once more under oxyfuel conditions or indirectly ([36]). Burning under oxyfuel conditions is, up to now, the most preferred solution to get out pure CO_2 but it has major disadvantages: First, oxyfuel calcinations need huge amounts of oxygen, that have to be

produced via cryogenic air separation. This leads to a large demand for electricity, as one ton of O_2 requires about 200 kWh to be produced[2] ([96]). Second, the sorbent is in direct contact with the fuel and therefore with its impurities leading, just like in the case of the AER process, to chemical phases with a low melting point. In addition, it is speculated that hot spots might lead to a very high thermal stress of the particle. However, oxyfuel combustion can be done with known technology and is therefore believed to be the easiest way to operate such a plant.
Due to the high temperature level of this process nearly all energy driven into the system can be recovered for the production of steam in the first, and electrical power in the second place. Losses occur from the air separation unit (ASU), the fans and from the reactors.
Calculations of EPPLE ET AL. [39] show that an efficiency penalty of 2.75% (CO_2 compression excluded) could be reached with the CL process. ROMEO ET AL. [98] estimated the capture costs at 16 €/t. These calculations do not take into account the possibilities improved sorbents may deliver.
Recent studies of the Technical University of Darmstadt showed ([40]) that an excellent, theoretical Ca-based sorbent could lower the efficiency drop from 3.35% to 2.75%. This is a reduction of 22% of the energy penalty that could be achieved only by a good sorbent. Chapter 4 is going to discuss in detail the effects of the sorbent on the process and will show what could be possible by an optimisation between product and process.

Even though that the AER and the CL process have different aims, reaction 1-6 is elementary for both. Therefore, the following chapter will give a closer look at the thermodynamics of this reaction and the crystal systems and characterisations of CaO and $CaCO_3$. Approaches for different kinds of sorbents will be discussed in chapter 3.

[2] 200 kWh is a state of the art power consumption for the production of one tonne of oxygen with a purity of 95%; 99.5% purity would require 250 kWh. Future AUS might only require 160 kWh per tonne of 95% oxygen.

2 Basics

2.1 Solid State Chemistry

2.1.1 Crystal Growth

Explanations for the habit of crystals date back to 1866 (BRAVAIS) and 1878 (GIBBS). The approach of BRAVAIS is based on geometrical assumptions, while GIBBS tried to explain the different habits by a thermodynamic approach.

Thermodynamic Explanation

According to GIBBS [50] a crystal has the lowest free enthalpy. This criterion can only be reached if the free surface energy is minimal.

$$G_{Surface} = \sum_i \sigma_i A_i \rightarrow \min \qquad 2\text{-}1$$

In case of isotropic surfaces, the equilibrium shape would be a sphere. Usually, in real life polyhedrons are observed. This observation is a result of the anisotropic free surface energy of the different planes of the crystal. Accordingly, WULFF [136] derived a theorem stating that the growth rate in a direction i is proportional in all directions to the quotient between the free surface energy and the central distance of the according surface h_i:

$$r_{growth} \sim \frac{\sigma_1}{h_1} = \frac{\sigma_2}{h_2} = ... = const. \qquad 2\text{-}2$$

Eq. 2-2 is the solution of eq. 2-1 and has the consequence that surfaces with a high free surface energy are growing faster than sites with a low free surface energy and, consequently, the fastest growing site will disappear if the growth time was sufficiently long. The construction according to WULFF describes the resulting equilibrium shape very well (see Fig. 2-1).

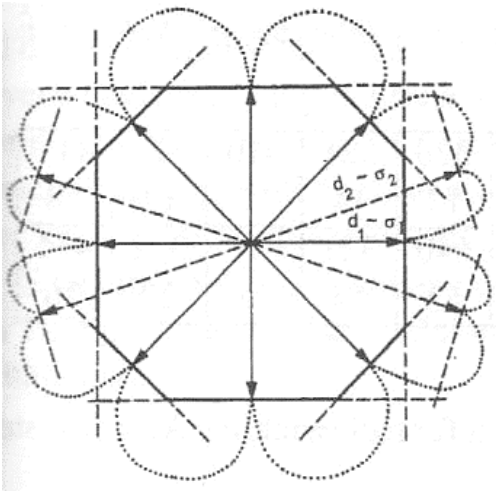

Fig. 2-1: Construction according to WULFF in two dimensions. Starting from a centre point lines are drawn in the direction of perpendiculars of the crystal plains. The length of these lines is proportional to the free surface energy. At the tip of the perpendiculars orthogonal lines are drawn. The resulting inner shape is the equilibrium state of the crystal. Picture is taken from [102].

As the concept of WULFF is able to explain the equilibrium shape very well, it does not allow to predict the habit of a crystal correctly without huge efforts, because the free surface energy is a function of temperature, supersaturation and pressure. It should be kept in mind that different additives are known to alter the habit by changing the specific free surface energy of specific planes.

Crystal Structure Explanation

BRAVAIS suggested that the growth of the morphological most important planes (crystal plains with the lowest growth rate) occur parallel to the crystal plain with the highest density of ions, i.e. the lowest distance between the plains. This concept works well for simple unit cells and geometries.

Atomic Theory of Crystal Growth

KOSSEL and STRANSKI ([63]) combined the models suggested by BRAVAIS and GIBBS into one theory based on energetic consideration of the adsorption and desorption of ions by and from a lattice.

Looking at the interaction of an ion on a two dimensional cubic lattice (see Fig. 2-2) it becomes obvious that this ion faces attractive and repulsive forces depending on the distance to other ions of the same or opposite charge.

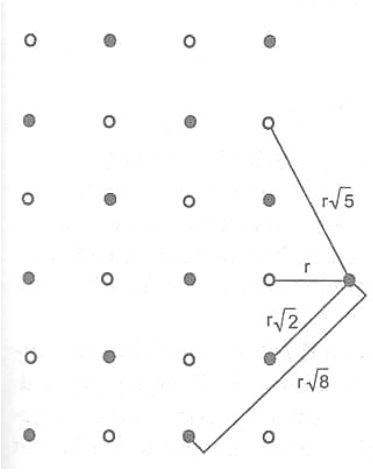

Fig. 2-2: Adsorption of an ion on the (1 0 0) plane of a sodium chloride crystal and the according distances to ions in the bulk. Figure taken from [102].

These distances contribute inverse to the binding energy

$$E_{Ion}^{Binding} = \phi \cdot \frac{e^2}{r}. \qquad 2\text{-}3$$

ϕ is the factor for the binding energy that summarises all inverse distances to other ions. Based on this concept it is possible to calculate the adsorption and desorption energies of an ion at different locations of a crystal and therefore understand the growth of it. Fig. 2-3 and Table 2-1 illustrate this concept.

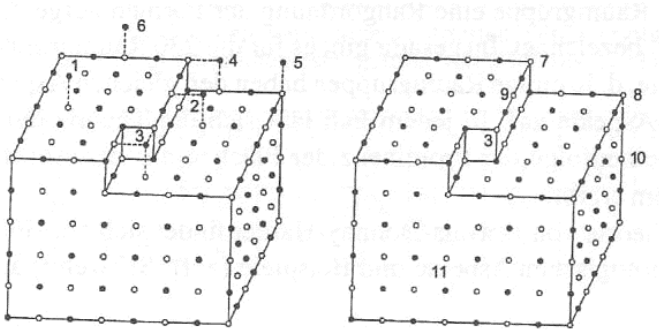

Fig. 2-3: Possible locations for the adsorption (left) and desorption (right) of ions onto and from the surface of a (1 0 0) NaCl crystal site. Picture taken from [102].

High ϕ values refer to a high energy value for the absorption and the desorption and, accordingly to a slow kinetic of both processes. This results in the growth of the crystal in the direction of the highest ϕ value or for the shrinkage, i.e. desorption of ions, into the direction of the lowest value.

Table 2-1: ϕ values of deposition and separation energies for a NaCl crystal.

Position of the Ion	ϕ values	
1	0.0662	Adsorption
2	0.1806	
3	0.8738	
4	0.4941	
5	0.2470	
6	0.0903	
7	1.1872	Desorption
8	1.3440	
9	1.5669	
10	1.5910	
11	1.6814	

According to Table 2-1 the adsorption of an ion on the (100) surface of a cubic space centred crystal will take place first at position (3) until the row is complete. Afterwards, another row will start from position (4). This process will continue until the plane is completed. The starting point for a new plane is position (6), the edge of the crystal.

The desorption of ions will start at point (8) followed by the desorption of ions in position (3) until it has vanished completely. Next, an ion in position (7) will desorb.

Even though the KOSSEL-STRANSKI theory explains the crystal growth very well, it was unclear for a long duration why the theoretical growth rates vary with some orders of magnitudes from experimental values. This misfit was overcome by BURTON, CABRERA and FRANK by the concept of a screw like crystal growth (see Fig. 2-4).

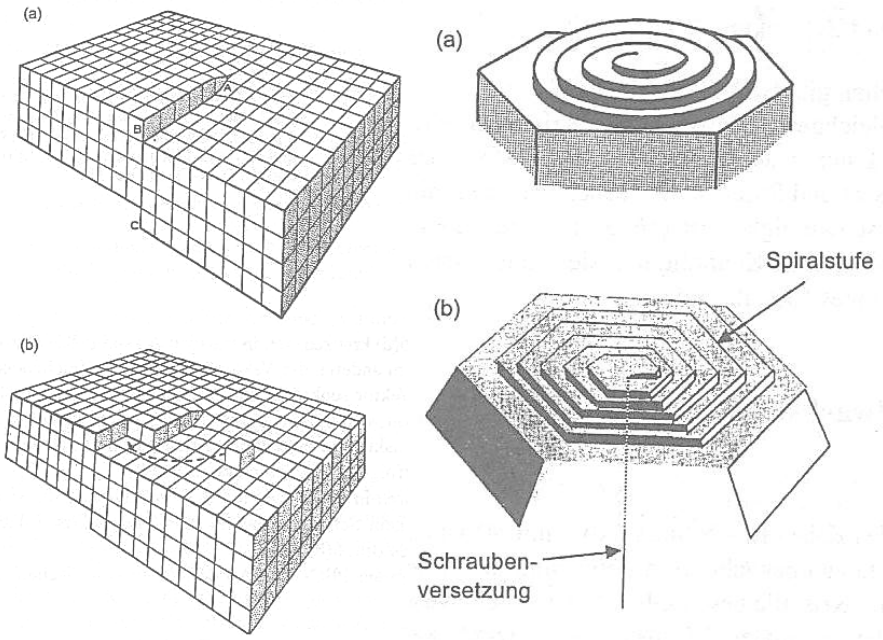

Fig. 2-4: Examples for a screw dislocation in a cubic (left) and hexagonal (righ)t crystal system. Figure taken from [102].

Due to screw dislocations incomplete rows are always present and enabling high growth rates.

2.1.2 Crystal Errors, Grain and Phase Boundaries

Crystal disorders can be classified into three categories.

- Zero-dimensional (point defects): vacancies and foreign atoms in the lattice
- One-dimensional: shiftings
- Two-dimensional: grain and phase boundaries

Only the occurrence of vacancies can be explained by thermodynamics ([102]). One- and two-dimensional disorders are the result of the formation (crystallisation) and the mechanical history of the crystal.

Mismatches in the crystal always cause an increase in the enthalpy. In contrast

$$G = H - TS \tag{2-4}$$

can only reach a minimum if the entropy is increased at the same time.

Regarding SAHM ET AL. [102], the concentration of crystal mismatches can be calculated according to

$$c_a = \exp\left(\frac{\Delta_F G}{k_B T}\right). \tag{2-5}$$

Where $\Delta_F G$ is the free formation energy of vacancies and k_B the BOLTZMANN constant.

Vacancies are important for the diffusive transport of ions in the lattice.

Transport Mechanisms in the Lattice

"Lattice diffusion takes place through the movement of point defects" ([66]). KOFSTADT ET AL. [66] describes three major diffusion mechanisms: Vacancy, interstitial and intersticialcy mechanism (see Fig. 2-5).

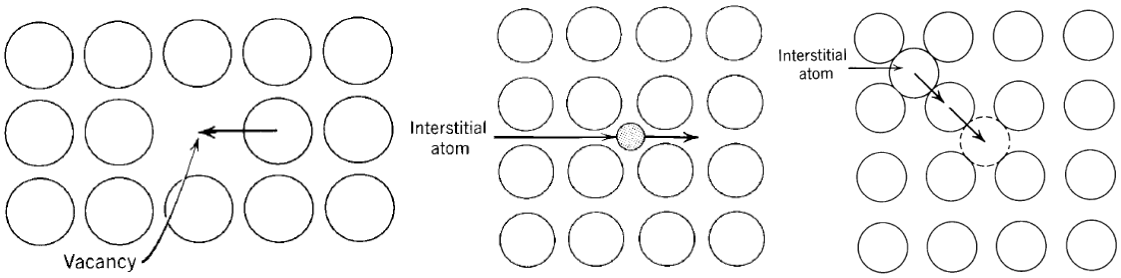

Fig. 2-5: Diffusion mechanisms according to [66]: vacancy (left) , interstitial (centre) and intersticialcy (right) mechanisms. Pictures taken from [66].

Solid transport by vacancy diffusion takes place if an atom on a normal site jumps into an adjacent, unoccupied lattice site. In contrast, atoms that are able to fit into lattice gaps of the lattice and jump from gap to gap cause diffusion by the interstitial mechanism. Of course, this mechanism prerequisites a wide lattice and small ions or atoms like H, C, N, O to work. The intersticialcy mechanism is a combination of vacancy und interstitial diffusion: "If the distortion becomes too large to make the interstitial mechanism probable, interstitial atoms may move by another type of mechanism. In the interstitialcy mechanism an interstitial atom pushes one of its nearest neighbours on a normal lattice site into another interstitial position and itself occupies the lattice site of the displaced atom" ([66]).

Mathematical Description of Lattice Diffusion

A time independent mas flow through a solid can be described according to FICK's first law.

$$J = -D\frac{dc}{dx} \qquad 2\text{-}6$$

J describes the mole flow through a given cross section; D is the diffusion coefficient and dc/dx the concentration gradient within the diffusion distance.

However, the diffusion coefficient is strongly temperature-dependent.

$$D = D_0 \exp\left(-\frac{Q}{RT}\right) = D_0 \exp\left(-\frac{q}{k_B T}\right) \qquad 2\text{-}7$$

The pre-exponential factor D_0 can be calculated according to

$$D_0 = \alpha a_0^2 \upsilon \exp\left(\frac{\Delta S_D + \Delta S_m}{R}\right). \qquad 2\text{-}8$$

α is a structure and mechanism-dependent factor, a_0 is the lattice parameter, υ the vibration frequency of a lattice atom (~10^{13}Hz) and ΔS_D and ΔS_m (<10 J/(molK)) are the change in entropy if vacancies are created or an atom moves from the equilibrium position to the top of the potential barrier. Usual values for D_0 are in the range of $0.2 \cdot 10^{-12}$ (Cl in a lattice of KCl) to $3.4 \cdot 10^{-12}$ m²/s (W in a lattice of W) ([62]).

The activation energy Q can be calculated by the sum of the change of enthalpies for the creation of vacancies (ΔH_D) and the difference of enthalpy between the equilibrium position and the top of the potential barrier (ΔH_m).

$$Q = \Delta H_D + \Delta H_m \qquad 2\text{-}9$$

However, values for the activation energy can be found in literature and estimated by the empirical formula

$$q/eV \approx 1.45 \cdot 10^{-3} T_S/K \text{ ([62]).} \qquad 2\text{-}10$$

T_s is the melting point of the according substance. Accordingly, activation energies for the creation of vacancies in $CaCO_3$ (T_S~1300 K) and CaO (T_S = 2834 K) range from 2 eV to 4 eV.

CHERNIAK ET AL. [32] investigated the diffusion of Sr and Pb in calcite. He reported an activation energy for the diffusion of Sr of (1.36 ± 0.06) eV and a pre-exponential factor of $0.21 \cdot 10^{-12}$ m²/s.

Fig. 2-6 illustrates the effect of the different activation energies for the creation of vacancies; taking a base temperature of 650°C the diffusion coefficient, i.e. the mole flux is increased by a factor of 10 and 100 if the temperature is increased by 100°C for $CaCO_3$ and CaO respectively.

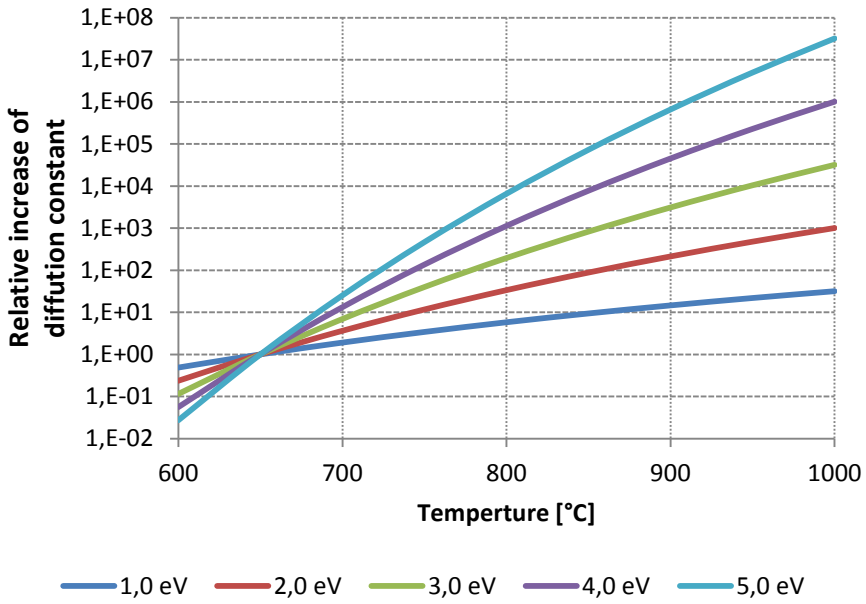

Fig. 2-6: Relative temperature impact on the diffusion constant in case of different activation energies for the creation of vacancies in a crystal lattice.

This effect has a huge practical impact: In case that the reaction rate of the re-carbonation is controlled by diffusion, an increase of the carbonator temperature by 50°C would raise the reaction rate by a factor of 10. Of course, this theoretical enhancement is too optimistic because other effects are going to counteract. However, section 6.1.1 contains a detailed discussion about this effect.

With respect to sintering it should be kept in mind that the self-diffusion coefficient in $CaCO_3$ at 650°C is an order of magnitude of 10^5 higher compared to CaO at 1000°C[3]. By this, sintering phenomena are much more likely to occur during the re-carbonation.

Grain Boundaries

Grain boundaries separate grains of the same phase but with different crystallographic orientation. These boundaries strongly influence the properties of a macroscopic crystalline substance because they counteract in dislocation motions and act as a source or sink of point defects. Fig. 2-7 illustrates a grain boundary between three different crystal orientations.

[3] D_0 was assumed to be in the order of magnitude of 10^{-13} m²/s while the activation energy for vacancies in $CaCO_3$ and CaO were believed to be 2 eV and 4 eV respectively.

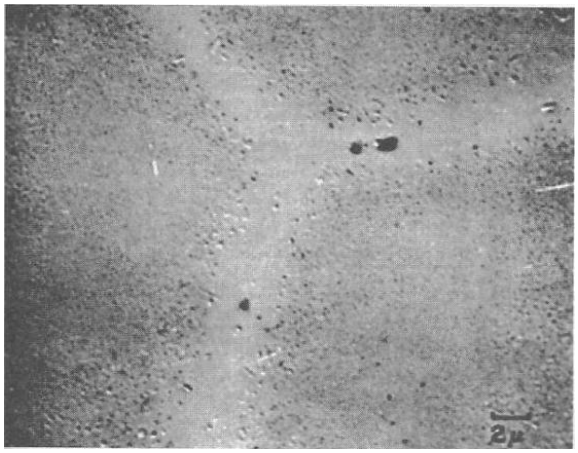

Fig. 2-7: Grain boundary as a sink of point defects between three different crystal orientations. Picture taken from [100].

Diffusion along grain boundaries is usually accelerated. By this, point defects vanish much faster at grain boundaries than in the lattice if the crystal is cooled down (see Fig. 2-7) ([105]). According to SAHM ET AL. [102], impurities can be enriched (segregated from the lattice) at grain boundaries if

- the specific surface energy can be reduced,
- the foreign atoms exceed more than 15% of the size of the lattice atoms (HUME-ROTHERY rule) and/or
- the chemical potential of the lattice can be lowered.

Tensions within the crystal can be decreased by an increase in temperature causing crystal dislocations to dissociate in grain boundaries.

One example of the defined control of the amount of grain boundaries is iron. Rapid cooling causes a creation of a fine grained texture that has a higher stability than normal steal but is very sensitive towards corrosion (the grain boundaries act as a starting point of the oxidation) ([128]).

Phase Boundaries

Phase boundaries can be classified as coherent (similar or equal crystal parameters of phase I and phase II) and incoherent (significant difference in the crystal parameters of the two phases). Naturally, mismatches cause an increase in energy. Therefore incoherent phase boundaries have always a higher energy than coherent ([102]).

Phase boundaries mark the starting point of the formation of new mixtures between two crystalline substances. By this, at least, two phase boundaries are likely to be observed. Thus, a microscopic approach to the arising problem is very difficult and unhandy. A more

macroscopic strategy will be shown in this work by the introduction of phase diagrams in Chapter 2.3.

2.2 Crystal Systems of the Main CL Substances

2.2.1 $CaCO_3$

The three main crystal systems of $CaCO_3$ are: calcite, aragonite and vaterite. Besides these modifications, water-containing $CaCO_3$ as monohydrocalcite ($CaCO_3 \cdot H_2O$) or Ikait ($CaCO_3 \cdot 6\ H_2O$) are known but not relevant for the scope of this work.

calcite is the only stable modification at high temperature and ambient pressure. aragonite and vaterite are metastable and transforms into calcite at temperatures above 420°C ([15]) and 400°C ([126]). However, even if these two modifications have no importance during the high-temperature conditions of the cycling of a Ca-based sorbent, they are important for the consideration of synthetic sorbents and for "low" temperature reactivation steps because they determine the initial texture and therefore the appearance of the resulting quick lime and so the re-carbonation behaviour.

Table 2-2: Compilation of the crystal parameters of $CaCO_3$ systems. Table according to [91].

Modification		calcite	aragonite	vaterite
Space group		$R\bar{3}c$	$Pmcn$	$P6_3/mmc$
Crystal system		trigonal	orthorhombic	hexagonal
Lattice constants [Å]	a	4.99	4.96	7.15
	b	=a	7.97	=a
	c	17.06	5.74	16.95
	α	90°	90°	90°
	β	$=\alpha$	$=\alpha$	$=\alpha$
	γ	120°	$=\alpha$	120°
Density [g/cm³]		2.71	2.94	2.54
Molar volume [cm³/mol]		36.9	34.0	39.4
Hardness (Mohs)		3	3.5-4.5	3

Fig. 2-8 illustrates the in Table 2-2 given values for the according crystal systems.

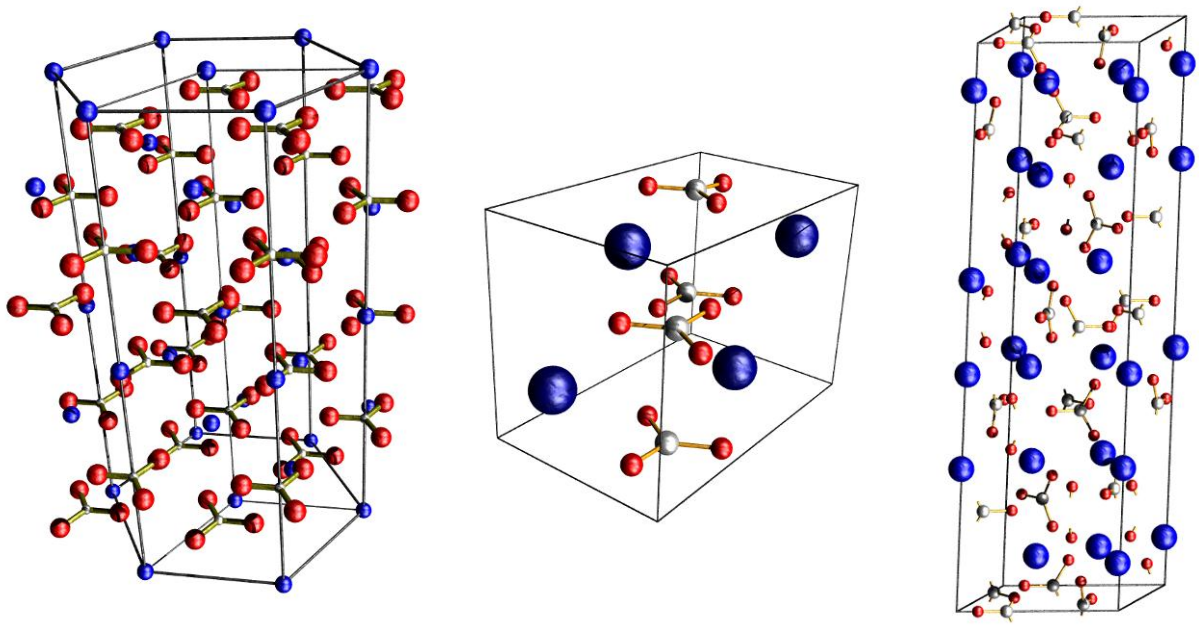

Fig. 2-8: Unit cells of calcite (left), aragonite (centre) and vaterite (right). Blue spheres are calcium, red are oxygen and whit are carbon. The crystal system of calcite and vaterite is hexagonal while aragonite is cubic. Note: To better illustrate the hexagonal crystal system of calcite three unit cells are displayed at once.

Even if the unit cell is fixed, the crystal may appear in various forms, so called habits. The different habits are resulting of different growth speeds of the crystal sites.

Fig. 2-9 explains this effect very good: Starting from a two-dimensional hexagonal unit cell, six different growth directions are possible resulting in six outer planes: (110), (1 $\bar{1}$ 0), ($\bar{1}$ 00), ($\bar{1}$ $\bar{1}$ 0), ($\bar{1}$ 10), (010). In this example, the growth rates in the directions ($\bar{1}$ 10) and (1 $\bar{1}$ 0) were lower than those in the (010), (110) and ($\bar{1}$ $\bar{1}$ 0) directions, while the growth in the ($\bar{1}$ 00) direction stopped spontaneously. These different growth rates result in a macroscopic shape that has nearly no similarity to the rhombohedral unit cell anymore.

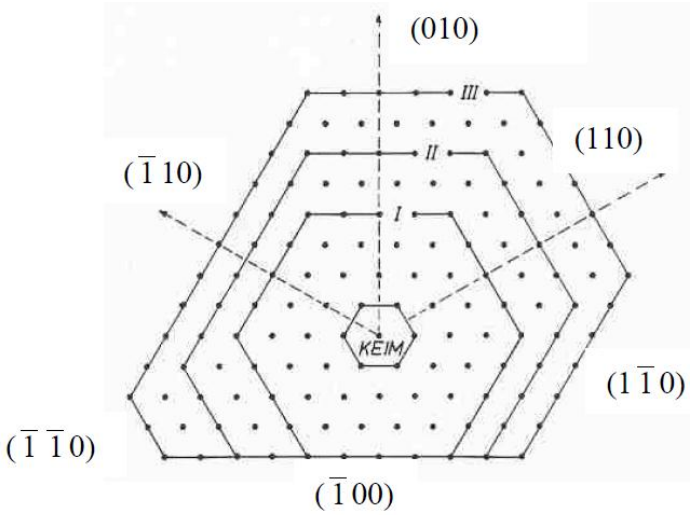

Fig. 2-9: Example of a hexagonal two-dimensional crystal system for the impact of different growth rates on the macroscopic appearance. Figure taken from [108].

In case of calcite six main habits are known. These are shown in Fig. 2-10.

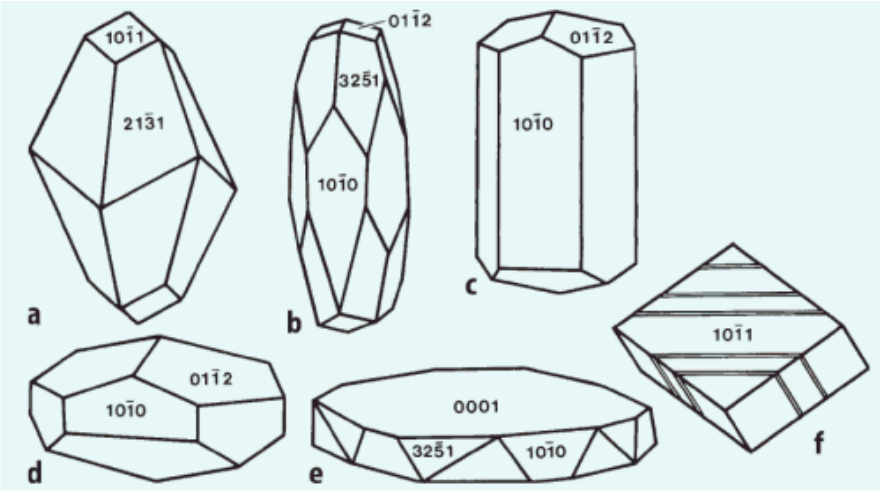

Fig. 2-10: Habit of calcite. a: Ditrigonal scalenoeder (21 $\bar{3}$ 1) combined with a rhombohedrum (10 $\bar{1}$ 1); b: Hexagonal prism (10 $\bar{1}$ 0) combined with a ditrigonal skalenoeder (32 $\bar{5}$ 1) and rhombohedrum (01 $\bar{1}$ 2); c: Hexagonal prism (10 $\bar{1}$ 0) combined with a rhombohedrum (01 $\bar{1}$ 2); d: Rhombohedrum (01 $\bar{1}$ 2) combined with a hexagonal prism (10 $\bar{1}$ 0); e: Basispinakoid (0001) dominates over prism and scalenoeder; f: Split rhombohedrum with twin siping caused by sliding along (01 $\bar{1}$ 2)[4]. Figure taken from [92].

These habits of calcite can occur on a microscopy (normal limestone and chalk) and on a macroscopic scale (calcspar) and can be influenced by the crystal growth conditions. Pressure and temperature variations are used, for example, to control the habit of calcite during the precipitated calcium carbonate (PCC) production in order to receive a filler or a coating

[4] Here, the „extended“ Miller indices are used: (hkil) while i = - (h+k).

substance for paper production. With scope on the CL process a modified PCC production route could be used to produce tailor made $CaCO_3$ that might be used as sorbent for CO_2.

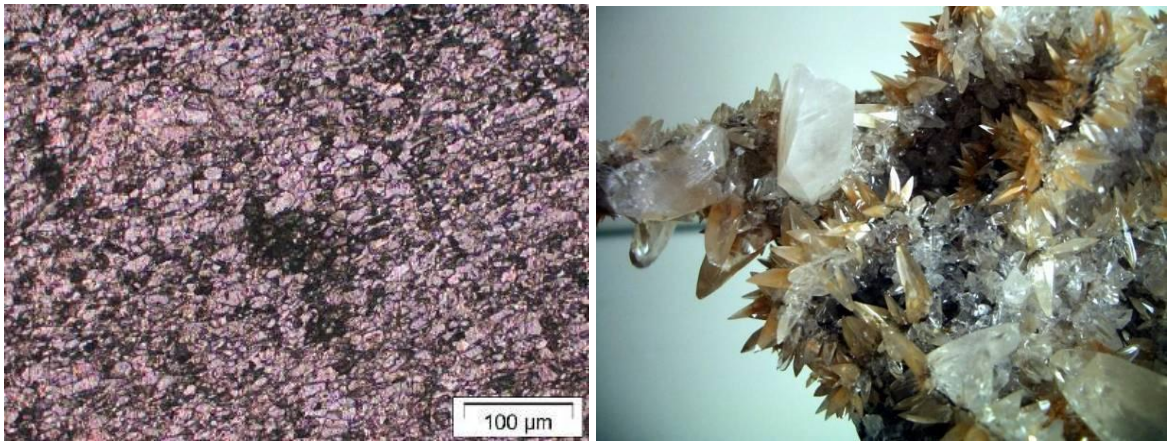

Fig. 2-11: Microcrystalline structure of Devonian limestone (left) (figure taken from [58]) and macro crystal scalenoeder (right).

Massive Devonian limestone usually comprises of small $CaCO_3$ crystals which are embedded in a matrix of $CaCO_3$ mixed with impurities like Al_2O_3, SiO_2, Fe_2O_3 and MgO (see Fig. 2-11, left) ([64]).

Calcspar is a pure limestone that has big elementary crystals that are in close contact with each other. Such stones tend to fall into pieces (decrepitate) during the preheating and heating within the kilns. Decrepitation is an effect caused by the crystal system: The thermal expansion coefficient of calcite is anistropic, i.e. the crystal expands in the c, but contracts in the a direction due to an increase of temperature (see Fig. 2-12).

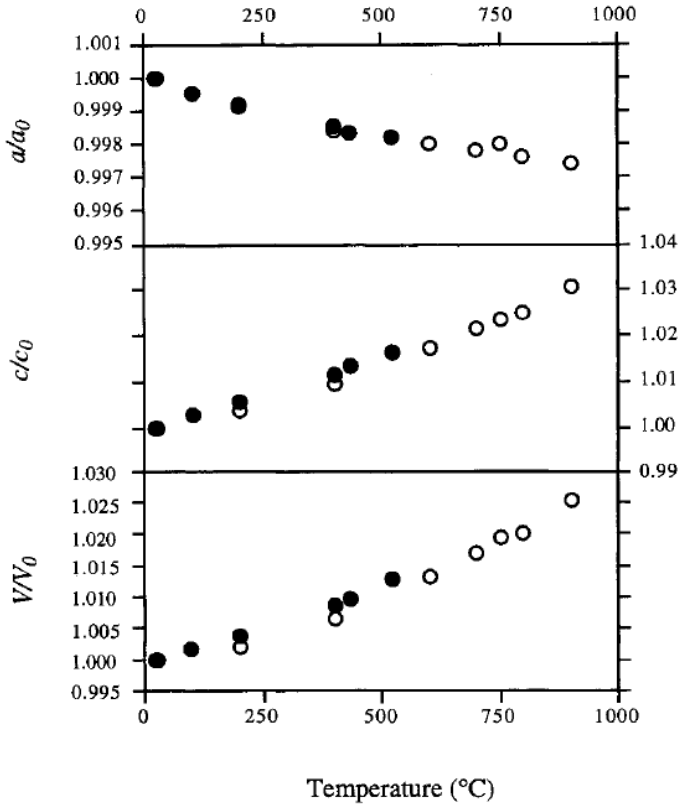

Fig. 2-12: Change in the lattice constants of calcite due to heating. The solid and the open circles present two different measurements of two authors. Figure taken from [134].

High tension forces are created on temperature increase, disregarding how slowly the heating takes place. These tensions lead, in the end, to cracks in the material and destruct it (dust generation) or weaken significant the mechanical strength. A more detailed discussion about this phenomenon can be found in section 2.7.

$CaCO_3$ has a TAMMANN[5] temperature of 533°C ([33]). The melting point of calcite under pressure is around 1300°C.

2.2.2 CaO

CaO only occurs in the form of lime. Lime is a manly artificial mineral that has a cubic space centred crystal system (see Fig. 2-13) and is produced by the thermal decomposition of either $CaCO_3$ (industrial process) or $Ca(OH)_2$ (lab process).

[5] The TAMMANN temperature is defined as starting point of the surface diffusion of metal and metal oxide particles ([124]). Usually, this temperature can be estimated by $T_{Tammann} \approx x\,T_{melting}$ while x can be 0.5 ([124]) or 0.75 ([28]). The TAMMANN temperature is measured by the microscopy observation of the temperature at that crystal edges become round.

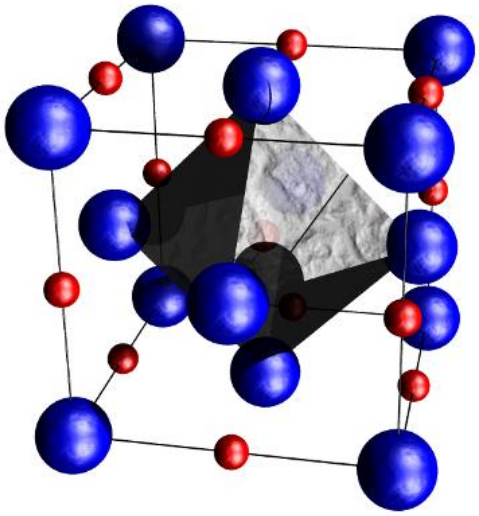

Fig. 2-13: Unit cell of lime according to the unit cell parameters given in Table 2-3. Blue spheres are calcium while red are oxygen.

Table 2-3: Crystal system parameters of CaO ([14]).

Formula		CaO
Name		Lime
Space group		$Fm\bar{3}m$
Crystal system		cubic
Lattice constants [Å]	a	4.8112
	b	=a
	c	=a
	α	90°
	β	$=\alpha$
	γ	$=\alpha$
Density [g/cm³]		3.37
Molar volume [cm³/mol]		16,6
Hardness (Mohs)		3.5

Due to its hydroscopic character CaO cannot be stored for a long duration under ambient conditions – it will react spontaneously with the humidity of the air and form $Ca(OH)_2$. Following, a rather slow reaction with CO_2 will take place and will form $CaCO_3$. The direct carbonation of CaO under ambient conditions is kinetically prohibited.

CaO has a TAMMANN Temperature of 1154°C ([33]), a melting point of 2570-2580°C and a boiling point of 2850°C. In conclusion, CaO is much more resistant towards sintering than $CaCO_3$.

Lime has, due to its origin from the decomposition of another solid, a sponge like structure with a porosity between 20 and 60% and a specific surface area between typically 0.3 to 5.3 m^2/g ([87]). Of course, the porosity and the specific surface area are a function of the sintering temperature, the sinter duration and the origin of the limestone. BORGWARDT ET AL. [24], for example, reported specific surface areas of nascent CaO produced from $Ca(OH)_2$ and $CaCO_3$ of 128 and 77 m^2/g respectively. These extremely high BET surfaces collapse nearly instantly if higher temperatures are applied (reduction of surface energy).

The series of pictures displayed in Fig. 2-14 illustrate the effect of temperature on the texture of lime.

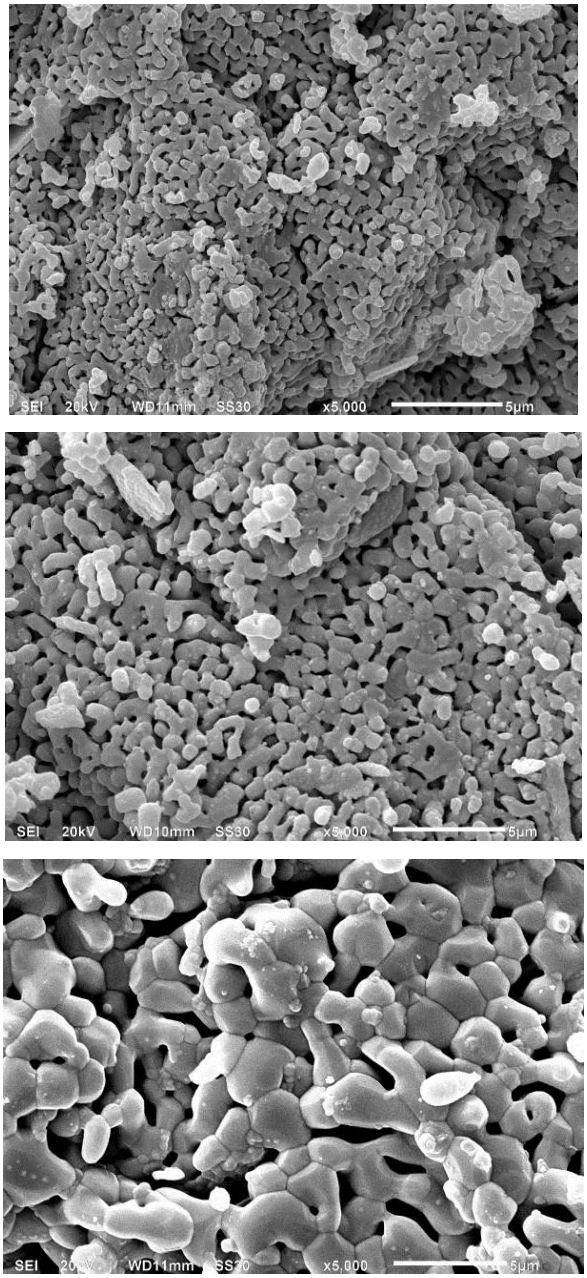

Fig. 2-14: Series of burning tests with D-2009-009 at different temperature levels. Scanning electron microscopy (SEM) pictures have a magnification of 5000 each. Calcination and sintering were done at ambient pressure under air for 2.5 h. The according temperatures were: Top 960°C, middle 1060°C, bottom 1200°C It should be noted that sintering effects become dominant if the TAMMANN temperature (1154°C) is crossed.

In case that the TAMMANN temperature is crossed, grain coarsening (viz. sintering) becomes dominant.

2.2.3 $Ca(OH)_2$

$Ca(OH)_2$ only occurs in the form of portlandite which has a layered structure that is connected via hydrogen bonds. It is rarely found naturally, because it will react slowly with the CO_2 provided by the air to form $CaCO_3$. Portlandite is produced industrially by the reaction of

water with lime. This reaction proceeds to its total end because it follows a dissolution-precipitation mechanism, first proposed by HEDIN in 1949. During this process, CaO is dissolved as $CaO \cdot 2\,H_2O$, which reacts in a liquid or in a pseudo-liquid phase (if steam hydration is applied) to $Ca(OH)_2$. This mechanism destroys the original crystal system and creates the new solid portlandite apart from the surface of CaO. This reaction normally occurrs at many sites of the CaO at once. Accordingly, a very fine powder is produced. Special conditions promoting a small supersaturation of $CaO \cdot 2\,H_2O$ and a constant growth of a limited number of $Ca(OH)_2$ crystals cause coarse portlandite particles. Another possible way to receive coarse $Ca(OH)_2$ is given by the introduction of high shear forces into a milk of lime. This fact can be explained by the structure of portlandite, which is presented in Fig. 2-15.

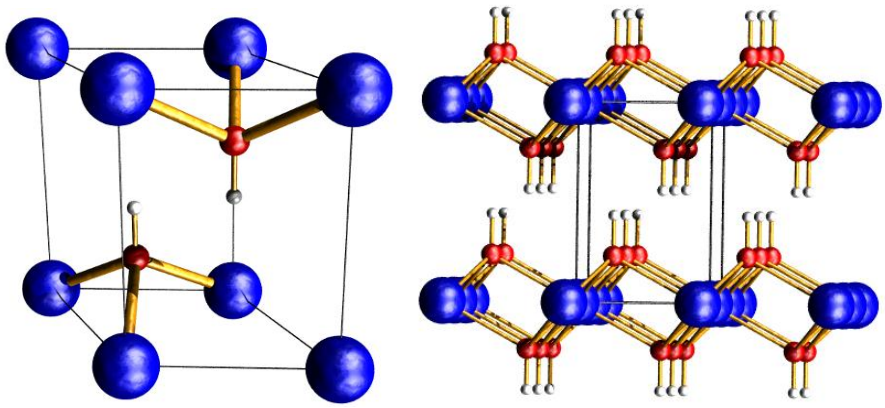

Fig. 2-15: Unit cell and layered structure of portlandite according to the unit cell parameters given in Table 2-4. Blue spheres are calcium while the red are oxygen. White spheres refer to Hydrogen.

Layers of $Ca(OH)_2$ are stacked on each other and connected with rather loss hydrogen bonds. This structure enables a “greasing” of new layers on top of the bulk material generating even coarser grains.

Table 2-4: Crystal system parameters of Ca(OH)2 ([14]).

Formula		$Ca(OH)_2$
Name		Portlandite
Space group		*P*3*m*1
Crystal system		trigonal
Lattice constants [Å]	a	3.5850
	b	=a
	c	4.8710
	α	90°
	β	$=\alpha$
	γ	120°
Density [g/cm³]		2.23
Molar volume [cm³/mol]		33.2
Hardness (Mohs)		2.5-3

$Ca(OH)_2$ decomposes, like $CaCO_3$, if it is heated above a certain temperature. The decomposition temperature depends on the partial pressure of H_2O in the atmosphere that surrounds the particle. Fig. 2-15 shows the equilibrium curve of the decomposition of $Ca(OH)_2$, which has been calculated according to the equation provided in paragraph 2.4.

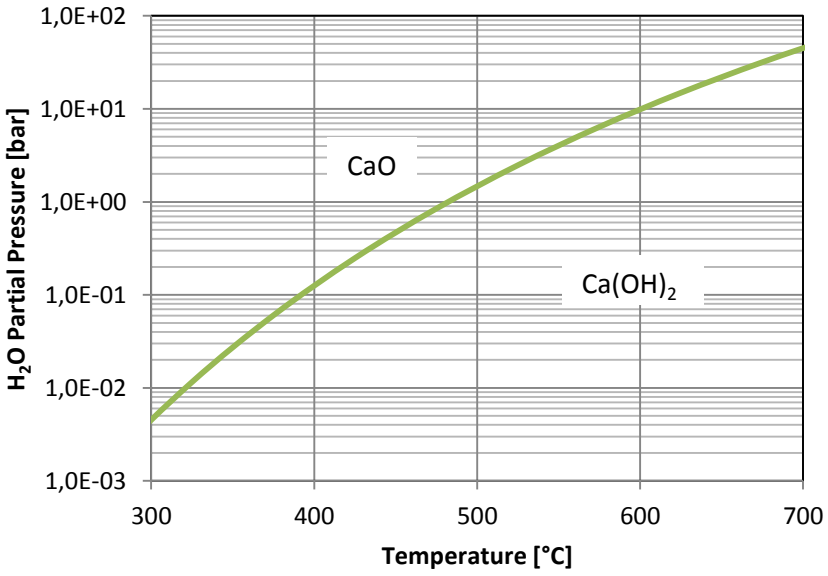

Fig. 2-16: H_2O partial pressure over a pure solid of $Ca(OH)_2$. The calculation of the curve was realised according to paragraph 2.4. with the used data, provided in Table 2-5. A value for $\ln K_a^{\Theta}$ of -26.23 was assumed.

Table 2-5: Thermodynamic data for the calculation of the equilibrium partial pressure of H_2O over $Ca(OH)_2$ in dependency of the temperature. Values taken from [95].

	a	b	c	c_p^Θ	$\Delta_B H^\Theta$
H_2O	34.40481	0.000628	0	34.59	-242.0
CaO	41.89000	0.020275	-452412	42.84	-635.5
$Ca(OH)_2$	89.56970	0.000000	0	89.57	-986.0
Δ	-13.27489	0.020903	-452412	-12.14	109.0

It can be stated, that the decomposition of $Ca(OH)_2$ starts at roughly 470 °C under atmospheric pressure. The melting point of $Ca(OH)_2$ can be investigated under extreme high pressure conditions and decreases with increasing pressure (see Fig. 2-17). This indicates that molten portlandite has a higher density than crystalline ([46]).

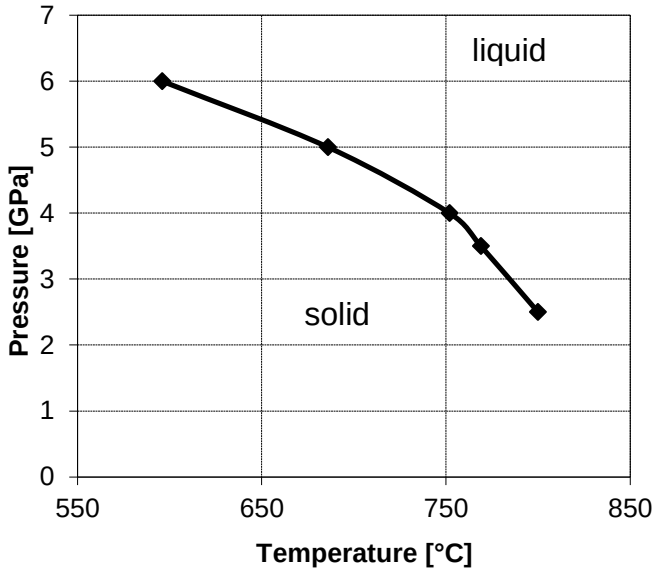

Fig. 2-17: Melting line of $Ca(OH)_2$. Values taken from [46].

2.2.4 $CaSO_4$

Three water free phases of anhydrite are known, anhydrite I, II and III ([20]). The crystal structure of Anhydrite II, the only water free thermodynamically stable modification is shown in Fig. 2-18.

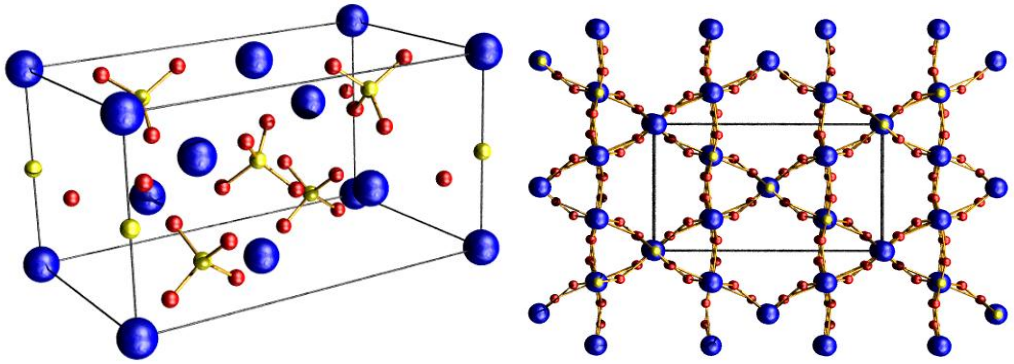

Fig. 2-18: Unit cell and top view of Anhydrite according to the unit cell parameters given in Table 2-3. Blue spheres are calcium while the red are oxygen. Yellow spheres refer to Sulphur.

According to BENEDIX ET AL. [20] anhydrite III forms after the dewatering of partial hydrated gypsum and is stable between 200 and 500°C. Anhydrite II forms at a temperature range between 500 and 600°C and is stable up to 1200°C. In case of heating anhydrite II above 1200°C, anhydrite I is formed.

The melting point of anhydrite is 1460°C ([116]).

Decomposition of $CaSO_4$ can take place at rather low temperatures if a reducing atmosphere surrounds it. [132], for example, proposed the decomposition of $CaSO_4$ into CaO, CaS and SO_2 by applying an atmosphere of CO and H_2 and temperatures between 1177 and 1232°C in a fluidised bed. The mechanisms and conditions of these reactions are discussed in paragraph 3.6.2 in more detail.

Besides, anhydrous $CaSO_4$ species, also three water containing ones are known: Calciumsulfate dihydrate ($CaSO_4 \cdot 2\ H_2O$) , α - calciumsulfate half hydrate ($CaSO_4 \cdot 0.5\ H_2O$) and β - calciumsulfate half hydrate ($CaSO_4 \cdot 0.5\ H_2O$).

Table 2-6: Compilation of the properties of the different CaSO4 species according to [20].

Formula	$CaSO_4 \cdot 2\ H_2O$	$CaSO_4 \cdot 0.5\ H_2O$	$CaSO_4 \cdot 0.5\ H_2O$	$CaSO_4$
Name	Gypsum	α -Bassanite	β - Bassanite	Anhydrite
Crystal system	monoclinic	monoclinic	orthorhombic	orthorhombic
Density [g/cm³]	2.31	2.757	2.619	2.93-2.97
Molar volume [cm³/mol]	74.5	52.7	55.4	45.9-46.5
Hardness (Mohs)	2	---	---	3-3.5

Water-containing $CaSO_4$ species are interesting in terms of sorbent reactivation and production of synthetic sorbents, because they provide a high molar volume and this, a very porous solid is formed after the dewatering.

2.3 Melting Phases due to Impurities

Coal is a very inhomogeneous substance composed of basically carbon, oxygen, hydrogen, nitrogen and sulphur. Fig. 2-19 shows an outtake of a part of a proposed chemical structure.

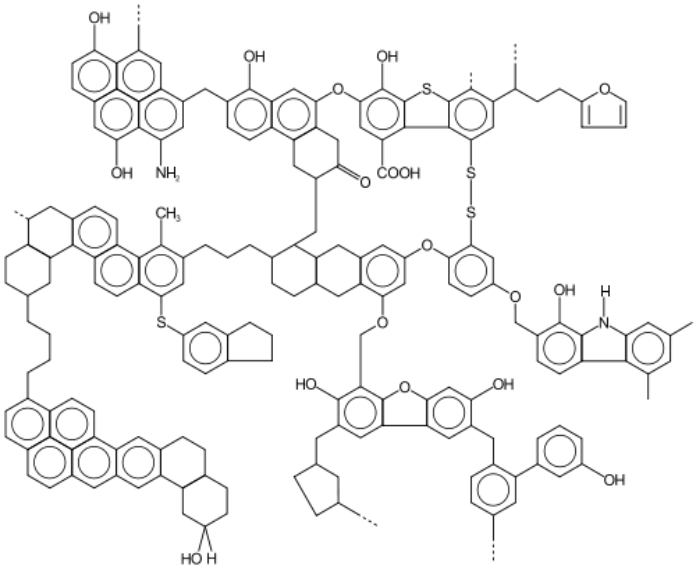

Fig. 2-19: Part of a proposed chemical structure of coal. Figure taken from [127].

Besides the basic elements, minor constituents like Na, Mg, Al, Si, P, K, Ca, Ti, Mn and Fe are present in the coal and causing the majority of sintering/ incrustation problems.

The number of trace elements found in the coal is nearly as large as the number of elements in the periodic table of elements (see Fig. 2-20 and Fig. 2-21).

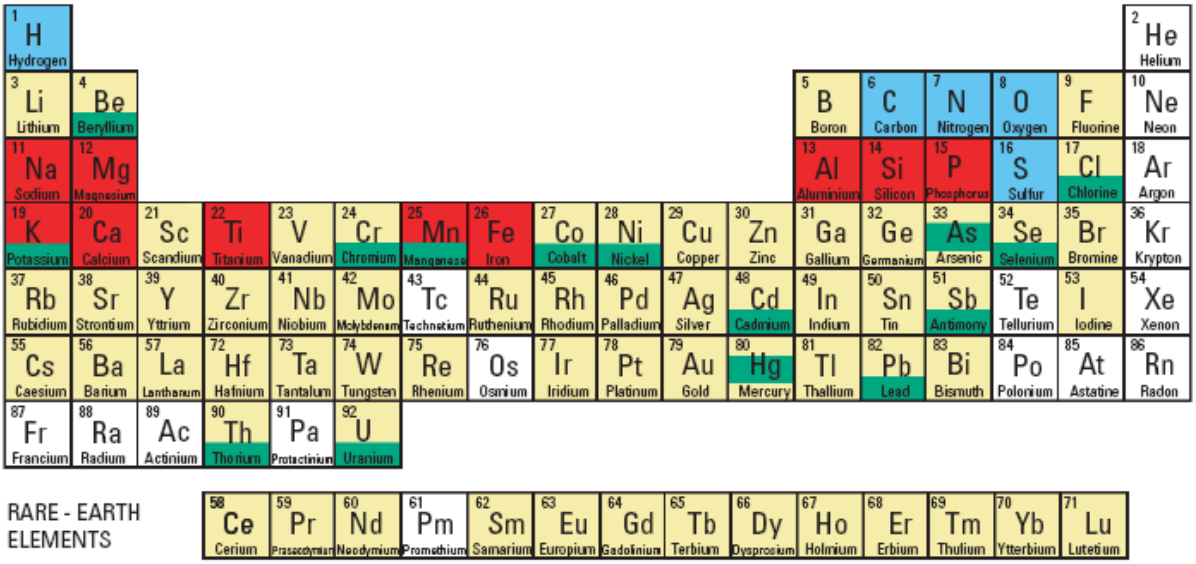

Fig. 2-20: Main (blue), minor (red) and trace (yellow) elements that can be found within coal. Elements that are marked green are classified as environmentally harmful. Picture taken from [113].

MUHAMMADIEH [88] investigated the formation of incrustations and melting phases in the boiler and on the heat exchangers due to the burning of lignite. He found that Ca, Fe and Al

are likely to form $Ca_2(Al, Fe)_2O_5$ (brownmillerite). Within melts of silicates, CaO increases the basicity and displaces alkali elements which, themselves, are forced into low melting sulphur compounds that are believed to be the seat of incrustations.

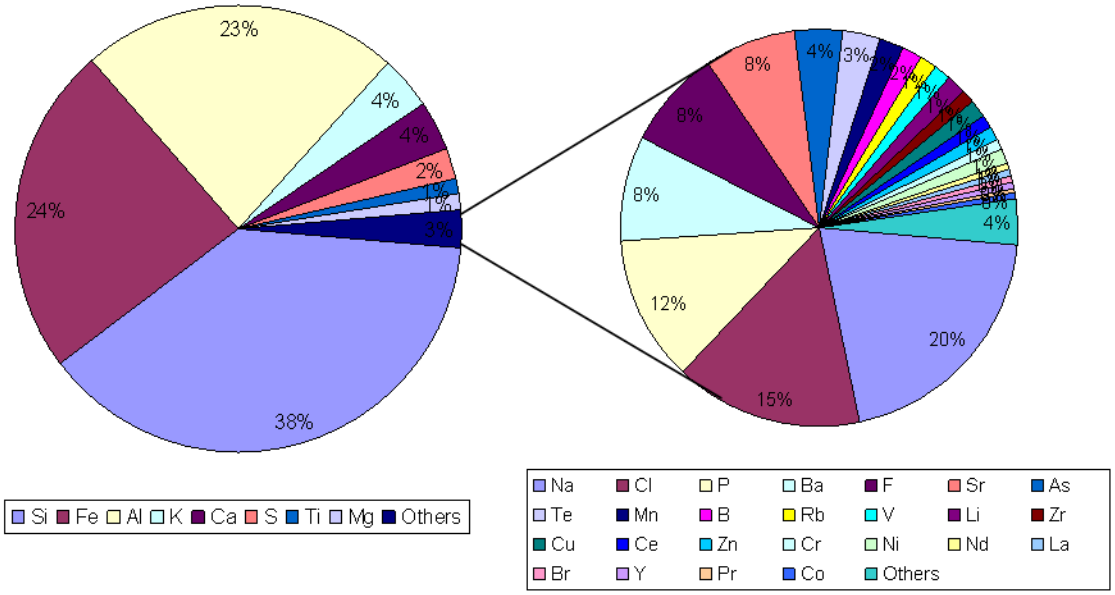

Fig. 2-21: Major and minor elements that can be found in the ash of lignite. Diagrams were created by using the average of 949 measurements of the chemical composition of wet lignite by the USGS [125]. The coal analysed can be found in the state of Alabama in the United States of America. The average ash content of these samples on a wet basis was 12.8%.

In terms of the CL process, impurities in the fuel of the calciner could become a challenge because they get concentrated by the cycles. Assuming that the controlled bleed and the make-up is the only possibility to refresh the interior in the CL process, it is shown in Fig. 2-22 that $CaSO_4$ could contribute manly to the total circulating mass (see chapter 4.5). This enrichment of impurities could cause considerable sintering and incrustation problems and could be a major challenge for the utilisation of the bleed. Also, the decay in CO_2 capture ability is very likely to be accelerated significantly.

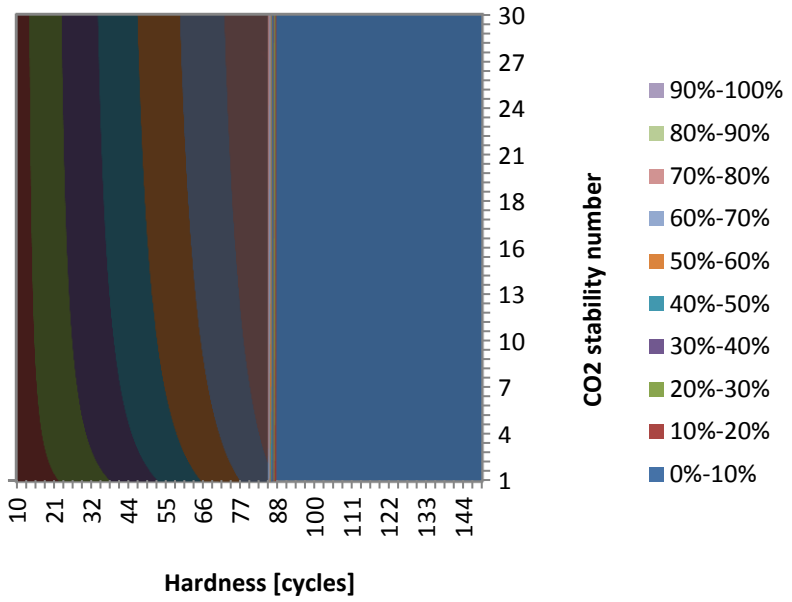

Fig. 2-22: Share of impurities ($CaSO_4$ and ash) of the circulating mass flow in the CL process in case of the use of hard coal. CL process would not run under the applied conditions with a lower bleed rate than 1.3% per cycle. This number equals a stability number of 80. Accordingly, the blue area to the right of a stability number of 80 reflects the breakdown of the system before a steady state could be reached. Explanations of the simulation are given in chapter 4.

Following, the description of binary and ternary systems via phase diagrams will be discussed. Examples of phases that are likely to form under the conditions of the CL process will be given.

2.3.1 Binary Phase Diagrams

Effects occurring by the change of the composition and the temperature of a homogeneous mixture of two solids can be explained very well with binary phase diagrams. Fig. 2-29 shows a very simple example of such a diagram. Commonly, the abscissa is used as composition scale that displays an increase of the solid S_2 if read from left to right. The share of the solid S_1 can be calculated accordingly by

$$S_1 = 100 - S_2 . \qquad 2\text{-}11$$

The temperature is drawn on the ordinate. Following, all important points of Fig. 2-29 will be explained shortly.

F and G are the melting points of the pure substances S_1 and S_2 respectively. C_1 is the eutectic point in which the two solid phases S_1 and S_2 and the liquid are in equilibrium. This point is invariant because any change of conditions (temperature or composition) will cause the disappearance of this equilibrium either into a pure liquid phase (temperature increase), a liquid phase and a solid of S_1 or S_2 (addition of S_1 or S_2) or a solid composed of S_1 and S_2

(temperature decrease). The lines $\overline{FC_1}$ and $\overline{C_1G}$ are the liquid curves. They separate the regions of the occurrence of a solid and liquid. For example, a mixture of two solids with composition A (13% S_2 and 87% S_1) and a temperature T_2 will occur as liquid that contains solid particles of S_1. The ratio between liquid and solid is given by the ratio $\overline{A_2B_2} / \overline{B_2C_2}$. At point C this ratio would result in infinite, meaning, that no solid would be present any more.

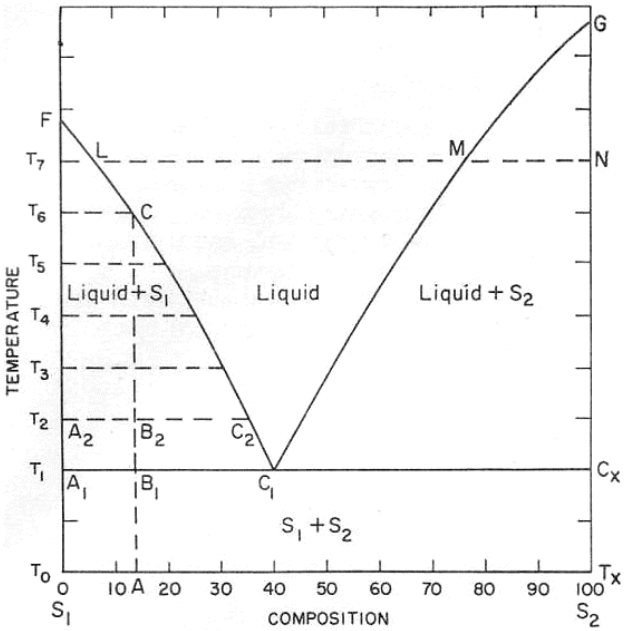

Fig. 2-23: Binary diagram with eutectic. Picture taken from [70].

Accordingly, two-phase areas are gaps in which no single phase can exist. Exactly these voids are believed to cause difficulties during the operation of the CL process: Impurities, especially if alkali metals are involved, are very likely to arrange in compositions that enable the creation of low melting eutectics. During this process, it is irrelevant if the precise composition of the eutectic is matched or not; liquid phases will be present possibly causing plugging of the surface of the sorbent or marking the starting point of incrustations. Two strategies could be applied to prohibit the expected problems: First, keep the temperature in both reactors as low as possible and second, avoid high contents of impurities in the system.
A detailed discussion about binary phase diagrams can be found in LEVIN ET AL. [70].

2.3.2 Ternary Phase Diagrams

Mixtures of three different substances are typically described with ternary diagrams and triangular coordinates. Fig. 2-29 shows an equilateral triangle of which the apexes are labelled with the components A, B and C. Each site of this triangle corresponds to a binary mixture, e.g. point F would correspond to a mixture of 65% A and 35% C. Determining the

concentration of the individual components in X is more sophisticated; for each component-site a parallel has to be projected through X, e.g. the parallel of the site $\overline{AB}$ is $\overline{FH}$. This parallel still reflects the shares of the substances of the original site. Therefore, the share of B in the composition in X can be calculated by $\overline{FX} / \overline{AB}$ (20%) while A would have a share of $\overline{XI} / \overline{AB}$ (45%). Component C would be $\overline{XJ} / \overline{AC}$ (35%).

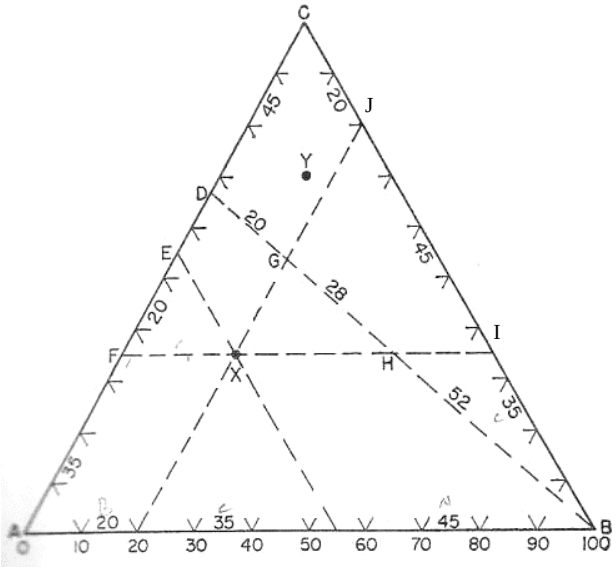

Fig. 2-24: General appearance of a simple ternary diagram. Picture taken from [70].

Melting points, i.e. the existence of liquid phases, cannot be displayed in a two dimensional plot but is often indicated by according lines.

Six of the major possible interactions of three substances are shown in Fig. 2-25.

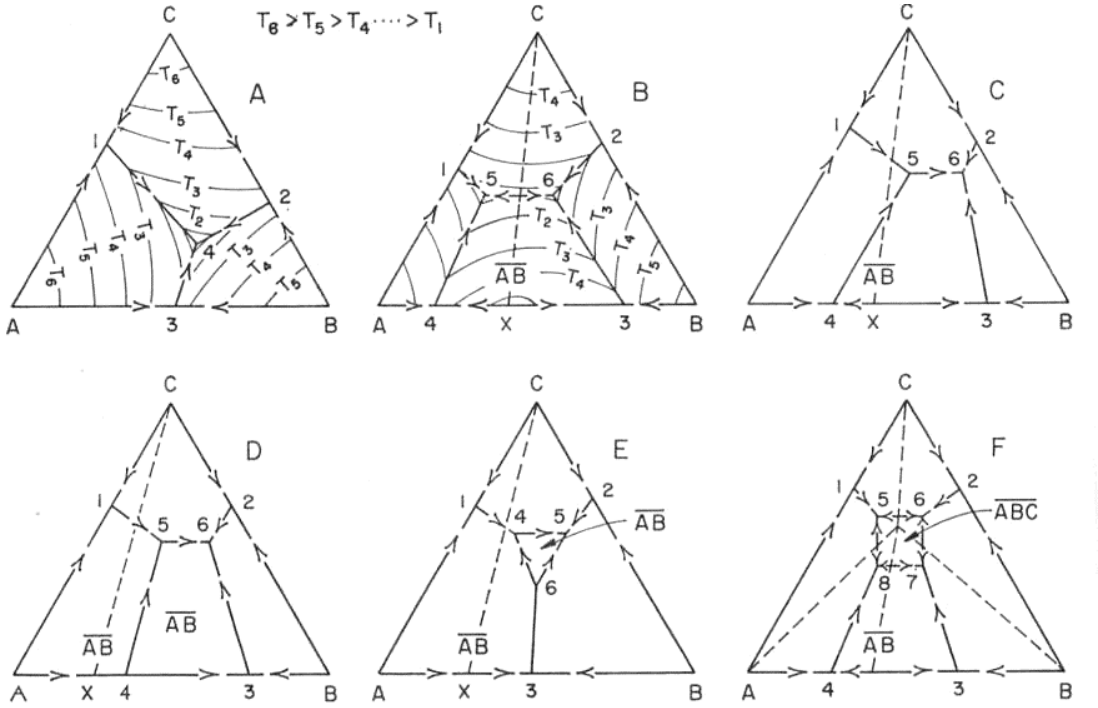

Fig. 2-25: Different principle effects of ternary mixtures: A: No binary or ternary compounds are present. One ternary eutectic can be found at point (4) (quadruple point) and three binary eutectics are present at point (1), (2) and (3). Hypothetical isotherms are inserted. B: Intersection line $\overline{CX}$ indicates a new compound AB and separates the ternary system in to two halves. Two eutectics (point (5) and (6)) can be seen. C: Similar situation like in B, but only one real eutectic present. D: New phase AB in the field (3)-(4)-(5)-(6). E: Phase AB is instable in a binary mixture of AB, but is stable in the presence of C. F: Occurrence of a ternary phase ABC. Arrows indicate the direction of falling temperature. Picture taken from [70].

As well, a detailed discussion of ternary phase diagrams is given elsewhere ([70]).

2.3.3 Important Binary and Ternary Phases

According to Fig. 2-21 the main impurities in coal are Si, Fe, Al, K. These elements may form oxides, carbonates, halogenates and sulphates and are able to interact with each other and with the Ca-based sorbent of the CL process.

Probably, one dominant reaction that could cause the loss of free CaO in the CL process is the reaction between CaO and SiO_2. Above a temperature of ~725°C both substances are able to react to calcium silicates disregarding their ratio (see Fig. 2-26). However, the kinetic of those reactions in relation to the possible interaction duration in a fluidised bed should be considered in detail to determine the extent of the formation of such phases.

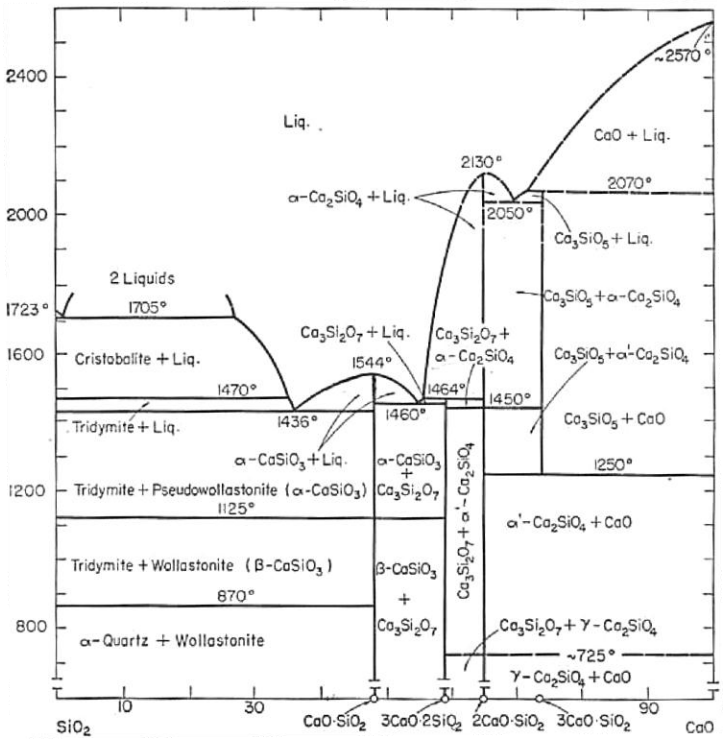

Fig. 2-26: System SiO_2-CaO. Picture taken from [70].

Another extreme critical chemical compound is K_2O. Together with SiO_2 and FeO or CaO it can form low melting glasses (see Fig. 2-27).

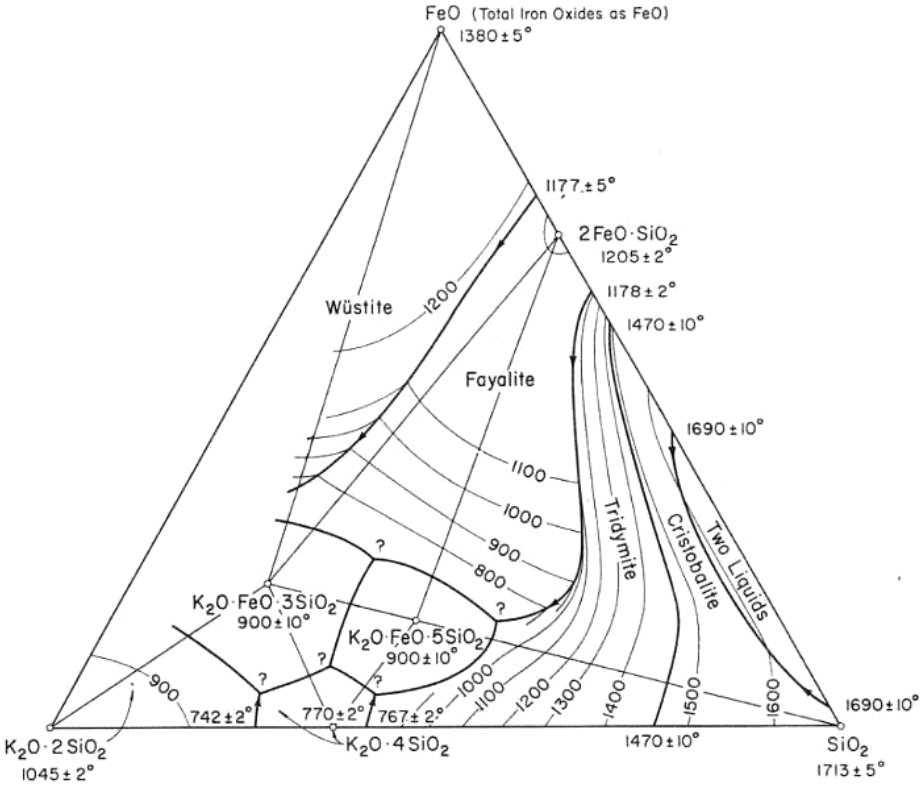

Fig. 2-27: System $K_2O{\cdot}SiO_2$-SiO_2-FeO. Picture taken from [70].

One chance to “neutralise” the impact of potassium might be the element Al. Slight amounts in the range of 10% are enough to create potassium aluminates and potassium silica aluminates (see Fig. 2-28).

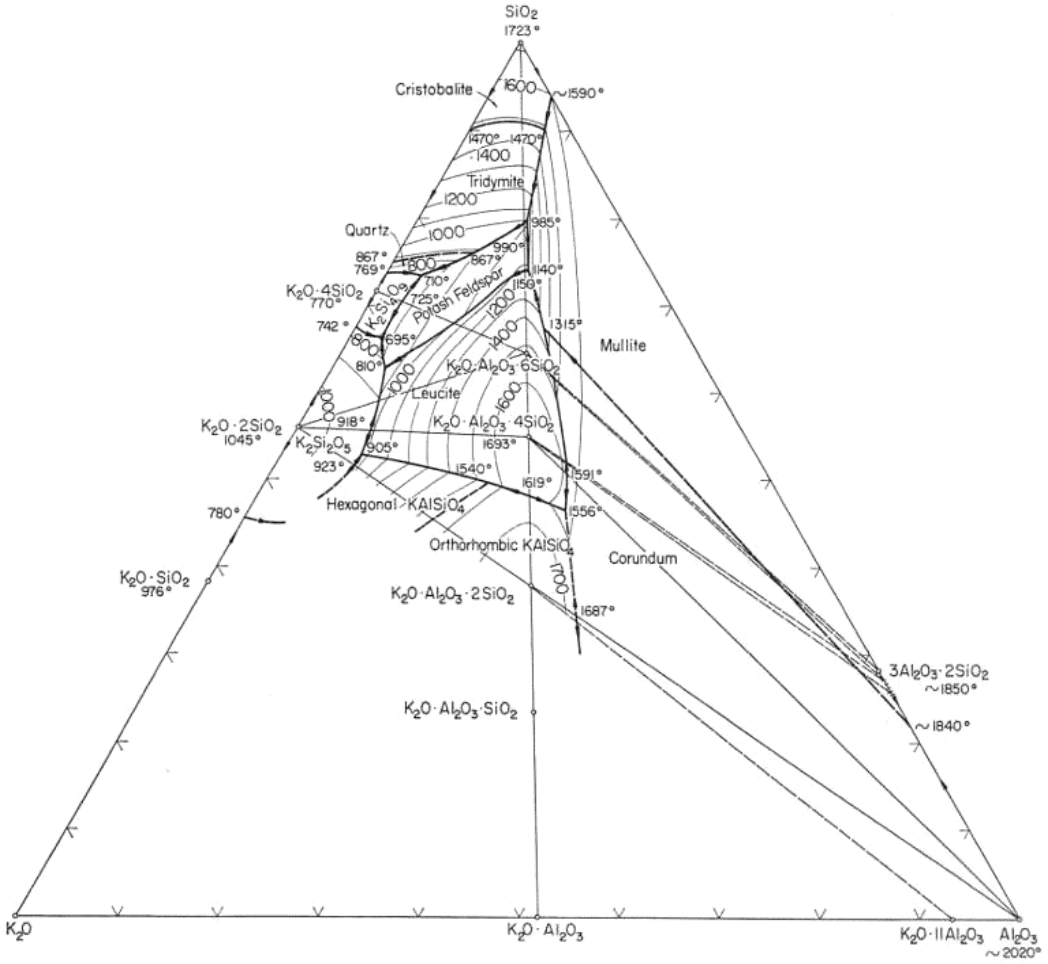

Fig. 2-28: System K_2O-SiO_2-Al_2O_3. Picture taken from [70].

In the end, interactions between the specific impurities expected in the CL process are very hard to foresee because their mass fraction and distribution is unknown today. However, thermodynamic modelling as done by MUHAMMADIEH [88] might be a good tool to control the CL process in a more sophisticated way.

Chlorides might be problematic as well. SUN ET AL. [120] pointed out that the expected operating temperature of the calciner in the CL process (>850°C) exceeds the melting points of $MgCl_2$ (714°C), $CaCl_2$ (675°C) and NaCl (800°C). This causing pore-mouth blockage and a possible decrease in the CO_2 capture ability during the calcination/carbonation cycles. However, $MgCl_2$ might decompose at higher temperatures.

2.3.4 Impact of the Atmosphere on Melting Points

Reducing atmospheres cause the creation of additional substances. One classical example for this effect is gypsum; $CaSO_4$ can be reduced to $CaSO_3$ and CaS. By this, a simple one-component system splits into a complex ternary.

SCHREINER ET AL. [109], for example demonstrated that ashes received from burning different biomasses showed a melting point between 650 and 1250°C under oxidising conditions, while the same ashes melted between 680 and 770°C under a reducing atmosphere. The gap between the melting point of a high temperature melting ash under reducing and oxidising conditions was more than 450°C. Consequently, special attention should be given to the design of the CL calciner.

2.4 Thermodynamics of the $CaCO_3$ Decomposition

The according equilibrium concentrations of CaO, $CaCO_3$ and CO_2 are temperature dependent and can be described according to the law of mass action and the reaction isobar according to VAN'T HOFF. The law of mass action can be written as

$$K_a = \frac{a_{CaO} \cdot a_{CO_2}}{a_{CaCO_3}}. \qquad 2\text{-}12$$

Chemical activities can be calculated employing the equation

$$a_i = f_i \cdot \frac{c_i}{c_i^{\Theta}}. \qquad 2\text{-}13$$

The activity is defined as the product of the activity constant f and the quotient of the concentration and the standard concentration. The activity constant describes non-linear interaction of the molecules in a mixture of substances. Upon close inspection, this coefficient depends on concentration, temperature and pressure but might be set constant for this derivation.

The division of the concentration by the standard concentration is needed to receive a dimensionless activity, e.g. if gases are involved in a chemical reaction the term for the mass action law is not a partial pressure like 0.1 bar but $\frac{0.1bar}{1bar} = 0.1$. Also, it should be noted that the activity of pure substances is set to one by definition.

The VAN'T HOFF equation is given by

$$\frac{d\ln K_a}{dT} = \frac{\Delta_R H}{RT^2}. \qquad 2\text{-}14$$

Before integrating eq. 2-14, one has to keep in mind that the reaction enthalpy is temperature-dependent. This dependency can be described as

$$\Delta_R H(T) = \Delta_R H^{\Theta} + \int_{T^{\Theta}}^{T} \Delta_R c_p dT. \qquad 2\text{-}15$$

The temperature dependency of the heat capacity can be approximated by

$$c_{p,i}(T) = a_i + b_i T + \frac{c_i}{T^2}. \qquad 2\text{-}16$$

a_i, b_i and c_i are substance specific parameter.

The overall difference in the heat capacities between products and educts can be described as differences in the coefficients a, b and c; eq. 2-16 can be written as

$$\Delta_R c_p(T) = \Delta a + \Delta b T + \frac{\Delta c}{T^2}. \qquad 2\text{-}17$$

Putting eq. 2-17 into eq. 2-15 delivers after integration

$$\Delta_R H(T) = \Delta_R H^{\Theta} + \Delta a(T - T^{\Theta}) + \frac{\Delta b}{2}(T^2 - T^{\Theta^2}) + \Delta c\left(\frac{1}{T^{\Theta}} - \frac{1}{T}\right). \qquad 2\text{-}18$$

All terms referred to the standard temperature can be put in one term

$$I^{\Theta} = \Delta_R H^{\Theta} - \Delta a \cdot T^{\Theta} - \frac{\Delta b}{2} \cdot T^{\Theta^2} + \Delta c \cdot \frac{1}{T^{\Theta}}. \qquad 2\text{-}19$$

Combining eq. 2-14, 2-18 and 2-19 leads to

$$\frac{d\ln K_a}{dT} = \frac{I^{\Theta} + \left(\Delta a \cdot T + \frac{\Delta b}{2} \cdot T^2 - \Delta c \frac{1}{T}\right)}{RT^2} = \frac{I^{\Theta}}{RT^2} + \frac{1}{R}\left(\frac{\Delta a}{T} + \frac{\Delta b}{2} - \Delta c \frac{1}{T^3}\right). \qquad 2\text{-}20$$

After integration we can find

$$\int_{K_a^{\Theta}}^{K_a} d\ln K_a = \int_{T^{\Theta}}^{T} \frac{1}{R}\left(\frac{I^{\Theta}}{T^2} + \frac{\Delta a}{T} + \frac{\Delta b}{2} - \Delta c \frac{1}{T^3}\right) dT$$

$$\ln\left(\frac{K_a}{K_a^{\Theta}}\right) = \frac{1}{R}\left[I^{\Theta}\left(\frac{1}{T^{\Theta}} - \frac{1}{T}\right) + \Delta a \ln\left(\frac{T}{T^{\Theta}}\right) + \frac{\Delta b}{2}(T - T^{\Theta}) + \frac{\Delta c}{2}\left(\frac{1}{T^2} - \frac{1}{T^{\Theta^2}}\right)\right]. \qquad 2\text{-}21$$

With the found temperature dependent expression for the equilibrium constant K_a the partial pressure of CO_2 above $CaCO_3$ can be described by

$$c_{CO_2} = \frac{a_{CaCO_3} K_a}{f_{CO_2} a_{CaO}} c_{CO_2}^{\Theta}. \qquad 2\text{-}22$$

Following, the equilibrium curve of the decomposition of limestone is shown with thermodynamic data taken from the second chapter of PERRY'S Handbook of Chemical Engineering [95] (see Table 2-7).

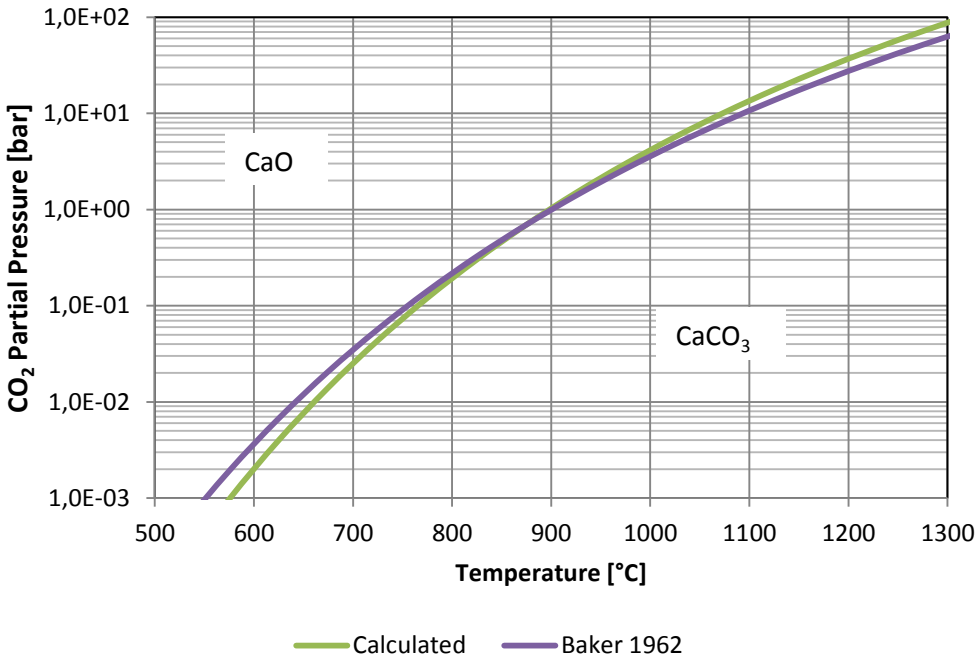

Fig. 2-29: CO_2 partial pressure over a pure solid of $CaCO_3$. For the calculation of the green curve eq. 2-21 and 2-22, the data provided in Table 2-7 and a value for $\ln K_a^{\Theta}$ of -54,70 were used. The violet line was calculated from the equations given by BAKER [19]: $\lg c_{CO_2} = 7.079 - \frac{38000}{4.574 \cdot T}$. BAKER's equation was derived from pressure measurements performed at temperatures above 897°C.

Two points of the equilibrium curve are very important: CO_2 partial pressure at 650°C, because this is the operating temperature of the carbonator and 900°C, because this is the temperature of complete dissociation of $CaCO_3$ at atmospheric pressure.

Table 2-7: Thermodynamic data for the calculation of the equilibrium partial pressure of CO2 over CaCO3 in dependency of the temperature. Values taken from [95].

	a	b	c	c_p^{Θ}	$\Delta_B H^{\Theta}$
CO_2	43.31426	0.011478	-818950	37.51	-394
CaO	41.89000	0.020275	-452412	42.84	-636
$CaCO_3$	82.43952	0.049807	-1288536	82.77	-1213
Δ	2.76474	-0.018055	17175	-2.42	183

According to the strict thermodynamic calculation, the CO_2 equilibrium partial pressure at 650°C is 0.75%. In contrast, BAKER's equation delivers 1.20%.

Examining eq. 2-22 a little bit further, some interesting facts can be revealed: First, impurities in the limestone can alter the activity of the $CaCO_3$ and CaO differently. In case that the interaction between the contaminations and the carbonate is stronger than those with the oxide the calcination temperature is increased while the CO_2 pressure at 650°C would be decreased. Second, the interactions of the impurities are stronger with the oxide than with the carbonate. This would lower the calcination temperature und increase the CO_2 equilibrium partial pressure at 650°C. In order to maintain the same capture efficiency in the carbonator, the temperature would have to be decreased.

The third possible case that could change the expected equilibrium CO_2 partial pressure is the presence of gases that interact with CO_2 and therefore lower the fugacity of the CO_2.

The following table gives fictive examples of the above mentioned cases.

Table 2-8: Fictive examples of the impact of impurities on the activities of CaCO3, CaO and CO2 and the resulting effects for the CO2 partial pressure at different temperatures.

Case	Base	I	II	III
a_{CaCO_3}	1	0.5	1	1
a_{CaO}	1	1	0.5	1
f_{CO_2}	1	1	1	0.5
	c_{CO_2} in shares of 1 bar			
625°C	0.4%	0.2%	0.8%	0.8%
650°C	0.8%	0.4%	1.5%	1.5%
680°C	1.6%	0.8%	3.1%	3.1%
855°C	0.50	0.25	0.99	0.99
900°C	1.02	0.51	2.03	2.03
947°C	2.02	1.01	4.04	4.04

The mentioned effects are important in several ways: First, while focusing on improved sorbents that may have been produced by the introduction of dopants it is not possible to compare these sorbents always using the same TGA test conditions. For example, it is speculated that sodium decreases the decomposition temperature of limestone. At the same time, it is known to cause coalescence. These two effects would require process and test conditions with a lower calcination and a lower re-carbonation temperature and accordingly, adapted residential times under calcination and re-carbonation conditions. Using a too high temperature might cause the destruction of the beneficial sorbent properties.

Second, if oxyfuel calcination is used, impurities will be introduced into the system via the fuel. Depending on the nature of the contaminants, this might cause a shift of operating conditions to, most likely, lower temperatures.
Third, depending on the oxygen excess during the oxyfuel calcination the calciner atmosphere might vary a lot, leading to, most likely, lower required calcination temperatures.

2.5 Kinetics of the $CaCO_3$ Decomposition

The reaction kinetic of the decomposition of $CaCO_3$ changes with the particle size. The calcination of limestone powder is controlled by the chemical reaction while heat transfer processes are rate determining when coarser particles are calcined ([60]).
Describing the kinetics and the elementary mechanism of $CaCO_3$, decomposition is a very difficult manner due to the fact that basic assumptions that are required to apply kinetic models like an ARRHENIUS plot are not given. Such models were developed for homogenous reactions in which the concentration and the distribution of reactants and products are homogenous. By this, it is assumed that the chemical potential for all reactants and reaction products is the same.
It is obvious, that these assumptions are not applicable for the decomposition of crystalline solids; the reaction occurs at a reaction front while the reactants are ahead of the front and the product are behind. Due to this configuration, an equal distribution of the substances involved is not possible.
Another hardly describable uncertainty is given by the kind, amount and distribution of impurities. MURTHY ET AL. [90] observed that small amounts of impurities enhance the decomposition of $CaCO_3$.
As well, processes at the reaction front are various. “Concurrent and/or consecutive processes taking place in the reaction zone (possibly with the participation of crystal imperfections) will involve more than one type of energy barrier and cause the numbers and the natures of these transition-states to change considerably during the course of reaction” ([49]).
Recent reviews reveal that there are still huge question marks all over the place in terms of solid state decomposition ([47], [48]).
For example, reported activation energies and pre-exponential factors for the decomposition of $CaCO_3$ vary between 23.9 and 956 kcal/mol and 10^2 and 10^{69} s^{-1} respectively ([17]).
An often quoted equation ([17]) believed to describe the calcination process in a good manner, is given below.

$$\frac{dx_k}{dt} = 3(1-x_k)^{\frac{2}{3}} k_0 \exp\left(-\frac{E_A}{RT}\right)\frac{M_{CaCO_3}}{\rho_{CaCO_3} r_{Particle}}. \qquad 2\text{-}23$$

x_k is the conversion ratio of limestone, t the time and k_0 the pre-exponential factor. This expression is known as shrinking core model.

However, work done by L'VOV ET AL. [76] gives at least a proposal for a decomposition mechanism at the reaction front that seems to be in good line with macroscopic observations: $CaCO_3$ sublimates into the gas phase before it decomposes into CaO and CO_2. Gaseous CaO condenses immediately on every surface while CO_2 is withdrawn. By this mechanism, one would expect that the CaO resulting of the decomposition of $CaCO_3$ is extremely porous and fine-grained. Thus, the high resulting surface area should collapse on heating due to the high specific surface energy.

The work of BORGWARDT ET AL. seems to confirm this mechanism. They decomposed $CaCO_3$ and $Ca(OH)_2$ under extremely mild conditions and found that nascent CaO has an initial specific surface area of 104 m²/g ([25]) while $Ca(OH)_2$ decomposed under a constant flow of N_2 at 370°C had a specific surface area of 128 m²/g ([24]). The high specific surface area of 128 m²/s collapsed within 15 seconds to 77 m²/g.

Fig. 2-30 reveals the coalescence curves of CaO prepared by the thermal decomposition of $Ca(OH)_2$ at different temperatures investigated by BORGWARDT ET AL. [24].

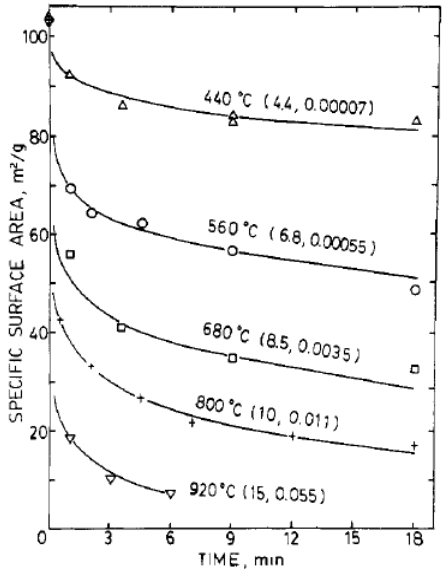

Fig. 2-30: Coalescence curves of CaO prepared by the thermal decomposition of $Ca(OH)_2$ at different temperatures. Figure taken from [24].

L'VOV ET AL. [76], as many others, reported kinetic data for his investigations. Unfortunately, these data are only of very limited practical use and will not be discussed further.

Nevertheless, approaches that are more empirical are described in literature, basically assuming heat transport to be the limiting factor.

WUHRER ET AL. [135] investigated the decomposition of limestones with different geometries: Plate, cylinder, cube and sphere. For each geometry, he derived a mathematical expression, for which he reported good accordance with measurements he performed. In case of a spherical geometry the expression is

$$t_{Full\ decomposition}^{CaCO_3} = \frac{\rho_{CaCO_3}\,\Delta_R H_{900°C}^{CaCO_3}\,r_{Particle}^{\,2}}{6\,\lambda_{CaO}\,(T_{Surface}^{Particle} - T_{Decomposition}^{CaCO_3})}. \qquad 2\text{-}24$$

ρ_{CaCO_3} is the density of the limestone, $\Delta_R H_{900°C}^{CaCO_3}$ the reaction enthalpy for the decomposition of $CaCO_3$, $r_{Particle}$ the radius of the particle, λ_{CaO} the heat conductivity of CaO and $T_{Surface}^{Particle}$ and $T_{Decomposition}^{CaCO_3}$ are the temperature of the surface of the particle and the decomposition respectively.

His research objections were put on limestones with a diameter between 20 and 400 mm. In this grain size, the rate of calcination is determined by the heat flow through the freshly created CaO layer. As Fig. 2-31 illustrates, this might not the case anymore for very small grains. In this case, it is more likely that the heat flow from the surrounding to the particles or the chemical reaction is the rate determining step[6]. However, if the surface temperature of a 700 µm particle is only 1°C above its decomposition temperature, full calcination will be achieved within 100 seconds. Note that the particle decomposition temperature is given by the local CO_2 partial pressure and not by the average concentration in the surrounding atmosphere. Accordingly, if the CO_2 transport from the inner site of the particle to the outside is slower than the decomposition of $CaCO_3$, the internal CO_2 partial pressure equals the overall outer pressure.

[6] Even if the rate of the decomposition of $CaCO_3$ at the reaction front would be rate determining, the consequence, in the end, would be a higher temperature on the CaO surface. This would lead to an accelerated decomposition at the reaction front due to a higher heat flow.

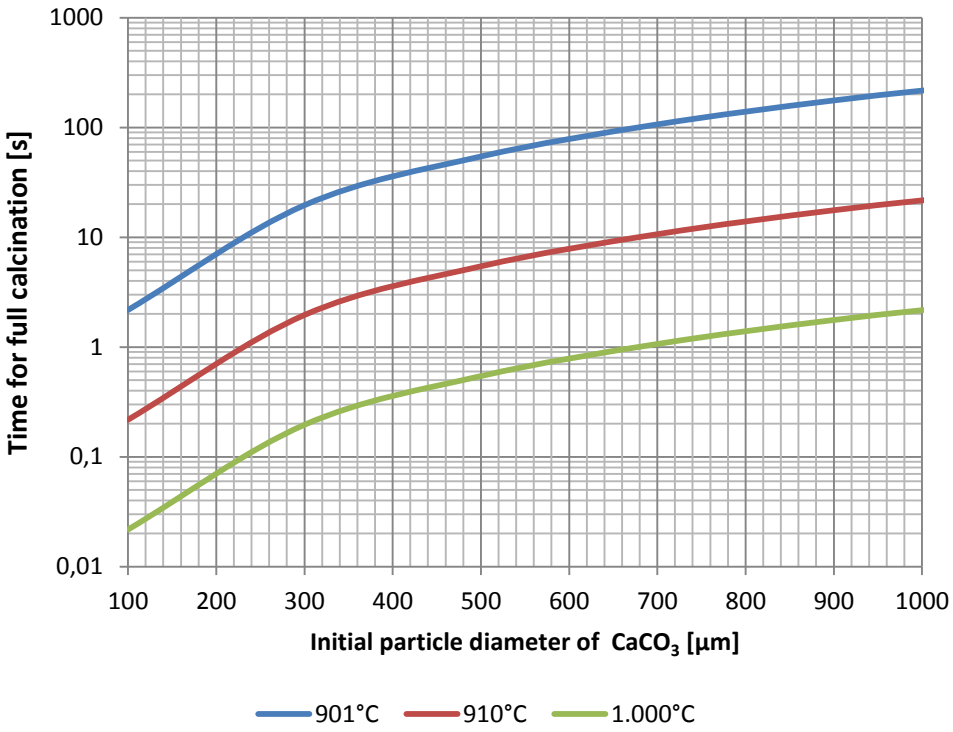

Fig. 2-31: Time of full calcination of $CaCO_3$ particles with a given diameter using eq. 2-24. The temperatures display the surface temperature on the particles. Used values for the creation of the diagram: $\rho_{CaCO_3} = 2600\,kg/m^3$, $\Delta_R H_{900°C}^{CaCO_3} = 1659\,kJ/kg$, $\lambda_{CaO} = 0.83\,J/(m\,K\,s)$, $T_{Decomposition}^{CaCO_3} = 900°C$.

It can be summarised that $CaCO_3$ will act as a perfect heat sink and so the required calcination time might only be a matter of an efficient heat transport in the calciner.

2.6 Kinetics of the Re-carbonation

Today, re-carbonation of CaO is widely used for the production of PCC and the hardening of lime-based mortar. Additionally, special production processes use a re-carbonation process ([9]).

However, most of these applications are liquid or pseudo-liquid processes at low temperatures in which, basically, $Ca(OH)_2$ is carbonated.

Before the CL process gathered a global interest in the scientific community, high temperature carbonation of CaO had neither a practical application nor an increased scientific awareness. Accordingly, dedicated work started only a few years ago in 2004 ([11], [68]). ALVAREZ ET AL. [11] focused on phenomena that reduce the overall CO_2 capture ability (sintering); kinetic effects were only secondary. Nevertheless, he created a link between product layer thickness, time and CaO conversion (see Fig. 2-32).

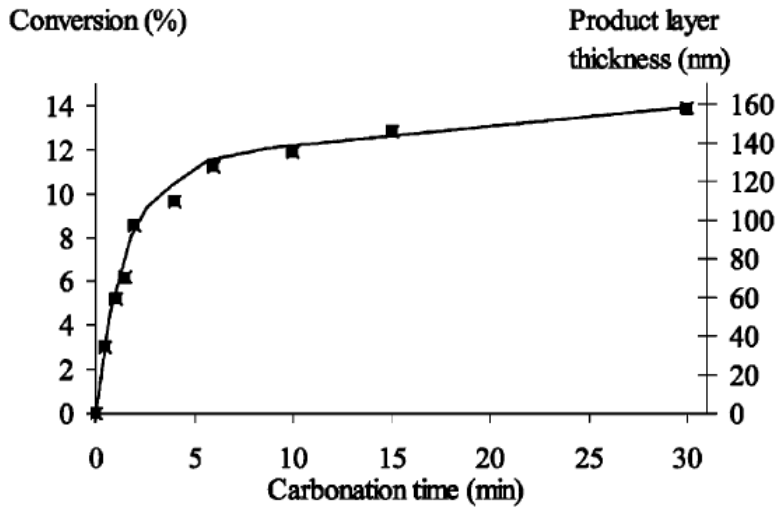

Fig. 2-32: CaO conversion and product layer thickness of $CaCO_3$ versus time on a CaO particle after 30 sucessive cylces of calcinatinon and re-carbonation. Picture taken from [11].

It is intersting to note that the re-carbonation reaction at 650°C is very fast unless the procuct layer thickness is not exeeding 100 nm. Afterwards, the rate is dramatically decreased while it seems to stabilise if the product layer thickness reaches about 140 nm. Pore closure by $CaCO_3$ and therefore a rapid loss of accessible surface area through which diffusion of CO_2 might take place, were discussed to be responsible for the shape of this graph. Further details of the work of ALVAREZ ET AL. [11] will be discussed in section 2.9.

LEE ET AL. [68] reported an empirical formula with that he was able to predict the extend of carbonation of CaO.

Reaction Mechnisms

BERUTO ET AL. [21] reported that the chemisorption of CO_2 on CaO takes place via the formation of carbonate ions at the locations of O^{2-} surface ions. Chemisorption enthalpies and entropies of -199 kJ/mol and 153 J/(mol K) were calculated corresponding to a higher enthalpy than for the re-carbonation of CaO of -178.4 kJ/mol ([58]). The suprising fact about this observation is that CaO seems to be able to minimise its specific surface energy by the adsorption of CO_2. It might be speculated that this difference of energy could be a reason for an equal distribution of carbonate ions across the CaO surface and this explaining the higher ion mobility and increased sintering of CaO in the precense of CO_2 which will be discussed in chapter 2.8.

SYMONDS ET AL. [122] investigated the effect of water vapour during the re-carbonation step. He figured out that the addition of steam contributes a lot to the extend as well as the rate of re-carbonation, if rather low temperatures are used (see Fig. 2-33).

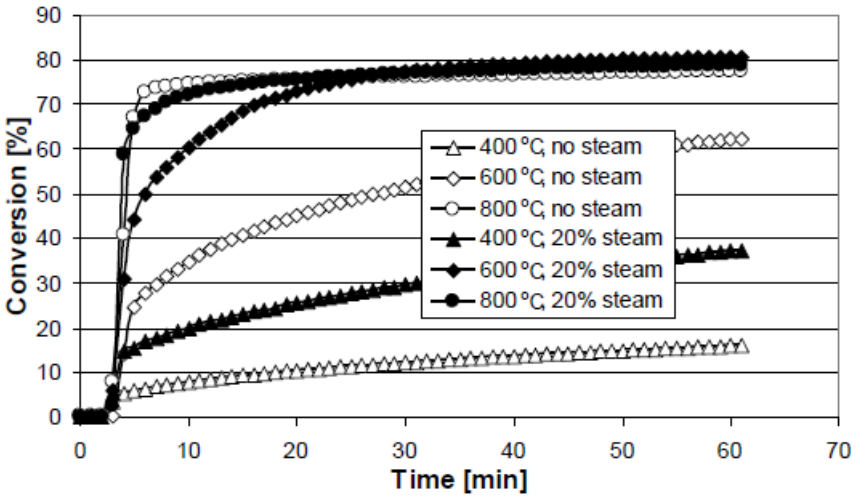

Fig. 2-33: CaO conversion over time at differnt partial pressures of watervapour and different temperatures. Addition of steam causes significant improvements at low temperatures. Figure taken from [122].

This effect might be explained by the binary phase diagram of $Ca(OH)_2$ and $CaCO_3$ (see Fig. 2-34): The melting temperature of $CaCO_3$ is ~1000°C while the TAMMANN temperature (temperature of significant improved ion mobility) is 533°C ([33]). During re-carbonation at temperatures above 650°C, ion mobility and therefore ductility and the diffusion coefficient of $CaCO_3$ are increased significantly, resulting in a very fast and maximal CaO conversion. Slight amounts of $Ca(OH)_2$ in $CaCO_3$ cause the occurrence of a liquid phase at rather low temperatures. This effect indicates that the ion mobility might be increased significantly if water vapour is present and the temperature of the hypothetical[7] mixture between $CaCO_3$ and $Ca(OH)_2$ is below ~680°C (occurrence of a liquid phase in the mixture).

[7] A mixture of $Ca(OH)_2$ and $CaCO_3$ cannot be observed under ambivalent pressure and temperatures above 470°C (stability of $Ca(OH)_2$). However, the law of chemical equilibrium determines the occurrence of $Ca(OH)_2$ at increased temperatures as long as CaO and H_2O are present.

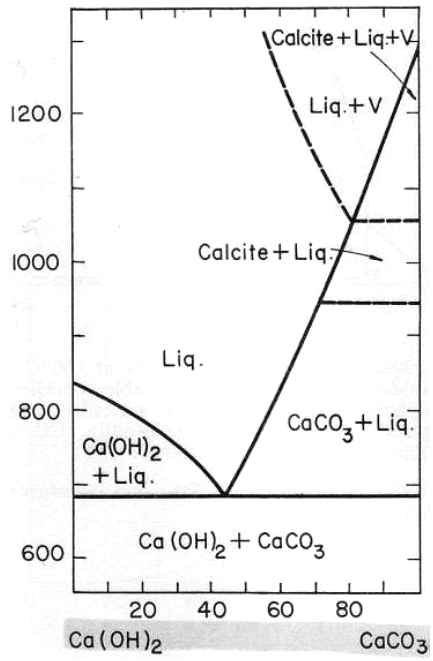

Fig. 2-34: Binary diagram of $Ca(OH)_2$ and $CaCO_3$ at 1000 bar. Figure taken from [70].

In addition to TGA investigations, SYMONDS ET AL. [123] also conducted circulating fluidised bed experiments in which he was able to show that the addition of water vapour has the same efficiency than shown before in his TGA experiments. He reported that the CaO conversion increased from 16.7% to 37.4%.

2.7 Calcination

Calcination of limestone is a large scale industrial process that results, only in Germany, in the annual production of 7 million tons of CaO ([27]). The major customer of these products is the steel industry.

The quality of lime is usually categorised in three classes: soft-, middle- and hard-burned lime. This classification is based on the t_{60} time[8]. Even though the t_{60} has some uncertainties and approaches are on-going to implement more accurate methods ([57]), it is the standard test in the lime industry and it is possible to give indications for the physical properties of the quick lime (see Table 2-9).

[8] The t_{60} test determines the time it takes to reach 60°C in a stirred DEWARD vessel if 150 g of quicklime are added to 600 g of de-ionised water with a temperature of 20°C. This method is standardised in DIN EN 459-2.

Table 2-9: Comparison between quick lime reactivity expressed as t60 and physical parameters. Table according to [107].

Burning degree	Soft	Middle	Hard
t_{60} [min.]	<2	2-6	>6
Particle density [g/cm³]	1.5-1.8	1.8-2.2	>2.2
Porosity [%]	46-55	34-46	<34
S_{BET} [m²/g]	>1.0	0.3-1.0	<0.3
Reactivity			
Wet slaking curve- R-value [°C/min]	>20	2-20	<2
Coarse grain titration 5-min value [ml 4 n HCl]	>350	150-350	<150

The decomposition of $CaCO_3$ to CaO and CO_2 can be described through five elementary steps ([1]): 1. Heat transfer from the gas phase to the $CaCO_3$ particle. 2. Heat conduction through a layer of CaO to the reaction zone. 3. Decomposition of $CaCO_3$ and therefore heat consumption, nucleation, growth and recrystallization of CaO. 4. Diffusion of the produced CO_2 through the layer of CaO to the surface of the particle. 5. Mass transfer from the particle surface into the surrounding. Depending on the raw material (chemistry, crystal size and crystal arrangement) and the calcination conditions, a wide variety of CaO textures can be formed. One extreme example is shown in Fig. 2-35: Calcspar is a macrocrystalline, dense form of $CaCO_3$. This kind of stone is normally very hard, except if share forces along the (1,0,1) plane of an elementary crystal are applied (good fissility), but is nearly destructed completely upon heating, disregarding the heating rate. As discussed in pragraph 2.2.1, the thermal expansion of calcite is anisotrope; the crystal expands in the *c* - while it contracts in the *a* -direction. This effect causes high tension forces on heating if the elementary crystals are packed very dense, are big and arranged randomly. On heating, these tensions will relax by the formation of cracks. In case that no calcination is done, the resulting material has lost some of its mechanical strength, but the $CaCO_3$ crystals are still able to interlog. On further temperature increase calcination takes places causing the shift of the crystal system to CaO that is not able to interlog anymore. This material has lost its mechanical strength completely.

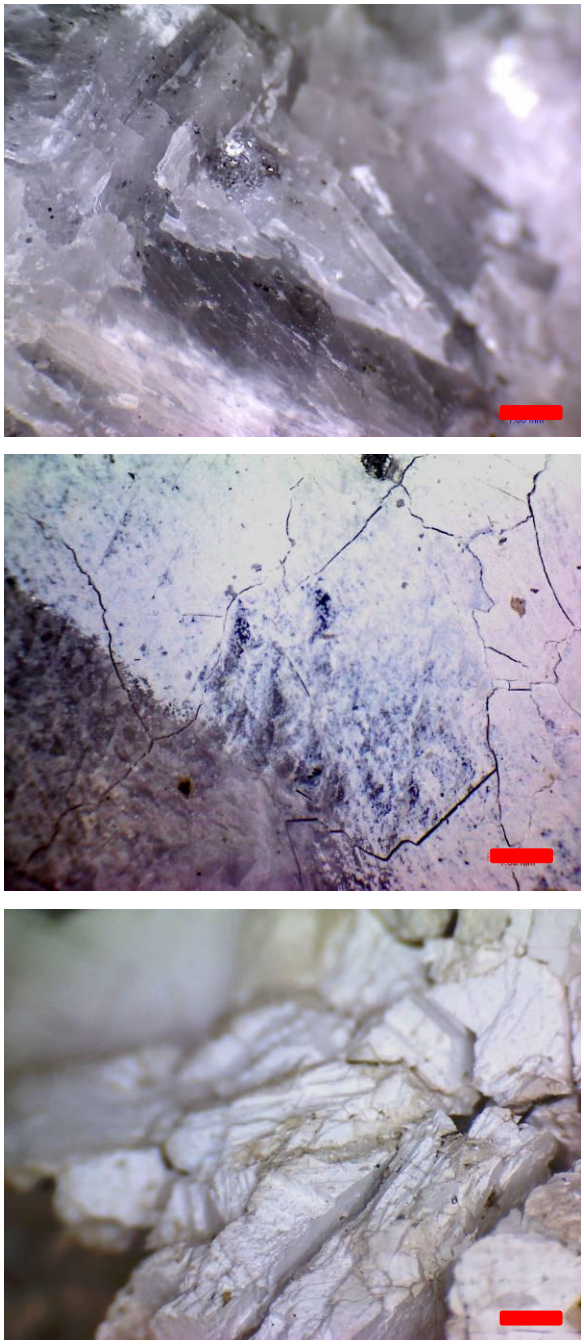

Fig. 2-35: Series of pictures of the same calcspar like substance with a constant magnifigation. The imprinted red bar refferes to a length of 1 mm. Top: Original Stone wih macroscopic cracks along the calcite crystal plane (1,0,1). It can be seen that the orientation of these elementary crystals is orthogonal. The displayed rock has a high mechanical strength; destruction between two hands is not possible. Middle: Macroscopic cracks on a stone that was heated within an hour to 800°C, maintained at this temperature for 10 minutes and withdrawn from the kiln after 10 further minutes (temperature at the time of removal ~750°C). Surface calcination can be noticed in the upper right region. This sample had lost most of its mechanical strength and could be destroyed by hand. Bottom: Gaps and cracks in the full calcined sample. At this test, the sample was heated from 20°C to 870°C during 5 hours, maintained their till full calcination and following slowly cooled. The sample had lost its entire mechanical strength and crumbled into peaces, probably of the sice of the original $CaCO_3$ crystals, if the slightes mechenical stress was applied.

Another example of the huge variety of limestones is the sensitivity towards the burning conditions, namely, the calcination temperature (see Fig. 2-36).

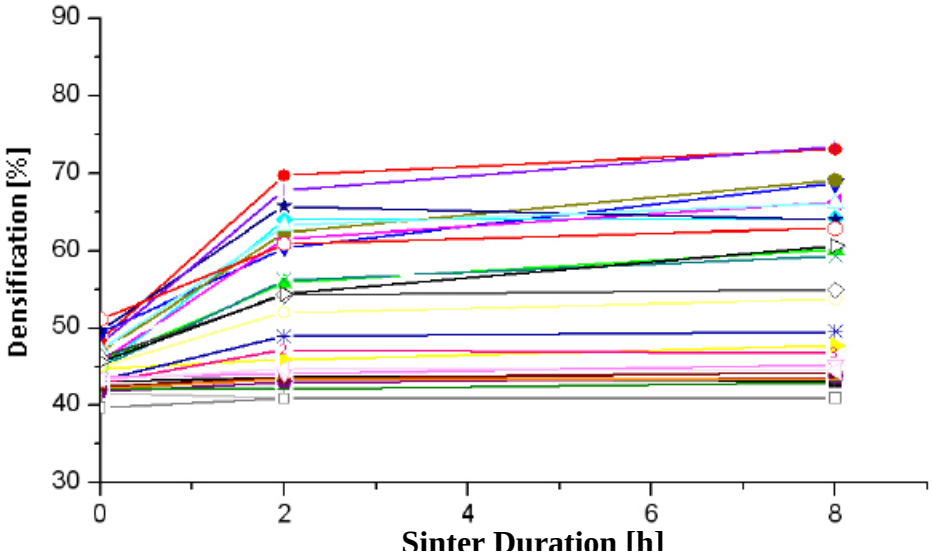

Fig. 2-36: Sensitivity of differen limestones towards densification at 1100°C. Figure taken from [58].

Some limestones respond very quickly to increased calcination temperatures by a significant shift in the t_{60} value (or densification) while others show nearly no reaction at all. The reasons for this behaviour could not be revealed so far but it is most likely that a special composition of impurities, that are equally distributed in the stone, benefit the sensitivity towards sintering. The issue of sintering will be discussed in more detail in the next paragraph.

During the formation of the CaO crystal FRENKEL (cation not at the right place) and SCHOTTKY (cation and anion missing within the crystal system) defects are the most likely defect structures that occur ([58]).

2.8 Sintering

The driving forces for sintering processes are the minimisation of the boundary layer energy and the minimisation of the specific surface energy. The specific surface energy is equivalent to not saturated bonds on the surface and therefore equal to the reactivity of the surface area ([58]). According to HOGEWONING ET AL. [58], sintering is preferably explained on the two-particle model (see Fig. 2-37).

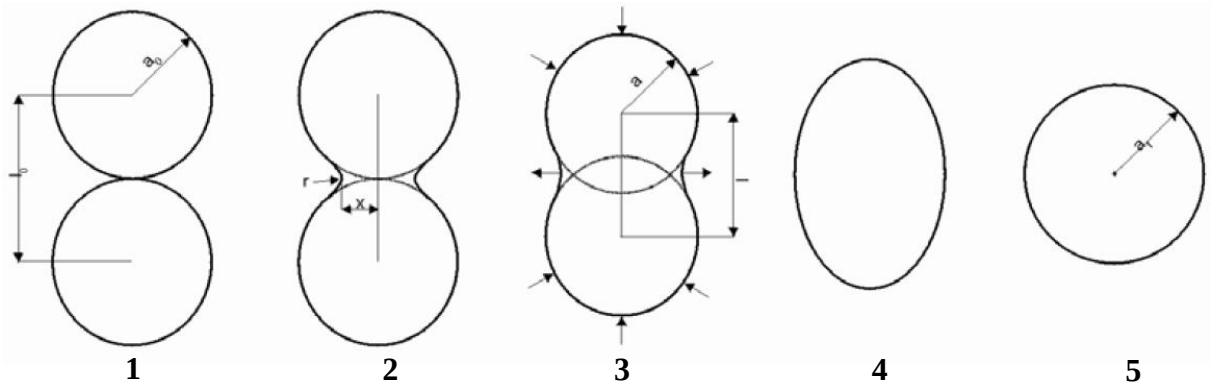

Fig. 2-37: Sinter stages of two particles. (1) Starting point with two separate grains. (2) Creation of a neck at the contact interface of the grains. (3) Shrinkage, i.e. the two centers of the grains approach to each other. (4) Late stage of sintering. (5) Equilibrium shape. Picture taken from [58].

The starting point are two spheres with the radius a_0 that are in contact with each other. Due to the minimisation of the specific surface energy given by the overall surface, the equilibrium shape of both grains would be a sphere with the radius

$$a_f = a_0 \sqrt[3]{2} \,. (5) \qquad 2\text{-}25$$

This equilibrium is reached under sintering conditions via evaporation and condensation mechanisms as well as through diffusion. Evaporation and condensation transports material from convex to concave surfaces at the neck of the two grains. During this process, the distance between the centres of the grains remains constant. On the other hand, diffusion is caused by a gradient of vacancies. High concentrations of vacancies are preferably located at concave surfaces. This flux causes a reduction of the distance of the centres of the grains (shrinkage). The distribution of vacancies and vapour on a curved surface can be seen in Fig. 2-38.

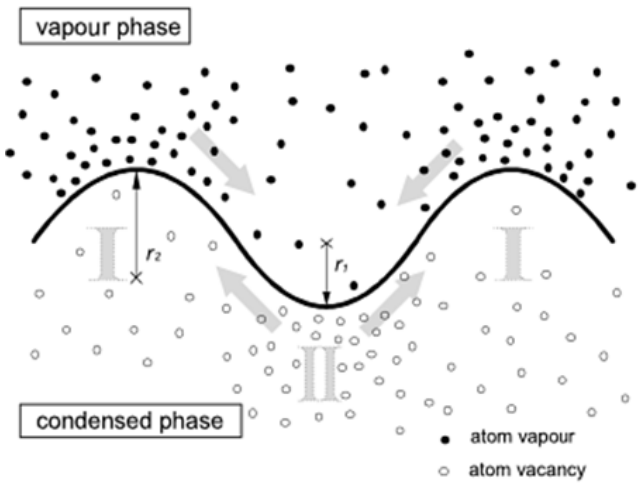

Fig. 2-38: Distribution of vapour (solid circles) and vacancies (empty circles). Figure taken from [61].

SUN ET AL. [119] figured out that lattice diffusion is the most common sintering mechanism in CaO while BORGWARDT ET AL. [24]supposed “that both grain boundary and surface diffusion mechanisms are operative” in the presence of H_2O and CO_2.

Impurities of the limestone can improve or constrain the sintering process. A slight iron content as well as sodium increases the ion mobility and therefore the tendency to sinter ([58]). Solid state reactions between silicon and calcium might also increase the sintering ([58]). But not only impurities benefit sintering, also very pure limestones tend to sinter very fast if the initial texture is beneficial. For example, Oolithes have a high sinter tendency ([58]).

Significant amounts of Mg prohibit the sintering in such a strong way that it is common sense that dolime follows other sintering patterns than lime ([58]) (see Fig. 2-39).

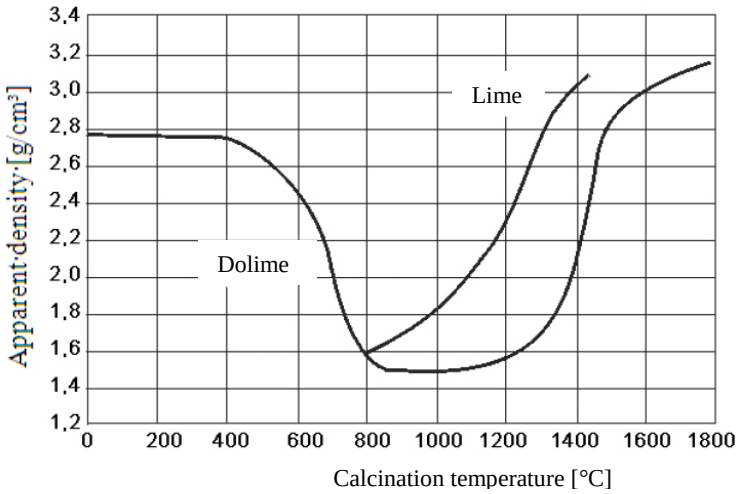

Fig. 2-39: Sintering expressed the change in the apparent density versus temperature. Figure according to [58].

In addition, the burning atmosphere has a strong impact on the sintering behaviour. SYMONDS ET AL. [122] mentioned the strength of different gases on sintering as $SO_2 > CO_2 > H_2O >$ Air $> N_2$. The sintering promoting effect of some gases is believed to occur due to dynamic absorption/desorption equilibria that improve the ion mobility and therefore the lattice diffusion ([58], [24]).

"Calculations by ANDERSON and MORGAN (1964) showed that a dynamic adsorption-desorption equilibrium with H_2O is possible in which short-lived surface hydroxyl groups may form. They propose that these groups accelerate the bonding of adjacent CaO lattices to eliminate surface and promote the mobility of O^{2-} along the surface" BORGWARDT ET AL. [24].

Besides chemical and process aspects, the impact of the geometry of the pores cannot be neglected. FIERRO ET AL. [44] investigated the effect of pore geometry on the sintering of Ca-

based sorbents. With his model he was able to predict the development of the specific surface area during and after calcination with an astonishing precision. The main conclusion of his work was that sorbents with cylindrical pores sinter to a greater extent than those with slit like pores.

HOGEWONING ET AL. [58] investigated 25 limestones to figure out which parameters are responsible for the sintering of CaO. She divided here samples into three groups based on its purity expressed as "Kalkstandard" (KS).

$$KS = \frac{C_{CaO}}{C_{CaO}^{Max}} \qquad 2\text{-}26$$

This concept was taken from cement producers. C_{CaO}^{Max} describes the amount of CaO that reacts with the impurities of the sample, namely Fe_2O, Al_2O_3 and SiO_2 to form cement phases. Its value can be calculated by

$$C_{CaO}^{Max} = 2.8\ C_{SiO_2} + 1.18\ C_{Al_2O_3} + 0.65\ C_{Fe_2O_3}. \qquad 2\text{-}27$$

Three groups were defined: Limestones with a high grade of impurities that do not tend to densify (KS < 10^3, C_{CaO} < 60%), limestones with medium impurities that show "normal" densification behaviour (10^3 < KS < 10^4, 60% < C_{CaO} < 99%) and high purity limestones that tend to very fast and intense densification (KS > 10^4, $C_{CaO} \geq 99\%$). This kind of classification shows, that cement phases are able to prohibit densification efficiently for temperatures up to 1300 °C. However, densification, even if the term sintering is used for it, should not be mismatched with the loss of specific surface area (coalescence). HOGEWONING ET AL. [58] reported that very impure samples showed signs of sintering (coarse grains and smooth surfaces), probably caused by the occurrence of local liquid phases, even though sintering was not conducted so far. In contrast, the high purity limestones showed no signs of sintering after the calcination at 1050°C; porous and fine grained solids were observed. However, if sintering was done at temperatures above 1100°C these samples tend to a high degree of densification.

Special elements should also be considered while talking of sintering and coalescence. For example, it is known that K, Na, Cl, F and P support the formation of low melting phases that cause a loss of surface area and in some cases densification. The impact of these elements might also be intensified if Si and Fe are present at notable amounts.

2.9 Loss of Specific Surface Area (Coalescence)

BORGWARDT ET AL. [24] showed that freshly produced CaO out of $CaCO_3$ and $Ca(OH)_2$ have specific surface areas of 104 and 76.7 m²/g, respectively. In case of vacuum calcination of $Ca(OH)_2$ or calcination under a pure atmosphere of nitrogen at 370°C specific surface areas of 128 m²/g can be reached. Subjection of such an oxide to 700°C caused a rapid decrease of the specific surface area to 77 m²/g within 15 seconds. BORGWARDT ET AL. [24] described the further decline of the specific surface according to

$$\left(\frac{S_0 - S}{S_0}\right)^{\gamma} = K \cdot t\,. \qquad 2\text{-}28$$

S_0 and S are the surface areas at the beginning and at the sintering time t respectively. γ is a mechanism-dependent parameter that was determined to 2.7. K is a sintering constant that increases exponentially with temperature. A γ value of 2.7 is believed to correspond to a lattice diffusion sintering mechanism. Unfortunately, this easy approach is only able to describe the initial sintering period up to 18 minutes satisfactory because the according function *S(t)* has a limit value of $-\infty$ for $t \to \infty$. However, a good accordance between measurement and model was achieved for this short period. Furthermore, it was shown that the γ value that is somehow linked with the ion mobility, increases exponentially with the temperature and linear with the partial pressure of H_2O and CO_2, while the water vapour contributed more to the observed loss in specific surface area. The first effect is in good accordance with temperature dependency of the diffusion coefficient as discussed in chapter 2.1.2.

Consequently, this finding indicates that it might be beneficial to inject steam into the calciner of the CL process, because the enhanced sintering by H_2O might be overcompensated (in a positive manner) by the exponential lower diffusity a temperature decrease in the calciner would cause.

SUN ET AL. [119] suggested that the loss in surface area due to sintering during successive calcination/carbonation cycles could be described as chemical reaction with an order of two.

$$\left(\frac{dS}{dt}\right)_{\mathrm{sin}\,tering} = k_S (S - S_a)^2 \qquad 2\text{-}29$$

S_a is the surface area after an infinite sintering time and k_S is the rate constant that depends on the partial pressure of CO_2 (p_{CO2}) in the sintering atmosphere and the temperature T.

$$k_S = 2.45 \cdot (1 + 10.3 \cdot p_{CO_2}^{0.67}) \cdot e^{-\frac{29}{T}} \qquad 2\text{-}30$$

Based on the equations 2-29 and 2-30, [119] performed modelling work regarding the CO_2 uptake after several calcinations/carbonation cycles. The results are shown in Fig. 2-40.

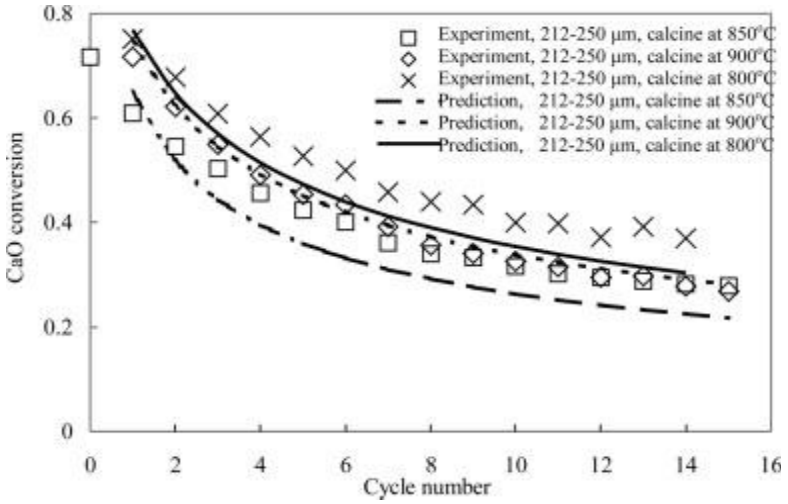

Fig. 2-40: Comparison of measured and predicted CO_2 uptake versus number of calcinations/ carbonation cycles [119]

However, only one limestone was investigated and a proof, that this approach could be used for other sorbents, was not published until 2011.

ALVAREZ ET AL. [11] investigated the textural evolution of a high purity limestone during 100 successive carbonation/calcination cycles in a fixed bed reactor which contained around 5 g of $CaCO_3$. The sample basket was moved automatically between a hot calcination zone at the bottom of the reactor (960°C) and a cooler carbonation zone at the top (650°C). The atmosphere was kept constant at 100% CO_2. Calcination and re-carbonation were carried out for 10 minutes and 5 to 30 minutes, respectively.

Probably the most important outcome of his investigations was that the drop in CO_2 capture ability during the cycling is not only an effect of a consequently decreasing surface area, but an effect of textural changes in a way that a lot of the particle porosity is blocked by a layer of $CaCO_3$ (pore-mouth closure) during the re-carbonation. Therefore, it becomes impossible for the CO_2 to reach the still active CaO sites in the particle. Fig. 2-41 illustrates that about 60% of the pore volume of a particle that had undergone 30 cycles were blocked if the CaO conversion reached a value of 14%.

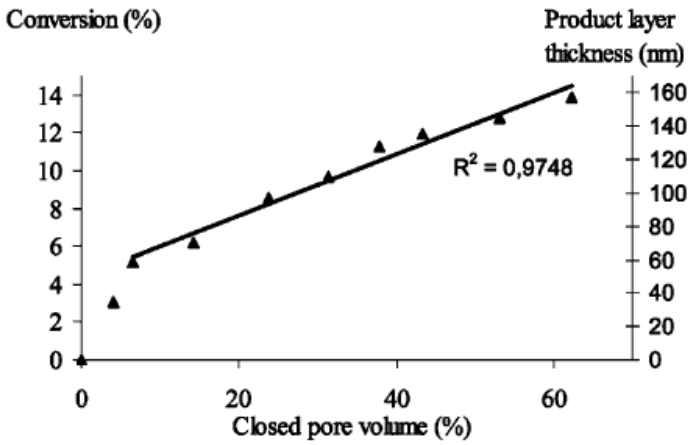

Fig. 2-41: CaO conversion and product layer thickness versus the closed pore volume of a sorbent that had undergone 30 cycles and a re-carbonation time of 30 minutes. Figure taken from [11].

Due to this observation, the positive effects of a thermal pre-treatment of a sorbent, as shown by MANOVIC ET AL. [80], becomes easier to understand: A thermal pre-treatment will allow the annealing of the CaO texture. By this, pore mouths become wider and are not able to close completely during the re-carbonation step anymore. Consequently, most of the surface is accessible during the re-carbonation step determining two effects: First, a high active surface area for the CO_2 uptake and, second, mildly "sintered" areas are going to be reactivated at each re-carbonation step.

According to the presented interpretation of "sintering", sintering is basically an effect of pore mouth blocking and slow annealing of CaO crystals in blocked regions of the particle.

Another important fact that should be kept in mind is the observation that the maximum size of the elementary grains in CaO is a function of temperature; higher temperatures allow bigger maximum grain sizes. Examples of this effect can be seen in Fig. 2-14 (lime) and 2-42 (copper). Copper and CaO show a similar sintering behaviour; the maximum densification degree is only a function of the temperature, while this maximum is reached exponentially with time.

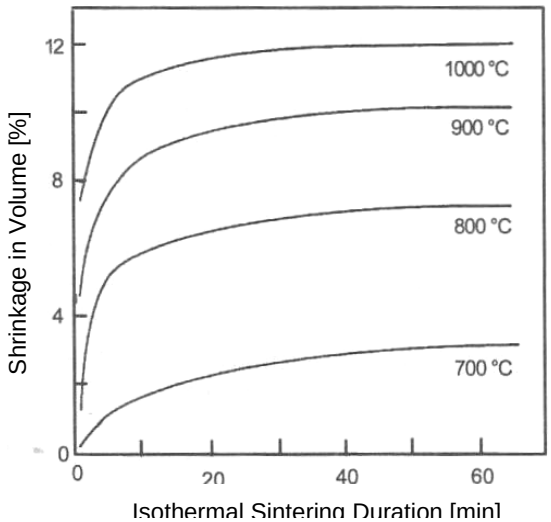

Fig. 2-42: Sintering of powder of Cu at different temperatures. Figure taken from [102].

The consequence for the CL process is that higher calcination temperature would require longer re-carbonation durations so that the annealed CaO surface is reactivated again. However, also in this case experiments should be carried out to determine the critical ratio between carbonation time and calcination temperature in which pore mouth blocking leads to a decrease in CO_2 capture ability.

LYSIKOV ET AL. [77] compared a Ca-based CO_2 sorbent that had undergone a large number of cycles with a refractory supported catalyst. This model assumes that unreacted CaO stays inside the sorbent particle after each cycle. These CaO grains are growing together due to sintering over the numbers of cycles to a bone like structure that supports the still active CaO. It is speculated that this kind of sintering mainly occurs during the carbonisation because of the low TAMMANN temperature of 533°C for $CaCO_3$. In the scope of the findings of ALVAREZ ET AL. [11], this may also be interpreted as closed pore volume due to a layer of $CaCO_3$.

Fig. 2-43 shows an interesting experiment that was performed by LYSIKOV ET AL. [77]; he subjected the very same sample to different re-carbonation durations for 80 subsequent cycles. After the 80th cycle he changed the duration of re-carbonation from 7.5 to 30 minutes and from 30 to 7.5 minutes for each experiment. He noticed a remarkable increase of the CaO conversion for the sorbent that was cycled with a carbonation duration of 7.5 minutes and a significant decrease for the one that was cycled with a carbonation duration of 30 minutes. Taking into account the findings of ALVAREZ ET AL. [11], this observation might be explained very well: Long re-carbonation durations determine a lot of pore mouth diameters with a diameter critical to blockage. Fast re-carbonation will be limited to the reaction of the porous CaO at the outside of the blocked pores. After this fast reaction, diffusion of CO_2 through the

product layer will become dominant. However, due to the high re-carbonation temperature of the experiment, this rate is still large enough to cause a significant better performance than the sample with the short duration of re-carbonation. On a shortening of this duration this product will respond with a lower CO_2 uptake because a lot of pores with a critical pore mouth diameter are present. Accordingly, the CaO conversion of this product will be beneath the product that had a shorter re-carbonation period from the beginning.

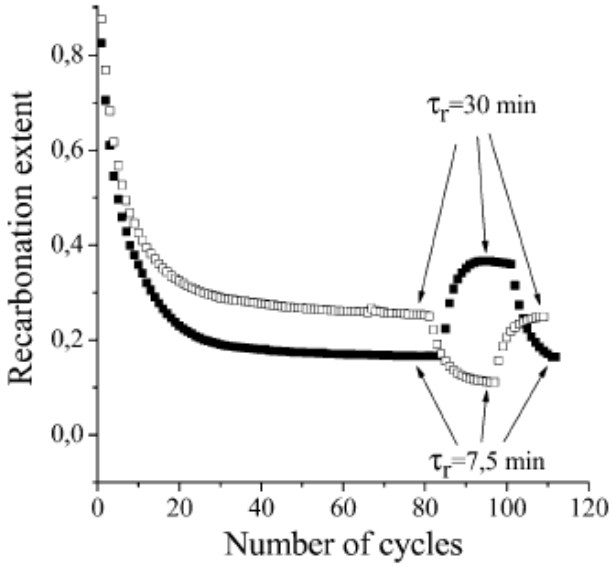

Fig. 2-43: Effect of the change of the re-carbonation time (τ_r) on the residual CaO conversion of the sample. Empty squares belong to a sequence of re-carbonation duration of 30, 7.5, 30 min. while black square have a sequence of 7.5, 30, 7.5 min. Both experiments were done isothermal (800 °C), while the partial pressure of CO_2 was changed between 0.33 atm (carbonation) and 0 (calcination). The calcination was performed under pure Ar. Figure taken from [77].

To the contrary, the sample that only had a limited re-carbonation duration right from the start was not able to develop as many pores with a critical pore much radius, because the ratio between freshly formed $CaCO_3$ and annealing of CaO prohibited this (creation of wider pore mouths). Consequently, this products outperforms the product with an initial carbonation duration of 30 minutes if the carbonation duration is shifted to the same value because of the significant increased accessible surface area. It might be speculated that this temporary outperformance could level out in a large amount of following cycles.

3 Carbonate Looping Sorbents

A Ca-based sorbent has to fulfil several requirements in order to keep the process simple and cost-effective. Chemical, mechanical and thermal stability are as important as high reaction rate constants, high CO_2 capture abilities (even after many cycles) and environmental harmlessness. Of course, the price has to fit into the framework of the just mentioned properties ([115]). In addition, the selectivity of the reaction should be very high, so that no problems with sulfation or other side reactions are likely to occur ([118]).

The general hope for improved sorbents is an improved process: A sorbent with a higher CO_2 capture ability would enable a higher CO_2 separation degree from the flue gas or a lower circulating mass flow. A harder sorbent would allow to operate the CL process with lower make up rates and this saving significant amounts of fresh sorbent. At the end, reduced capital expenditures and operational costs might be achieved (see Fig. 3-1).

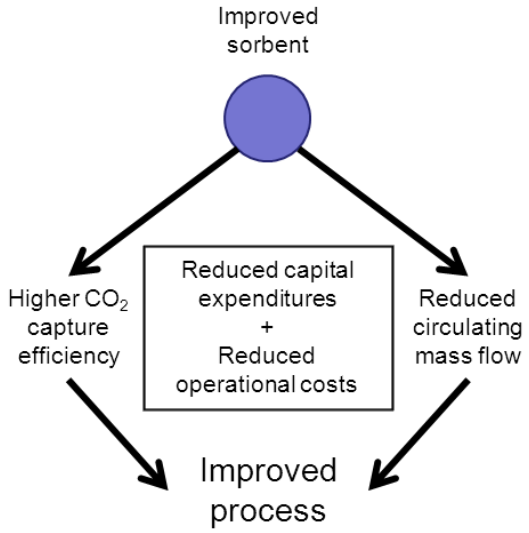

Fig. 3-1: Improved sorbents might lead to improved process conditions and this saving captial expenditures and operational costs.

Sorbent research activities can be divided into two groups: First, basic understanding of the lime behaviour within the process for a better design of the utilities and second, improvements of the used Ca-based sorbent for process improvements.

Before a critical assessment of approaches for improved sorbents, reported in the literature, can be done, desired sorbent properties have to be defined.

3.1 Ideal Sorbent Properties

Describing and understanding the interactions between the individual parameters within a CL looping systems requires a detailed and sophisticated model. The basic problem of this system is the interaction between the mass and heat balance. At low make-up rates, for example, the sorbent particles would have to stay much longer in the system. This means that the sorbent loses very much of its CaO conversion ability and this leads to an increased mass flow and an increased heat demand. This heat demand would be satisfied with the addition of more coal, causing a higher level of impurities in the system and this increasing the mass flow again while the heat demand is increased accordingly.

Even though some process models have been reported ([99], [38], [106], [7]) proving the theoretical feasibility of the CL process, only one author ([73]) investigated the impact of improved sorbents on the process in detail. Some authors provided assumptions that seem to be too optimistic. LISBONA ET AL. [73], for example, assumed a price for the raw limestone of 6 €/t. However, standard limestone sand in the required grain size and needed quality would cost at least 20 €/t ex works. Transportation costs would contribute between 2 and 6 € per ton and 100 km on top of this price.

Accordingly, the author of this work decided to set up his own model that has a clear aim of describing the process in terms of sorbent properties. Chapter 4 is only dedicated to this topic. The following figures are a result of the model described in Chapter 4. They are shown here to illustrate beneficial sorbent properties in the best possible way.

Fig. 3-2 and 3-4 show the efficiency drop without CO_2 compression of a coal fired power plant operated with two different impure coals versus the particle stability, i.e. hardness expressed in cycles and CO_2 capture stability respectively. Both independent variables will be described in detail later on. However, the hardness number defines the average cycles between calciner and carbonator one particle can withstand until full attrition or purge via the bleed and the CO_2 stability number expresses the rate of deactivation of the sorbent. An average hardness of 50 cycles (~2% make-up per cycle) and a CO_2 stability number of 9 would refer to an average CaO conversion of 29%. Both variables would determine a make-up rate of ~160 kg_{CaCO3}/t_{CO2}.

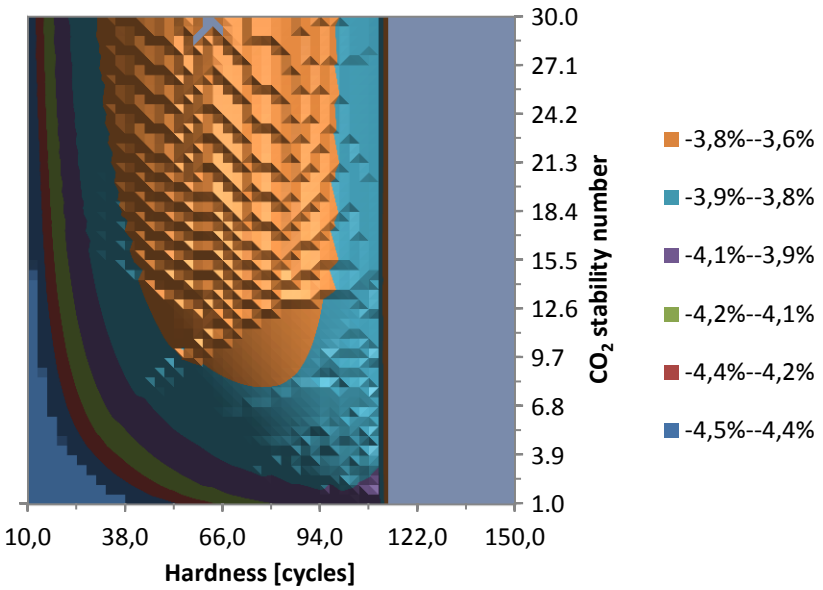

Fig. 3-2: Efficiency drop of a power plant described in Chapter 4 using a coal with 1.2% S, 16.7% ash, 10% moisture and a heating value of 24.5 MJ/kg. The process could not be operated if the sorbent would be kept in the system for more than 130 cycles (~0.75% make-up per cycle) because of sulphation of the sorbent. In addition, if the sorbent would be kept longer in the loop than 90 cycles, the investment cost would exceed 2 billion € for a 1 GW_{el} base power plant. The minimal efficiency drop in this calculation is 3.59% while the maximum is 7.11%. 2,500 possible operating points were calculated to plot this figure.

Impurities clearly determine the optimal operating conditions. Especially, the sulphur content of the coal will transform into SO_2 and SO_3. Both gases are able to react with CaO spontaneously to form $CaSO_3$ and $CaSO_4$. CaO intended for CO_2 capture is removed by this reaction leading to less active sorbent material in the loop and higher circulating mass flows. It can be seen that high particle stabilities, referring to a low make-up, would not be beneficial for the overall process, even though, a too small make-up would cause the system to collapse because of the absence of free CaO in the system. This point is reached if the make-up would be below 0.6% of the inventory per cycle.

Fig. 3-3 shows the dependency of the make-up flow versus the mechanical and CO_2 capture stability. It can be noticed that the minimum of the make-up flow is not the optimum for the efficiency drop. Depending on the cost of the sorbent the economical optimum might be in-between the two optima of Fig. 3-2 and 3-3.

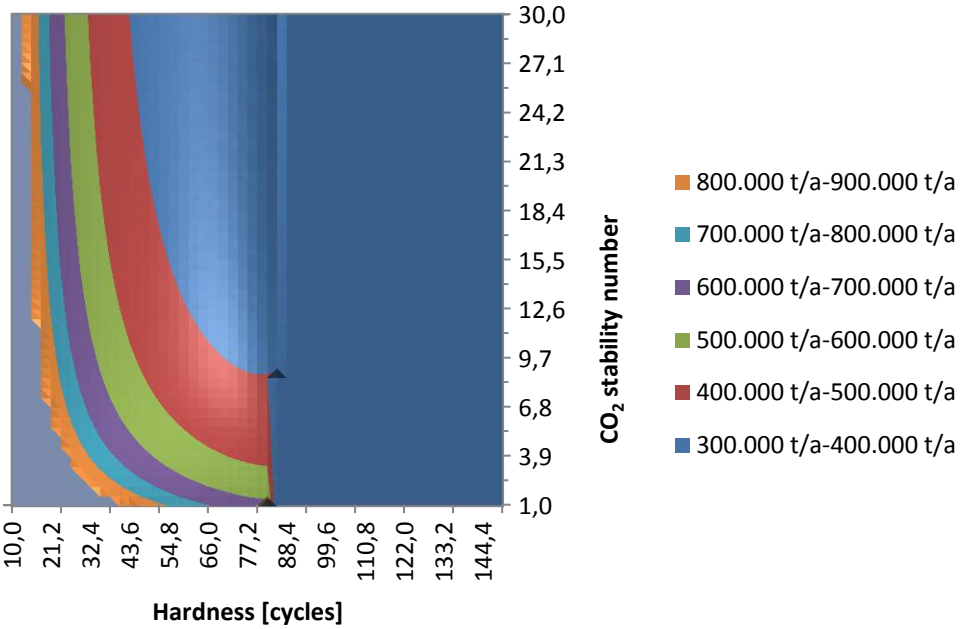

Fig. 3-3: **Make-up of CaO expressed as tons per year of a power plant described in Chapter 4 using a coal with 1.2% S, 16.7% ash, 10% moisture and a heating value of 24.5 MJ/kg. The process could not be operated if the sorbent would be kept in the system for more than 130 cycles (~0.6% make-up per cycle) because of sulphation of the sorbent. In addition, if the sorbent would be kept longer in the loop than 90 cycles, the investment cost would exceed 2 billion €. The minimal make-up in this calculation is 307,000 t/a while the maximum is infinite. 2,500 possible operating points were calculated to plot this figure.**

The whole picture looks completely different if the impurities of the coal would not interact with the sorbent and the CL system. Such a case is illustrated in Fig. 3-4 and 3-5; neither a local optimum nor a theoretical boundary in the operating conditions can be recognised.

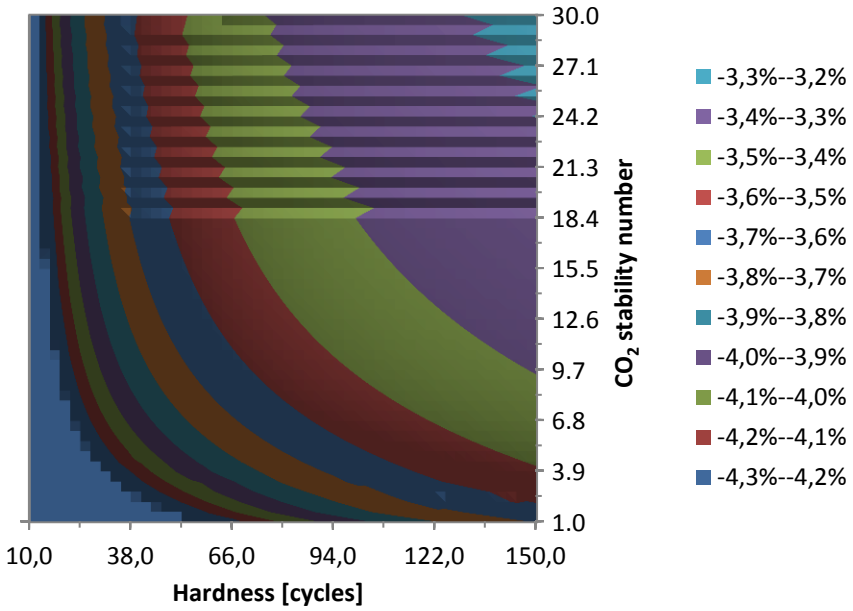

Fig. 3-4: **Efficiency drop of a power plant described in Chapter 4 using a hypothetical coal without impurities. The minimal efficiency drop in this calculation is 3.28% while the maximum is 7.21%. 2,500 possible operating points were calculated to plot this figure.**

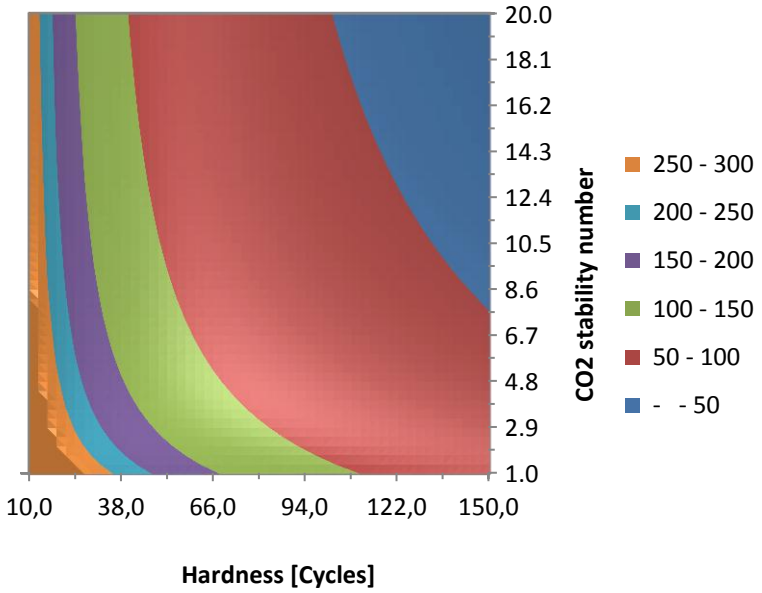

Fig. 3-5: **Make-up of $CaCO_3$ expressed as tons per hour of a power plant described in Chapter 4 using a hypothetical coal without impurities. The minimal make-up in this calculation is 48 t/h. 2,500 possible operating points were calculated to plot this figure.**

However, the small hardness scale is hiding the whole picture. Fig. 3-6 and 3-7 show the same case like Fig. 3-4 and 3-5 but with a 20 times extended hardness scale.

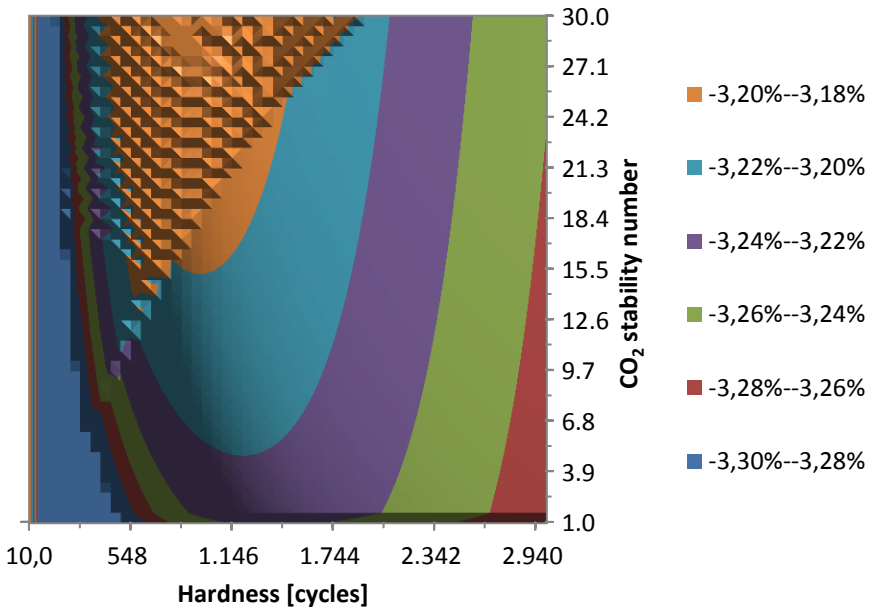

Fig. 3-6: **Efficiency drop of a power plant described in Chapter 4 using a hypothetical coal without impurities. The minimal efficiency drop in this calculation is 3.17% while the maximum is 7.21%. 2,500 possible operating points were calculated to plot this figure. Note: The hardness scale is extended to show effects of sorbent deactivation correctly. The scattering in the graph occurs from numerical deviations.**

By the observation of Fig. 3-6 it becomes obvious that the optimum operation may be achieved if the sorbent is cycled for 500 times, accounting for 0.2% of make-up after each cycle.

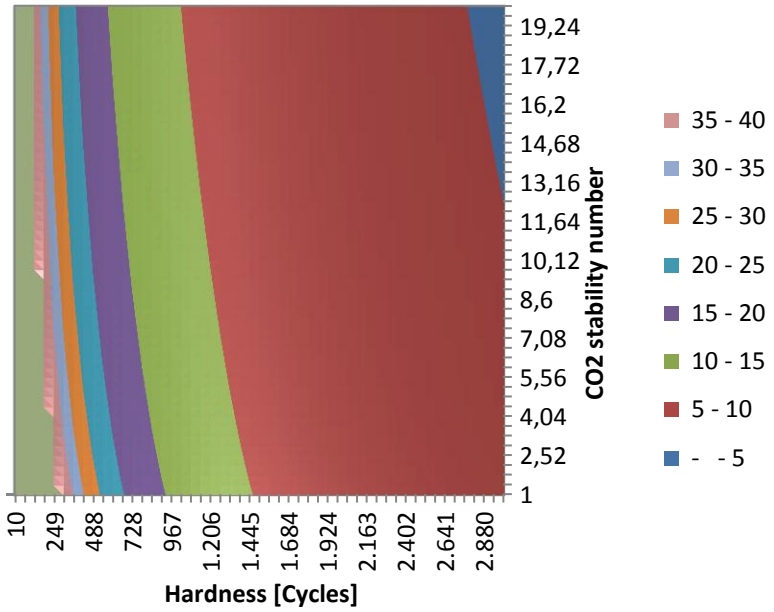

Fig. 3-7: Make-up of $CaCO_3$ expressed as tons per hour of a power plant described in Chapter 4 using a hypothetical coal without impurities. The minimal make-up in this calculation is 4.76 t/h. 2,500 possible operating points were calculated to plot this figure. Note: The hardness scale is extended to show effects of sorbent deactivation correctly.

Due to the remaining residual CaO conversion of the sorbent even after 1000 cycles it is common sense that the make-up rate will decrease monotonous with the number of cycles (see Fig. 3-7).

Following the presented simulation results, desired sorbent properties can be defined according to the cases as given in the following table.

Table 3-1: Desired sorbent properties for the cases of an introduction of impurities and no impurities. The impurity sulphur was considered to react with the sorbent and decreased its CO_2 capture ability linear while the ash was considered as inert that gets enriched in the cycle. Optimisation was done with respect to the overall efficiency drop.

	Hardness	**CO_2 stability number**
Introduction of impurities	40-80 cycles	As high as possible
Virtually no impurities	500-1000 cycles	No impact, because residual CO_2 capture ability is reached after 100 cycles → high residual CO_2 uptake important

From a strict scientific point of view, improved sorbents may not be interesting for systems that are operated with a fuel that introduces significant amounts of impurities because

standard $CaCO_3$ particles offer a CO_2 capture stability of ~3[9]. Therefore, the potential of sorbents with a lasting high CO_2 uptake is limited because of the required high bleed rate. By this, increased power plant efficiencies may not be overcompensated by the costs of an artificial sorbent that might be ten times higher than the costs for limestone sand. However, the potentially low requirements in terms of hardness, might enable the use of mechanical weaker agglomerated products that can be produced out of lime and limestone fines.

Applying high grade fuels in the CL process, however, requires mainly hard sorbents that are able to withstand complete attrition for at least 300 cycles. Of course, the residual CaO conversion should still be in an acceptable range, say between 10 and 20%.

Economical assessments conducted in Chapter 4 will reveal under which circumstances higher grade sorbents might be used to achieve an overall economic optimum. These simulations will also show economical advantages of tailor made sorbents.

Another issue that has to be taken into account besides CO_2 capture ability and hardness is the grain size distribution of the sorbent that can be used in the CL process. In order to achieve a circulating operation, the drag force F_{Drag} one particle experiences has to be at least equal to the gravitational force $F_{Gravity}$.

$$F_{Drag} = F_{Gravity} \tag{3-1}$$

Solving this equations with respect to the particle diameter delivers

$$d_{Particle} = \frac{3 c_W \rho_{Gas}}{2(\rho_{Particle} - \rho_{Gas}) g} v_{Gas}^2 . \tag{3-2}$$

c_W is the drag coefficient, $\rho_{Particle}$ and ρ_{Gas} are the apparent density of the particle and the gas, g is the gravitational constant and v_{Gas} is the superficial velocity. The temperature dependency of the gas that surrounds the particle can be described according to the law of ideal gases by

$$\rho_{Gas} = \frac{p \overline{M_{Gas}}}{RT} . \tag{3-3}$$

p is the outer pressure, $\overline{M_{Gas}}$ the average molar mass of the gas (~28 g/mol in the carbonator and ~43 g/mol in the calciner), R the universal gas constant and T the temperature.

[9] See Chapter 4 for a detailed explanation of the concept of the CO_2 stability number. A CO_2 capture stability numbers of 3 indicates a rather quick loss of the CO_2 capture ability towards the residual CaO conversion of ~11%.

While the particle diameter remains nearly unchanged during the cycling (neglecting attrition and densening), the apparent density changes drastically by the first calcination from ~2600 kg/m³ to ~1600 kg/m³. During the cycling, the change of the apparent density is less drastic from around 2000 kg/m³ in the partial carbonated state to ~1600 kg/m³ in the calcined state. Fig. 3-8 shows the working area of the CL process and the according maximal particle diameters to achieve a circulating fluidised bed operation.

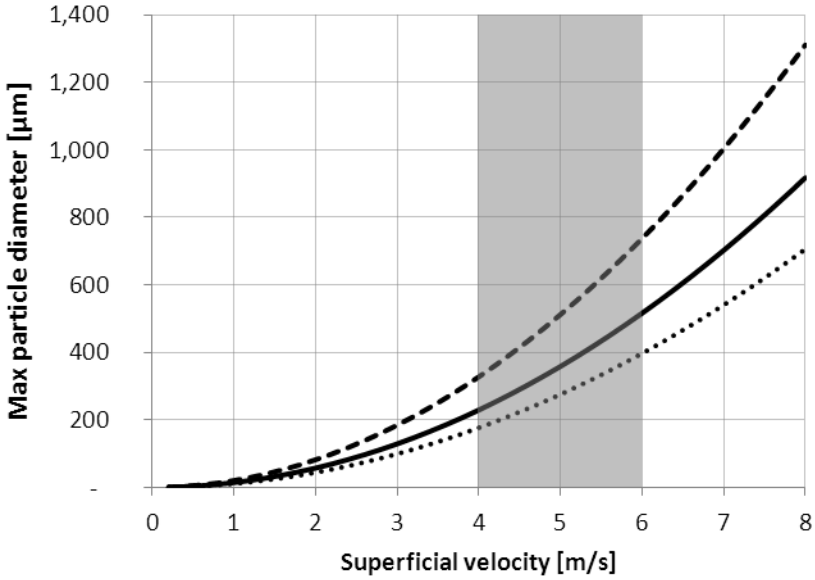

Fig. 3-8: Max particle diameter of limestone, lime and partial carbonated lime in the CL process versus the superficial gas velocity. The grey area marks the expected working area expected for the CL process. Solid line: Carbonator with partial carbonated particles (2000 kg/m³, 650°C, $\overline{M_{Gas}}$ =28.4 g/mol), dashed line: Calciner with lime particles (1600 kg/m³, 950°C, $\overline{M_{Gas}}$ =43 g/mol), fine dashed line: Carbonator with original limestone (2600 kg/m³).

Due to the higher density of the calciner gas (higher molar mass of CO_2) and the lower apparent particle density, the calciner could be operated at lower superficial gas velocities than the carbonator. Assuming that the maximal fluidisation velocity in the carbonator is 6 m/s, the maximal diameter of a partially carbonated particle could be around 500 µm. Besides this boundary, it is also obvious that it might not be a good idea to introduce fresh make-up into the carbonator because the maximal diameter in this case would be 400 µm; coarser particles would get concentrated at the bottom leading to a higher pressure drop and, in the worst case, to a blockage of the reactor. This particles could only be transported to the calciner if they would get attired or if higher fluidisation velocities would be applied. Both cases are not favourable.

However, in terms of the research on a CL sorbent, particle size distributions between 100 and 500 µm will be considered as good. The lower boundary is a result of the efficiency of the

used cyclones. It is assumed that 100% of particles coarser than 100 µm will be separated from the gas streams.

3.2 Tests to Characterise Hardness and CO_2 Capture Ability

Two types of new test methods are needed to characterise sorbent properties: First, a test to determine the mechanical stability of lime and limestone particles with a grain size below 1000 µm and second, a test to determine the chemical activity of different sorbents regarding the rate of CO_2 uptake and the total amount of CO_2 captured.

This section will provide an overview of the literature approaches for the two tests.

3.2.1 Tests for the Mechanical Stability

3.2.1.1 Attrition Mechanisms

SALATINO [103] classified attrition, according to their mechanisms, into three different groups;

- Attrition by primary fragmentation,
- attrition by surface wear and
- attrition by impact loading.

Attrition by primary fragmentation is associated with the rapid release of gases in the particle that cannot escape at an appropriate rate and lead to a micro-scale explosion. This case could happen in the CL process, if the heating rate of the particle is higher than its decomposition rate or if the outer surface is deeply sintered or melted, before full calcination is achieved. The first case is unlikely, because of the high self cooling effect during the calcination of $CaCO_3$. Also it is more likely that the second case takes places at very high temperatures before the first one could be noticed. The first continuously operated oxy-fuel calciners are going to demonstrate the occurrence or absence of such effects.

Attrition by surface wear is conveyed by friction, which in turn causes shear forces on the surfaces of particles that are attrited. SALATINO [103] pointed out that this attrition mechanism is poorly characterised and that “crack formation/propagation, fatigue and delamination jointly play a role in determining the attrition pattern”. However, he claimed that surface attrition could be described sufficiently with a simple equation.

$$\left(\frac{dm_{Attrited}}{dt}\right) = R_{AttritionS}^{Particle} = k_{AttritionS}\, m_{Bed}\, (U - U')^2 \qquad 3\text{-}4$$

$k_{AttritionS}$ is a material dependent factor associated somehow with material parameters (shape, density, specific surface area), operating conditions and the utility design (efficiency of energy flow leading to attrition), U is the superficial velocity and U' is the difference between incipient velocity (U_{mf}) and a threshold velocity beyond which attrition becomes noticeable. Disregarding that Eq. 3-4 might only have limited practical use, it gives at least an idea of the proportionalities. Assuming that the lost sorbent material will be refilled continuously in the CL process, the eluted mass is directly proportional to the inventory of the reactor and proportional to the kinetic energy ($E \sim (U - U')^2$) that is put into the system.

Attrition by impact loading generally occurs if particles are accelerated in a gas stream and subjected to collisions with other particles, walls or reactor internals. These particles can either show brittle (limestone) or ductile behaviour (quick lime) on impact stress. Fig. 3-9 illustrates the difference between the two cases very well.

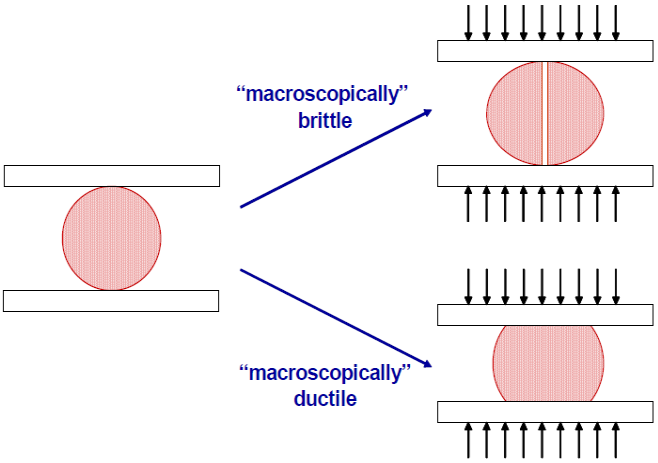

Fig. 3-9: Different apparent behaviours of macroscopic brittle and macroscopic ductile particles. Figure taken from [103].

Macroscopic brittle substances are forming cracks or propagating cracks from the impact point into the particle (see Fig. 3-10).

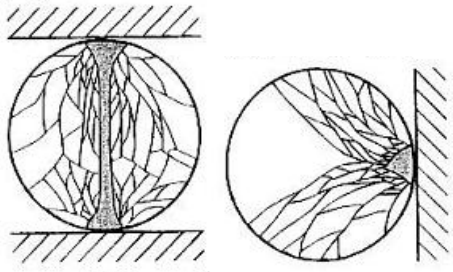

Fig. 3-10: Breakage patterns of balls when exposed to mechanical stress (left: pressure, right: impact). Figure taken from [110].

3.2.1.2 Determination of Dominant CFB Attrition Mechanism

Particle attrition within fluidised bed reactors can be influenced by a wide variety of matters:

- Properties of the particles (density, shape, size, assembly - single or multi layer, content and nature of binder, crystal size, shape and alignment, brittleness, elasticity)
- Layout of the used reactors (way of fluidisation, walls, fixtures in the system, design of cyclones)
- Kind of fluidised bed (stationary or circulating)
- Process parameters (fluidisation velocity, temperature, moisture, mass loading of system, make-up rate, circulating mass streams)

As discussed before, three attrition mechanisms are known (primary fragmentation, surface wear, impact load). Primary fragmentation could take place, if extremly high temperatures would be applied in the calciner, causing higher heating than calcination rates and leading to micro-explosions that destroy or damage the particle. No data is available so far, to prove or refuse the activity of this mechanism in the CL system. Therefore, it will not be discussed any further.

Attrition by surface wear is supposed to become important, if high mass loads and low fluidisation velocities are applied; attrition through impact might become dominant if low reactor mass loads and high fluidisation velocities are applied and unfavorable layouts of the cyclones or the fluidisation nossles are present leading to a high rate of impact of the particles (see Fig. 3-11).

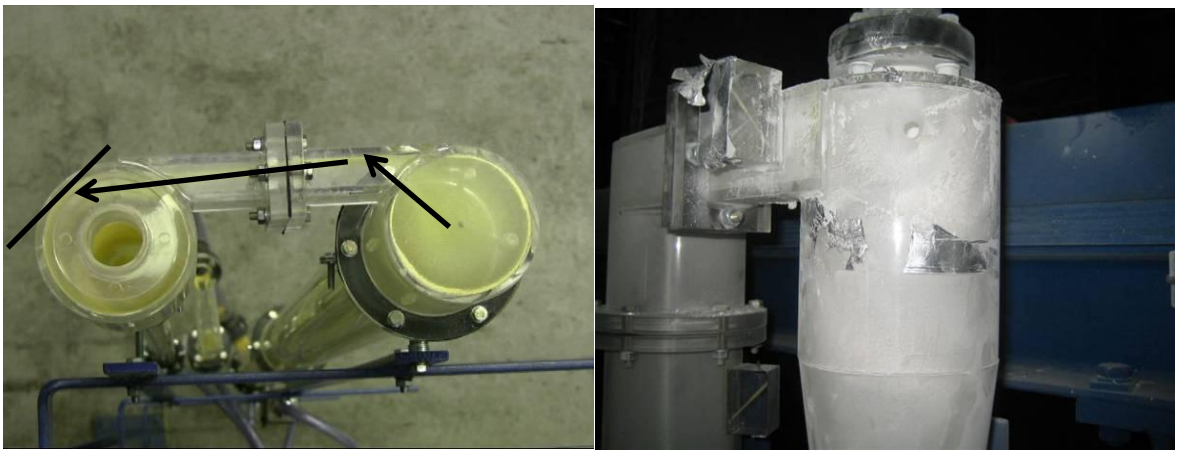

Fig. 3-11: Example of an unfavourable layout of a cyclone. Particles from the standpipe enter the connection to the cyclone with an angle of ~45° (right arrow of the left picture), are accelerated to the cyclone and collide with the wall of the cyclone with an angle of ~45° (arrow and straight in the left picture. Accordingly, high mechanical stress it put onto the product as well as abbreviation is observed at the cyclone (left picture). Pictures taken by Alexander Galloy.

However, as will be shown later, experimental evidence was received that surface wear might be dominant in a well designed test CFB test unit.

Keeping in mind that the superficial velocity in the reactors is going to be between 4 ([26]) and 6 m/s ([38]), the resulting speed in the cyclons wil be significant higher. In case of an unfavorable flow, particles are likely ot collide with the walls of the cyclones at this speed leading to impact attrition.

Of course, "particle attrition may […] also be induced by […] the gas distributor and/or bed internals such as heat exchange tubes" CHEN ET AL. [30].

Consequently, two or more lab based hardness tests would be required to determine the breakage pattern and to investigated the resistance of the particles towards surface wear and impact.

3.2.1.3 Literature Findings

Fluidised Bed Tests

CHEN ET AL. [30] investigated the attrition in a heated fluidised bed system between 25 and 850°C (see Fig. 3-12). The inner diameter of the riser was 40 mm while the height was given by 2 m. The original grain size of the samples was between 550 and 950 µm.

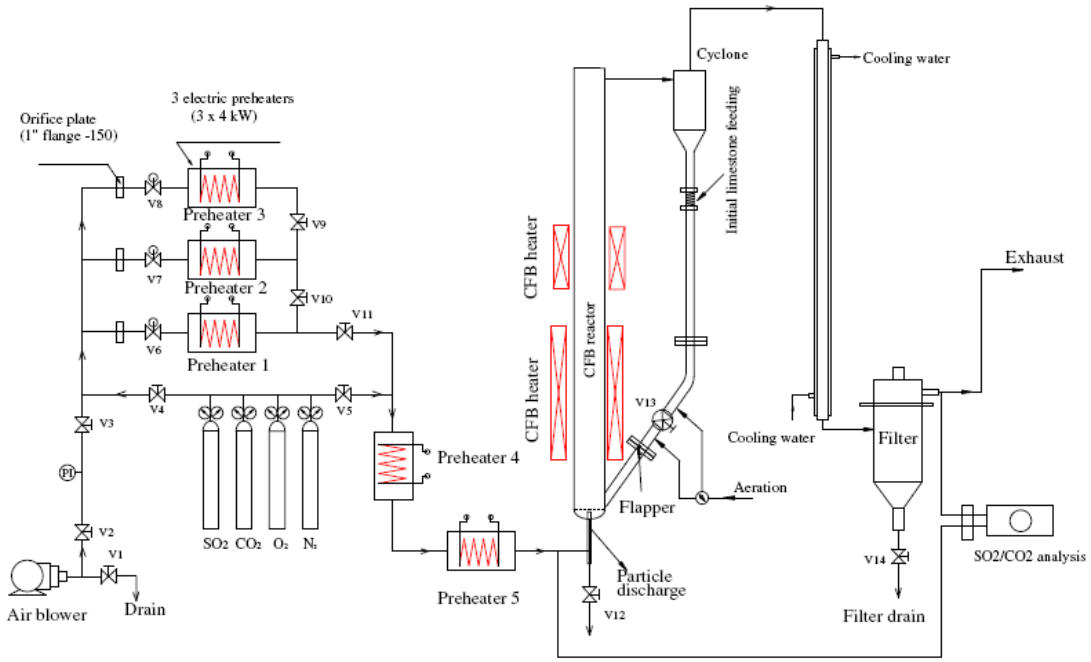

Fig. 3-12: Experimental setup for the investigation of attrition phenomena performed by [30]. Figure taken from [30].

Based on the particle size evolution CHEN ET AL. [30] suggested that the attrition mechanism was surface wear during his experiments. He also stated that the ratio between initial SAUTER diameter d_0^{Sauter} and SAUTER diameter at a given time d_t^{Sauter} increases linear with time.

$$\frac{d_0^{Sauter}}{d_t^{Sauter}} = k_{Attrition}^{Chen} \cdot t + 1 \qquad 3\text{-}5$$

$k_{Attrition}^{Chen}$ is an attrition rate constant that is dependent from the superficial velocity, t is the time.

$$k_{Attrition}^{Chen} = k'^{Chen}_{Attrition} \cdot (U_g - U_{mf})^2 \qquad 3\text{-}6$$

U_g is the superficial gas velocity, U_{mf} the minimum fluidisation velocity and $k_A^{'}$ an attrition rate constant. The correlation between attrition rate constant and excess gas velocity can be seen in Fig. 3-13.

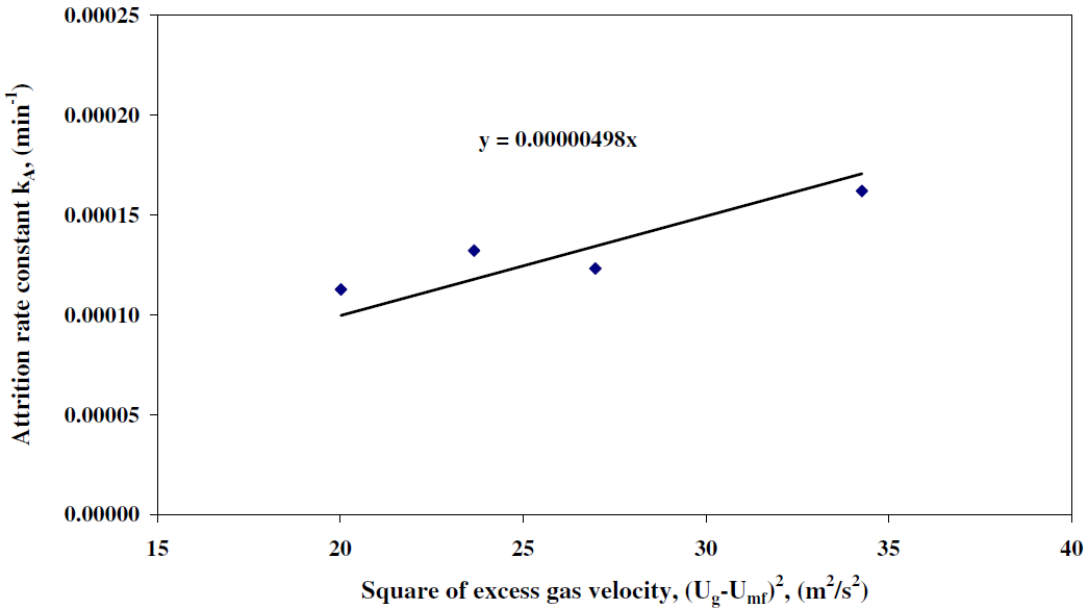

Fig. 3-13: Correlation between the attrition rate constant and the excess energy driven into a fluidised bed [30].

CHEN ET AL. [30] also posted a relationship between the creation of surface area S_t, temperature T, excess gas velocity and time t.

$$\frac{S_t - S_0}{S_0} = \frac{S_t}{S_0} - 1 = \frac{d_0^{Sauter}}{d_t^{Sauter}} - 1 = k_0 e^{\frac{-E}{RT}} (U_g - U_{mf})^2 t \qquad 3\text{-}7$$

k_0 is a pre-exponential factor, E the activation energy and R the universal gas constant. Eq. 3-7 "implies that the generation of new surface area of particles in the continuous CFB attrition system is proportional to the total excess kinetic energy (above minimum fluidization) consumed and the attrition time, whereas the generation of new surface area decreases exponentially with temperature. Therefore, the limestone attrition in the circulating fluidized

bed system reasonably follows RITTINGER's surface theory" ([30]). The activation energy and pre-exponential factor were determined to be -4,35 kJ/mol and $1.46 \cdot 10^{-8}$ s/m² for a temperature range from 25 to 580°C. After the calcination of the sample at 850°C for 1 h the attrition rate was more than 10 times bigger than expected from the strict extrapolation of the results achieved for temperatures up to 580°C. This indicating, that the resistance of CaO to attrition is much lower. Even though the work of CHEN ET AL. [30] is very interesting, only one material was investigated. A prove of concept for different sorbents is missing and the temperature dependence on the attrition rate might be interpreted as reduction of the density of the gases flowing through the test rig on elevated temperatures. Another weakness of this study is the discharge of the fines from the filter systems.

JIA ET AL. [59] defined an attrition rate constants with the approach of a first order attrition kinetic to describe the attrition of lime and limestone in a small quarz reactor and a small pilot scale fluidised bed reactor.

$$k_{Attrition}^{Jia} = -\frac{1}{m}\frac{dm}{dt} \qquad 3\text{-}8$$

He defined attrition as particles smaller than 75 µm. Five different limestones were tested at temperatures up to 900°C. Within his small test rig, agglomeration problems were reported, being the reason for tests in a larger BFB. The fluidisation velocities for the small (40 mm inner diameter) and large (100 mm inner diameter) FB were 3.5 and 1.4 m/s respectively. Cycling experiments were done within the large FB. Calcination was carried out under mild conditions at 850°C and a superficial velocity of 0.35 m/s.

Notably, JIA ET AL. [59] pointed out that particles that were grinded with a disc pulveriser showed a significant tendency to break into smaller grains and this showing a higher attrition rate than particles that were crushed with a jaw crusher. One possible explanation given was the different macroscopic particle shape; plate like in case of a disc pulveriser and more spherical in case of the jaw crusher. Another important outcome is the severe production of fines during the first and second calcination. One possible explanation for this observation will be given by the end of this section. Even though that Eq. 3-8 was proposed by JIA ET AL. [59], no attrition rate constants were evaluated or given.

Static Tests

Probably one of the most often used historical test methods is the Hard Grove test. 50 g of sample with a grain size between 590 and 1190 µm are introduced into a grinding bowl. 8 milling balls with a diameter of 25.4 mm are added. On top of the balls a weight with a mass

of 30 kg is set. After 60 complete rounds of the balls over the bed of material, the milled product is sieved. The mass that passes a 74 µm sieve (D) is the measured value that goes into the calculation of the HGI (Hard Grove Index). The experimental setup can be seen in Fig. 3-14. This test was designed for the determination of the hardness of coal to predict its graindability and is still a standard test. In addition, it was and is used to get basic ideas for the dimensioning of grinding equipment for different applications. Good accordance between the HGI and energy consumption of the mills was reported ([8]). The HGI is calculated according to

$$HGI = 13 + 6.93D. \qquad 3\text{-}9$$

Obviously, low HGI refer to hard particles. The grinding occurs approximately to 90% through pressure.

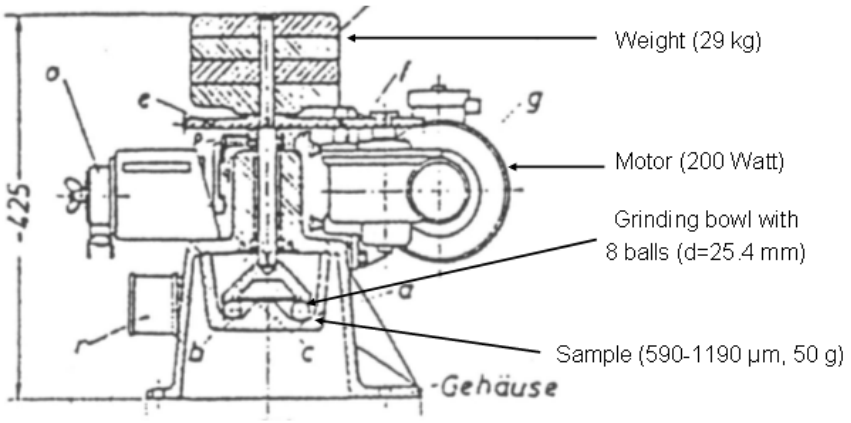

Fig. 3-14: Experimental setup of the Hard Groove test. Fig. taken from [75].

The Centre for Solar Energy and Hydrogen Research (ZSW) designed another test, similar to the Hard Grove procedure: 32 ml of sample with a grain size between 600 and 710 µm is introduced into a grinding beaker with a volume of 80 ml that belongs to a Fritsch Pulverisette 6, a planetary mill ([140]). 5 achat grinding balls with a diameter of 20 mm are added. Therefore, the milling vessel is filled to approximately 66%. After 5 minutes of grinding with a rotation speed of 440 turns/minute the amount of sample that is smaller than 200 µm is measured. Fig. 3-15 shows the correlation between the HGI and the ball mill test.

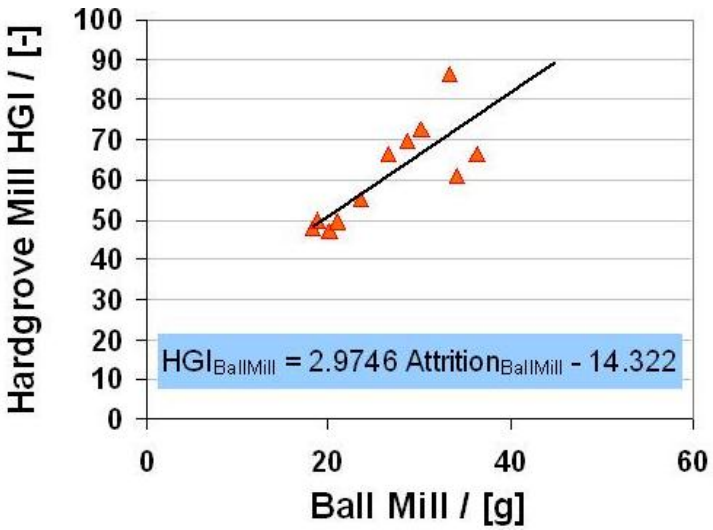

Fig. 3-15: Correlation between HGI and ZSW Ball Mill Test [138].

Based on the defined test procedure the ZSW investigated various limestones and limes since 2004 (see Fig. 3-16).

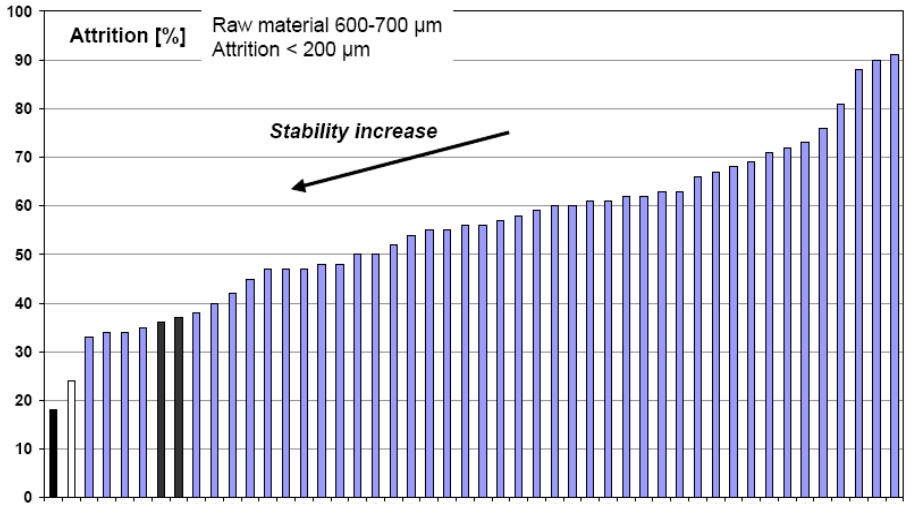

Fig. 3-16: Attrition values for limestones determined by the ZSW. Figure taken from [139].

Pressure forces of the grinding balls, due to the high rotational speeds, usually cause particle destruction in a planetary mill. However, while choosing a too low or a too high loading of the grinding vessel shifts in the attrition mechanism can occur (see Fig. 3-17).

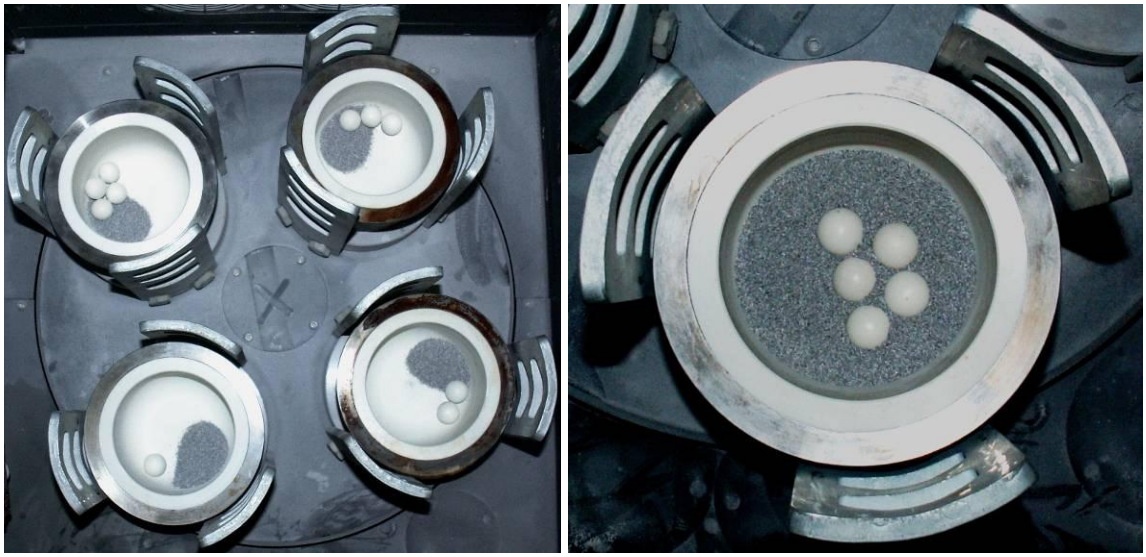

Fig. 3-17: **Possible distribution of particles and grinding balls in a planetary mill. Both pictures were taken during the operation of the mill. The large plate moves clockwise with 70 rpm while the vessels move counter clockwise with roughly 120 rpm. The grain size of the particle was 600-710µm. The masses were 14 g (left) and 100 g (right, ~20% filling of the vessel). It can be seen that only some grinding base are in contact with the particles if the filling is too low (left) and that the grinding balls are likely to assemble themselves in the middle if the filling level is to high (right). Attrition mechanisms are: Pressure and surface wear, i.e. friction (left) and surface wear (right).**

Within the ZSW test it is likely that a too high loading was chosen, leading to the attrition mechanism of surface wear.

However, in the scope of this work a test based on physical properties of the materials was desired. One possibility to do so is the precise recording of the energy that is put into the material followed by the determination of the increase of outer surface area. The quotient between introduced energy and created outer surface area should deliver a material parameter. SCHUBERT ET AL. [110] describes the fundamentals of such a test precisely. The two most important figures of his explanations shall be shown here.

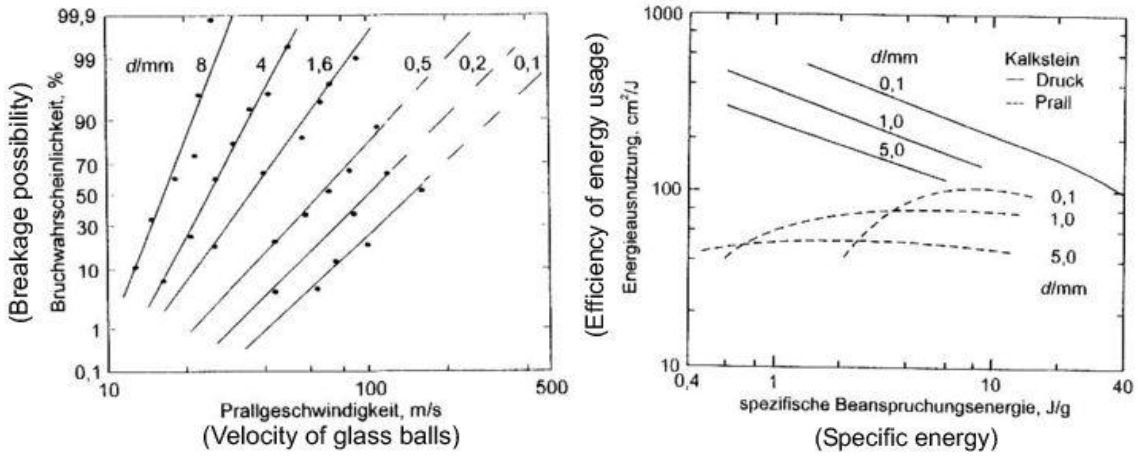

Fig. 3-18: Left: Possibility of breakage of glass balls with different diameters versus the velocity of these balls. Note the double logarithmic plot. Right: Comparison of the efficiency of the energy usage versus the specific energy that was put into different grains of limestone for grinding. Pressure is usually more effective regarding particle breakage for low energy amounts and small grains. Figures taken from [110].

Fig. 3-18 shows the breakage possibility versus the speed of glass balls and the efficiency of energy usage versus the specific energy that is put into a particle. By examining the left picture it becomes obvious, that the breakage possibility by impact will be extremely low in the bottom of a FB. Only if higher fluidisation velocities are applied, say >10 m/s, which might be the case at the tips of the fluidisations nozzles and in the cyclone, the possibility of breakage on a single impact is up to a maximum of 1%. In this case, only the rate of impacts would determine the overall particle size reduction. By this, it could be argued that a poorly designed fluidisation grid might contribute much more to the overall attrition than a poorly designed cyclone.

However, the right picture of Fig. 3-18 reveals that it should be possible to establish a hardness ranking of limestone particles that have suffered pressure stress. The straight shape in the double logarithmic diagram indicates that a normalisation is possible, which would not be the case if impact stress is applied. It should be mentioned that stress patterns in the particle, i.e. crack patterns, are very similar in the impact and the pressure case (see Fig. 3-10).

The derived test procedure “delta-test” will be described in detail in chapter 5.2.

Such a tests can be used if the particles react brittle on pressure, statements about the behaviour on impact stress with rather high velocities is desired and the particles are not able to behave ductile (e.g. soft burned lime or agglomerates).

Limitations of Lab-Based Hardness Tests

At a closer look, four different kinds of particles are present in the CL process: $CaCO_3$, highly porous CaO (freshly calcined), sintered CaO and "mixed" particles consisting of a skeleton or a core of CaO and a dense shell of $CaCO_3$. Pure $CaCO_3$ particles are only present at the beginning or if a constant make-up is adjusted.

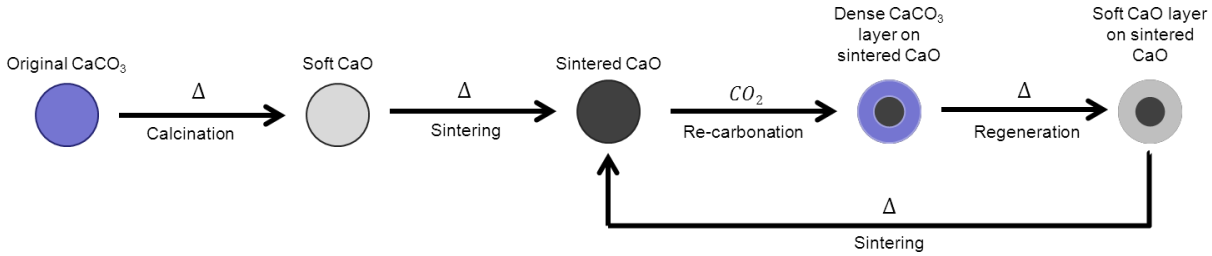

Fig. 3-19: Different stages of Ca-based sorbent particles in the CL process. Highly porous CaO is formed after each cycle creating attrition sensible surfaces.

As soon as these particles enter the calciner, a calcination very close to the equilibrium temperature of the decomposition of $CaCO_3$ will take place leading to a highly porous material. Eventually, the residential time in the calciner is sufficient for annealing processes in the CaO. This processes are associated with a densification and hardening of the particle. Afterwards, the lime particles are subjected to the carbonator to react with the CO_2 to $CaCO_3$. A dense outer layer of $CaCO_3$, which contains CaO at the inside, is formed. At the next step, theses carbonated particles are calcined again leading to a layer of highly porous CaO on a skeleton of dense lime. This process is illustrated in Fig. 3-19. Each stage has its own mechanical reaction towards different stress patterns that are summarised in Table 3-2.

Table 3-2: Possible reaction of the particles of the different sorbent stages on attrition conditions "surface wear" and "impact.

	Surface wear	**Impact**
Original, dense $CaCO_3$	Low attrition, chipping of edges	Inelastic breakage patterns, lots of fines
Soft CaO (freshly calcined)	High attrition, generation of very fine dust	Ductile behaviour, erosion on the impact point, fine dust, no particle breakage
Sintered CaO	Medium attrition	Behaviour between ductile and inelastic, no complete destruction of the particle
$CaCO_3$ covered CaO	Very low attrition, smooth surfaces	Elevated destruction resistance due to $CaCO_3$ shell. if shell brakes: possible completed destruction of particle and high dust production

Accordingly, two different hardness tests, one for surface wear and one for impact resistance would have to be carried out for each stage resulting in eight tests for each product.

Investigations carried out by CHEN ET AL. [31] strongly support this theory; he reported a decrease in attrition resistance on his successful attempt to improve the CO_2 capture ability of Ca-based sorbents.

However, up to now there are several uncertainties regarding final layout and operations of the CL looping system, prohibiting the design of highly specific tests. Up to now, for example, it is unknown, which overall and CaO surface temperatures the oxyfuel calcination will cause. Besides that, the interactions of impurities coming from the coal with the product are unknown. For sure, it is known that sulphation is able to lower the attrition rate but no data is available on the interaction between the coal ash and the sorbent. On top, the author of this thesis was not able to find any publication, discussing the dependency of attrition mechanisms on fluidisation velocities, cyclone geometries and roughness of the reactor walls at different temperatures.

Tests carried out in the scope of this work try to give a first indication for the behaviour in the real process.

Possibilities to Improve the Attrition Resistance

There is evidence that spherical particles are more resistant towards impact stress. This could be caused by the good force drainage of spheres. Smooth surfaces could lower the attrition as well because the energy exchange would be lower during the interaction between two particles or a particle and the wall of the reactor.

Besides geometrical aspects, the history of the product seems to be important. Crushing equipment that is grinding due to pressure is very likely to leave micro carcks within the particles. These pre-carcks can be considered as starting points for further destruction of the particles.Accordingly, bowl mill crushers might deliver mechanical weaker partikel than impact mills.

3.2.2 Tests for the CO_2 capture ability

Three different test procedures for the determination of the CO_2 capture ability are known in the literature:

- Classical thermo-scale design: Sample in small crucible, temperature of furnace is changed for every cycle

- Static Temperature: Sample is heated up to 750°C (equilibrium temperature for the dissociation of limestone) → Atmosphere changes for calcinations (100% N_2) and carbonation (100% CO_2)
- Two zone TGA: Crucible with sample or whole oven is moved, to change between the hot oven zone (calcinations) and the cold one (carbonisation), normally no change in atmosphere is applied
- Fluidised bed: Calcinations and carbonisation within fluidised bed environment

Because of its commercial availability the classical thermo-scale is the widest used technique. Normally the atmosphere (e.g. 10% CO_2, 30% H_2O, 60% N_2) is not changed between calcination and carbonisation. The temperature for calcination is usually in the range from 840 to 950°C. Carbonisation is mostly done at 650°C. Heating and cooling rates of about 20 K/min are usually used. Fig. 3-20 shows the typical graphs of a TGA cycle experiment. Mainly due to pore mouth blocking and sintering effects, the CO_2 capture ability decreases with the numbers of cycles.

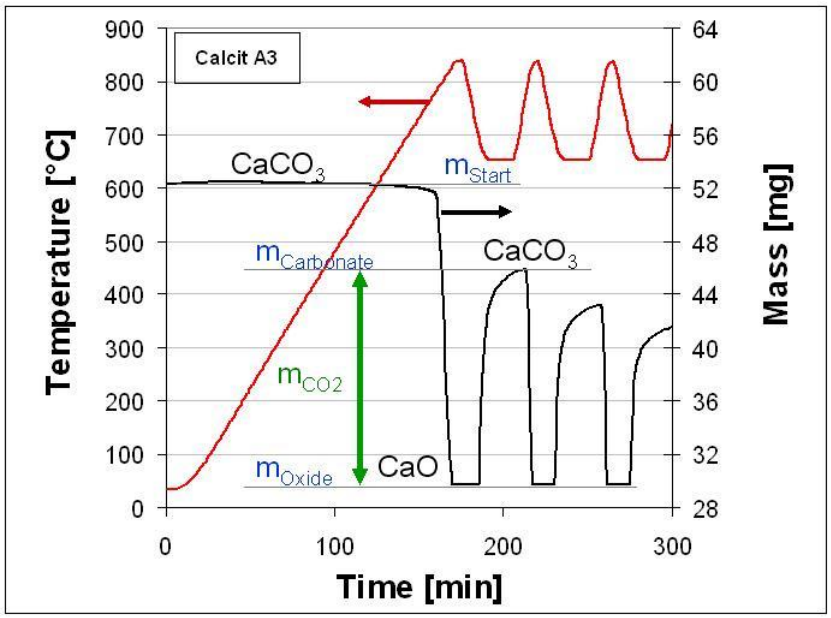

Fig. 3-20: Cyclic CO_2 absorption experiment with classical TGA. Figure taken from [138].

FENNELL ET AL. [42] suggested the second strategy to perform cyclic calcinations carbonation tests: The calcinations could be conducted under an atmosphere of pure nitrogen at 750°C and the carbonation under a pure CO_2 atmosphere. This approach has the advantage that the cycle tests can be conducted within furnaces that cannot be heated and cooled so rapidly like small TGAs. Coalescence is, of course, very minor due to the low calcinations temperature but this

also is an advantage if the influence of acidic gases like SO_2 or HF is investigated and sintering phenomena should be masked. As well, larger quantities of cycled sorbent can be provided for further tests.

The probably most advanced test procedure for the cyclic CO_2 capture ability is the use of a two zone TGA. ALVAREZ ET AL. [10] and GRASA ET AL. [51] presented two different designs for such an experimental setup (see Fig. 3-21). To be precise, the experimental setup of ALVAREZ ET AL. [10] is no real TGA, but it offers the possibility of rapid cycles and bigger sample amounts, that gives the possibility of the collection of a lot material for tests at different cycle numbers. ALVAREZ ET AL. [10] calcined 5 g of $CaCO_3$ for 10 min at 960°C and re-carbonated it at 650°C. Both steps were done under an atmosphere of 100% CO_2. GRASA ET AL. [51] was only able to test 15 mg. Calcination and re-carbonation was done at 860 and 650°C for 10-20 min in an atmosphere containing 10% CO_2 and 90% Air/N_2.

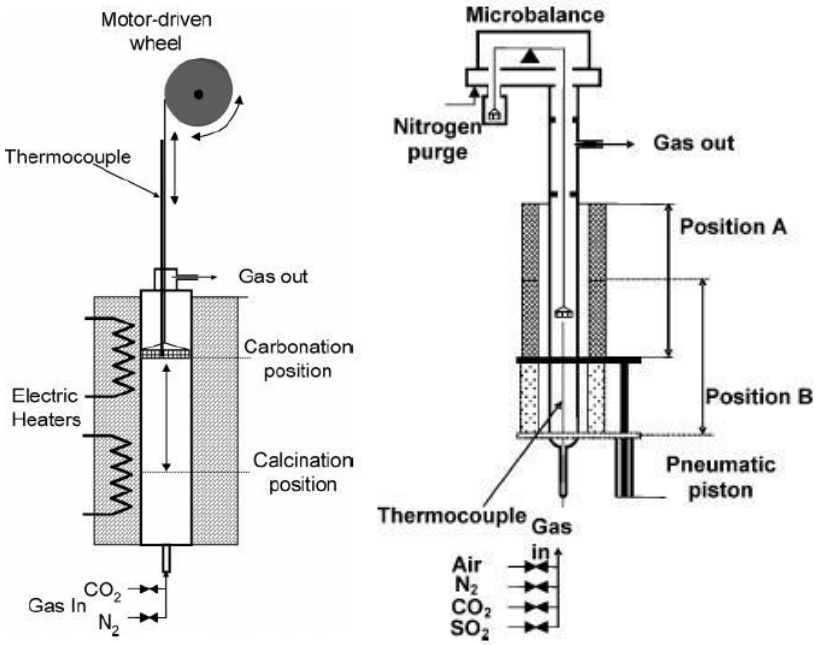

Fig. 3-21: Design of a two zone TGA proposed [10] (left) and [51] (right).

Results in this thesis include standard TGA experiments and CFB tests.

3.3 Limestones Investigated in Literature

About 50 different limestones have been investigated and the results have been published in scientific papers between 2004 and 2010 (see Table 3-3).

Table 3-3: Examples for authors who conducted investigations on the topic of Ca-based sorbents for the CL process. Approaches for synthetic sorbents are not taken into account in this listing.

Publication	Year of publication	Number of Limestones	Chem.	Thin section	Pore Structure	Surface Area	Mechanical stability	CO_2 capture ability
[10]	2005	5	no	no	yes	yes	no	yes
[30]	2008	1	yes	no	no	no	yes	no
[43]	2007	5	no	no	yes	yes	no	yes
[51]	2006	6	no	no	no	no	no	yes
[52]	2007	1	no	no	no	no	no	yes
[53]	2008	1	no	no	no	no	no	yes
[56]	2008	1	no	no	yes	yes	no	yes
[58]	2008	25	yes	yes	yes	yes	partly	no
[59]	2007	3	yes	no	no	no	yes	no
[118]	2007	2	no	(SEM-Images)	no	no	no	yes
[119]	2007	1	no	yes	yes	yes	no	yes
[121]	2008	1	no	(SEM-Images)	yes	yes	no	yes
[130]	2007	1	yes	no	no	no	no	yes

However, this thesis summarises the results achieved on more than 50 different samples collected around the world.

3.4 Behaviour of Natural Sorbents

The CL plant design and therefore the investment- and operating costs are very sensitive towards the CO_2 capture ability and costs of the sorbent; high deactivation rates regarding the CO_2 capture ability or high sorbent costs lead to a significant increase of the costs referred to one ton CO_2 avoided.

GRASA ET AL. [51] was able to show in long series of carbonation/calcinations cycles that common limestones and dolomites have the same decay in CO_2 capture ability (see Fig. 3-22). This decay is closely referred to sintering and pore mouth blockage and therefore to the loss of porosity (pores in the range of 200 nm) and specific surface area.

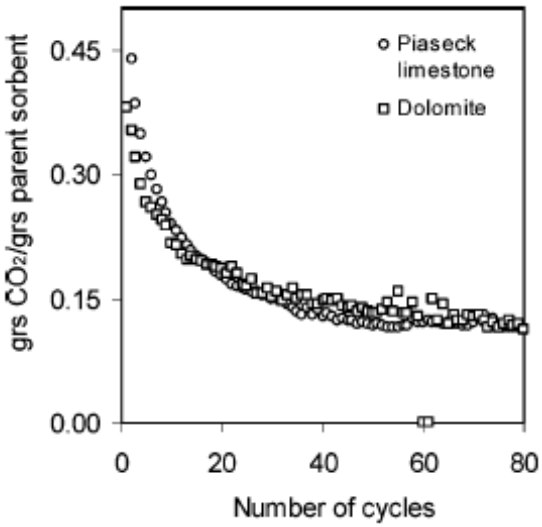

Fig. 3-22: "Comparison of sorbent capture capacity (for Piaseck limestone and dolomite) along the cycles in terms of grams of CO2 captured per gram of parent sorbent. Calcination temperature 900 °C, 10 min.; carbonation temperature 650 °C, 10 min; pCO2 2 of 0.01 MPa." [51]

Graphs of different limestones that only consider the conversion of free CaO into $CaCO_3$ show noticeable variations regarding the sorbent performance (Fig. 3-23).

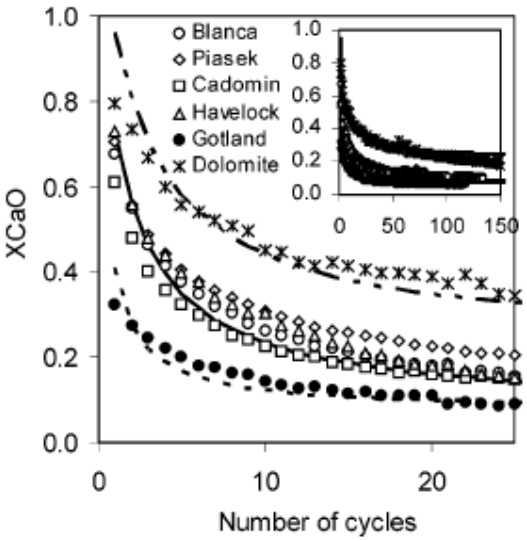

Fig. 3-23: "Conversion versus number of cycles for experiments carried out with different types of limestones. Particle size 0.4-0.6 mm. Calcination temperature 850 °C, 10 min; carbonation temperature 650 °C, 10 min; pCO2 of 0.01 MPa." [51] Note that the conversion of CaO is printed on the ordinate.

However, this presentation method of obtained raw data has no real impact on the process itself because the mass flows from the carbonator to the calciner and backward will be the same. Only slight improvements for the process could be obtained if the heat capacities of the inert substances that are cycled are significantly lower than the heat capacity of CaO.

Residual CaO conversions rates below 10% were reported ([121], [51]). SUN ET AL. [121] showed that this residual conversion can easily be influenced by the residence time of the CaO in the carbonator (see Fig. 3-24). This observation is not surprising because the carbonation of CaO can be devided into 3 different rate determining reaction steps ([140]): 1. Fast surface reaction, 2. Pore diffusion and 3. Slow solid state diffusion through a product layer of $CaCO_3$. Depending on the porosity and probably other parameters of the product, only reaction step 1 and 2 (see Fig. 3-25) or 1 and 3 (see Fig. 3-26) can be observed within reasonable time spans.

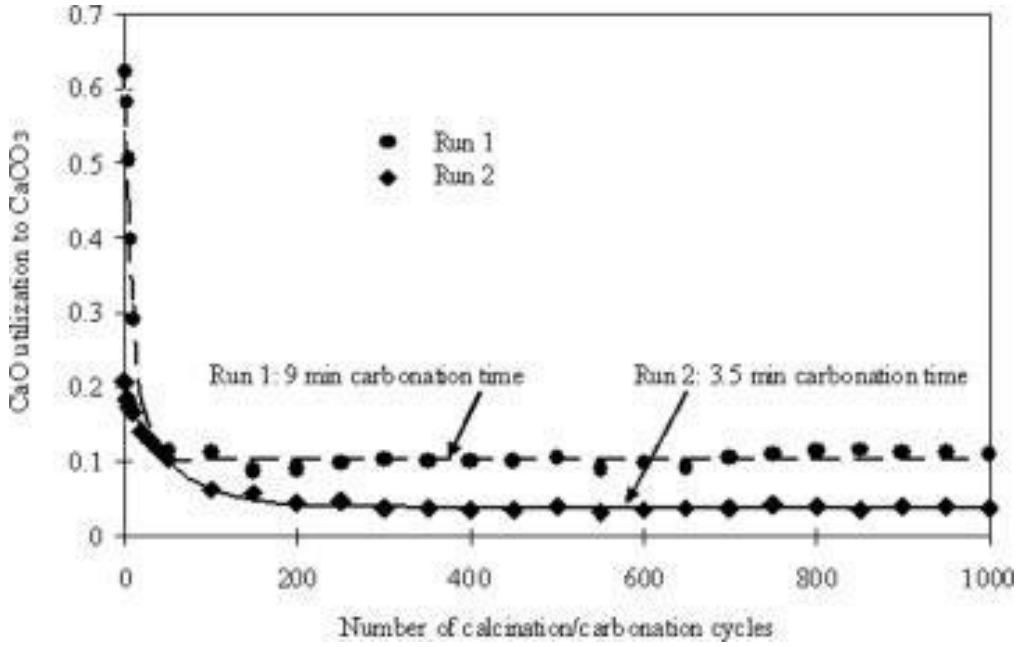

Fig. 3-24: "Cyclic performance of Strassburg-limestone derived sorbent over 1000 calcination and carbonation cycles: with Eq. 1 fitted lines. Every 50th point plotted except at the beginning (calcination times: 8 min run 1 and 4.5 min run 2)" [121].

EPPLE ET AL. [40] has investigated the economical impact of advanced Ca-based CO_2 sorbents on the CL process that is applied to a 1.000 MW power plant. It turned out that a product with a residual CaO conversion of 50% could reduce the cycling mass flows by 86% (1.800 t versus10.000 t) compared to a standard limestone with a residual CO_2 capture ability of 7%. The investment costs for the calciner could be lowered by 82% (30.1 Mio. € versus 173.5 Mio. €), the net efficiency of the power plant could rise about 0.6% points (43.25 % versus 42.6 %) and due to the higher efficiency fuel savings of 2.2 Mio. € per year would be achievable.

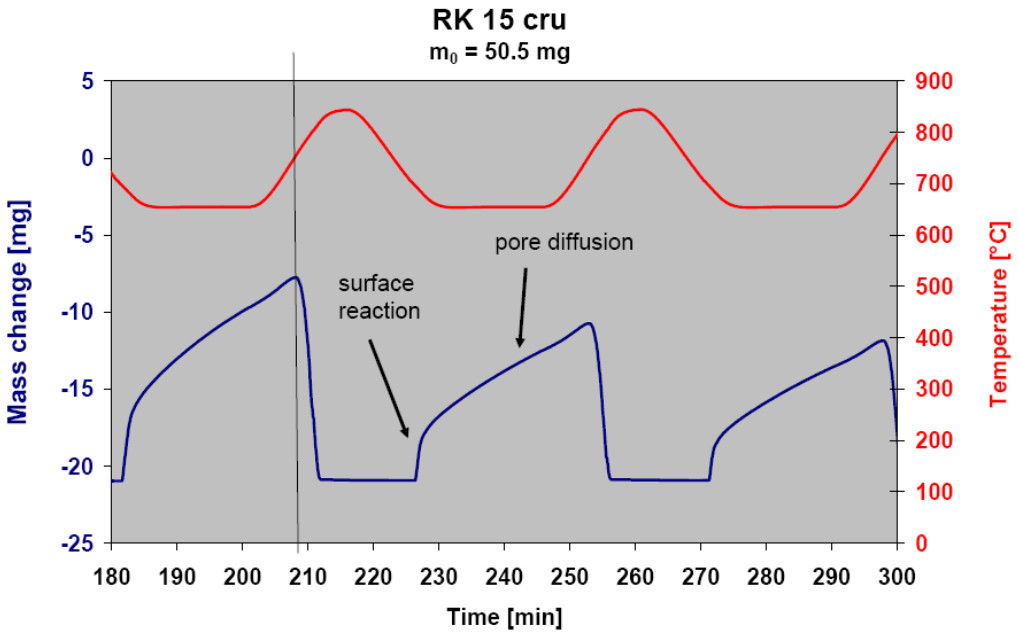

Fig. 3-25: Rate determining reaction steps within the cyclic carbonation/calcination of limestone. Only surface reaction and pore diffusion apparent. Figure taken from [140].

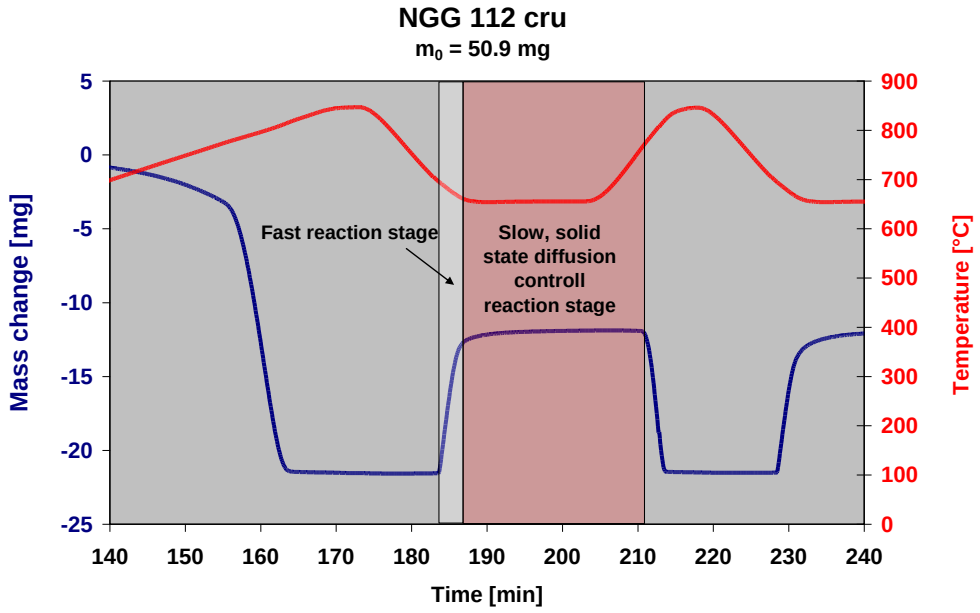

Fig. 3-26: Rate determining reaction steps within the cyclic carbonation/calcination of dolomite. Only surface reaction and solid state diffusion apparent. Figure taken from [140].

PACCIANI ET AL. [93] was able to synthesise a Ca-based CO_2 sorbent with a precursor method that had a ground structure of Mayenit ($Ca_{12}Al_{14}O_{33}$). This sorbent had an incredible mechanical strength and an increasing CO_2 capture ability over the numbers of CO_2 capture cycles. Cost neutrality regarding the CL process for this kind of sorbent was reported ([56]).

3.5 Approaches for Advanced Product

The test protocol for the determination of the CaO conversion has not been harmonised yet, leading to results of different work groups that are very hard to compare. Nevertheless, the most important publications of scientists around the world, trying to create improved products by special pre-treatments, doping, precipitation, agglomeration and sole-gel-processes, will be discussed and critically evaluated.

3.5.1 Extended Calcination as Pre-Treatment and Reactivation Step

MANOVIC ET AL. [82] investigated the effect of long calcination under a pure atmosphere of CO_2. He subjected about 3 g of different limestones with different origins, chemical composition and grain size into a tube furnace and exposed them to different temperatures (900°C, 950°C, 1000°C, 1100°C) and for different durations (6h, 24h, 64h). After the treatment, the samples were characterised in terms of specific surface area, pore volume distribution, morphology (SEM pictures) and, of course, the development of the CO_2 capture ability versus extended carbonation/calcination cycles.

The sorbents were collected from Canada (Kelly Rock), Spain (La Blanca) and Poland (Katowice). The chemical compositions can be seen in Fig. 3-27.

Compound	Kelly Rock	La Blanca	Katowice
Al_2O_3 (wt%)	1.0	< 0.10	0.24
CaO (wt%)	51.61	54.39	54.10
Fe_2O_3 (wt%)	0.37	< 0.01	0.09
K_2O (wt%)	0.27	< 0.02	0.06
MgO (wt%)	0.52	0.11	0.89
Na_2O (wt%)	< 0.10	1.07	< 0.20
SiO_2 (wt%)	3.70	< 0.10	0.85
TiO_2 (wt%)	0.06	< 0.03	< 0.03
Loss on fusion (wt%)	41.69	44.20	43.64
Sum	99.32	99.77	99.96

Fig. 3-27: Chemical Analysis of the pre-treated sorbents investigated by [82].

The TGA test condition were isothermal at 800°C. The atmosphere was switched between 100% N_2 (calcination) and 50% CO_2 (N_2 balance) for re-carbonation. The duration for both steps was 15 min.

Limestone from Canada and Poland showed an increasing CO_2 capture ability over 10 to 30 cycles after a pre-treatment at 1000°C in a 100% CO_2 atmosphere. After roughly 10 cycles the CO_2 uptake was higher than that of the original sample after 10 cycles. Limestone from Spain

did not show this behaviour; the performance was in all cases worse than the untreated stone. This was believed to be a result of the unusual high sodium content.

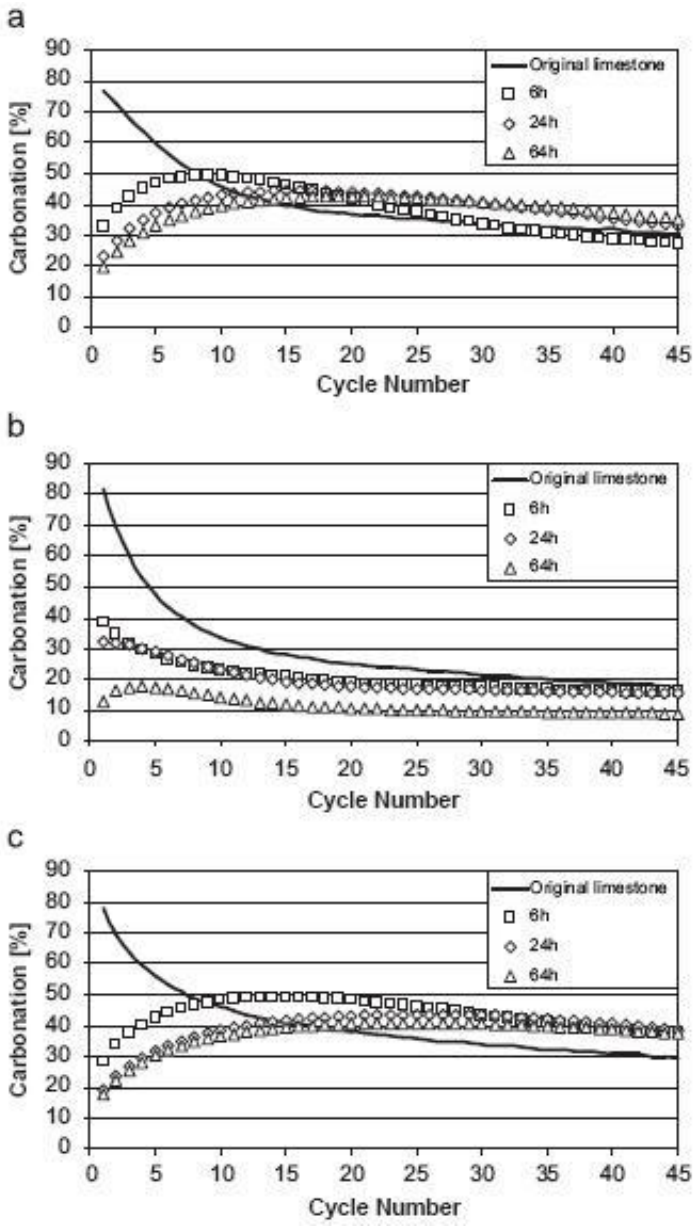

Fig. 3-28: CO_2 uptake of pre-treated products: "Carbonation–calcination cycles (isothermally 800°C, carbonation in 50% CO2 and calcination in 100% N2, each for 10 min) of limestone samples pre-treated for different durations at 1000 ◦C: (a) Kelly Rock, (b) La Blanca and (c) Katowice" MANOVIC ET AL. [82].

The observed effects were explained with the recrystallization of CaO in the presence of CO_2, that benefits the recrystallisation but does not enhance significantly bulk diffusion ([82]). Therefore, the "pre-treatment leads to formation of recrystallized CaO that is a very stable structure and prevents sintering during cycles. […] During the first cycle, carbonation takes place at that less-reactive surface and is limited by the processes in the hard skeleton. During

this step and following calcination, a less-stable structure (soft skeleton) of CaO, which is more reactive, is formed." MANOVIC ET AL. [82].

These findings might be explained according to chapter 2.9; a pore mouth blockage is prohibited by the formation of large pores while the inner surface is consequently reactivated by the high temperature and high CO_2 partial pressure during the cycling. However, it could be speculated that these outstanding results could be lowered significantly if lower CO_2 partial pressures and re-carbonation temperatures would be applied.

CHEN ET AL. [31] studied the effect of long thermal treatment of a limestone and a dolomite with the chemical composition given in Fig. 3-29.

composition (wt%)	Strassburg limestone	Arctic dolomite
CaO	53.7	30.51
MgO	1.25	21.25
Al_2O_3	0.19	0.17
Fe_2O_3	0.94	1.3
K_2O	0.08	0.04
Na_2O	0.02	0.15
SiO_2	0.94	2.12
loss on ignition	42.9	44.4

Fig. 3-29: Chemical composition of the products investigated by [31].

Both sorbents were thermally pre-treated at 1000 and 1100°C for 6 and 24 hours. Afterwards, the received materials were subjected to 1000 subsequent cycles of calcination and re-carbonation under isothermal conditions at 850°C. Carbonation was done under 100% CO_2 for 9 min while calcination was done under pure N_2 for 8 min. The results of his experiments are shown in Fig. 3-30. It can be noticed that only a long thermal pre-treatment resulted in the desired significant increase of CaO conversion. It is remarkable that the CaO conversion of the pre-treated products remained nearly unchanged at 18% for more than 1000 cycles compared to ~10% in case of the original materials.

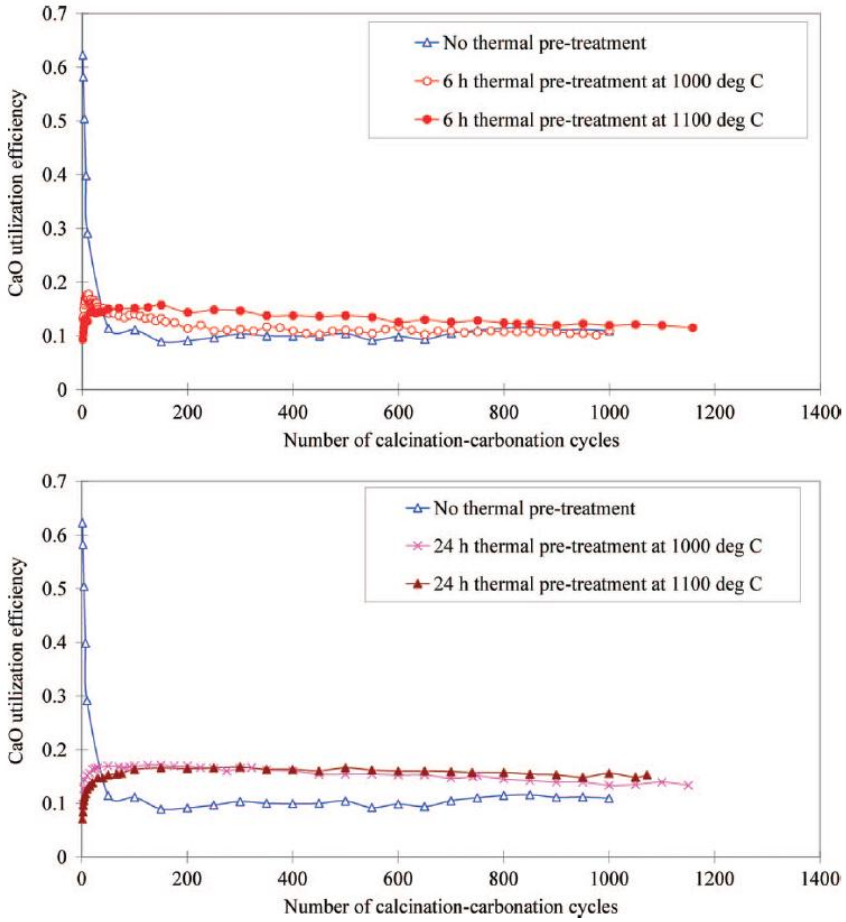

Fig. 3-30: Outcomes on Strassburg limestone. Figure taken from [31].

CHEN ET AL. [31] investigated also the effect of very long re-carbonation durations to study the effect on the following performance of the sorbent. The outcomes can be seen in Fig. 3-31.

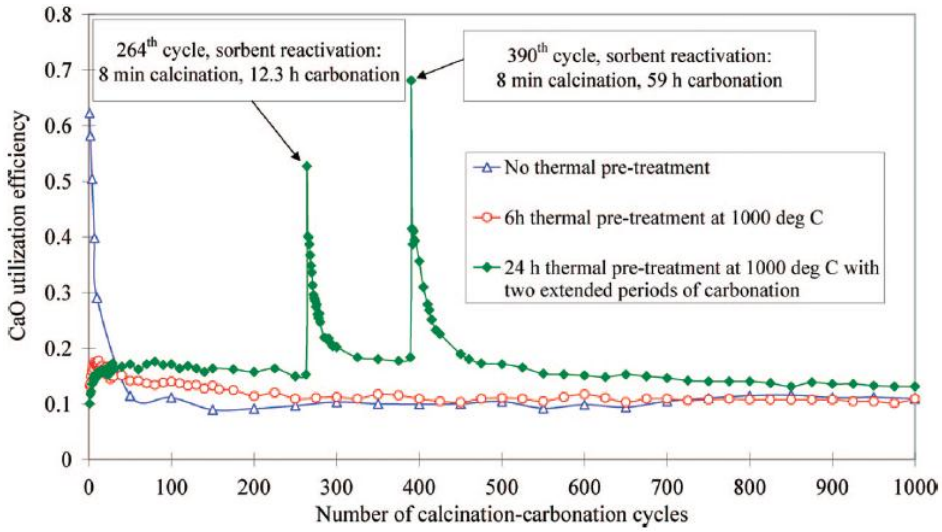

Fig. 3-31: Effect of very long re-carbonation for Strassburg limestone. Figure taken from [31].

This strategy resulted in a remarkable increase of CaO conversion for some cycles. However, it was noticed, that the sorbent tends very fast to reach its equilibrium CaO conversion again. Thermal pre-treatment lead in case of dolomite to a significant increase of the CaO conversion compared to the untreated sample for the first 50 cycles (see Fig. 3-32).

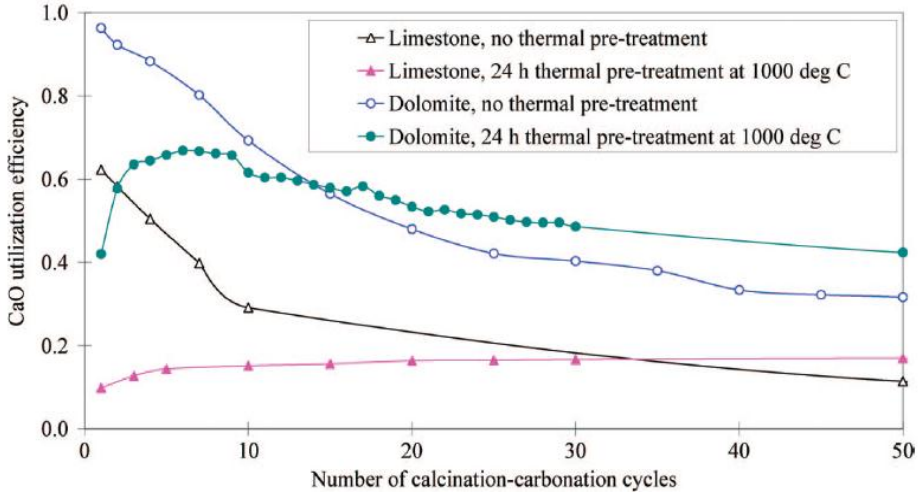

Fig. 3-32: First 50 cycles of dolomitic and calcitic sorbents with and without pre-treatment. Figure taken from [31].

It was figured out by CHEN ET AL. [31] that untreated and pre-treated dolomite showed a superior CaO conversion under the given test conditions. For example, the pre-treated dolomite showed an average CaO conversion for the first 30 cycles of 60%. This value refers to a specific CO_2 uptake of 25.4 g_{CO2}/g_{Oxide} and would be equal to a CaO conversion in lime of roughly 30%. Unfortunately, this gap in the performance is nearly completely lost after 300 cycles; the specific CO_2 uptake of the pre-treated dolomite was nearly equal with that of untreated limestone.

However, from a global point of view it seems like each set of test conditions causes an equilibrium uptake that is reached more or less rapidly and that depends on the history of the sorbent. Fig. 3-23, for example, illustrates the specific CO_2 uptake of different dolomites that have been tested under quite different conditions than in case of CHEN ET AL. [31].

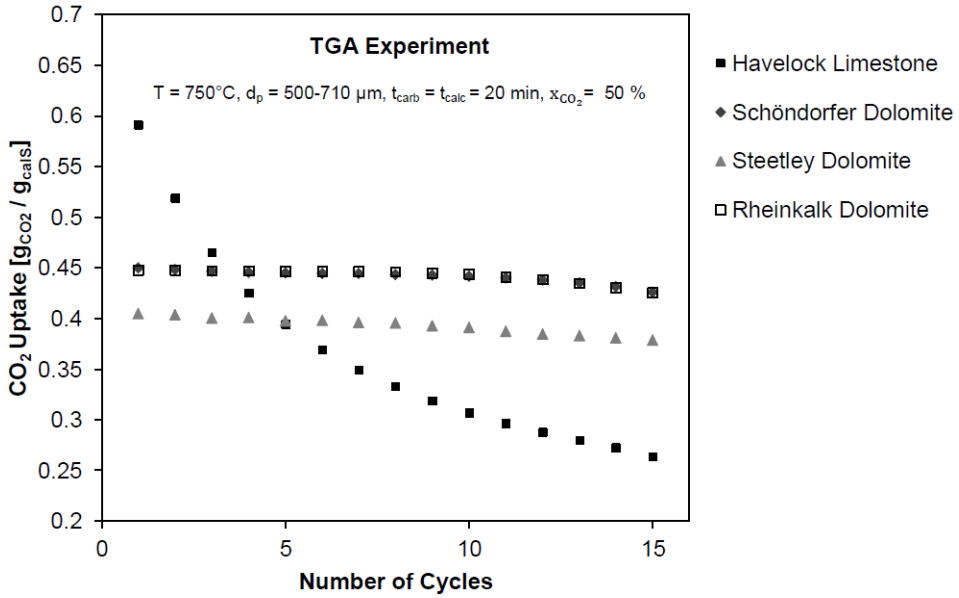

Fig. 3-33: CO_2 uptake of different dolomites. Note: Dolomite from Schöndorfer and Rheinkalk show a performance close to the theoretical maximum Figure received from [89].

It can be seen that a decrease of the temperature by 100°C causes the dolomites to show nearly 100% CaO conversion over the first 15 cycles.

By this, it is very likely that a fortunate or unfortunate constellation between test conditions and nature of the product cause the statement of some scientist that reactivation with CO_2 works HARRIS ET AL. [56]) or not SUN ET AL. [117].

However, the operators of the CL processes have to determine within which boundaries their utility can be operated. This information would have to be used, to determine the optimal conditions for the sorbent performance under TGA conditions resulting in a probably much improved real process performance.

3.5.2 Doping

Doping is probably one of the easiest procedures to modify the properties of natural occurring Ca-based CO_2 sorbents. Usually, a solution containing the dopant is sprayed equally onto the limestone. Another possibility is to suspend the limestone in a solution of the desired dopant.

During the calcination the dopants, like sodium, are likely to form local, low melting compounds that can be transported into the bulk of the particle[10] and distributed evenly. However, this will only be the case for a few dopants, especially alkali elements[11].

[10] A similar process is applied for the purification of Si. This process is called floating zone melting.

SALVADOR ET AL. [104] "prepared […] 20 wt.% aqueous NaCl and Na_2CO_3 solutions, which were then poured over prescreened limestone samples with a particle size range of 650–1675 µm. The amounts of solution used in TGA investigations were equivalent to 0.5, 1, 2 or 3 wt.% of salt in limestone. The wet mixture was blended for 20 min and dried overnight at 120°C" SALVADOR ET AL. [104]. TGA tests were performed under an atmosphere of 15% CO_2 in N_2 while calcination was done for ~10 min at 850°C and re-carbonation was done for ~50 min at 700°C.

SALVADOR ET AL. [104] found that the addition of Na_2CO_3 and NaCl resulted in a dramatic decrease in the overall CO_2 capture ability within the fluidised bed environment. On the contrary, he reported an increased CO_2 capture ability under TGA conditions for doping with NaCl (see Fig. 3-34).

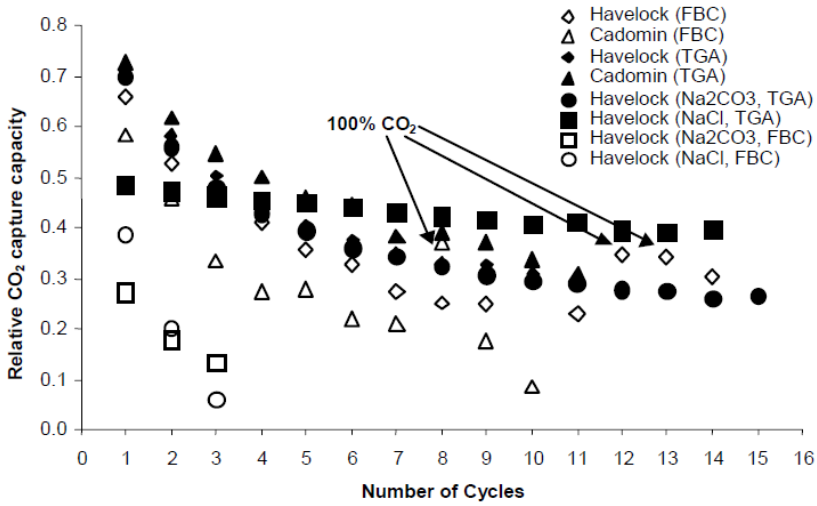

Fig. 3-34: CO2 uptake of behaviour of different limestones that were doped. Figure taken from [104].

This observation might be contributed to the mild TGA test conditions consisting of long re-carbonation durations and low calcination temperatures. However, these conditions are far from reality and could explain why this effect was not recognised during his FB experiments.

FENNELL ET AL. [43] also tried doping with $NaCO_3$ and NaCl. He added 10 g of limestone to a flask with 400 ml of a solution of the salts and let it stir for 36 h, afterwards the limestone was dried at 70°C overnight. Only samples treated with a low concentrated Na_2CO_3 solution (0.1 M) yielded in a slower decay in the CO_2 capture ability during the tests in a small fluidised

[11] Note that this process could alter the sorbent properties unintentionally if according impurities or an unfortunate combination of impurities would be present in the CL process.

bed; higher concentrations of both dopants resulted in an rapid decrease of the CO_2 capture ability. The experiments were carried out isothermally at 750°C while calcination was conducted under a pure flow of N_2 and the re-carbonation was done using an unknown concentration of CO_2. Both steps took about 500 s.

In summary, it can be stated that doping with sodium salts might show slight advantages, if the introduced amount of dopant is very low and the test conditions are quite soft. Positive effect for CFB plants are questionable.

3.5.3 Hydrolysis

SUN ET AL. [120] tested 13 different substances ($Al(NO_3)_3 \cdot 9H_2O$, Al_2O_3, Ca-acetate, SiO_2 gel, SiO_2 sand, kaolinite, ZrO_2, MgO, TiO_2, $MgSO_4 \cdot 7H_2O$, NaCl, $MgCl_2$, $CaCl_2$) for their suitability to improve the CO_2 capture ability of lime and limestone. In total 41 different experiments were carried out. He pre-weighed the lime and the modifier precursor (~1.5g) and mixed them into 70 ml of deionised water. 5 ml of ethanol were added as dispersant. This mixture was stirred over a heating plate at 150°C until dry.

Cycling was done in a small FB under isothermal conditions at 850°C. The atmosphere was switched between 100% N_2 to 100% CO_2 for calcination and re-carbonation respectively. Re-carbonation was stopped as soon as the slow reaction stage was recognised.

The investigations of him lead to the conclusion that “most of the additives [showed] disappointing results” SUN ET AL. [120]. Only a mixture of CaO and Al_2O_3 in a molar ratio of ~1:1 resulted in promising outcomes regarding the free CaO conversion (see Fig. 3-35).

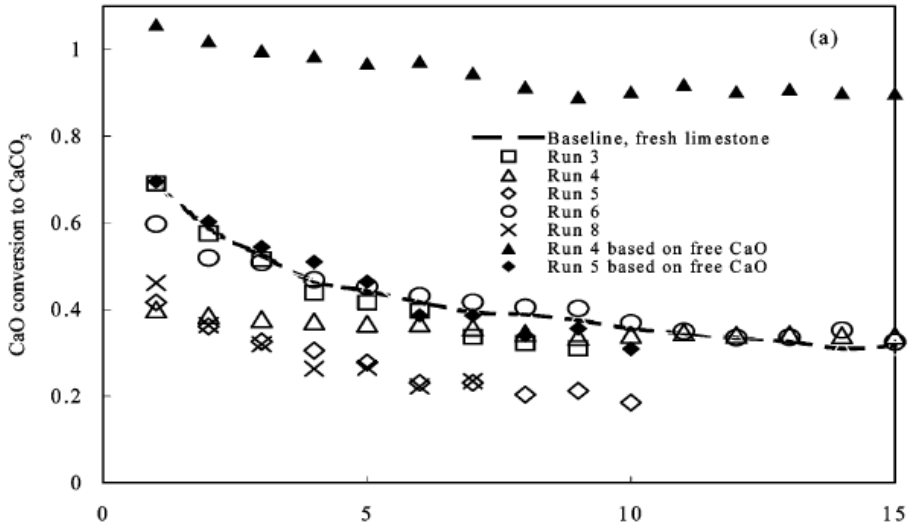

Fig. 3-35: CaO conversion of synthetic Ca-based sorbents for CO_2 separation versus cycle number. Run 3: 36.3 wt % Limestone + Al_2O_3, Run 4: 37 wt % calcined lime + Al_2O_3, Run 5: 53.7 wt % calcined lime + Al_2O_3, Run 6: 83.1% calcined lime + Al_2O_3, Run 8: 81.7 wt % calcined lime + acetate + Al_2O_3. Figure taken from [120].

The amount of free CaO in this sample was very high because Mayenite was the predominant phase. It becomes obvious that the performance of this most promising sample is as good as fresh limestone if it is referred to the same mass.

PACCIANI ET AL. [93] tested the influence of different amounts of $Al(NO_3)_3$ and $Mg(NO_3)_2$. He used a "reagent grade powdered CaO (Fisher) [and] added [it] to a solution of $Al(NO_3)_3$ (or $Mg(NO_3)_2$) in a mixture of 75 vol% water and 25 vol% 2-propanol. The amounts of CaO and salt were chosen in such a way that the mass ratio of CaO to inert in the final sorbent was 25:75, 50:50, 63:37, 75:25, or 85:15. The solution was stirred at 75°C at 700 rpm for 1 h and then dried overnight in an oven at 120°C. When dry, the cake was crushed into a fine powder and roasted at 500°C in an oven to decompose each nitrate to its oxide. […] The powder was then brought into pellets by adding water and afterwards calcined at 850, 900 or 1000◦C in an oven for 1.5 h" PACCIANI ET AL. [93]. The sieved pellets (500-700 µm) were tested in a small fluidised bed under isothermal conditions at 750°C. Calcination and re-carbonation were done under an atmosphere of pure nitrogen and 15% CO_2 (N_2 balance) and for 500 s.

The sorbents named HA-75-850 (75% CaO, initialy calcined at 850°C) and HA-85-850 (85% CaO, initially calcined at 850°C) showed an even or increasing CO_2 capture ability while the other approaches were worse than a natural occurring limestone (see Fig. 3-36).

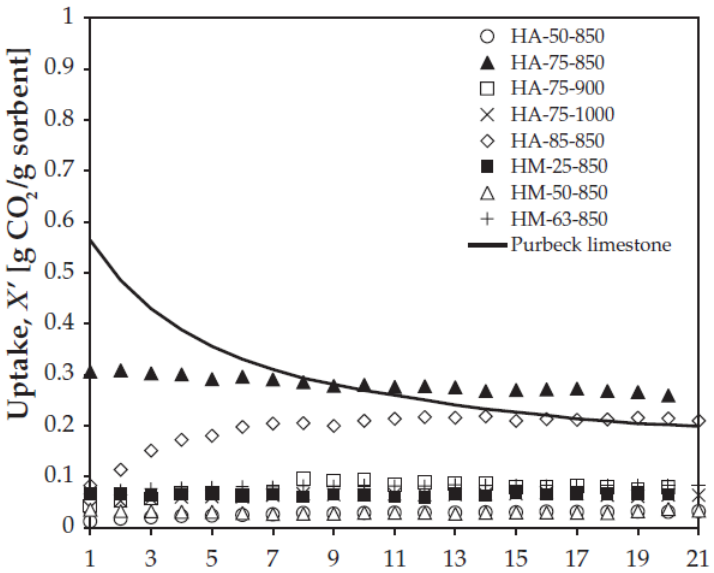

Fig. 3-36: CO_2 uptake of different synthetic syntphetic Ca-based CO_2 sorbents prepared by hydrolysis (H) and with Mayenite (A) or Magnesium Oxide (M) as basic structure. Figure taken from [93].

However, the advantage over a natural sorbent was minor under the given conditions. Nevertheless, the experimental setup was used as well to observe the attrition resistance (see Fig. 3-37).

Table 2. Loss in mass of selected synthetic sorbents prepared by hydrolysis during attrition tests

Sorbent	Mass loss percent after 20 cycles
HA-50-850	1.0±1.5
HA-75-850	9.0±1.9
HA-85-850	9.0±0.9
HM-50-850	5.0±1.1
HM-63-850	22.0±2.6
Steetley dolomite	24.0±7.1

Fig. 3-37: Attrition behaviour of different Ca-based CO_2 sorbents compared to a dolomite reference. Figure taken from [93].

It can be seen that Mayenite supported sorbents show somehow a bigger resistance towards attrition than a normal dolomite. It should be noted that dolomites usually show significant decrepitating on a rapid increase of temperature. This effect was not investigated resulting in an unknown reference point.

Besides the investigation of CO_2 uptake and hardness, PACCIANI ET AL. [93] also varied the CO_2 concentration during the re-carbonation step. It turned out the sample named HA-85-850 responses extremely positive to this change of conditions (see Fig. 3-38). The highest CO_2 uptake measured after 60 cycles was 0.45 $g_{CO2}/g_{Sorbent}$. The reason for this unusual behaviour

was not explained. Perhaps it is a beneficial combination of sorbent properties and process conditions again.

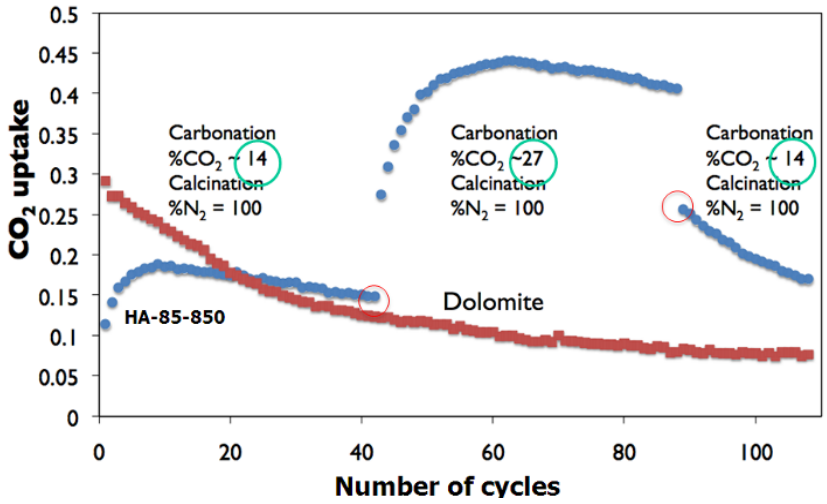

Fig. 3-38: Increased CO_2 uptake due to a higher CO_2 concentration during the carbonation of a synthetic sorbent with 85% CaO. Theoretical maximum CO_2 uptake of this sorbent was 0.67 $g_{CO2}/g_{Sorbent}$. Figure taken from [35].

However, it stays unclear why no response of the behaviour of the dolomite was observed.

ROESCH ET AL. [97] studied the performance of a CaO supported caesium sorbent. He prepared a slurry of analytical grade CaO and a 50% CsOH solution. After diluting this mixture by 100:1 with deionised water, the suspension was heated and stirred till all water was evaporated. Afterwards, the received cake was grounded, dried and calcined at 750°C for 5 h. The received product had a grain size smaller than 100 µm and a share of 20 wt % Cs. The mean particle diameter was between 10 and 20 µm. Based on single adsorption experiments done at different temperatures with a not specified CO_2 partial pressure for 5 h ROESCH ET AL. [97] reported an CO_2 uptake of 66% $g_{CO2}/g_{Sorbent}$ at 600°C. It should be noted that even natural sorbents with this grain size perform equal or better, under similar conditions for the first cycle without the efforts of using costly Cs.

3.5.4 Co-Precipitation

The process of co-precipitation is very similar to hydrolysis: CaO is put together with a dopant into water. There, the dopant, usually a highly soluble salt, is dissolved and the CaO reacts to $Ca(OH)_2$. Following, a flow of CO_2 is subjected through the slurry causing a decrease of the pH-value, the formation of carbonate ions and therefore the precipitation of $CaCO_3$. During this process hardly soluble salts of the dopant, e.g. $Al(OH)_3$, are precipitated

as well. Consequently, the only difference between hydrolysis and co-precipitation is the use of CO_2 for the precipitation of Ca and dopant salts.

FLORIN ET AL. [45] investigated the possibility to produce Ca-based sorbents with improved hardness and CO_2 capture ability by co-precipitation in a slurry bubble column. He used $Ca(OH)_2$, $Al(NO_3)_3 \cdot 9H_2O$ and 2-propanol as dispersant. The mean particle diameter he was able to achieve was 2.3 µm. TGA tests were done at a constant atmosphere of 15% CO_2 in N_2. Calcination and carbonation were done at 900°C for 5 min and 650°C for 10 min respectively. It should be noted that these temperatures refer to the kiln temperature. In order to test these materials in a small fluidised bed he used an extruder to conduct a shaping.

Fig. 3-39 shows the comparison between different kinds of co-precipitated products and a PCC sorbent.

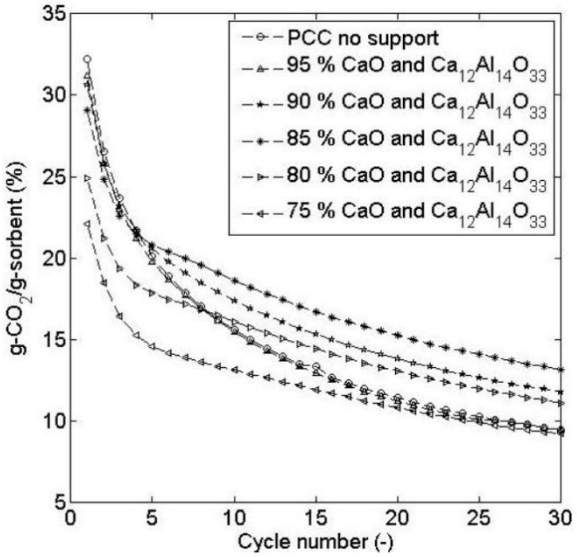

Fig. 3-39: Comparison of the CO_2 uptake of different co-precipitated products and a PCC sorbent. Figure taken from [45].

It can be seen that the aluminium doped sorbents show a significant better performance after five cycles of calcination and re-carbonation.

However, the performance of these products after a shaping step that would have enabled the comparison with the performance of coarse materials was not reported.

PACCIANI ET AL. [93] used a slightly different route to receive co-precipitated products. He started from a solution of $Ca(NO_3)_2$ and $Al(NO_3)_3$ or $Mg(NO_3)_2$ which he mixed in the desired ratio. Afterwards, he added a solution of $Na_2(CO_3)$ to precipitate $CaCO_3$ and $Al(OH)_3$ or $MgCO_3$. The precipitate was washed several times with deionised water until no sodium was recognised anymore in the washing solution (detection via the conductivity). The received solid was dried at 150°C and calcined at 850°C. This process led to the formation of

agglomerates in case of the use of $Al(NO_3)_3$. Co-precipitates with Mg did not show any agglomeration. These agglomerates were sieved to 500 to 700 µm and tested in a fluidised bed described in subsection 3.5.3.

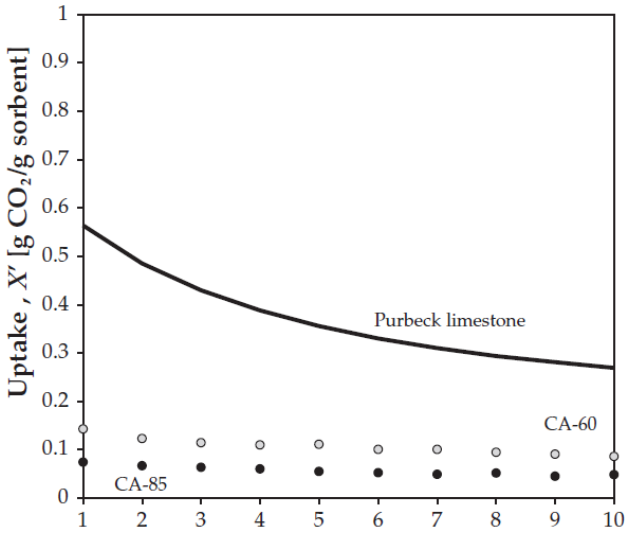

Fig. 3-40: Comparison of the CO_2 uptake of Al co-precipitated products and a Purbeck limestone. Figure taken from [93].

As illustrated in Fig. 3-40 the results of this approach were disappointing; the performance of these synthetic products was more than 66% below the natural limestone after 10 cycles.

It should be noted that PACCIANI ET AL. [93] observed agglomeration upon calcination of a mixture between CaO and Al_2O_3 during 1.5 h at 850°C. This can only be explained by some sort of sintering phenomena. This indicates that the addition of aluminium might not prohibit sintering as discussed very often in the literature.

3.5.5 Ca-Acetate Precursor

LI ET AL. investigated the use of acetic acid to modify natural limestones ([71]) and dolomites ([72]) to receive improved sorbents. The same procedure was used for the preparation of the two modified sorbents; 50 vol % acetic acid solution was put together with a limestone or a dolomite with a grain size smaller than 125 µm in a beaker. The chemistry for the two original products is given in Table 3-4. The molar ratio between acetic acid and Ca or (Ca + Mg) was 1.5:1. After 2 h of reaction time the beaker was put into a drying cabinet at 120°C.

However, LI ET AL. did not reveal how much of the limestone or dolomite was dissoluted by the acetic acid. The molar ratio would have enabled the dissolution of the original sorbent up to 75 wt%. Another thing one has to keep in mind and that was not discussed by LI ET AL. is

the fact that calcium acetate is a highly soluble salt (374 g/l) which will precipitate from the solution on evaporation of water.

Table 3-4: Chemistry of the natural sorbents Li et al. used for his investigations for improved sorbents produced by acetic acid. Values taken from [71] and [72].

	CaO	MgO	Al_2O_3	Fe_2O_3	SiO_2	Others	LoI
Limestone	54.70	0.36	0.05	0.04	1.18	0.52	43.15
Dolomite	30.11	20.41	0.44	0.20	2.01	0.51	46.32

Cycling investigations were carried out in a fixed bed reactor under altering temperatures and atmospheres. Calcination was done for 15 min between 920 and 1100°C under an atmosphere of 80% CO_2 and 20% O_2 while the re-carbonation was done for 20 min between 550 and 750°C under an atmosphere of 15% CO_2 and 85% N_2.

Fig. 3-41 and 3-42 show a good summary of the results achieved by LI ET AL..

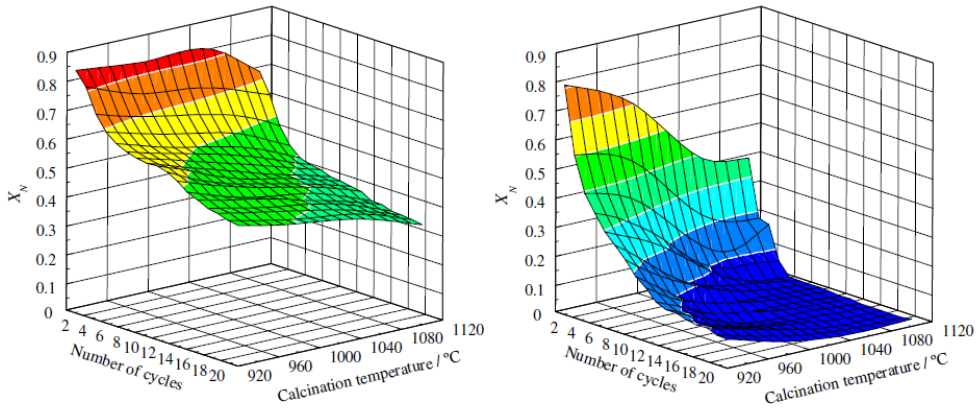

(a) Modified limestone (b) Original limestone

Fig. 3-41: Performance of limestone modified with acetic acid. Figure taken from [71].

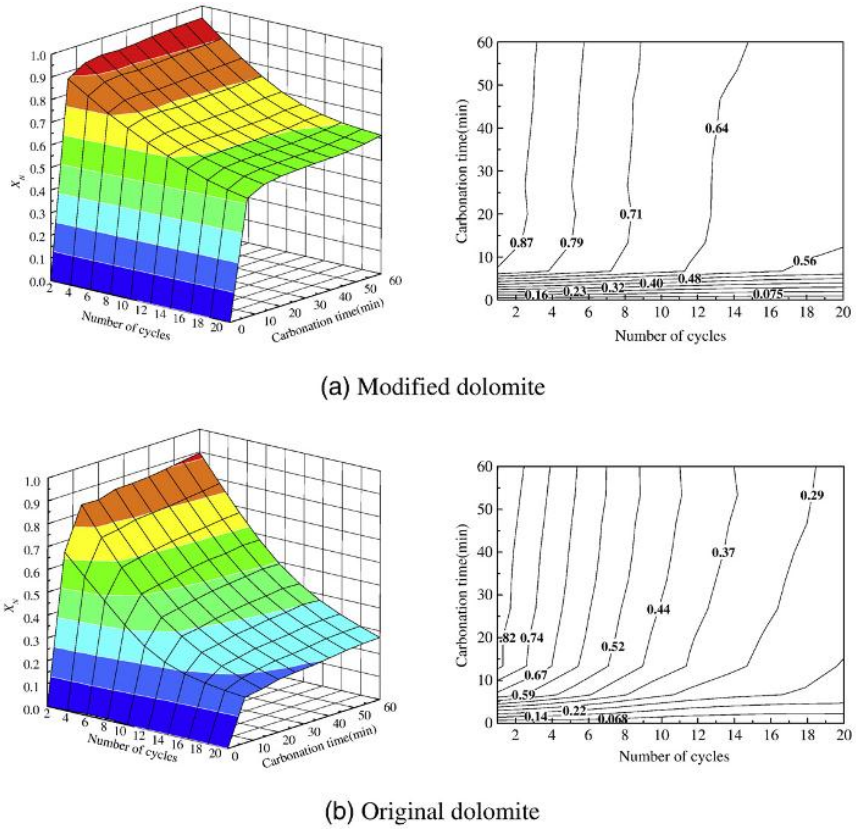

Fig. 3-42: Comparison of original and modified dolomite. Carbonation and calcination were done at 650 and 920°C respectively. Figure taken from [72].

LI ET AL. [72] explained that the outstanding behaviour of the modified sorbents is an effect of textural changes in the sorbent. They reported smaller elementary grains and higher specific surface areas for these sorbents. Even though, the decay rate in the specific surface area in case of the limestone (see Fig. 3-43) seems to be comparable. However, it takes place at an elevated plateau.

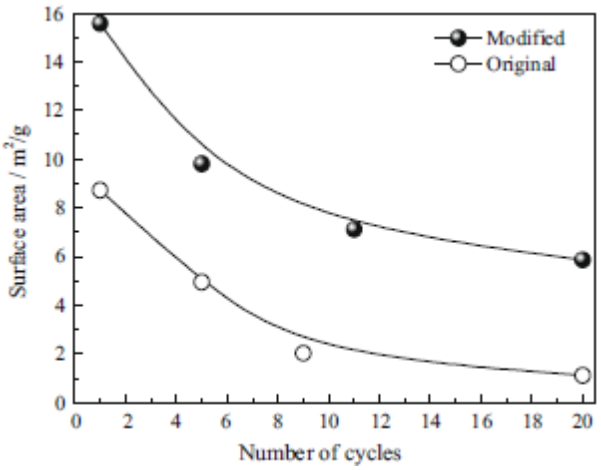

Fig. 3-43: Comparison of the loss of surface area during cycling for the case of original and acetic acid modified limestone. Figure taken from [71].

However, LI et al. provoked probably two effects that they did not include in their explanations. First, the process of re-crystallisation causes most likely a purification of the product. Secondly, calcium acetate is a very fine grained, fragile salt that will cause a much smaller grain size distribution of the CaO of the modified sorbent than that obtained from the original sample.

3.5.6 Sorbent Derived from Nano $CaCO_3$

Nano $CaCO_3$ is produced by the precipitation of $CaCO_3$ (PCC) by the introduction of CO_2 into a slurry of $Ca(OH)_2$. Depending on the process conditions, the crystal shape and size can be influenced leading to the wide variety of appearances discussed in paragraph 2.2.1. As well, it is possible to introduce doping atoms into the crystal system of PCC.

HARRIS ET AL. [56] investigated the adaptability of nano-sized $CaCO_3$ for the CL process. He used $CaCO_3$ from the Nanomaterials Technology Pty Ltd (Singapore) which had an apparent particle diameter of 40 nm. Carbonation and calcination were done with 5 mg $CaCO_3$ equivalent at 650°C and 850°C and under an atmosphere of 15% CO_2 in N_2 and 100% N_2. Carbonation and calcination took 20 and 10 min respectively. In addition to simple carbonation/calcination tests, the influence of pre-sintering and extended carbonation time was tested.

HARRIS ET AL. [56] reported that the material had no “skeleton” so the small grains grew together over the numbers of cycles. Therefore, it is not surprising that the CO_2 capture ability decay is very similar to “normal” limestone (see Fig. 3-44). Remarkable is the fact that the material that was pre-sintered for 12 h at 900°C first showed a rise in the CO_2 uptake followed by a decreases much slower than the untreated one. However, a residual CaO conversion of about 20 % was reached regardless if it was pre-treated or not.

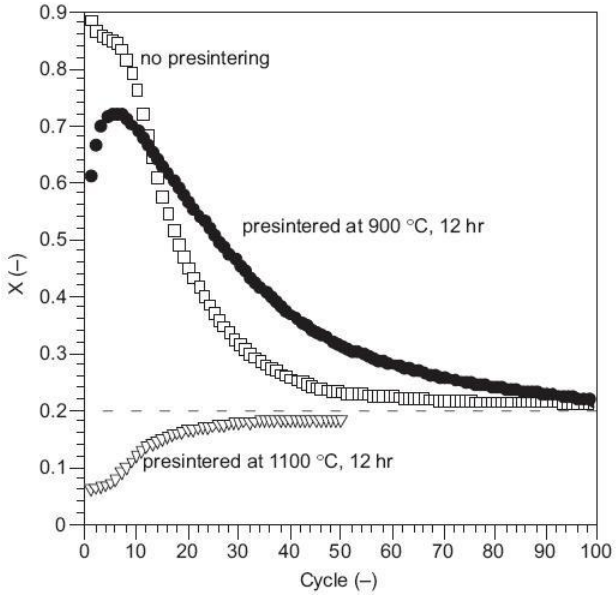

Fig. 3-44: HARRIS ET AL. [56]: Calcination/carbonation cycles for nano-sized $CaCO_3$ with a mean initial diameter of 40 nm

HARRIS ET AL. [56] explained this outcome: "The decay asymptote represents the establishment of an equilibrium between the pore volume and surface area loss during thermal sintering; and the pore volume and surface area regeneration as a consequence of a solid-state diffusion mechanism, and the subsequent release of CO2 in the next calcination cycle" HARRIS ET AL. [56]. This explanation is supported by the experimental outcome that a complete re-carbonation of CaO derived from nano-sized $CaCO_3$ is possible if the duration of re-carbonation is 24 h. Even though, 4 h might be enough considering the kinetic of re-carbonation that was reported.

The work done by HARRIS ET AL. [56] indicates that normal PCC might not offer any advantages over natural sorbents. However, the specific introduction of impurities could lead to the desired success.

3.5.7 Cement Granules

MANOVIC ET AL. [80] investigated the long term behaviour of pellets supported by calcium aluminate cement. He screened various cement types in a pre-study ([81]) concluding that calcium aluminate cements show the most promising impact on the CO_2 capture ability. In addition, he concluded that bentonite cements are not favourable because of the formation of calcium-silica compounds with low melting points; $Ca_5(SiO_4)_2CO_3$ was reported as dominant phase. MANOVIC ET AL. [80] prepared the granules by calcining an impure limestone (see Fig. 3-45) with a grain size between 250 and 1400 µm at 850°C for 2 h. This material was mixed

with a calcium aluminate cement that contained ~71% Al_2O_3, ~28% CaO and ~1% impurities, in a ratio of 90% CaO and 10% cement. Water was added until a mortar like gel was received that was shaped by the extrusion through a 1 mm sieve. After air-drying for 24 h, the pellets had a reported diameter of 800 µm. Additionally, pellets with a diameter of ~10 mm were prepared to assess the mechanical strength.

component	content
SiO_2, wt %	5.47
Al_2O_3, wt %	1.54
Fe_2O_3, wt %	0.61
TiO_2, wt %	<0.03
P_2O_5, wt %	<0.03
CaO, wt %	50.67
MgO, wt %	0.55
SO_3, wt %	<0.10
Na_2O, wt %	<0.20
K_2O, wt %	0.35
Ba, ppm	618
Sr, ppm	272
V, ppm	<50
Ni, ppm	<50
Mn, ppm	1132
Cr, ppm	<50
Cu, ppm	36
Zn, ppm	78
loss on fusion, wt %	40.48
sum, wt %	99.98

Fig. 3-45: Chemical composition of Cadomine limestone used for the production of cement granuales. Figure taken from [80].

TGA tests were done isothermally at 800°C. Calcination and re-carbonation were carried out for 10 minutes under an atmosphere of 100% and 50% CO_2 (balance N_2) respectively.

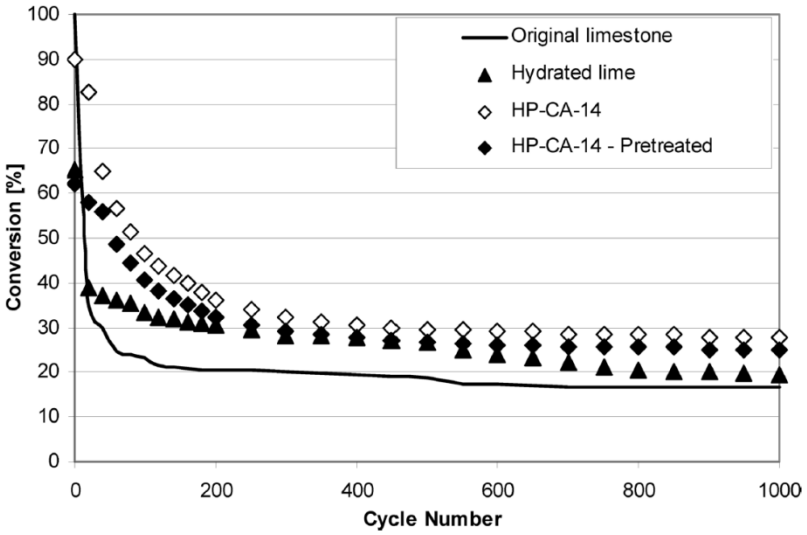

Fig. 3-46: CaO conversion for granules of hydrated lime and aluminate supported CaO pellets. The original limestone is also shown as reference. Figure taken from [80].

MANOVIC ET AL. [80] was able to demonstrate that his pellets had an outstanding performance compared to the original limestone under the given test conditions (see Fig. 3-46). As well, he

showed that the produced particles, which had a diameter of 10 mm reduced their mechanical strength on calcination. After 300 cycles the mechanical strength was lowered further. A comparison with normal limestone was not given. As well, it should be kept in mind that cement granules need a certain diameter to develop their full hardness. Therefore, the hardness tests done should not be overemphasised because it is very likely that the small cement supported sorbents are much more fragile.

3.5.8 Outlook

A lot of approaches for the production of synthetic, or at least improved, CL sorbents have been tested so far. However, even "promising" results reported are hard to compare and to evaluate because of the absence of a common TGA test protocol. Indications provided by the work of all authors suggest a huge impact on the measured sorbent performance by the process conditions. In addition, the residual CO_2 capture ability that is reported for all sorbents, might only be the equilibrium between loss of surface area during the calcination and its regeneration during the next re-carbonation step. Consequently, the chemistry of the sorbent determines the rate of the loss of surface area during the calcination and therefore the drop of CO_2 uptake during the cycling and the residual CaO conversion. The negative effect of elevated contents of alkali metals, for example, might be compensated by lower calcination temperatures. In case of a faster diffusion of CO_2 through a product layer of $CaCO_3$ such products might even outperform sorbents with a low amount of impurities under special test conditions.

However, a thermal pre-treatment, especially of dolomites ([82]) seems to offer good opportunities for high CaO utilisations and hard products. Another, more expansive approach for which good results were reported ([45]) is the intentional introduction of aluminium and therefore the formation of Mayenite.

3.6 Reactivation of Spent Sorbent

Two different reactivation processes have to be distinguished: Mechanical and chemical reactivation. Mechanical reactivation describes the recycling of fines that are produced within the fluidised bed and lost through the cyclones. These fine could be agglomerated or dissoluted and precipitated for a re-coarsening and reintroduction into the CL system.

Chemical reactivation means that the sorbent that is taken out of the system, either through the bleed or the cyclones and filters, is treated in a way that it could be reused for the CL process or for the flue gas desulfuration (FGD) unit ([37]). If the material should be used for FGD the reactivation step "is allowed" to destroy the material mechanically. Actually, the finer the particles become, the better it is for the FGD. However, if the chemical reactivation is meant to increase the CO_2 capture ability or to remove impurities from the sorbent, the particles should stay intact and should not lose any of their mechanical strength.

3.6.1 Mechanical Reactivation

The coarsening of fines, e.g. attrition of sorbent particles, is a very delicate task because technologies for producing the desired CL grain size are rare.

CURRAN ET AL. [34], for example, developed a melting process that uses an eutectic in the system CaO-$CaCO_3$-$Ca(OH)_2$. He reported that pressures between 21 and 69 bar and temperatures between 650 and 760°C would be sufficient to receive a melt that could be prilled. The grain size of the particles after spraying the melt into a prilling tower could be 0.6 to 2 mm. However, industrial handling of a molten salt under such high-pressures and at the given temperature is tremendously expensive or even hardly possible.

Agglomeration can be done industrially by rotating plates, mixers or in fluidised beds. Mechanisms are various and include VAN-DER-WAALS forces, electrostatic forces, solid and liquid bridges and geometrical surface interactions, e.g. interlocking ([55]). During the agglomeration process a constant growth and destruction of particles up to a certain diameter is observed ([94]). However, if particles have achieved a critical diameter and the process is not selectively destroying coarse particles, e.g. by the use a special design, a constant growth is noticed leading to bigger and bigger particles. A process used within the lime industry is the agglomeration of limestone with hydrated lime in a rotating disk (see Fig. 3-47). Hydrated lime and limestone are premixed and water is added successively to conduct the agglomeration.

Fig. 3-47: Rotating dishes used in the lime industry for the production of $CaCO_3$ granules.

At a certain point, the first formation of granules can be observed. The smallest, stable particles received from the process have a diameter of ~1 mm. In case of a change of the raw materials, the optimal ratio between $CaCO_3$, $Ca(OH)_2$ and water has to be determined again empirically.

During an extrusion process, material with a high viscosity, e.g. mortar, is forced through a die that shapes the mass into a desired two-dimensional geometry. Depending on the nature of the material and the die used, e.g. a sieve, even very small shaping dimensions can be realised. Moreover, strengthening of the particles usually includes drying and/or additional chemical reactions like carbonation or calcination.

A dissolution/precipitation process might also coarsen fines. CaO reacts in water to $Ca(OH)_2$ that can react to $CaCO_3$ in the presence of carbonate ions. The size of the received particles can be adjusted from nano-calcium carbonate (PCC) with an average diameter of 40 nm up to some millimetres, in special cases even centimetres in the case of a controlled crystal growth. Especially the last case is worth mentioning: Hard water (water containing a too high amount of Ca^{2+} and HCO_3^-) is treated with $Ca(OH)_2$ to transform the hydrogen carbonate into carbonate. By this, a supersaturated $CaCO_3$ solution is formed. This water is directed through a fluidised bed of sand on which $CaCO_3$ is precipitated and slowly growing. At the end of the process, perfectly round grains with a narrow particle size distribution and an extreme hardness are received. These grains are called “Reaktorkorn”. Unfortunately, this product loses its entire hardness on calcination.

Melting, agglomeration, extrusion and dissolution/precipitation are processes that could be used to reshape fines into useful CL sorbents again. All processes react sensitive towards changed raw materials. Consequently, a need of empirical investigations to find the optimal operating conditions and, as well, the best after treatments is inevitable. Unfortunately, up to the mid of 2011 there was no CL process operated with coal, delivering a suitable attrition to perform this kind of tests. Besides shaping processes, purification processes would have to be considered as well.

3.6.2 Chemical Reactivation

Chemical reactivation could be done either to regain the CO_2 capture ability of the sorbent or to purify the CL sorbent bed from impurities like sulphur. Both possibilities shall be explained in the next passages.

Based on the experience of the FGD, water and water vapour is usually discussed as reactivation substance ([74], [117], [79]). It is reported that this step could lead to a superior SO_2 sorbent ([16]). Also a higher reactivity towards the capture of CO_2 is reported ([137]). These experiments were all conducted within a thermo-balance, therefore the change in the mechanical stability was never considered. According to the discussion in subsection 2.2.3, CaO reacts with water according to a mechanism proposed by HEDIN. Due to this mechanism fine particles are always formed during the hydration of lime. Only if high temperatures and a high H_2O partial pressure are applied, annealing of the $Ca(OH)_2$ can take place leading to coarse portlandite particles. However, the intermediate stage of very fine particles arranged loosely cannot be avoided. This fact requires a very special process layout to avoid a complete loss of the sorbent due to the production of fines; a process proposed by MATERIC ET AL. [85] might give the solution to this problem.

MATERIC ET AL. [85] proposed a process called Superheated Dehydration (SD); a “spent” sorbent particle is cooled down to 300°C after each third calcination/carbonation cycle and treated for 45 minutes in an atmosphere of 25% steam (N_2 balance). After this hydration, the atmosphere is changed to 100% CO_2 and the sample is heated up to 520°C and maintained at this temperature for 25 min (annealing time) before it is heated further to 620°C where it dehydrates completely (see Fig. 3-49).

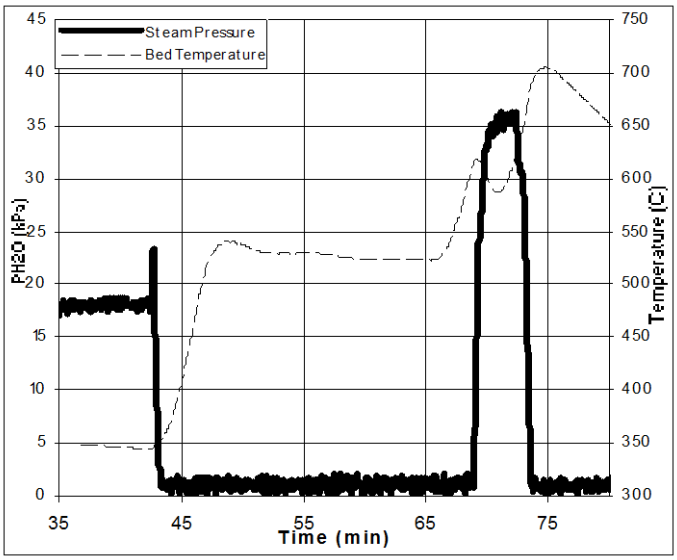

Fig. 3-48: Temperature and steam development during the SD process. Figure taken from [85].

However, the start of the dehydration depends on the CO_2 partial pressure (see Fig. 3-49).

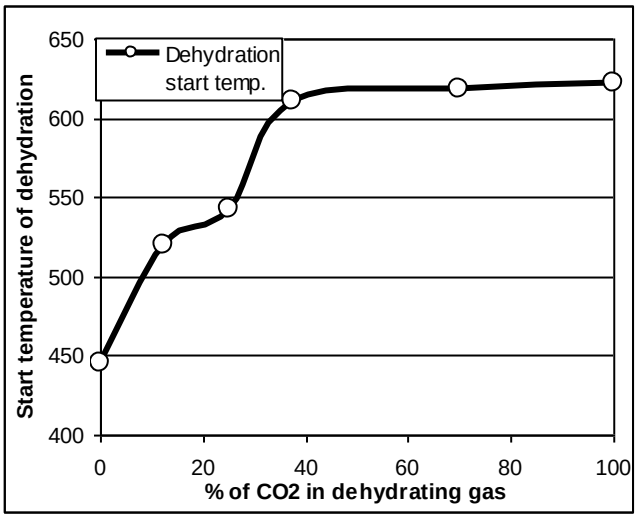

Fig. 3-49: Start of the decomposition of $Ca(OH)_2$ versus the partial pressure of CO_2. Figure taken from [85].

Consequently, after the decomposition of $Ca(OH)_2$ carbonation takes place immediately. MATERIC ET AL. [85] reported significant CaO conversion reactivation effects and a much lower rate of the production of fines during the cycling in a fluidised bed compared to a conventional hydration step and only a minor increase compared to the original sorbent. His explanation for the observed behaviour is the annealing of $Ca(OH)_2$ during the superheated state. This description corresponds to know-how available in the lime industry. However, a fast decrease of the CO_2 capture ability after the reactivation was reported, causing the repetition of the reactivation after each 3rd cycle. Nevertheless, the SD process might be the

only opportunity so far for the reactivation of Ca-based CL sorbents in terms of increasing the CO_2 capture ability again.

In general, chemical bound impurities of the CL sorbent can only be removed easily, if they can be decomposed thermally into a solid and gas. The only impurities which fulfils this requirement is sulphur. However, sulphur bound in the form of anhydrite is very stable and will melt at 1460°C (see subsection 2.2.4), but if reducing atmospheres are applied $CaSO_4$ can be reduced to $CaSO_3$ that decomposes at temperatures higher than 960°C ([67]).
SUN ET AL. [120] investigated the decomposition of $CaSO_4$ in the presence of CO. He reported that the anhydrite he used was fully decomposed at a temperature of 950°C and a molar ratio between CO and CO_2 of 0.12 (11% CO and 89% CO_2). Furthermore, he explained that a share of CO during the calcination did not yield in improved CO_2 capture abilities, if a co-capture of CO_2 and SO_2 was implemented during the carbonation. Nevertheless, this process could be used for a batch wise purification of the CL sorbent. WHEELOCK ET AL. [132], for example, proposed a process for the production of high grade CaO by the reductive thermal decomposition of $CaSO_4$. He claimed that his process is enabling a fast and effective decomposition of $CaSO_4$. By this, a split stream of the masses cycled in the CL process could be treated continuously in such a fast purification step.

4 Process and Cost Model

In order to observe the theoretical possible process impacts of an improved sorbent, a sophisticated process model of the whole CL process was created. This model was setup in MS® Office Excel while using Visual Basic for Application (VBA) to conduct all iterations and sensitivity analysis.

4.1 Assumptions

The whole model is based on the flow scheme developed by EPPLE ET AL. [39, 41] (see Fig. 4-1). Besides the two "hearts" of the system, the carbonator and the calciner, all basic auxiliaries (heat exchangers, pre-heaters, fans and the air separation unit) are displayed in this scheme.

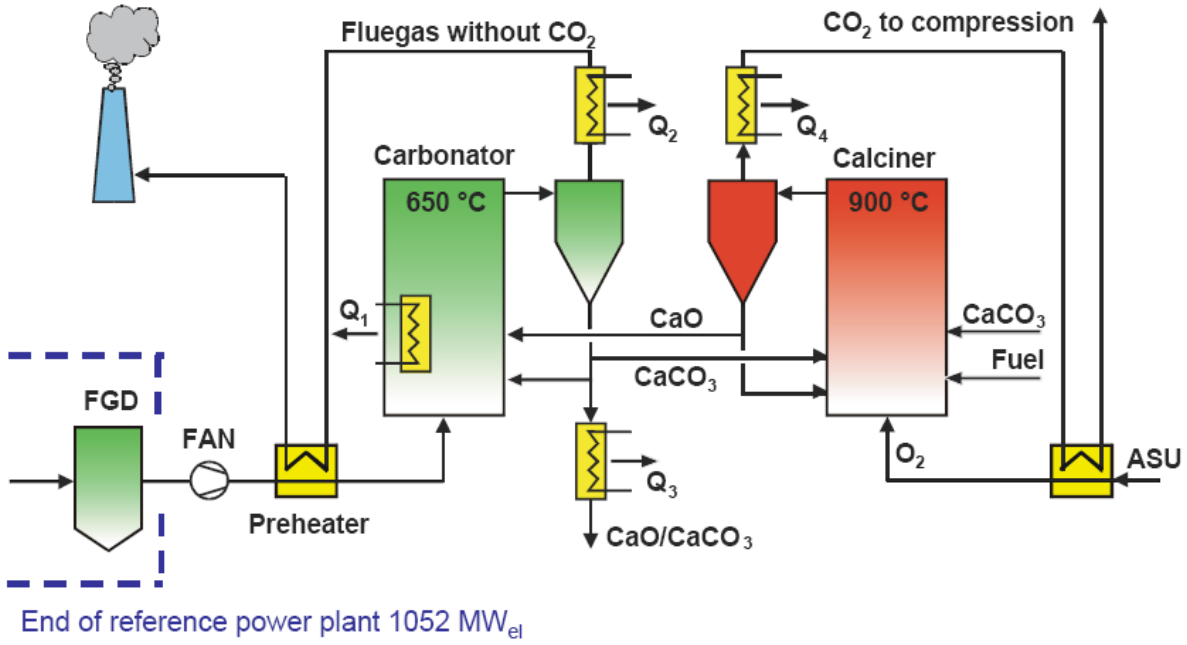

Fig. 4-1: Flow scheme of CL plant [39, 41].

It should be mentioned that this approach is considered as "standalone"- CO_2 separation, all mass and heat streams do not interact with the basic power plant; no modification of the original power plant would have to be made, excluding the flue gases. These would not enter the chimney directly but would go through the carbonator and enter the chimney afterwards. Therefore, the energy required for this process is entered by additional fuel in the calciner and is recovered by an individual steam cycle and turbine. Usually, this fuel is the regional available lignite or the imported coal already used on the spot.

4.1.1 Fuel

Coal is a very inhomogeneous substance, mainly composed of carbon, oxygen, hydrogen, nitrogen and sulphur (see Fig. 2-19). However, salts and inorganic compounds contribute as well to the overall composition of the coal.

Regarding the calculation, the carbon, sulphur and the ash contents are the important material values for a general mass balance. CO_2 is formed out of carbon as well as SO_2 and SO_3 is formed out of the contained sulphur. The ash, even though it is composed of various substances (see Fig. 2-21), is treated in the calculation as inert with one heat capacity that is not interacting with the sorbent and is only withdrawn from the process by the bleed.

Due to the circumstance that not only carbon and sulphur but also hydrogen react with the oxygen in the combustion atmosphere and, on top, the oxygen of the fuel also takes part in the reactions, the oxygen demand for the specific coal is calculated via a combustion calculation module.

However, the calorific value of the coal cannot be determined by calculations because the precise chemical state of each element is unknown. Consequently, experimentally determined values have to be used.

For the purposes of the simulations carried out in this work, a fuel, believed to be an average hard coal ([131]), will be used on the one hand and a lignite form RWE Power ([114]) will be used on the over hand. Both compositions are shown in Table 4-1.

Table 4-1: Composition of the hard coal and lignite used for the calculations.

	Hard coal	**Pre-Dried Lignite**
Carbon	69.50	60.71
Hydrogen	1.00	1.03
Oxygen	1.00	21.68
Nitrogen	0.50	0.72
Sulphur	1.20	0.36
Chlorine	0.10	---
Moisture	10.00	11.36
Ash	16.70	4.13
LHV [MJ/kg]	24.51	22.20
Fuel costs [€/t]	50	30

4.1.2 Power Plant

The main purpose of the power plant is the transformation of the chemical energy stored in the fuel to electrical power. This transformation is done with a certain efficiency. Depending mainly on the steam parameters, different efficiencies are achievable. Modern power plants are operating with an efficiency up to 43% (Niederaußem, Block K, [101]). Older boilers reach an efficiency of around 35% (Jänschwalde, [129]). A net efficiency of a state of the art power plant and for the steam cycle of the CL process of 45% (internal requirements for electrical power is subtracted individually in case of the CL process) is assumed for the simulation.

In order to burn the fuel completely the power plant is operating the combustion with an oxygen excess. This so called lambda value ranges between 1.1 and 1.3, as 1 refers to the theoretical minimum that is needed to burn the fuel completely. A lambda value for the power plant of 1.29 and for the oxyfuel calciner of 1.06 is stated here.

The heat capacity of the flue gas after FGD is needed within the calculation for the general heat balance and varies according to the lambda value, nature of the coal and the water content (operating temperature of the FGD unit). Accordingly, this value is calculated and ranges from 1.0 to 1.2 kJ/(kg K).

The SO_x content after the FGD is usually in the range between 200 and 400 mg_{SO2}/Nm^3_{dry} (~60-120 $g_S/t_{flue\ gas}$). This content could cause the formation of $CaSO_3$ or $CaSO_4$ in the carbonator of the CL system, which itself would lead to a faster deactivation of the sorbent. Within the calculation a value of 90 $g_S/t_{flue\ gas}$ which will be captured to an extend of 80% is assumed.

4.1.3 CL Process

The CL process itself is, in the end, a large oxyfuel combustion boiler that has the potential to separate additional CO_2 from a conventional combustion. The main cost and efficiency benefits result out of the fact that less oxygen has to be separated than in a normal oxyfuel combustion. As well, the re-circulation of CO_2 can be avoided due to the containing limestone acting as a heat sink.

The power plant operator may want to choose how much flue gas he is willing to treat. For example, legislations may only require the separation of a certain amount of CO_2 from a power plant in order to reach a previously set technical emission limit.

From a thermodynamic point of view the equilibrium of $CaCO_3$ decomposition enables to capture 85 to 90% (depending on the initial partial pressure of CO_2 in the flue gas) of the total CO_2 entering the carbonator at 650°C. Pilot plant trials indicate that CO_2 separation degrees up to 90% ([81]) are no problem if highly reactive sorbents are used, an initial CO_2 partial pressure of 16% is present and the carbonator is operated under isothermal conditions. The university of Stuttgart reported CO_2 uptakes between 55 and 96% based on the maximum CO_2 uptake possible at a given temperature ([29]). Assuming a CO_2 capture of 80% of the total CO_2 in the flue gas is therefore considered as realistic.

The CaO-cycles per hour refer to the average mass transfer from the carbonator to the calciner and back in relation to the total interior. Of course, the operation conditions of the plant strongly influence the cycle rate; it may vary from 5 to 50 and will be set for the further calculation to 30.

Probably the two most important parameters of the whole process are the CaO conversion and the lifetime of the sorbent particles, meaning the mechanical stability of the sorbent expressed in a theoretical number that indicates how many cycles it will take, until the whole sorbent interior of the system is lost due to attrition. GRASA ET AL. [51] reported residual CaO conversions of 7.5 % after 500 cycles. Attrition rates of 2%/h, while the utility was operated with 10 cycles per hour, are reported by CHARITOS ET AL. [29]. However, these two numbers will always be varied during the simulations to demonstrate the impact of improved sorbents on the process conditions and the associated economics.

4.1.4 Energy Issues

The flue gas stream is enriched in water while passing by the FGD unit. It shall be assumed that the flue gas is completely saturated with water after the FGD that shall be operated at a temperature of 60°C and thereby causing a H_2O partial pressure in the off gas of the FGD of ~20%. Before this gas enters the carbonator of the CL process, it is pre-heated in a heat exchanger by CO_2 depleted off-gas coming from the exit of the carbonator.

The carbonator is operated at a temperature of 650°C. Within several TGA experiments it was figured out that this temperature is the best compromise between the thermodynamics and the kinetics of the reaction of CaO and CO_2 to $CaCO_3$ ([71]).

The heat balance of the carbonator is given by the specific heats of the gases and solids that enter and leave the carbonator and the reaction enthalpy of the formation of $CaCO_3$. Gases

and solids enter the carbonator with ~100[12] and 950°C respectively and leave with 650°C (operating temperature of the carbonator). The reaction enthalpy of the carbonation is believed to be 165 kJ/mol at this temperature level and is as well assumed during the calcination.

The specific heats are calculated using the temperature dependency of the specific heat capacity. The factors for Eq. 2-16 are taken from [95] and can be seen in the following table.

Table 4-2: Factors for the specific heat capacity of the gases and solids occurring in the CL process. The according equation is given by Eq. 2-16

	a	b	c
N_2	6.5	0.001	0
O_2	8.27	0.000258	-187700
H_2O	8.22	0.00015	0.00000134
CO_2	10.34	0.00274	-195500
CaO	10.00	0.00484	-108000
$CaCO_3$	19.68	0.01189	-307600
$CaSO_4$	18.52	0.02197	-156800

The decision, whether a calcined or carbonated sorbent is going to be used as make-up is also very critical because a calcined sorbent could improve the power plant efficiency. The base scenario foresees the use of a carbonate as make-up. However, the impact of a pre-calcined sorbent could be calculated.

It is expected that the sulphur, introduced via the fuel that is burned in the calciner, shall be captured to an extend of 99% by the sorbent in the form of $CaSO_4$.

4.1.5 CO_2 Handling and Auxiliaries

To be able to make statements about the drop in the overall electrical efficiency of the power plant, assumptions regarding the CO_2 handling have to be made.

In order to recover a nearly pure stream of CO_2 at the outlet of the calciner, the fuel has to be combusted with pure oxygen. This oxygen is produced in an air separation unit that consumes between 160 to 200 kWh/t_{O2} ([96]). For the simulation a value of 170 kWh/t_{O2} will be used.

The separated CO_2 has to be compressed in order to transport and store it. A value of 100 kWh/t_{CO2} is assumed. A lump consumption of auxiliaries, e.g. fans is set to 62 kWh/t_{CO2}.

[12] This temperature is a result of the difference in the specific heats of the gases (CO_2 rich and depleted flue gas) that enter the first pre-heater prior to the carbonator.

4.2 Modell Description

Prior to the detailed discussion of the individual calculation steps, it should be mentioned that the mass and energy balances are coupled in a way that the mass balance interacts with the heat balance. For example, the introduction of impurities into the CL process via the fuel leads to an increased mass flow between calciner and carbonator. Therefore a higher amount energy is transported from the calciner to the carbonator by accompanying substances that have to be heated up again as soon as they are transported back to the calciner. By this, more fuel has to be burned in the calciner leading to a higher mass flow and again, to a higher energy demand. Due to a constant make-up and a constant bleed, this coupled process reaches a steady state. However, a general analytical solution for this problem is unknown. Accordingly, intensive numerical computation is needed. Fig. 4-2 shows the general steps of the iteration.

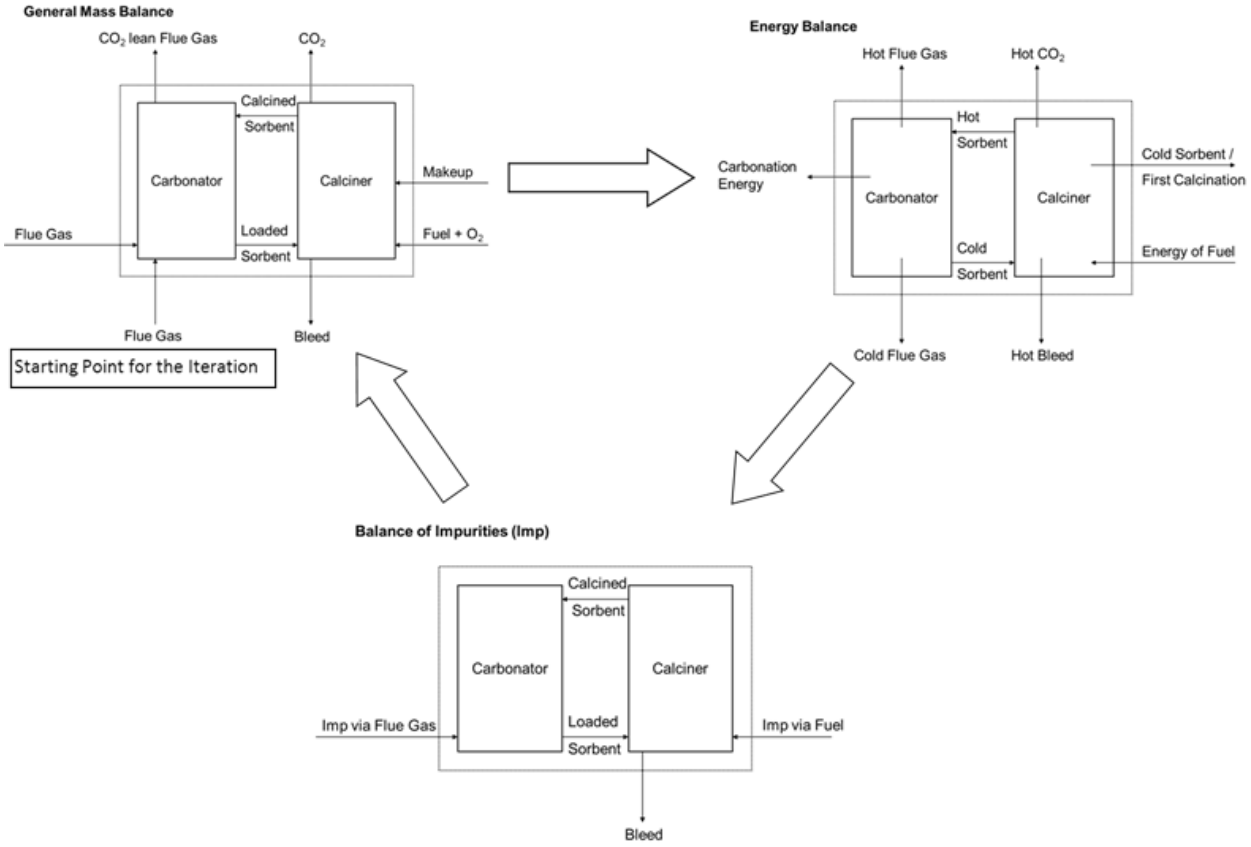

Fig. 4-2: General logic of the iteration process for the process model of the CL process.

It can be seen that the starting point of this iterative process is a general mass balance while the flue gas from the power plant is the first boundary. Usually, it takes maximal eight of these circles to reach a converged solution.

The used symbols in the following detailed mathematical explanations are described in the preface. Values that have been used for the sensitivity analysis in chapter 4.5 are given in square brackets.

4.2.1 Mass and Energy Balance for the Power Plant

The power plant is designed to produce a certain amount of electrical energy [1000 MW_{net}]. With the knowledge of the electrical efficiency [45 %], the thermal output can be calculated on top of this:

$$P_{Thermal}^{Power\ planet} = \frac{P_{Electrical}^{Power\ plant}}{\eta_{Electrical}^{Power\ plant}}\left(1-\eta_{Electrical}^{Power\ plant}\right) \quad 4\text{-}1$$

The total thermal power generated by the boiler through burning of the coal is given by the sum of the electrical and the thermal (waste) energy.

$$P_{Total}^{Power\ plant} = P_{Thermal}^{Power\ plant} + P_{Electrical}^{Power\ plant} \quad \textbf{4-2}$$

Out of this number the needed coal flow can be calculated accordingly.

$$\dot{m}_{Coal}^{Power\ plant} = \frac{P_{Electrical}^{Power\ plant}}{\eta_{Electrical}^{Power\ plant} H_{Fuel}} \quad 4\text{-}3$$

The CO_2 production of the power plant is linked with the coal flow and the carbon content of the coal.

$$\dot{m}_{CO_2}^{Power\ plant} = \frac{M_{CO_2}}{M_C}\dot{m}_{Coal}^{Power\ plant} C_{Carbon}^{Fuel} \quad 4\text{-}4$$

As well as the CO_2 production, the SO_2 formation is linked with the nature of the coal: The sulphur content of the coal determines the SO_2/SO_3 content of the flue gas. Usually, this acidic gas is captured with limestone (only in some cases with $Ca(OH)_2$ or CaO or other bases) in the FGD unit. The demand for the FGD unit is calculated with Eq. 4-5. About 90% of this sulphur shall be captured in the wet scrubber.

$$\dot{m}_{CaCO_3\ demand}^{FGC} = \frac{M_{CaCO_3}}{M_S}\dot{m}_{Coal}^{Power\ plant} C_{Sulphur}^{Fuel} \quad 4\text{-}5$$

The calculation of the flue gas flow after the FGD and before the CL process is more complex: The main components of this stream after the FGD unit are nitrogen, water, carbon dioxide and oxygen.

$$\dot{m}_{beforeLLCR}^{Flue\ gas} = \dot{m}_{N_2}^{Flue\ gas} + \dot{m}_{H_2O}^{Flue\ gas} + \dot{m}_{CO_2}^{Flue\ gas} + \dot{m}_{O_2}^{Flue\ gas} \quad 4\text{-}6$$

Nitrogen is introduced with the burning air and is considered as inert (the formation of NO_x is dismissed). The excess of N_2 is linked with the O_2 level of the burning air[13], the oxygen demand for a complete cobustion of the introduced coal and the oxygen excess (lambda value).

$$\dot{m}_{N_2}^{Flue\,gas} = \dot{m}_{Coal}^{Power\,plant} D_{Oxygen}^{Fuel} \lambda \frac{C_{Oxygen}^{Air}}{(1 - C_{Oxygen}^{Air})} \frac{M_{N_2}}{M_{O_2}} \qquad 4\text{-}7$$

The water vapour content of the flue gas after the wet scrubber is given by the equilibrium partial pressure of water at the outlet temperature of the FGD reactor [60°C].

$$C_{Water}^{Flue\,gas} = \exp\left(\frac{\Delta_V H}{R}\left(\frac{1}{T_{Exit}^{FGD} + 273} - \frac{1}{373}\right)\right) \qquad 4\text{-}8$$

$\Delta_V H$ is set to 41 kJ/mol. According to Eq. 4-8, the mass stream can be calculated consequently by

$$\dot{m}_{Water}^{Flue\,gas} = \dot{n}_{beforeFGD}^{Flue\,gas} \frac{C_{Water}^{Flue\,gas}}{1 - C_{Water}^{Flue\,gas}} M_{H_2O}. \qquad 4\text{-}9$$

The flow of carbon dioxide is given by the amount of burned coal that itself is given by the total power production and was calculated earlier (see Eq. 4-3).

$$\dot{m}_{CO_2}^{Flue\,gas} = \dot{m}_{CO_2}^{Power\,plant} \qquad 4\text{-}10$$

The content of oxygen present in the flue gas results out the oxygen excess and can be calculated by

$$\dot{m}_{O_2}^{Flue\,gas} = \dot{m}_{Coal}^{Power\,plant} D_{Oxygen}^{Fuel} (\lambda - 1). \qquad 4\text{-}11$$

4.2.2 Mass Balance for the CL process

The CL process could be designed to separate up to 90% of the CO_2 that is in the treated flue gas stream. The total separation degree is given by the following equation.

$$\eta_{Totalseparation}^{CO_2\ flue\,gas} = \eta_{CO_2\,treatment}^{FlueGas} \cdot A_{Treated}^{Flue\,gas} \qquad 4\text{-}12$$

With this value the mass flow of the separated CO_2 can be calculated according to

$$\dot{m}_{CO_2\,separated}^{Power\,plant} = \eta_{Totalseparation}^{CO_2\ flue\,gas} \dot{m}_{CO_2}^{Power\,plant}. \qquad 4\text{-}13$$

[13] Air is considered as a two-component gas comprising of about 21% oxygen and 79% nitrogen.

To separate this amount of CO_2 it is necessary to introduce a certain amount of CaO into the carbonator. It is assumed that the CaO conversion (to $CaCO_3$) within the model can be reached by the applied process parameters[14].

$$\dot{n}_{Sorbent}^{LLCR} = \frac{\dot{m}_{CO_2\ separated}^{Power\ plant}}{M_{CO_2} X_{CaCO_3}^{LLCR}} \qquad 4\text{-}14$$

Taking this number into account, the needed flow of CaO to the carbonator can be calculated accordingly.

$$\dot{m}_{CaO}^{LLCR} = \dot{n}_{Sorbent}^{LLCR} M_{CaO} \qquad 4\text{-}15$$

Of course, the mole flow of Ca between the carbonator and the calciner increases significantly if the formation of $CaSO_3$/$CaSO_4$ is included in the overall balance. The degree of sorbent inhabitation is calculated with an iteration and will be explained later on.

$$\dot{n}_{Ca}^{LLCR} = \frac{\dot{n}_{CaO}^{LLCR}}{1 - X_{CaSO_3/CaSO_4}^{LLCR}} \qquad 4\text{-}16$$

The mass flow of the partially re-carbonated sorbent to the calciner will be larger than the pure mass flow of CaO and can be calculated according to

$$\dot{m}_{CaO/CaCO_3}^{LLCR} = \dot{n}_{CaO}^{LLCR} (X_{CaCO_3}^{LLCR} M_{CaCO_3} + (1 - X_{CaCO_3}^{LLCR}) M_{CaO}) . \qquad 4\text{-}17$$

On top of this mass flow, the flow of $CaSO_3$/$CaSO_4$ has to be considered as well. BLAMEY ET AL. [22] calculated that the dominant phase under the conditions of the CL process should be $CaSO_4$ (see Fig. 4-3).

Temperature, T (K)	Oxidising conditions	Reducing conditions
$T < 723$	$CaSO_3$	
$723 < T < 973$	$CaSO_3$, $CaSO_4$	$CaSO_3$, $CaSO_4$, (CaS)
$T > 973$	$CaSO_4$	
$T > 1103$		$CaSO_4$, (CaS)

Fig. 4-3: Predominant calcium-sulphur species at different temperatures and under different atmospheres. Figure taken from [22].

Consequently, it is assumed that the whole interior of sulphated CaO consists of $CaSO_4$.

$$\dot{m}_{CaO/CaCO_3/CaSO_4}^{LLCR} = \dot{m}_{CaO/CaCO_3}^{LLCR} + \dot{n}_{CaO}^{LLCR} \frac{X_{CaSO_3/CaSO_4}^{LLCR}}{(1 - X_{CaSO_3/CaSO_4}^{LLCR})} M_{CaSO_4} \qquad 4\text{-}18$$

[14] Note that the ratio between CaO and CO_2 that enters the carbonator limits the maximum CaO conversion in the first place. The second limiting step is the chemical reaction, i.e. the applied space time (ratio between active sorbent mass in the carbonator and the flow of CO_2 into the reactor).

The needed CaO amount in the system results out of the assumed cycles performed per hour and the mole flow of CaO into the carbonator.

$$m_{Sorbent}^{LLCR} = \frac{\dot{n}_{CaO}^{LLCR}}{Z} M_{CaO} \quad 4\text{-}19$$

Here as well, if sulphation is taken into account too, the mass of material in the system rises.

$$m_{CaO/CaSO_4}^{LLCR} = \frac{\dot{n}_{Ca}^{LLCR}(X_{CaSO_3/CaSO_4}^{LLCR} M_{CaSO_4} + (1 - X_{CaSO_3/CaSO_4}^{LLCR}) M_{CaO})}{Z} \quad 4\text{-}20$$

The make-up of CaO is determined by the mole flow of Ca and the assumed lifetime of the sorbent.

$$\dot{m}_{CaOMakeup}^{LLCR} = \frac{\dot{n}_{Ca}^{LLCR}}{L} M_{CaO} \quad 4\text{-}21$$

This number can also be expressed in terms of mass of $CaCO_3$.

$$\dot{m}_{CaCO_3\,Makeup}^{LLCR} = \frac{\dot{n}_{Ca}^{LLCR}}{L} M_{CaCO_3} \quad 4\text{-}22$$

The loss of active sorbent due to sulphation is taken into account on two occasions: In the calciner due to the sulphur content of the fuel and in the carbonator due to the residual SO_2 that was not captured in the FGD unit. Of course, within the two reactors different S capture rates might be observed [99% in the calciner, 80% in the carbonator].

$$\dot{m}_{CaCO_3\,losstotal}^{LLCR} = \dot{m}_{CaCO_3\,losscarbonator}^{LLCR} + \dot{m}_{CaCO_3\,losscalciner}^{LLCR} \quad 4\text{-}23$$

$$\dot{m}_{CaCO_3\,losscalciner}^{LLCR} = \dot{m}_{Coal}^{LLCR} C_{Sulphur}^{Fuel} \eta_{Sulphurcapture}^{Calciner} \frac{M_{CaCO_4}}{M_S} \quad 4\text{-}24$$

$$\dot{m}_{CaCO_3\,losscarbonator}^{LLCR} = \dot{m}_{beforeLLCR}^{Fluegas} C_{Sulphur}^{Fluegas} \eta_{Sulphurcapture}^{Calciner} \frac{M_{CaCO_4}}{M_S} \quad 4\text{-}25$$

The mass stream of bleed that leaves the system can be calculated with the help of the mass flow of the sorbent in the reactor and the guessed average lifetime of the sorbent

$$\dot{m}_{Bleed}^{LLCR} = \frac{\dot{m}_{CaO/CaCO_3/CaSO_4}^{LLCR}}{L} \quad 4\text{-}26$$

In theory, the bleed could also be taken after the calcination but additional energy losses would be the result. Therefore this option is dismissed.

The sulphation degree is influenced by the additional energy needed for the operation of the CL process (sulphur content in the fuel). On the other hand, the additional energy needed for the CL process is influenced by the sulphation degree. This mathematical problem can only be solved by two iterations. Within the created calculation the EXCEL internal solver calculates

the needed energy demand. Afterwards, the new according sulphation level is calculated using the parameters calculated by the new energy demand. With this result the iteration for the energy demand is carried out again. This cycle is carried out as long as the difference between introduced sulphur (by the fuel and the flue gas) and disposed sulphur (through the bleed) becomes equal. This approach has a very good convergence order and radius: In normal cases it takes only 10 iteration steps until the final result is displayed.

A simple sulphur mass balance calculates the sulphation level.

$$\dot{n}_{Sulphurin}^{LLCR} - \dot{n}_{Sulphurout}^{LLCR} = \frac{\dot{m}_{CaCO_3 losstotal}^{LLCR}}{M_{CaCO_3}} - \dot{n}_{Sulphurout}^{LLCR} = 0 \qquad 4\text{-}27$$

The mole flow of sulphur out of the CL process is given by the amount of total moles leaving the system and the according sulphation level of the bleed.

$$\dot{n}_{Sulphurout}^{LLCR} = X_{CaSO_3/CaSO_4}^{LLCR} \dot{n}_{Bleed}^{LLCR} \qquad 4\text{-}28$$

The mole flow of the bleed can be calculated with the mass flow and the average mole mass of the bleed.

$$\dot{n}_{Bleed}^{LLCR} = \frac{\dot{m}_{Bleed}^{LLCR}}{X_{CaSO_3/CaSO_4}^{LLCR} M_{CaSO_4} + X_{CaCO_3}^{LLCR} M_{CaCO_3} + (1 - X_{CaCO_3}^{LLCR}) M_{CaO}} \qquad 4\text{-}29$$

The mole flow of sulphur entering the CL process is determined by the captured sulphur in the calciner and in the carbonator.

$$\dot{n}_{Sulphurin}^{LLCR} = \frac{\dot{m}_{CaCO_3 losscarbonator}^{LLCR} + \dot{m}_{CaCO_3 losscalciner}^{LLCR}}{M_{CaCO_3}} = \frac{\dot{m}_{CaCO_3 losstotal}^{LLCR}}{M_{CaCO_3}} \qquad 4\text{-}30$$

Combining the Eqs. 4-18 and 4-26 - 4-30 and considering Eq. 4-31, we receive a quiet complex expression that can be considered as quadratic equation regarding $X_{CaSO_3/CaSO_4}^{LLCR}$.

$$X_{CaCO_3}^{LLCR} = X_{CaCO_3}^{LLCR0} (1 - X_{CaSO_3/CaSO_4}^{LLCR}) \qquad \textbf{4-31}$$

This equation has the following general form

$$\alpha (X_{CaSO_3/CaSO_4}^{LLCR})^2 + \beta X_{CaSO_3/CaSO_4}^{LLCR} + \gamma = 0 \qquad \textbf{4-32}$$

and can be solved by

$$X_{CaSO_3/CaSO_4}^{LLCR} = -\frac{\beta}{2\alpha} + \sqrt{\left(\frac{\beta}{2\alpha}\right)^2 - \frac{\gamma}{\alpha}}\,. \qquad \textbf{4-33}$$

The factors alpha, beta and gamma result out of the quadratic equation received by the above mentioned combination of the given expressions.

$$\alpha = L\dot{n}_{Sulphur\,in}^{LLCR}(X_{CaCO_3}^{LLCR,0}M_{CaCO_3} + M_{CaO} - X_{CaCO_3}^{LLCR,0}M_{CaO} - M_{CaSO_4}) - \dot{n}_{Sorbent}^{LLCR}M_{CaSO_4} + \dot{m}_{CaO/CaCO_3}^{LLCR} \quad \textbf{4-34}$$

$$\beta = L\dot{n}_{Sulphur\,in}^{LLCR}(2X_{CaCO_3}^{LLCR,0}M_{CaO} + M_{CaSO_4} - 2X_{CaCO_3}^{LLCR,0}M_{CaCO_3} - M_{CaO}) - \dot{m}_{CaO/CaCO_3}^{LLCR} \quad \textbf{4-35}$$

$$\gamma = L\dot{n}_{Sulphur\,in}^{LLCR}(X_{CaCO_3}^{LLCR,0}M_{CaCO_3} + M_{CaO} - X_{CaCO_3}^{LLCR,0}M_{CaO}) \quad \textbf{4-36}$$

With this number the new maximum conversion of the bed material to $CaCO_3$ can be estimated by

$$X_{CaCO_3}^{LLCR} = (1 - X_{CaSO_3/CaSO_4}^{LLCR})X_{CaCO_3}^{LLCR,0}. \quad \textbf{4-37}$$

This value could also be understood as share of the conversion of all Ca atoms in the bed to $CaCO_3$.

The heat capacity of the bleed and therefore the heat capacity of the material coming out of the carbonator is calculated by the molar heat capacities of $CaCO_3$, CaO and $CaSO_4$ and the according shares of these substances regarding the whole bleed.

$$c_p^{Bleed} = X_{CaSO_3/CaSO_4}^{LLCR}c_p^{CaSO_4} + X_{CaCO_3}^{LLCR}c_p^{CaCO_3} + X_{CaO}^{LLCR}c_p^{CaO} \quad \textbf{4-38}$$

The flue gas stream after the CL process equals Eq. 4-6, but, of course, is corrected by the separated CO_2.

$$\dot{m}_{after\,LLCR}^{Flue\,gas} = \dot{m}_{before\,LLCR}^{Flue\,gas} - \eta_{Total\,Separation}^{CO_2\,flue\,gas}\,\dot{m}_{CO_2}^{Power\,plant} \quad \textbf{4-39}$$

Due to the fact that ash is only introduced via fuel, content of ash in the cycle and in the bleed is:

$$C_{Ash}^{Bleed} = \frac{C_{Ash}^{Fuel}\dot{m}_{Fuel}}{C_{Ash}^{Fuel}\dot{m}_{Fuel} + m_{Bleed}^{LLCR}} \quad \textbf{4-40}$$

Accordingly, the total amount of bleed can be calculated by

$$\dot{m}_{Bleed,total}^{LLCR} = \dot{m}_{Bleed}^{LLCR}\left(1 + \frac{C_{Ash}^{Bledd}}{1 - C_{Ash}^{Bledd}}\right). \quad \textbf{4-41}$$

The total mass flow from the calciner to the carbonator is calculated the same way.

The mass flow of coal into the CL process is a result of the energy balance (see section 4.2.4) and is calculated by

$$\dot{m}_{Coal}^{LLCR} = \frac{P_{ThermalIn}^{LLCR}}{H_{Fuel}}3600. \quad \textbf{4-42}$$

Of course, if coal is burned within the CL process, additional CO_2 has to be produced.

$$\dot{m}_{CO_2}^{LLCR} = \dot{m}_{Coal}^{LLCR} C_{Carbon}^{Fuel} \frac{M_{CO_2}}{M_C} \qquad \textbf{4-43}$$

Consequently, the total flow of CO_2 leaving the system is given by the sum of separated CO_2 and CO_2 produced by the burning of the fuel in the calciner.

$$\dot{m}_{CO_2}^{Total} = \dot{m}_{CO_2}^{LLCR} + \dot{m}_{CO_2\ separated}^{Power\ plant} \qquad \textbf{4-44}$$

4.2.3 Average Maximum CaO Conversion

The decay of the CaO conversion of natural occurring limestones that are rather pure, that have not been pre-treated and were tested under TGA conditions can be described satisfactory with an expression according to

$$X_{CaO}(n) = \frac{f}{n+a} + b \qquad \textbf{4-45}$$

that is similar to other equations proposed in the literature BLAMEY ET AL. [22].

The parameters *f* and *a* determine the rate of the decay of the CO_2 capture ability while *b* describes the residual CaO conversion.

Fig. 4-4 illustrates the good accordance of the expression compared to TGA experiments that will be explained later on.

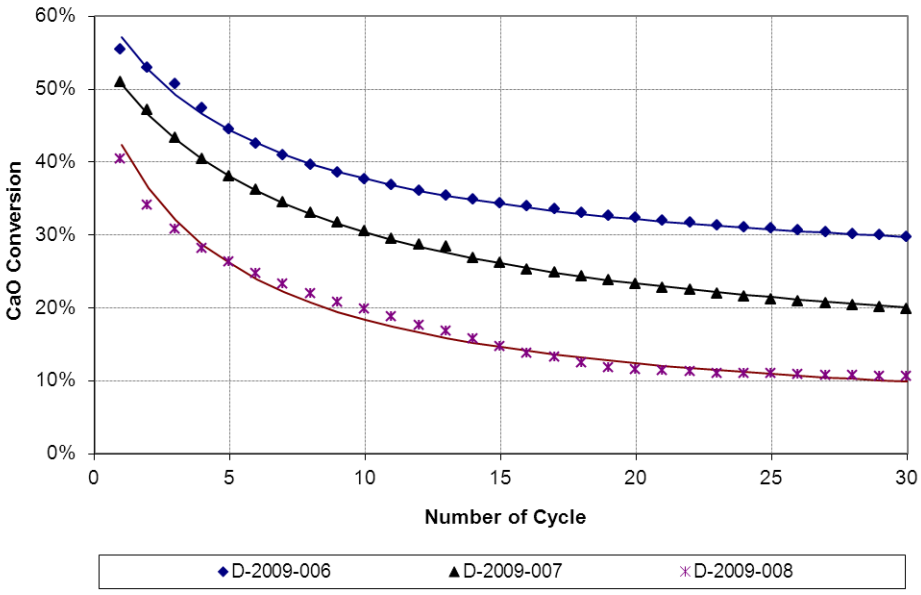

Fig. 4-4: Decay of the CaO conversion of different sorbents tested in a TGA described in chapter 5. Eq. 4-45 has been used to fit the curves onto the measured data.

Table 4-3 shows the received values for the best fit parameters of Eq. 4-45 for the data shown in Fig. 4-4. It can be seen that the residual CaO conversion varies between 3.7 and 23.6% for

different products. In addition, it should be noted that the ratio between a and f is in the range of 2.1 to 2.5.

Table 4-3: Parameters used for a best fit of Eq. 4-45 to the data provided in Fig. 4-4.

	D-2009-006	D-2009-007	D-2009-008
f	2.20	3.69	2.12
a	5.56	8.07	4.50
b	23.6%	10.0%	3.7%
a/f	2.53	2.19	2.12

Therefore, the parameter a shall be set to

$$a = 2.25 f \ . \qquad \textbf{4-46}$$

Accordingly, Eq. 4-45 can now be written as

$$X_{CaC} = \frac{f}{n + 2.25 f} + b \ . \qquad \textbf{4-47}$$

For the following simulations f shall be named as "CO_2 stability number"; this number will be varied under the assumption that the residual CaO conversion is constant and has a value of 11%.

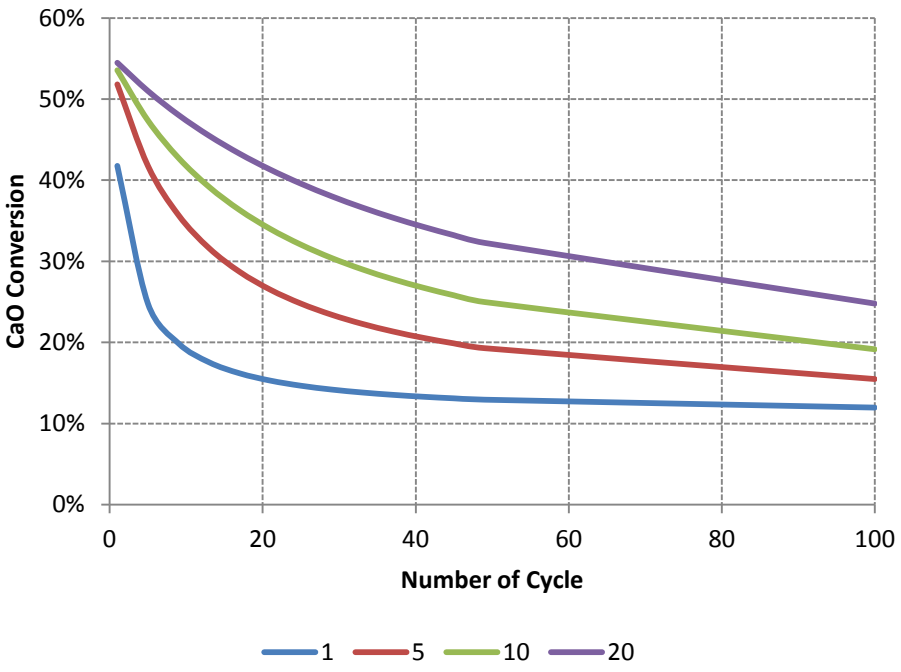

Fig. 4-5: CaO conversion decay curves of the numbers of cycles for different CO_2 stability numbers and a residual CO_2 capture ability of 11%.

Now, a link between the bleed rate and the average CO_2 capture ability of the sorbent bed in the CL process has to be set up.

ABANADES ET AL. [4] proposed a link between share of particles that have undergone a given numbers (r_n) of cycles (n) the make-up-rate (F_0) and the flow of Ca between the calciner and the carbonator (F_R).

$$r_n = \frac{F_0 F_R{}^{n-1}}{(F_0 + F_R)^n}. \qquad \textbf{4-48}$$

Through this expression, the average CaO conversion can be calculated quite easily by the following sum.

$$X_{CaCO_3}^{LLCR} = \sum_{n=1}^{\infty} r_n X_{CaO}(n). \qquad \textbf{4-49}$$

However, numerically it is not beneficial to integrate to infinite. Therefore, the addition is stopped as soon as $\sum_n r_n$ = 99.9%.

Limitations of this Description

Even though, the expressions given above are the best available to describe the average CaO conversion in a CL system, it is known that the sorbent particles have some sort of memory of the cycle conditions they have experienced (see chapter 3). Consequently, a particle that stayed for a longer duration in the carbonator or calciner than another will show a different CO_2 capture behaviour during the next cycle.

Another limitation is given by the possibilities to operate the CL process. CaO conversions recorded in a TGA are usually done in an excess of CO_2; as well, the duration of re-carbonation surpasses the fast re-carbonation reaction stage. These two facts lead to an overestimation of the product performance and would, if the large CL plant was operated according to the TGA conditions, lead to an undesired bad CO_2 separation from the flue gas. In a worst case scenario, the process conditions could limit the product performance to its residual CaO conversion. Several R&D groups around the world are working on the determination and optimisation of the real process conditions. Therefore, it is believed that it will be possible to operate the plant very close to the theoretical possible one day.

4.2.4 Energy Balance

Carbonator and calciner are two similar parts of the CL process in terms of the heat balance. Each part can be described by three different accounting grids, First, the pre-heater, second, the reactor and third the cooling of the of gases. These three grids can be seen in Fig. 4-6.

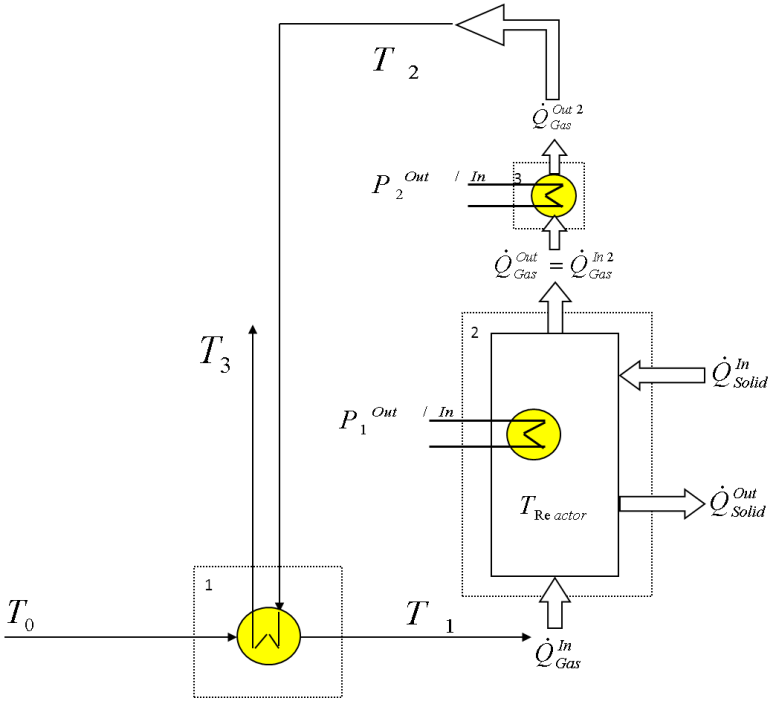

Fig. 4-6: Three accounting grids of the calciner and the carbonator. Temperatures, heat in- and outputs and power outputs are illustrated.

Most important for the energy balance of the process are the according temperature levels that are assumed. These are summarised in Table 4-4.

Table 4-4: Temperature levels of gases and solids in the CL process as assumed for the simulations below. T1 is a result of the temperature levels T0 and T3.

	carbonator	calciner
T_0	60°C	-100°C
T_1	calculated	calculated
$T_{Reactor}$	650°C	950°C
T_2	150°C	150°C
T_3	80°C	80°C
$T_{Make-up}$	---	25°C

The flue gas enters the CL with the temperature level of the FGD unit and is pre-heated before entering the carbonator in a gas-gas pre-heater by the hot off-gas, coming from the exhaust of the carbonator. The temperature T_1 is limited by the remaining enthalpy of the CO_2 depleted flue gas after it has passed the heat exchangers for the steam production. This pre-heated gas

enters the carbonator, which is operated at 650°C. 950°C hot solids from the calciner enter the carbonator, are cooled down; the active CaO part reacts with the CO_2 of the flue gas and releases the according reaction enthalpy and the 650°C hot partially carbonated solids leave the reactor again. In order to maintain the carbonator temperature, energy in the form of steam (P_1) has to be removed from the reactor. The carbonator off-gases, now at a temperature level of 650°C, are directed through a series of gas-liquid heat exchangers to produce steam and to be cooled down to a temperature level of 150°C (P_2). For the sake of simplicity, this cascade of heat exchangers is just symbolised with one pictogram. The 150°C CO_2 depleted off-gas is now cooled down to 80°C in the pre-heater and subjected to the stack. Further cooling might be possible but, even now, the temperature difference of 20 K in this heat exchanger is considered as very low.

The bleed, a partially re-carbonated solid, is cooled from 650°C down to 110°C by a solid-liquid heat exchanger. The heat is used for the production of steam.

As indicated, the calciner can be described in the same way as the carbonator. Cold oxygen from the ASU with a temperature of -100°C is directed into a pre-heater and heated up to a temperature determined by the enthalpy of the still hot CO_2 from the calciner. Afterwards, it enters the calciner, which is operated at a temperature level of 950°C. The “cold” partial re-carbonated solid from the carbonator as well as the make-up (T ~25°C) enters the calciner. Both solids are calcined; the according reaction enthalpy has to be provided by the fuel. The amount of fuel needed is calculated by the power P_1. The enthalpy of the introduced fuel is set to zero because the chemical state of the atoms in the fuel is unknown. Accordingly, the heat capacity is not certain. The 950°C hot exhaust gases of the calciner are directed through a series of gas-liquid heat exchangers to produce steam and to be cooled down to a temperature level of 150°C (P_2). This temperature will be decreased further in the pre-heater for the oxygen to 80°C.

The enthalpy of the individual compounds was calculated using the primitive of Eq. 2-16 and the parameters given in Table 4-2. The reference temperature was set to 273 K. However, the reference temperature has no impact on the outcome of the calculation because macroscopic heat phenomena are a result of the difference in enthalpies of the compounds entering and leaving the accounting grid. By this approach, the powers of the heat exchanges Q1 to Q4 of Fig. 4-1 have been calculated.

Accordingly, the total thermal power output is given by

$$P_{Thermal}^{All\ heat\ exchangers} = P_{Thermal}^{Q1} + P_{Thermal}^{Q2} + P_{Thermal}^{Q3} + P_{Thermal}^{Q4}. \qquad \textbf{4-50}$$

Energy losses in the system are taken into account by the model through the difference in the temperature of the gases and solids entering and leaving the system. However, thermal losses due to other effects, like radiation from the reactor walls, were not taken into account.

The recovered thermal power can be used for the production of electricity. As the CL process has an individual steam circuit, this power production might be implemented with a higher efficiency than the original power plant.

$$P_{Electrical}^{LLCR} = P_{ThermalOut}^{LLCR} \eta_{Electrica,net}^{LLCR} \quad \textbf{4-51}$$

This effect results in some cases in an increase in the overall plant efficiency. This is unique within all the CCS technologies available today.

Besides, the electrical energy production, energy is needed for the operation of the ASU, the CO_2 compression and supporting units. The energy demand for the ASU can be estimated by

$$P_{O_2\,\mathrm{Production}}^{LLCR} = \dot{m}_{Coal}^{LLCR} D_{Oxygen}^{Fuel} \lambda E_{Oxygen}^{\mathrm{Production}}. \quad \textbf{4-52}$$

The electrical power for the CO_2 production can be estimated with the following equation.

$$P_{Auxilliar}^{LLCR} = E_{Auxillarie}^{LLCR} \dot{m}_{CO_2}^{Total} \quad \textbf{4-53}$$

Moreover, the needed power for the CO_2 compression can be estimated with

$$P_{CO_2\,Compression}^{LLCR} = E_{CO_2}^{Compression} \dot{m}_{CO_2}^{Total}. \quad \textbf{4-54}$$

Consequently, the net power output of the system is

$$P_{Electrical,cross}^{LLCR} = P_{Electrical}^{LLCR} - P_{O_2\,\mathrm{Production}}^{LLCR} - P_{Auxilliar}^{LLCR} - P_{CO_2\,Compression}^{LLCR} \quad \textbf{4-55}$$

The results of the energy balance mark the starting point for a new calculation of the mass balance, which determines a new heat balance causing a new calculation of the mass balance and so on. This iterative process converges within eight cycles and is only needed due to the cumulation of impurities that are driven into the process by the flue gas and by the fuel.

4.2.5 Overall Plant Efficiency

The specific energy needed for the separation of one ton of CO_2 can be calculated according to

$$\pi = \frac{P_{ThermalIn}^{LLCR}}{\dot{m}_{CO_2}^{Total}}. \quad \textbf{4-56}$$

It should be noted that this energy amount **is not** lost but can be recovered to a certain extend.

The additional energy demand for the CL process is calculated by

$$\delta = \frac{P_{ThermalIn}^{LLCR}}{P_{Total}^{Power\ plant}}. \quad \textbf{4-57}$$

This value indicates the additional size of the CCS system.

The electrical net power production without CO_2 compression is given by the power production of the plant itself and the CL system minus the energy needed for the ASU and the supporting CL units.

$$P_{Electrical}^{Total\ w/o\ compression} = P_{Electrical}^{LLCR} + P_{Electrical}^{Power\ plant} - P_{O_2\ Production}^{LLCR} - P_{Auxilliar}^{LLCR} \quad \textbf{4-58}$$

The overall plant efficiency is defined by the output of electrical power divided by all the energy put in the system.

$$\eta_{CO_2\ treatment}^{Total\ w/o\ compression} = \frac{P_{Electrical}^{Total\ w/o\ compression}}{P_{ThermalIn}^{LLCR} + P_{Total}^{Power\ plant}} \quad \textbf{4-59}$$

The change in efficiency follows directly by

$$\Delta\eta_{CO_2\ treatment}^{Total\ w/o\ compression} = \eta_{CO_2\ treatment}^{Total\ w/o\ compression} - \eta_{Electrical}^{Power\ plant}. \quad \textbf{4-60}$$

Including the CO_2 compression, the Eq. 4-58 to 4-60 are changed accordingly to

$$P_{Electrical}^{Total\ incl.\ compression} = P_{Electrical}^{LLCR} + P_{Electrical}^{Power\ plant} - P_{O_2\ Production}^{LLCR} - P_{Auxilliar}^{LLCR} - P_{CO_2\ Compression}^{LLCR} \quad \textbf{4-61}$$

$$\eta_{CO_2\ treatment}^{Total\ incl.\ compression} = \frac{P_{Electrical}^{Total\ incl.\ compression}}{P_{ThermalIn}^{LLCR} + P_{Total}^{Power\ plant}} \quad \textbf{4-62}$$

$$\Delta\eta_{CO_2\ treatment}^{Total\ incl.\ compression} = \eta_{CO_2\ treatment}^{Total\ incl.\ compression} - \eta_{Electrical}^{Power\ plant}. \quad \textbf{4-63}$$

4.3 Economical Estimations

The CL process requires significant investment costs (CAPEX - capital expenses) due to the full erection of a second power plant besides base power plant and according high operating costs (OPEX-operational expense) due to the need of fuel and sorbent. All costs were based on existing CFB units that were installed recently ([131]).

4.3.1 Estimation of the CAPEX

Table 4-5 shows a list with the associated costs for the calciner and the carbonator and the according scaling exponents.

Table 4-5: Costs of the components of the CL looping process referred to a power plant built in Europe with an electrical cross efficiency of 43% and a power production of 400 MW_{el}. The costs are given in million $ and are based on the year 2006. The costs are referred to a retrofit.

	Calciner	Carbonator	Scaling exponent
Boiler island complete	170.00	80.00	0.55
Turbine island complete	53.30	---	0.65
Coal/Ash handling	17.62	---	0.65
Flue gas cleaning	18.33	11.60	0.65
Waste/Water handling	3.20	---	0.6
Miscellaneous equipment	1.05	0.40	0.8
Air separation	40.00	---	0.9
Civil works	73.00	14.50	0.5
Electric./control package	31.60	8.70	0.45
Piping	34.90	2.00	0.6

The baseline for the cost scaling was the combustion power (1070 MW_{th}) in the case of the calciner and the flue gas amount (1,134,000 Nm^3/h) in the case of the carbonator.

With this list and the base values it is possible to estimate the costs for larger or smaller equipment according to the easy approach

$$K_2 = 1.03^{J-2006}\left(\frac{Q_2}{Q_{2006}}\right)^{\Gamma} K_{2006}. \qquad \textbf{4-64}$$

It can be seen that the price increase due to inflation was set to 3%.

The following overheads were added onto the sum of the utility costs:

- Engineering 10%
- Contingency 12%
- Start up 2.5%
- Spare parts 1%

Accordingly, the total costs were calculated by the sum of the utilities and overheads. This amount is considered in the OPEX in the form of capital expenditures.

In case that the CL process should be constructed on a green field together with the power plant, cost savings are possible. These are given in the following Table.

Table 4-6: Possible cost savings for the greenfield erection of the CL process.

	Calciner	Carbonator
Boiler island complete	---	8%
Turbine island complete	2%	---
Coal/Ash handling	21%	---
Flue gas cleaning	7.50%	9.50%
Waste/Water handling	23%	---
Miscellaneous equipment	1%	12%
Air separation	---	---
Civil works	7%	4%
Electric./control package	8%	7%
Piping	2%	9%

In order to convert $ into € a fixed exchange rate of 1.25$ per € was applied.

4.3.2 Estimation of the OPEX

The operational costs have to be subdivided into two groups; fixed and variable. Fixed operating costs are costs for the capital service, staff, insurance, maintenance and repair and administration. Variable costs are include all consumable goods like fuel, sorbent and water.

4.3.2.1 Fixed Operational Costs

It is assumed that the rate of interest is 7% and that the depreciation period is 15 years. Further, it is assumed that the plant is fully financed by a loan. CFB systems are believed to be available at full load for 85% of the year resulting in 7446 full-load operating hours. Insurance is set to 0.6% of the total erections costs per year. Disregarding the size of the process, it is believed that one plant manager, 5 engineers and 20 shift men will be needed on top of the staff of the power plant team to maintain the operation. Administration costs are set to 2 € per kW_{th} installed, while the annual costs for maintenance and repairings are estimated to be 2.5% of the total erection costs (see Table 4-7).

Table 4-7: Fixed operational costs of the CL process.

Rate of interest	7%	
Interest payments	15	Years depreciation
Rate of return for investors	0%	
Capacity factor	85%	
Annual operating hours	7446	
Insurance	0.60%	Erection cost
Staff Costs	100,000	1 Chief engineer
	90,000	5 Engineers and technicians
	60,000	5 Shifts with 4 shift men
Administration	2	€/kW_{thi}
Maintenance & repair	2.50%	Of total erection costs

4.3.2.2 Variable Operating Costs

According to the two cases (calcination with lignite or hard coal) that shall be investigated, the specific fuel costs are 30 and 50 €/t. However, due to the double energy content of natural gas, the price difference based on the heating value is given by a factor of five. The start up fuel which is believed to be needed once a year, is taken into account with 500 €/t. Cooling water und auxiliary material are based on the MWh_{el} that are produced by the generator of the CL looping process; the specific costs are 0.75 and 0.3 € respectively. The sorbent cost is based on a CaO value and estimated to be 80 €/t_{CaO}. This prices refers to a $CaCO_3$ price of ~40 €/t that is seen as appropriate because of the high material requirements (high purity and mechanical strength and a very special grain size). The residual, i.e. bleed, that is withdrawn from the process could be processed to be suitable either for the on-site FGD unit or for other applications. Due to the enrichment of impurities in the system in case of the calcination with lignite, only 50% of the bleed might be reclaimed. The other 50% have to be dumped for 150 €/t. The processing of the bleed is accounted by 20 €/t_{Bleed}. Table 4-8 gives a summary of the before discussed values.

Table 4-8: Variable operational costs of the CL process.

Normal fuel (99%)	30/50	€/t
Start-up fuel (1%)	500	€/t
Cooling water	0.75	€/MWh
Sorbent costs	80.00	€/tCaO
Auxiliary materials	0.3	€/MWh
Processing of bleed	20	€/t
Usable material of bleet	50/100%	
Waste	150	€/t

4.3.2.3 Benefits

Something unique of the CL process compared to other CO_2 capture technologies is the presence of benefits; electrical power can be sold and processed bleed could be used for the FGD or other applications like the cement industry. The internal benefit for the use in the FGD is accounted by 50 €/t_{Bleed}, for external applications by 10 €/t_{Bleed}. The first price is a normal market price for a FGD sorbent while the second is a known price cement producers would pay for such a residue. As well, electrical power can be sold on the market. The price for this benefit is set to 50 €/MWh. Table 4-9 summarises the benefits.

Table 4-9: Benefits occurring due to the operation of the CL process.

New raw material for FGD	50	€/t_{Bleed}
New raw material for Other applications	10	€/t_{Bleed}
Sale of power	50	€/MWh

4.4 Key Performance Indicators

Following two approaches with an opposite point of view that offer the possibility to understand the economics of the process are presented.

The first number Ψ_{CO_2} assumes that a CL process would require a certain amount of money for the CO_2 separation. In this case, only the net costs of the CL process are considered; the electricity produced by the CL process is already sold to a price of 50 €/MWh as well as the by-products. By this approach, the CL process becomes directly comparable to amine scrubbing processes.

In the second case, the number $\Psi_{MWh_{el}}$ shows how high the cost of CO_2 allowances would have to be to justify the increased production costs of electricity by operating the power plant and the CL process together. In addition, it is taken into account that a certain amount of CO_2 still leaves the stack for which certificates have to be purchased. Consequently, this number is important because it shows the difference of the production costs if the CL process is applied or not and therefore the economical break even in terms of costs for CO_2 emission allowances.

Following, both benchmark numbers are described shortly.

CO_2 Related Costs

The very popular number costs per ton of CO_2 avoided can be defined in the various ways as indicated in Table 4-10.

Table 4-10: Possible combinations of the key number costs for one tone of CO2 avoided.

		Costs			
		Without CO_2 compression		With CO_2 compression	
		Total	Net	Total	Net
CO_2 from	Power plant	*X*	*X*	*X*	*X*
	Power plant + CL	*X*	*X*	*X*	Ψ_{CO_2}

In the scope of this work only one combination is believed to be meaningful: The overall net costs of the CL process divided by the amount of CO_2 that is produced by the power plant AND the CL process. This number is further marked as Ψ_{CO_2}. The overall net cost of the CL process is defined by the difference of operating costs subtracted by the benefits including the costs of the compression of all CO_2. By this approach all merits and drawbacks of the CL process are accounted leading to a number that can be used to decide whether it is useful to run the CL process or to simply buy CO_2 emission certificates. This means the cost for one certificate has to be higher than calculated because the costs for the CO_2 transport and storage have to be covered as well.

Electrical Power Related Costs

Another approach to deduct if it is useful to run the CL process or not is the comparison of the production costs of one MWh of electrical power with the purchase of CO_2 allowances compared to the operation of the CL process that enables the separation of CO_2.

These two values are defined as

$$K_{MWh_{el}}^{Power\ plant} = K_{MWh_{el},original}^{Power\ plant} + S_{MWh_{el}}^{CO_2} K_{Certificate}^{CO_2} \qquad \textbf{4-65}$$

$$K_{MWh_{el},CCS}^{Power\ plant} = X_{\text{Production}}^{Power\ plant} K_{MWh_{el},original}^{Power\ plant} + X_{\text{Production}}^{LLCR} K_{MWh_{el}}^{LLCR} + S_{MWh_{el}}^{CO_2} K_{Certificate}^{CO_2} \qquad \textbf{4-66}$$

Subtracting Eq. 4-65 from 4-66 causes a benefit in case of negative values. This value shall be used further under the term $\Psi_{MWh_{el}}$

$$\Psi_{MWh_{el}} = K_{MWh_{el},CCS}^{Power\ plant} - K_{MWh_{el}}^{Power\ plant} \qquad \textbf{4-67}$$

4.5 Impact of Sorbent Parameters on the CL Process

Following, circulating mass flow, required calciner power, efficiency penalty, price per ton of CO_2 (Ψ_{CO_2}) and production costs of electrical power in case of CO_2 separation with the CL process will be shown and discussed for a power plant with a power output of 1000 MW_{el} and an electrical net efficiency of 45%. The ratio of the electric gross power and the amount of heat transferred to the steam circuit in the CL process was set to 50.3% [141].

The two variables that are going to be varied for every analysis are hardness and CO_2 stability number. Each case is calculated with two different fuels shown in Table 4-1.

As a pre-note, the hint shall be given, that the calculations are based on the separation of a certain amount of CO_2. Therefore, the heating power of the calciner is set as a free variable leading to the circumstance that some operating points would require an enormous power input into the calciner. This would require utilities which would exceed capital expenses of two billion €. These cases are dismissed because it is believed to be unlikely that a power plant owner would invest more than twice as much for a CO_2 separation technology as he had to invest for the whole power plant. Those operating points can be seen in all diagrams for hard coal as a plane area.

4.5.1 Circulating Mass Flows

Fig. 4-7 and 4-8 show the hourly mass flow form the carbonator into the calciner with varying hardness and CO_2 stability number, if the calciner is operated with hard coal or lignite, respectively.

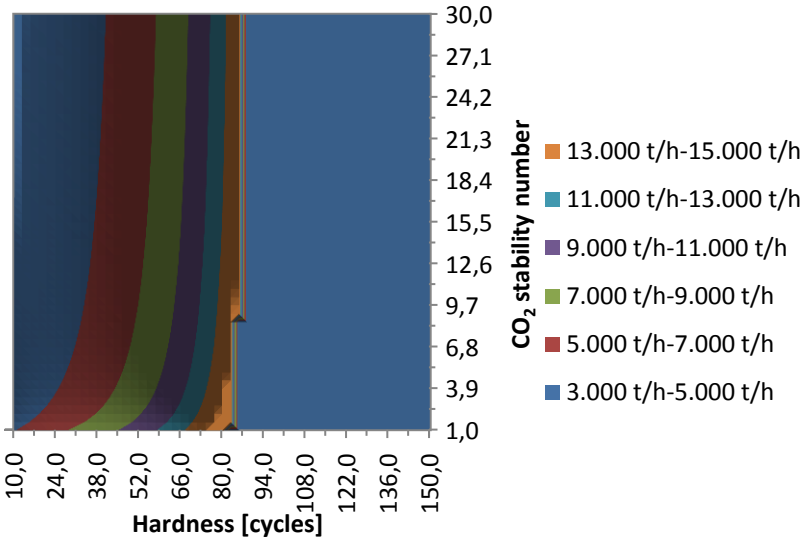

Fig. 4-7: Flow of solids from the carbonator to the calciner in case of hard coal. The minimal hourly flow in this simulation is 2.815 t/h while the maximum is infinite because of the enrichment of impurities.

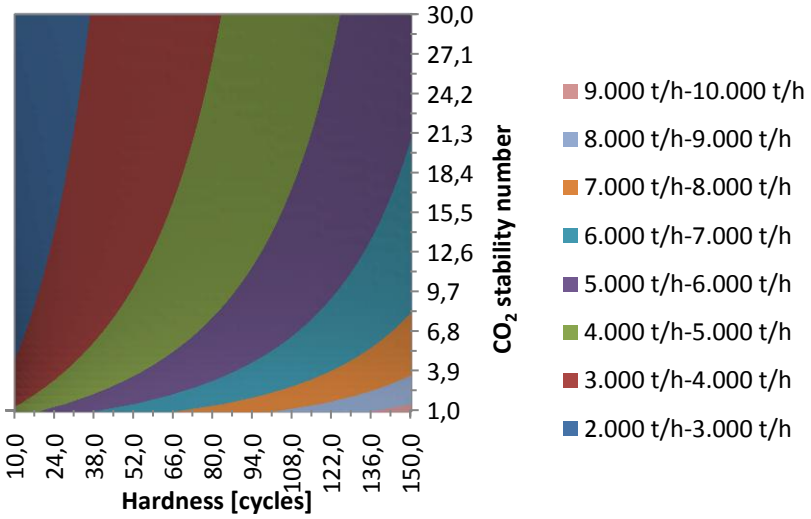

Fig. 4-8: Flow of solids from the carbonator to the calciner in case of lignite. The minimal hourly flow in this simulation is 2,406 t/h while the maximum is given by 9,447 t/h.

Both cases illustrated that due to the prohibition of significant enrichments of impurities, the lowest mass flow can be achieved at high make-up rates and high CO_2 stability numbers. However, a mechanical stability of the sorbent bigger than 90 cycles would not be beneficial for the process if the calciner would be operated with hard coal because the amounts of inerts would out rule the sorbent mass. Accordingly, a far too high heating power would have to be applied in the calciner leading to unreasonable high investment costs.

4.5.2 Required Calciner Power

As indicated before, the accumulation of impurities in the CL process leads to a major increase of the heat demand in the calciner. However, due to the heat consumption of the first calcination of the sorbent, local optima of the heating power depending on the hardness and the CO_2 stability number can be noticed in Fig. 4-9 and 4-10.

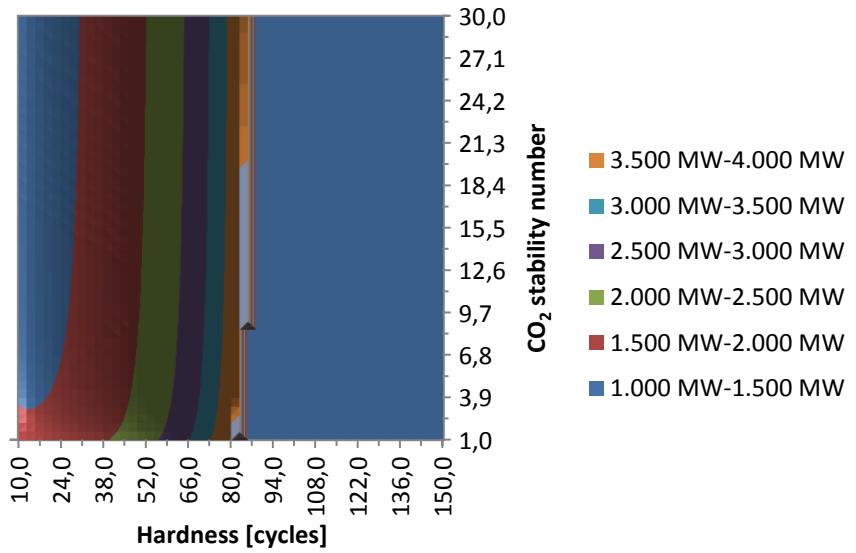

Fig. 4-9: Heat requirement of the calciner in case of the use of hard coal. The minimal power needed in this simulation is 1,327 MW while the maximum is infinite because of the enrichment of impurities.

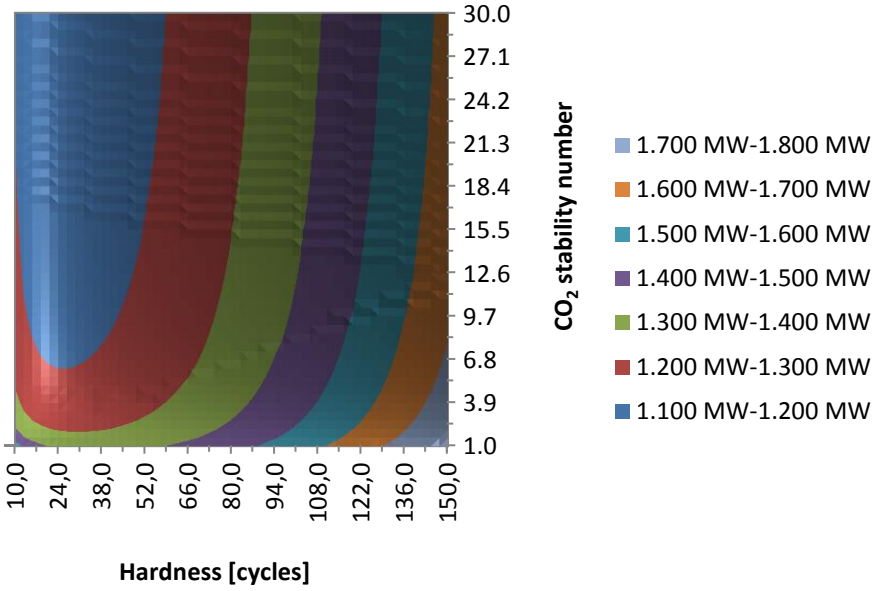

Fig. 4-10: Heat requirement of the calciner in case of the use of lignite. The minimal power needed in this simulation is 1127 MW while the maximum is 1836 MW.

Both cases indicate that a stability of the sorbent of 30 cycles would be sufficient to reach the local optima. Of course, the CO_2 stability number would have to be at least three, meaning that the CaO conversion in the 30^{th} cycle should be around 30%. The product D-2009-006 could fulfil this requirement.

4.5.3 Efficiency Penalties without Compression

As shown in Fig. 4-11 and 4-12, the efficiency optimum is not the same optimum than the optimum for the required calcination power. This effect is caused by the combination of different parameters. However, the biggest impact is given by the required power for the supporting units. This value was assumed to be 62 kWh per ton of CO_2 captured. Comparing the efficiency optimum in case of lignite with the calciner power optimum, around 7% more energy would be needed but the additional energy demand for the supporting units would only be 3% because the sum of CO_2 from the power plant and the CL process is only increasing by this this amount. A more sophisticated model might calculate the energy demand for the supporting units out of process parameters. However, the most important parameter to do so, the amount of reactor internal cycles, is not known yet. Nevertheless, the now chosen approach points into the right direction: An increase of CO_2 produced by the CL process causes an increase of the power demand for the supporting units, e.g. the power needed for the milling of the coal that is fed into the calciner.

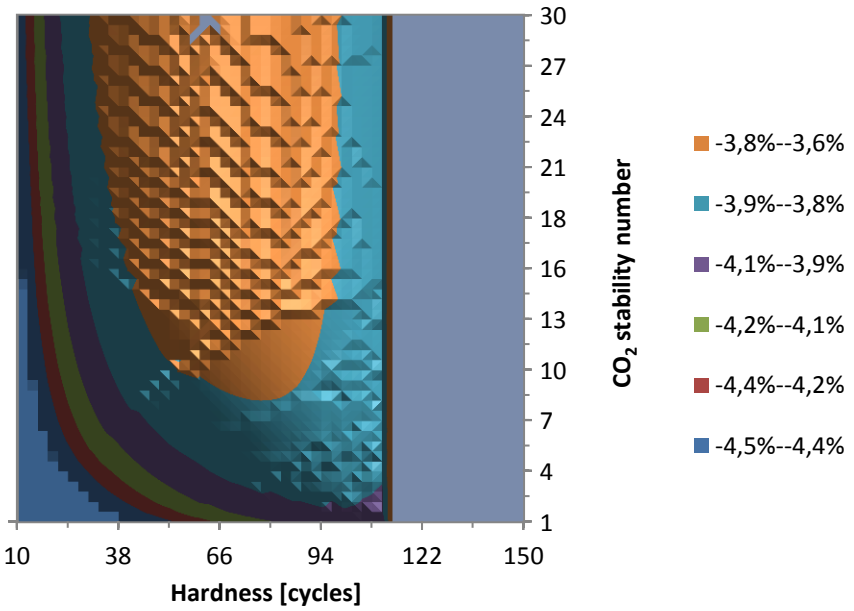

Fig. 4-11: Efficiency penalty in case of the use of hard coal. The minimal efficiency penalty in this simulation is 3,59% points while the maximum is 7.11% points.

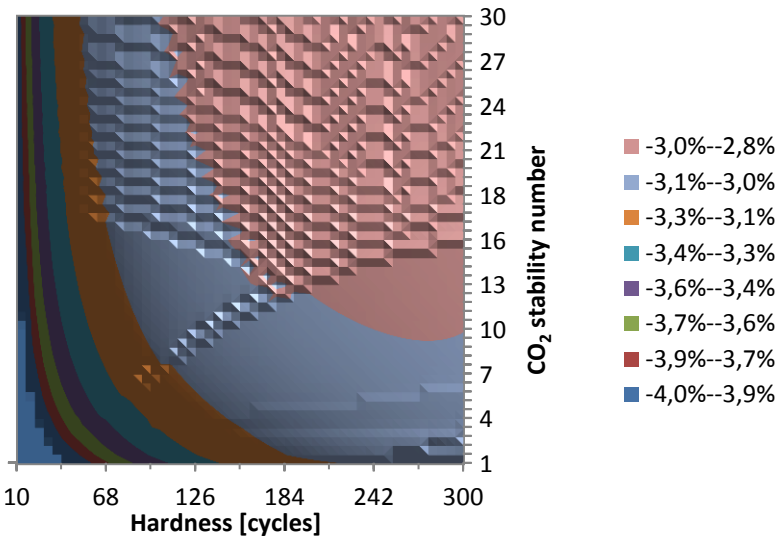

Fig. 4-12: Efficiency penalty in case of the use of lignite. The minimal efficiency penalty in this simulation is 2.89% points while the maximum is 6.64% points.

The optima are, as expected, associated with an average to low required hardness and an outstanding CO_2 stability number of the sorbent. However, the response on improvements of the CO_2 capture ability would be more significant in case of hard coal.

The best achievable efficiency penalties that could be expected, if the process would be run at the optimal operating points with a sorbent that enables this operation would be 4.0 and 4.8 % for lignite and hard coal respectively.

4.5.4 Costs per Ton of CO_2 Captured

Fig. 4-13 and 4-14 illustrate the impact of the sorbents properties on the costs for one ton of separated CO_2, Ψ_{CO_2}. At a first glance the shape looks a little bit contra expectation because one might have guessed that the specific capture costs would have to be in line with the outcomes of the efficiency penalty. However, this guess would have been incorrect because here, the costs per ton of CO_2 capture are considered. By this, the devisor (total amount of CO_2) is increased if the efficiency of the total power plant is decreased. Additionally, the exponential lowering of the specific costs on the increase of machinery capacity overcompensate losses that result out of a poorer process performance.

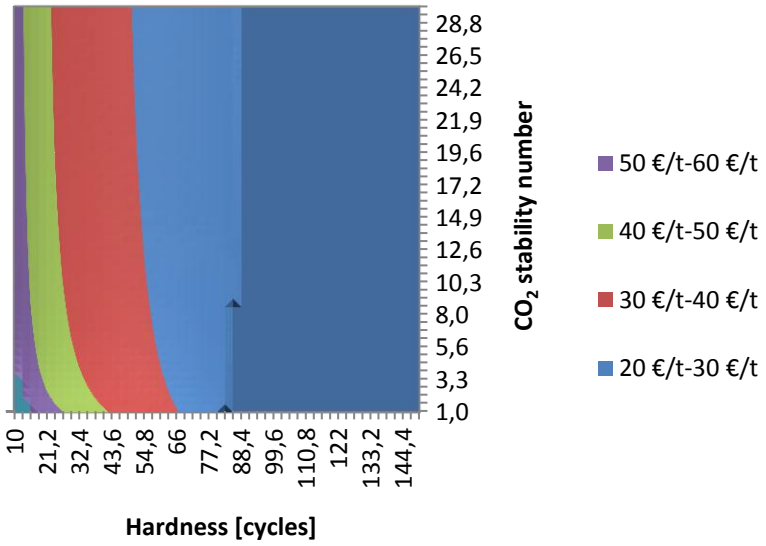

Fig. 4-13: Price per ton of capture CO_2 in case of the use of hard coal. The minimal price per ton in this simulation is 23€ while the maximum is 80€.

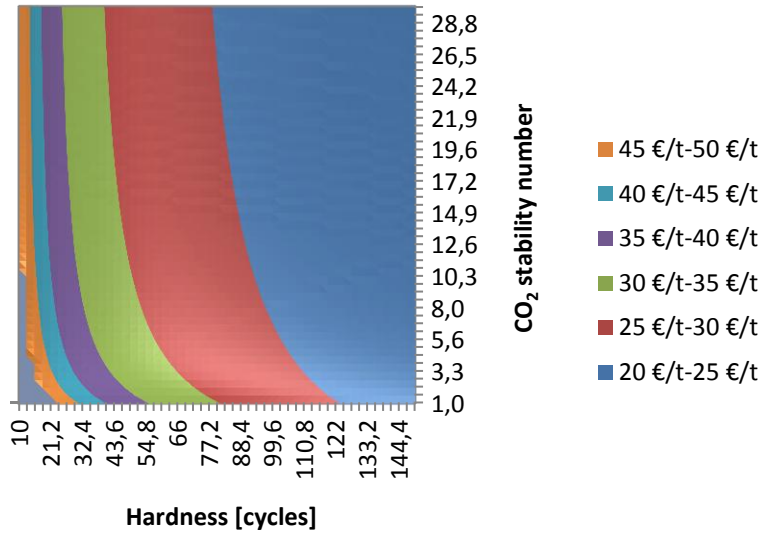

Fig. 4-14: Price per ton of capture CO_2 in case of the use of lignite. The minimal price per ton in this simulation is 20€ while the maximum is 77€.

From this point of view the sorbent would only have to fullfill two requirements: Being as hard and as cheap as possible becauses capital costs would become more and more unimportant compared to the costs of the consumables like sorbent or fuel. However, the scaling exponents are only applicable up to a total utility cost of two billion €. As well, larger combustion units are hard to imagine considering the size and the infrastrutural requirements. Nevertheless, it can be seen that CO_2 capture costs of 25-30 and 30-40 €/t_{CO2} can be reached if the process layout would be done for the lowest efficiency penalty.

4.5.5 Production Costs

The production costs of one MWh_{el} without CCS and without the purchase of CO_2 emission certificates are 29 and 33 € for lignite and hard coal, respectively ([133]). Therefore 30 €/MWh_{el} were set as cost bases, on which the normalised costs for the CO_2 capture with the CL process were added. This approach was chosen because the CL process produces additional electrical power that can be sold on the market. Fig. 4-15 and 4-16 show the overall production costs for one MWh_{el} that is produced together by the power plant and the CL process after the energy demand for the CO_2 compression had been removed.

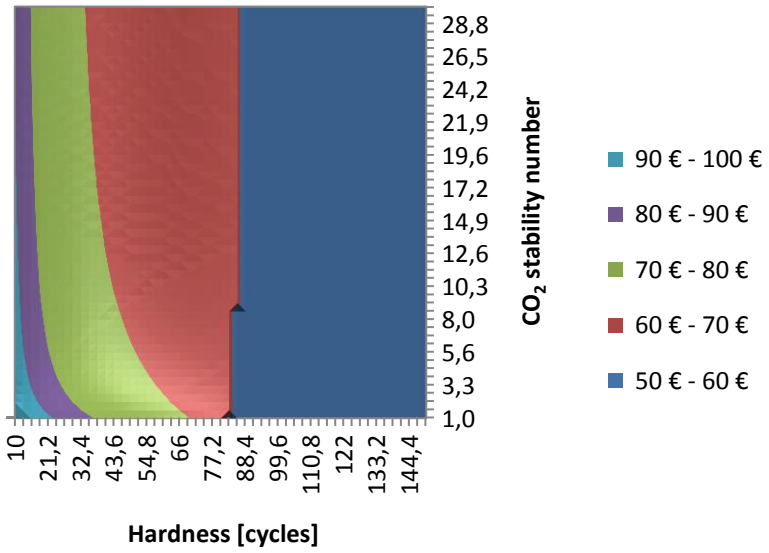

Fig. 4-15: Production costs of one MWh_{el} in case of the use of hard coal. The minimal production costs are 64 €/MWh_{el} while the maximum is 117 €/MWh_{el}. CO_2 compression is included.

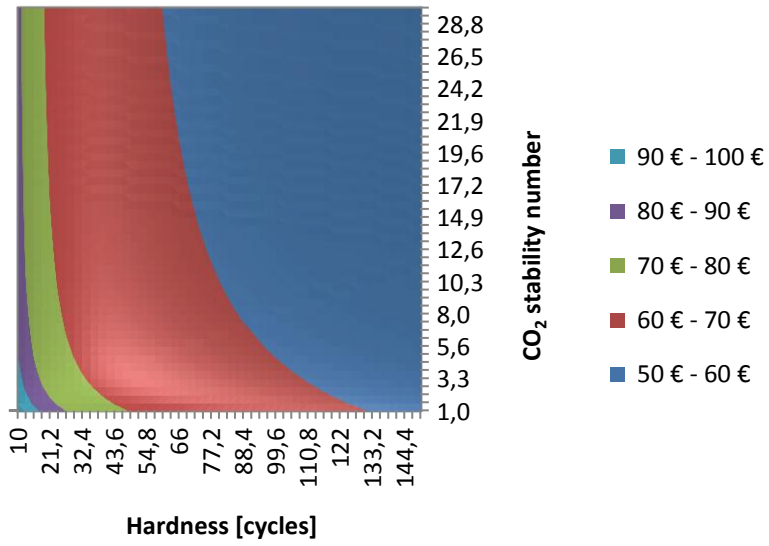

Fig. 4-16: Production costs of one MWh_{el} in case of the use of lignite. The minimal production costs are 56 €/MWh_{el} while the maximum is 109 €/MWh_{el}. CO_2 compression is included.

Still, a part of the CO_2 produced by the power plant is emitted in the air (20%). For this share CO_2 certificates with a specific price of 25 €/t_{CO2} have to be purchased. This amount has already been added to the production costs.

However Fig. 4-15 and 4-16 deliver similar results as Fig. 4-13 and 4-14: The product would have to be basically hard, while the CO_2 stability number is of a minor importance. These outcomes are again contributed to the exponential impact of specific cost reductions, achieved if large CL processes would be built. As well, the product would have to be as cheap as possible to benefit the process economics because of the before discussed reasons.

Nevertheless, it can be seen that the production costs for electricity for a technical optimal operating CL process (optima of the efficiency) would be in the range of 60-70 and 70-80 €/MWh_{el}. For this reason, the specific production costs would be more than doubled.

4.5.6 Annual Sorbent Make-up

As shown in Fig. 4-17 and 4-18, the annual supply of a CL process with sorbent will be a huge logistic challenge.

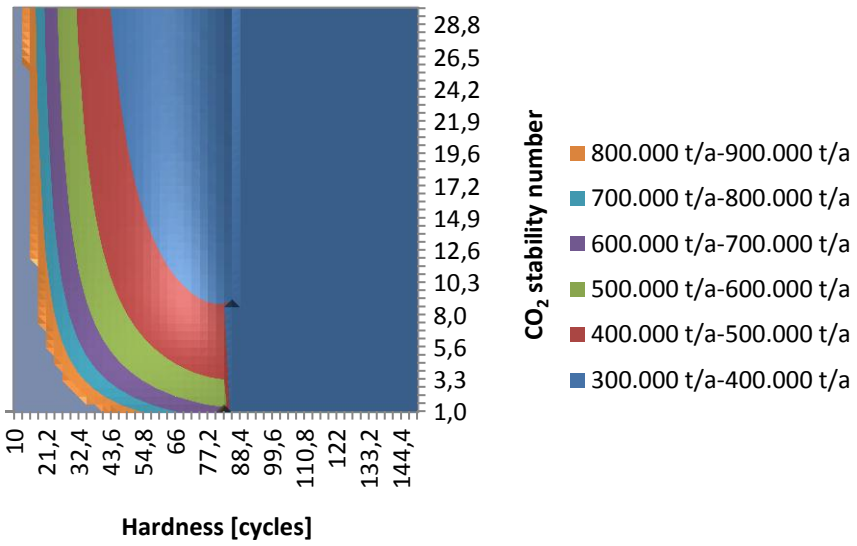

Fig. 4-17: Annual sorbent make-up in case of the use of hard coal. The minimum make-up in this simulation is 307,000 t_{CaO} per year.

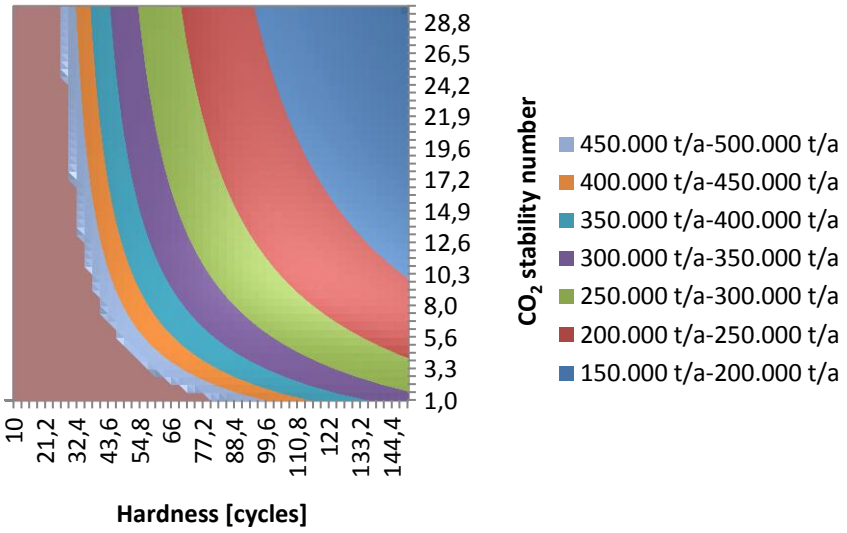

Fig. 4-18: Annual sorbent make-up in case of the use of lignite. The minimum make-up in this simulation is 149,200 t_{CaO} per year.

In best cases, around 150 (lignite) and 300 kt_{CaO} per year (hard coal) would be needed for the operation of the CL process. Considering the case of lignite, a global minimum of the make-up could be found for a hardness of ~300 cycles and a CO_2 stability number bigger than 20. In this case, the annual make-up would be in the range of 100 kt_{CaO}. However, this possible operating point is far beyond an energy efficient operation of the process and therefore not shown.

For an energy efficient operation of the CL process between 300 (lignite) and 600 kt_{CaO} (hard coal) would be required every year.

For comparison, 150 to 200 kt_{CaO} is the amount of FGD products one large lignite power plant (1 GW) requires per year for its flue gas desulfurization.

4.5.7 Main Conclusions from the Simulations

The simulations demonstrated the huge impact of the fuel and the sorbent properties on the CL process. However, it was shown that quite different sorbent properties would be required to achieve an optimisation of different target numbers. Table 4-11 summarises the findings.

Table 4-11: Compilation of learnings from the simulations presented. The given numbers refer to the optimum conditions of the target number. Only the fuel case "lignite" is shown.

Optimised parameter	**Hardness [Cycles]**	**CO_2 stability number**	**Remarks**
Circulating mass flow	0[15]	Infinite	The higer the make-up rate and the higher the CaO conversion, the lower the circulating mass flow. Hardness should be increased on decreasing impurities in the fuel.
Calciner power	15-35	>6	The higher the impurities, the lower the needed sorbent stability.
Efficiency penalty	~300	>20	High impurities of the fuel increase the minimal possible efficiency drop.
Ψ_{CO_2}	Up to 400*	0[16]	Large CL plants benefit low capture costs.
$\Psi_{MWh_{el}}$	Up to 400*	>3	Large CL plants benefit low production costs of electrical power.
Sorbent make-up	300	Infinite	Reasonable make-ups only at the optimum.

In Terms of economics it turned out that only very large CL plants have the potential to operate at a reasonable specific price level. Consequently it is uneconomic to treat low flue gas amounts with the CL process. However, in case of large flue gas amounts compromises between a good efficiency and logistical challenges (transport of the make-up and the waste) have to be found.

The sorbent price was set in these estimations to 80 €/t_{CaO}. This price, even though it is average, causes a contribution of the sorbent costs to the total costs of only 10%.

By this, it is unlikely that higher prices for even improved sorbents are realistic. Accordingly, approaches for synthetic products would have to prove in a very early stage that these are economically feasible.

[15] A hardness of 0 cycles indicates that the makeup should be as high as possible.

[16] A CO_2 stability number of 0 equals a constant residual CaO conversion of 11%.

5 Experimental Section

Research efforts carried out in the scope of this work are categorised by the nature and the availability of the products. Consequently, three different material types were defined.

- ***Basic Materials***: Limestone that is already industrial available. This research step includes a basic categorisation and evaluation of the potential of existing quarries.
- ***Advanced Materials***: Materials that have been treated somehow with existing equipment, e.g. calcination, to improve the hardness or CO_2 capture ability or both.
- ***Synthetic Materials***: Ca-based CO_2 sorbents with outstanding hardness or CO_2 capture ability or both that cannot be produced with the existing equipment in lime plants.

Within this chapter, the unit g_{CaO} is meant to describe the mass of calcined sorbent material in grams even though other elements like aluminium were in the sample.

5.1 Experimental Approach

The starting point for the material screening was the determination of the hardness as carbonate and as oxide. This was done with the delta test that made it possible to evaluate the hardness of a material very quickly with a low sample demand. After the determination of the hardness the pore size distribution and specific surface area of the oxide were measured.

In order to have a high transport stability, a high hardness as carbonate is needed. A high delta value as oxide is seen as good sign because it is believed that this will lower the losses if the carbonate is burned for the first time. Pore size distribution and specific surface area are linked to the CO_2 capture ability and therefore deliver an idea of the expected performance during the CO_2 capture ability test. 100 g_{CaO} were needed for the first characterisation step. In parallel, a TGA test was conducted to get an idea of the CO_2 capture ability during prolonged cycles. In total 30 calcination/re-carbonation cycles were carried out. The sample mass that was needed for this test was in the range of 50 mg_{CaO}. In the event of a successful outcome, a larger quantity of cycled material was produced in a special pilot furnace that is able to change the atmosphere and temperature automatically. Eight cycles were carried out; the procedure stopped with the re-carbonation and delivered additional information regarding the cycling behaviour. Again, the hardness as carbonate (re-carbonated, cycled material) and the oxide were measured. As well, the pore size distribution and the specific surface area were determined. The last step, as the first, had also a sample demand of 100 g_{CaO}.

Taking into account that the BET and Hg intrusion measurement also consume slight amounts of the sample and backup samples had to be kept, the sample demand from the beginning until

the end was about 250 g_{CaO}. In addition to the small lab tests which consumed only a few grams of material, large pilot investigations were carried out, too. By this, lab based results should have been confirmed and a correlation between those and the real process should have been established.

5.2 Experimental Setups

5.2.1 Assessment of the Hardness by the Delta Tests

The delta test was designed and developed to determine the hardness of Ca-based products with a grain size between 100 and 500 µm. The general idea was to introduce a defined amount of energy into a solid bed of particles and measure the change of the outer surface area. Energy was introduced via a press that was able to record the force and the form feed. The change of the outer surface area was calculated with the help of a particle size measurement before and after the introduction of energy into the particle bed. By a mathematical model ([111]), it was possible to compare macroscopic brittle products. It turned out that nearly every limestone and sintered[17] lime can be tested by this test. However, the assessment of the mechanical strength of agglomerates and other substances that show a ductile behaviour on pressure stress could not be performed because the basic assumptions of the test were not fulfilled (see section 3.2.1).

The PSD measurement was carried out with a BECKMAN-COULTER 13 320LS laser light diffraction. Methanol was used as dispersant. During the loading and the measurement, ultrasonic with a relative intensity of three was applied.

The press used and produced by iGM (Ingenierie Générale de Mesures) can be seen on Fig. 5-1. The maximum pressure during one experiment was 28.3 MPa (20 kN on 7 cm²). The form feed velocity was set constant at 10 mm/min. Usually the resulting pellet felt apart if slight tangential forces were applied.

[17] In this scope, the term sintered refers to a CaO with strong interconnections between the CaO grains that lead to a macroscopic brittle breakage pattern.

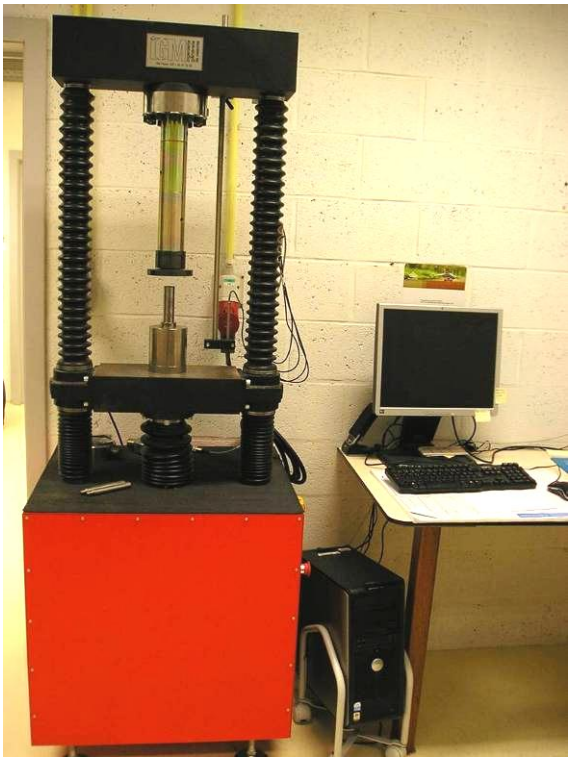

Fig. 5-1: Press with stamp, force recorder and form feed measurement.

5.2.2 Preparation of Calcined Material

The calcination was carried out with ~125 g_{CaO} to get an impression of the properties of the freshly calcined sorbent that has not suffered mechanical stress or sintering. The crucible with the material was put into a normal lab furnace at 900°C. Due to the low temperature of the crucible and the sample (room temperature) the furnace temperature dropped. As soon as the furnace was heated up to 900°C again, the time for the one hour calcination started. After one hour, the crucible was taken out of the kiln and cooled down to room temperature. The burned product was characterised further by BET, Hg-intrusion and delta test measurements.

5.2.3 Five Points BET Measurement

Surface area analysis by nitrogen absorption-desorption (BET method) was only conducted on the calcined product because the specific surface area of carbonates (limestones) was only determined by the outer surface area. Only very few limestones are porous. However, all of those are known to be very soft.

The surface area was measured with a “Tristar 3000” produced by Micromeritics; about 0.6 g of the sample were put into a sample tube. Afterwards, this tube was put under vacuum.

Heating of the sample for two hours to 190°C was necessary to remove already adsorbed gas molecules completely. The temperature of the sample was afterwards to -195°C (evaporation point of liquid nitrogen) to start the measurement of adsorption of nitrogen on the surface of the sample. The adsorption isothermal was used to calculate the specific surface area. This was done automatically by the "Tristar 3000".

5.2.4 Hg-Intrusion

The mercury intrusion porosimeter Micromeritics 9215 was used for the analysis of the distribution of the pore volume according to the diameter of the pores in a range from a few nanometres to several µm. About 0.8g of calcined material was put into a penetrometer, which was connected to low pressure to degas the sample. After the degasing, the penetrometer was filled with mercury and the analysis was started, beginning from low pressure of 40 kPa up to a final pressure of 420 MPa.

5.2.5 Particle Size Distribution (PSD)

In the standard procedure, the PSD was measured with a BECKMAN-COULTER 13 320LS laser diffraction. However, in terms of pilot attrition testing this high precision was neither needed nor handy. Therefore, sieve analysis were done with mesh widths of 125, 250, 300, 350, 500, 630, 800, 1000, 1250 and 2000 µm. The RETSCH sieving tower was operated with a sieving force of 1.5 g and sieving intervals of 10 seconds for 3 minutes.

5.2.6 Preparation of Cycled Material

A special furnace that was equipped with a balance at the bottom and a gas inlet system (see Fig. 5-2) was used to produce sufficient amounts of cycled material for hardness tests. In addition, it provided additional information of the CO_2 capturability over eight cycles that were compared to the results achieved within the TGA.

About 112 g_{CaO} were subsequently calcined at 920°C in an atmosphere of 79% N_2 and 21% H_2O and re-carbonated at 820°C under an atmosphere of 79% CO_2 and 21% H_2O. One cycle took, due to the slow heating and cooling rates, about two hours. Consequently, calcination and re-carbonation lasted for roughly one hour. The volume flow of the gases was fixed to 8 l/min for calcination and re-carbonation.

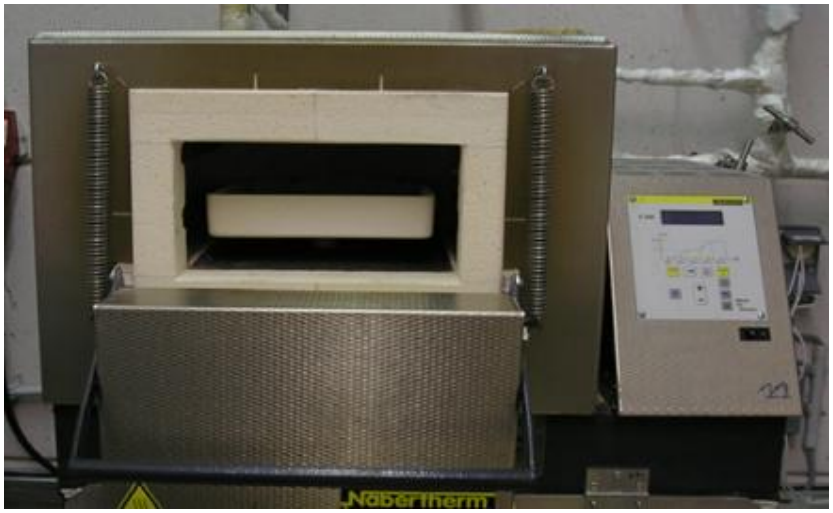

Fig. 5-2: Pilot kiln that was used to produce cycled sorbent material for further investigations.

5.2.7 TGA Procedures

Standard thermo-gravimetric analysis was done with the water vapour furnace "STA 449 F3 Jupiter" produced by NETZSCH. Thirty calcination and re-carbonation cycles were done under a constant gas atmosphere by changing temperatures. However, to see the impact of different test conditions on the performance of the product, two different procedures were defined that are summarised in Table 5-1.

Table 5-1: Special and standard test protocol used for the TGA investigations.

	Special	**Standard**
PSD	600-710 µm	250-500 µm
Mass	~28 mg_{CaO}	~50 mg_{CaO}
Heating rate	20 K/min	25 K/min
Cooling rate	20 K/min	25 K/min
Calcination		
CO_2	0%	12%
H_2O	33%	42%
N_2	66%	46%
O_2	0%	0%
Duration	5 min	~10 min >850°C
Temperature	840°C	920°C
Carbonation		
CO_2	10% (start and stop at 690°C)	12%
H_2O	30%	42%
N_2	60%	46%
O_2	0%	0%
Duration	20 min	~25 min < 750°C
Temperature	650°C	650°C

In order to compare all sorbents, the results of the TGA experiments will be reported in g_{CO2}/g_{CaO}. The term for this unit will be 'CO_2 uptake.

5.2.8 CFB Investigations

Cold CFB Tests

In order to validate the accuracy of the delta value, cold circulating fluidised bed experiments with selected carbonates and oxides were conducted. The arrangement of the riser, cyclone, standpipe, bunker, loop seal and filter can be seen in Fig. 5-3.

One unique feature was the on-line attrition mass recognition that was realised by three mass probes located beneath the filter. By this, it was possible to record attrition curves for a long duration.

The fluidisation was done through a double wall pipe in that the fluidisation air was introduced into the outer wall and directed through a slit between the inner and outer wall at the bottom of the pipe into the reactor. Through this arrangement a soft fluidisation was achieved.

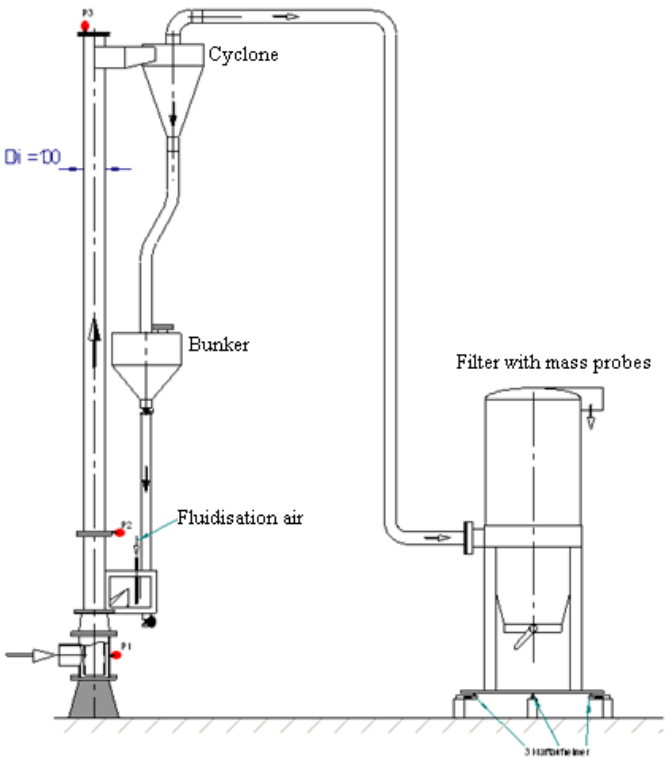

Fig. 5-3: Experimental setup of the CFB test designed and operated by the IRKB.

The inner diameter of the riser was 100 mm while the height was around 5 m. The loop seal and therefore the reintroduction of the cycled material was placed around 0.5 m above ground. The bunker had a capacity of 20 kg carbonate. The cyclone was able to separate particles larger than 13 µm to 100% from the gas stream. Pressure probes were placed in the rises at the bottom, above the loop seal and at the top. Via those pressure information the mass

loading in the reactor was recognised. Furthermore, the air flow used for the fluidisation was measured to derive the amount of circulating mass with the help of a calibration curve that was recorded before the tests with a carbonate and with an oxide. For each test, about 20 l of sorbent (~20 kg_{CaCO3} or 13 kg_{CaO}) were used.

The particle size of the sorbents was always kept constant between 260 and 500 µm. However, few experiments were done with the product D-2011-008 to see the impact of a sieving step and different grain sizes on the overall attrition. An industrial available fraction between 300 and 700µm was sieved into two fraction, 260-500µm and 500-800µm. Fines were discharged. The original, the sieved and the re-mixed fraction comprising of the same share of particles between 260-500 and 500-800µm like in the original product, were investigated.

Hot Bubbling Fluidised Bed Tests

Tests in hot bubbling fluidised beds were intended as a first step of the upscaling of the lab experiments. Therefore, tests were carried out in a small and a large fluidised bed. The scope of the small fluidised bed experiments was only the assessment of the mechanical hardness of different sorbents, while large tests were intended to give indications for the CO_2 uptake and the hardness at the same time.

Small bubbling fluidised bed tests were done with four different sorbents in a tube reactor with an inner diameter of 21 mm. The experimental setup is shown in Fig. 5-4.

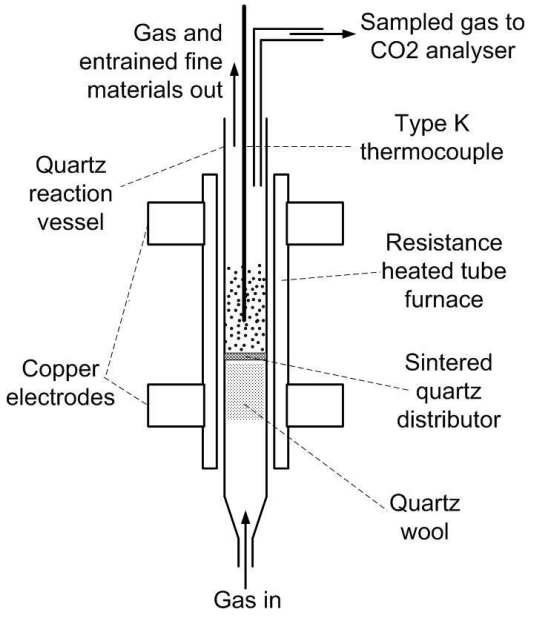

Fig. 5-4: Experimental setup of small hot BFB attrition experiments. Figure taken from [23].

The mechanical stability as carbonate and as oxide was investigated by means of the bed loss during one experiment that lasted one hour. The size of the particles was between 400 and 500 μm. The investigation for the evaluation of the hardness of the carbonate was done at 650°C in 15% CO_2 in N_2. The superficial velocity was 0.25 m/s, while the bed volume was about 10 ml. Particles were directly introduced into the reactor at the operating temperature.
Oxides were prepared from the carbonates in the reactor. Calcination was done at 900°C under fixed bed conditions (minor N_2 fluidisation, superficial velocity <0.01 m/s) and was finished after 10 to 20 min. In summary, the total calcination duration was one hour. The received calcined particles (about 10 g) were unloaded and transferred to a dessicator for cooling. Attrtition tests were done at 850 °C in 15 % CO_2 in N_2. The superficial velocity during these experiments was 0.1 m/s.

5.3 Basic Materials

More than 50 different natural sorbents have been investigated. However, due to the unhandy amount of the produced data, only eleven different sorbents will be discussed in detail. Wherever possible, the number of displayed sorbents will be increased to show the accuracy of trends in a better way. For a better comparison of the results to literature findings, samples from the most often investigated limestones (La Blance, Cadomin and Havelock) had been organised and tested under the conditions described in subsection 5.2. Table 5-2 gives an overview of the sorbents that were used for different tests.

Table 5-2: Tests performed on selected sorbents.

	TGA		Delta test		Pilot	Cold	Hot BFB	
Sorbent	**Standard**	**Specialised**	**Carbonate**	**Oxide**	**furnace**	**CFB**	**Small**	**Large**
D-2009-002	X	X	X	X	---	X	X	---
D-2009-003	X	X	X	X	---	X	X	---
D-2009-009	X	X	X	X	---	---	X	---
D-2009-010	X	---	X	X	---	---	---	X
D-2010-002	X	---	X	X	---	X	---	X
D-2010-006	X	X	X	X	X	---	X	X
D-2011-001	X	---	---	---	---	X	---	---
D-2011-002	X	---	---	---	---	X	---	---
D-2011-006	X	---	---	---	---	X	---	---
D-2011-007	---	X	X	X	---	X	X	---
D-2011-008	---	---	---	---	---	X	---	---
Havelock	X	---	---	---	---	---	X	---
Cadomin	X	---	---	---	---	---	X	---
La Blanca	X	---	---	---	---	---	X	---

The chemical composition of the products is summarised in Table 5-3.

Table 5-3: Chemical composition of selected products. Red marked samples are CaO. The chemical composition of limestone from Havelock, Cadomin and La Blanca was taken from [13].

wt%	CaO	MgO	SiO_2	SO_3	Fe_2O_3	Al_2O_3	Mn_2O_3	K_2O	Cl	LoI
D-2009-002	54.88	0.52	0.59	0.01	0.06	0.12	0.03	0.02	0.00	43.45
D-2009-003	54.75	0.48	1.05	0.05	0.07	0.03	0.03	0.00	0.00	43.43
D-2009-009	54.60	0.70	0.84	0.09	0.14	0.17	0.05	0.04	0.00	43.40
D-2009-010	54.73	0.51	1.32	0.00	0.23	0.57	0.00	0.08	0.00	43.53
D-2010-002	54.83	0.52	0.54	0.00	0.10	0.16	0.03	0.00	0.00	43.60
D-2010-006	55.20	0.45	0.53	0.03	0.12	0.26	0.00	0.00	0.03	43.40
D-2011-001	90.92	1.39	3.48	0.59	0.43	1.38	0.08	0.27	0.00	1.45
D-2011-002	96.11	0.55	0.75	0.01	0.21	0.26	0.02	0.03	0.00	1.40
D-2011-006	91.95	1.67	2.69	0.18	0.35	0.42	0.09	0.10	0.00	1.79
D-2011-007	54.52	0.42	0.28	0.00	0.04	0.13	0.03	0.01	0.00	43.84
D-2011-008	55.05	0.39	0.14	0.00	0.02	0.04	0.03	0.01	0.00	43.81
Havelock	54.9	0.33	0.51	n.a.	0.11	0.25	n.a.	0.07	n.a.	43.34
Cadomin	51.97	2.55	0.79	n.a.	0.14	0.42	n.a.	0.2	n.a.	44.61
La Blanca	55.67	0.15	0	n.a.	0	0	n.a.	0.04	n.a.	43.96

5.4 Advanced Sorbents

Many efforts had been undertaken to repeat and prove the promising literature findings discussed in paragraph 3.5. For example, the product D-2010-002 was thermally pre-treated between 1.25 and 24 h under air and pure CO_2 at a temperature between 840 and 1100°C. Afterwards, extended re-carbonation for three hours under a pure atmosphere of CO_2 at 650°C was done in some cases. In total eleven different combinations of temperature, duration, atmosphere and optional re-carbonation were tested. Additional sixteen tests were carried out with other materials. However, none of these efforts resulted in the creation of a sorbent that exceeded the average CO_2 capture ability of the best untreated basic material D-2010-002. Accordingly, only one example of this outcome will be displayed in chapter 6.

5.5 Synthetic Sorbents

The particle size requirement of the CL process caused several problems during the investigation of synthetic sorbents because modifications on an atomic scale require very small particle sizes, this leading to powdered substances that have to be shaped somehow. Common agglomeration techniques (see section 3.6.1) create particles larger than 1 mm. On top, not every mixture can be shaped as it is, but has to be treated with agglomeration supporting substances, thus making it impossible to see only the effect of dopants on the

sorbent performance. Another critical issue is the destruction of the sorbent properties due to the physical parameters, like high pressure during the shaping. Due to these difficulties, some of the approaches have only been tested by TGA as powder.

The products that have been shaped could not be tested with respect to attrition resistance parameters because the delta test would not work for those products and other tests would require material amounts that could not be produced on a lab scale. However, the standard calcination procedure was executed (see subchapter 5.2), thus indicating that most of the calcined agglomerates lost their mechanical stability completely.

The following subsection shall only give a general overview over the conducted experiments. Details and results will not be shown in this work because of intellectual property issues.

5.5.1 Extrusion

The powdered product was mixed with water and (in some cases) with additional substances like $Ca(OH)_2$, to receive a mortar-like gel that was put into an extruder and then pressed through a 1 mm mesh. The cylinder like particles with a length of some millimetres were dried and in some cases re-carbonated to increase their strength or to alter their texture. Afterwards, the particles were crushed and sieved to 260-500 µm in order to remain a constant grain size fraction for the TGA tests. Fig. 5-5 shows the used extruder and the shape of the received particles.

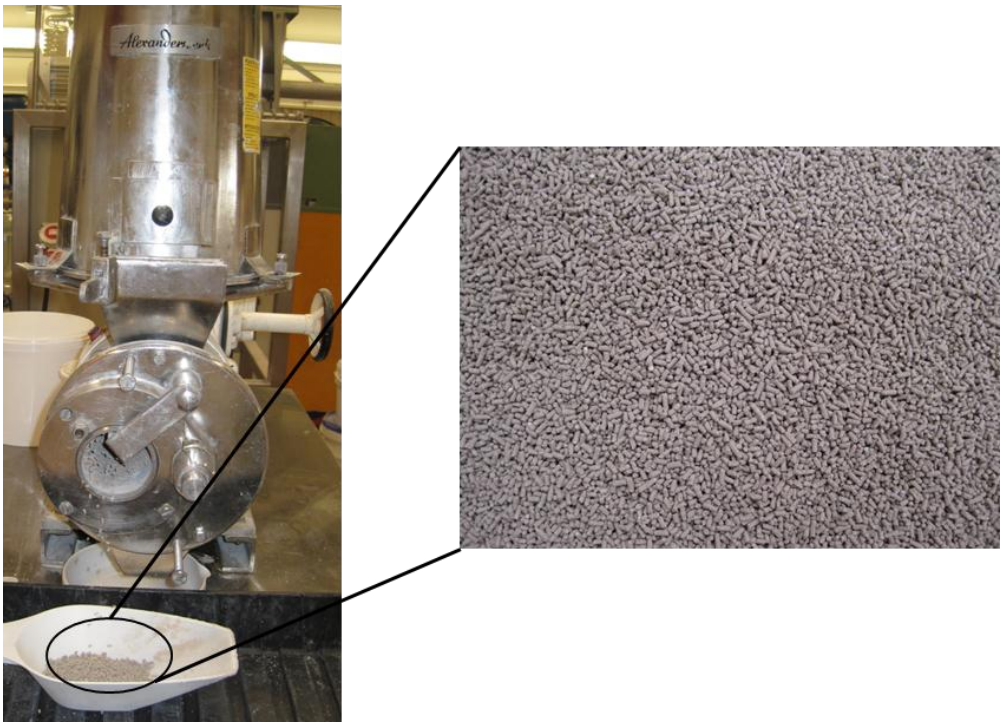

Fig. 5-5: Extruder used for the shaping of powders and according appearance of the particles produced by this technique.

5.5.2 Hydrolysis

Hydrolysis describes the exothermic reaction of CaO with water to $Ca(OH)_2$. By the choice of the right amount of water, temperature and additive a $Ca(OH)_2$ powder with an optimised pore structure can be produced. However, the internal texture and the associated high specific surface area of more than 40 m²/s of such special product appeared to be sensitive up on mechanical stress (sifting or agglomeration).

5.5.3 Co-Precipitation and Nano-Sized Sorbents

Milk of lime was produced with limes coming from different origins. CO_2 was directed through those suspensions in a stirred reactor leading to the formation of different kinds of PCC that was classified according to its habit (see subsection 2.2.1). Besides the investigation of different types of PCC, organic and inorganic additives were added, too. In order to coarsen the very fine powder $Ca(OH)_2$ and other products, additives had to be added for the extrusion.

5.5.4 Ca-Acetate Precursor

Acetic acid and limestone was mixed according to the procedure provided by [72]. As well, pure and commercially available calcium acetate powder was completely dissoluted in water and slowly precipitated at the edge of a beaker. By this process, a very porous, highly aerated and broccoli-like solid (see Fig. 5-6) was received. This solid was crushed and sieved to 260-500 µm and tested for its CO_2 capture ability. Hardness tests were not performed because of the very fragile nature of this kind of product.

Fig. 5-6: Precipitated calcium acetate received from dissoluted analytical grade calcium acetate.

6 Results and Discussion

6.1 Basic Materials

6.1.1 CO_2 Capture Ability

6.1.1.1 TGA Test with Standard Conditions

The sorbents D-2009-003, D-2009-009 and D-2011-001 have been chosen to illustrate different observed effects in a good manner.

First, the maximum conversion within the standard test procedure is shown in Fig. 6-1.

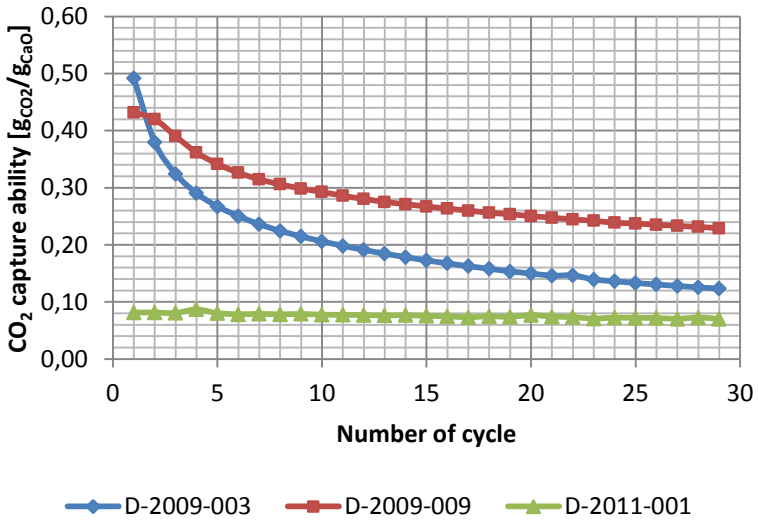

Fig. 6-1: CO_2 capture ability versus cycles under standard conditions. Re-carbonation duration of the CO_2 capture ability points is 25 min. Maximum re-carbonation duration was 25 min.

It can be seen that the sorbent D-2011-001 has a very poor but constant CO_2 capture ability. This product is an industrial available sintered lime. D-2009-003 has the best CO_2 capture ability at the first cycle. Unfortunately, the drop in the CO_2 capture ability is very fast and after 29 cycles only 5 percent points higher than D-2011-001. One of the best performing products tested was D-2009-009. This sorbent has a good initial CO_2 uptake and a slow decay in the CO_2 capture ability. One very similar product to D-2009-009 was delivered to the TU Darmstadt for pilot testing.

One very important question that has to be answered for the operation of the CL process is the CaO conversion, i.e. CO_2 capture ability, on shorter re-carbonation durations.

Fig. 6-2 and 6-3 show the CO_2 capture ability at different timings of the re-carbonation that lasted 25 minutes in total.

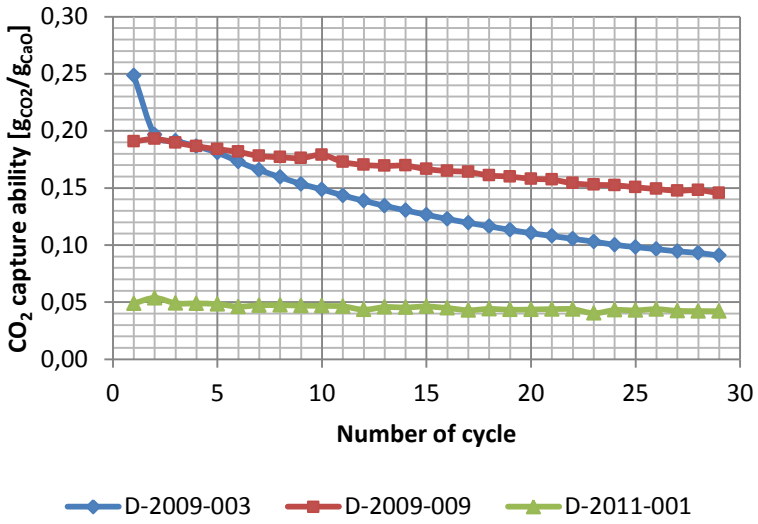

Fig. 6-2: CO_2 capture ability versus cycles under standard conditions. Re-carbonation duration of the CO_2 capture ability points is 10 min. Maximum re-carbonation duration was 25 min.

It is likely that the re-carbonation degree up to the 10th minute is limited by the mass transport of CO_2 from the atmosphere to the active surface sites of the sorbent particle. Comparing the product D-2009-003 with D-2009-009 (see Fig. 6-2) it shows that both sorbents act nearly the same up to the sixth cycle. Afterwards D-2009-003 decreases its CO_2 capture ability much faster.

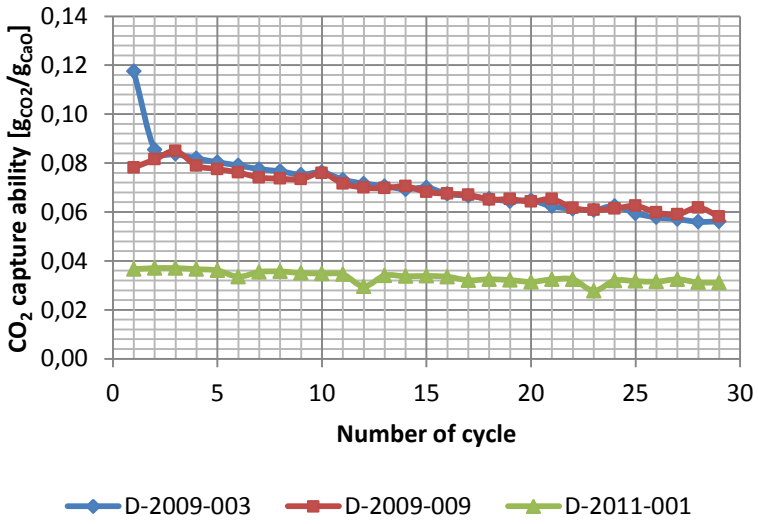

Fig. 6-3: CO_2 capture ability versus cycles under standard conditions. Re-carbonation duration of the CO_2 capture ability points is 5 min. Maximum re-carbonation duration was 25 min.

This effect is believed to be caused by pore mouth blocking that seems to take place much faster in the product D-2009-003 than in D-2009-009. As figured out (results not presented here), the CO_2 capture ability in the fast re-carbonation region is directly linked with the specific surface area. Accordingly, the products D-2009-003 and D-2009-009 lose about 0.1% of their active surface area during each cycle but D-2009-003 would lose its surface area

proportionally fast after the sixth cycle (considering the CO_2 uptake after 10 min). This can only be explained by a pore mouth blocking.

Fig. 6-4 allows a closer look on the kinetics of the CO_2 uptake of the sorbents during the 13th cycle and the associated processes in the particles.

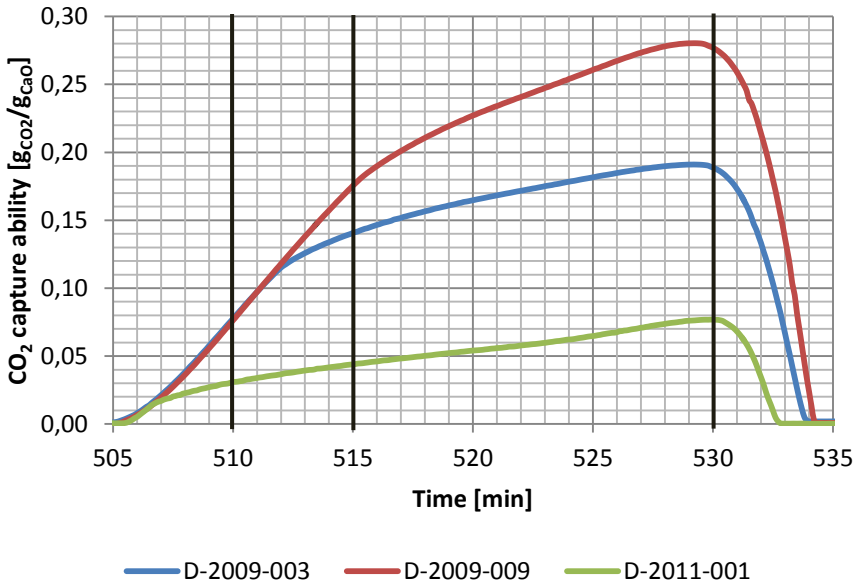

Fig. 6-4: CO_2 capture ability versus cycles under standard conditions. The 13th cycle is displayed. Re-carbonation durations of 5, 10 and 25 minutes are highlighted.

Two different re-carbonation regimes can be noticed: First, a fast surface reaction that is finished after two minutes for D-2011-001, but lasts for more than ten minutes in case of D-2009-009. Second, a diffusion-controlled stage in which the CO_2 capture occurs only due to the diffusion of CO_2 through a layer of $CaCO_3$. The kinetic of the first stage is controlled by the mass flow of CO_2 to the active CaO cites while the second is diffusion controlled. It is extremely important to note that the rate of CO_2 uptake in the diffusion-controlled regime of the sorbents D-2009-003 and D-2011-001 is nearly the same (~0.003 $g_{CO2}/(g_{CaO}$ min)). This can only be explained by nearly equal specific surfaces areas both products offer for the diffusion. D-2011-001 had an initial specific surface area of 0.3 m^2/g_{CaO} while D-2009-003 had 8.8m^2/g. Consequently, pore mouth blocking must have taken place in case of the product D-2009-003, leading to a very low accessible specific surface area below 0.3 m^2/g_{CaO}. In case of the sorbent D-2009-009 the rate of CO_2 uptake in the diffusion controlled regime is in a range of ~0.006 $g_{CO2}/(g_{CaO}$ min), indicating that the specific surface area for the diffusive flow is double and that somehow pore mouth blocking is lower than in case of D-2009-003.

With the given numbers, it is possible to estimate the flux of CO_2 through a layer of $CaCO_3$, which has a thickness of 100 nm (see section 2.6 or [11]) on a CaO structure at a temperature of 650°C.

$$J_{650°C}^{12.5\%_{CO_2}} \approx \frac{0.003\frac{g_{CO_2}}{g_{CaO}\min}}{0.3\frac{m^2}{g_{CaO}}} = 0.01\frac{g_{CO_2}}{\min m^2} = \underline{\underline{3.8\cdot10^{-6}\frac{mol_{CO_2}}{s\cdot m^2}}} \qquad \textbf{6-1}$$

This would equal a growth rate of ~9 nm_{CaCO3}/min.

According to FICK's first law (see eq. 2-6), the diffusion coefficient at this temperature can be calculated according to

$$D_{650°C} = J_{650°C}^{12.5\%}\frac{\Delta x}{\Delta c} = 3.8\cdot10^{-6}\frac{mol_{CO_2}}{s\cdot m^2}\cdot\frac{10^{-7}m}{(12\%-1\%)} = \underline{\underline{3{,}4\cdot10^{-12}\frac{mol_{CO_2}}{s\cdot m}}}. \qquad 6\text{-}2$$

The difference in concentration was set to shares of one atmosphere. This unit is more handy because the equilibrium partial pressure of CO_2 above CaO, according to BAKER's equation is given in the same unit.

D_0 of Eq. 2-7 can be calculated using this diffusion constant and assuming an activation energy for the diffusion of CO_2 in a solid of $CaCO_3$ of 2 eV.

$$D_0 = D_{650°C}\exp\left(\frac{q}{k_B T}\right) = 0.28\frac{mol_{CO_2}}{s\cdot m} \qquad 6\text{-}3$$

Now, it is possible to predict the maximum mole flux of CO_2 through a 100 nm thick layer of $CaCO_3$ by a given CO_2 partial pressure and a given temperature

$$J = D_0\exp\left(-\frac{q}{k_B T}\right)\frac{(p_{CO_2} - p_{CO_2,eq.})}{\Delta x} = D_0\exp\left(-\frac{q}{k_B T}\right)\frac{\left(p_{CO_2} - 10^{7.079-\frac{38000}{4.574T}}\right)}{\Delta x}. \qquad 6\text{-}4$$

Ion mobility and chemical potential (difference between equilibrium CO_2 partial pressure and CO_2 partial pressure in the surrounding atmosphere) counteract each other. Consequently, optima for different combinations of CO_2 partial pressures and temperatures exist (see Fig. 6-5). These calculations show the importance of the process condition on the evaluation of the overall sorbent performance. High re-carbonation temperatures and high CO_2 partial pressures are potentially able to increase the performance of the same product in the diffusion controlled stage significantly because the CO_2 flux of CO_2 through the product layer can be increased by several orders of magnitudes. However, these positive effects might only be observed for as long as no pore mouth blocking is taking place.

In terms of the real CL process, these findings are important as well because they illustrate that the diffusion-controlled regime will be of minor importance for the overall CO_2 capture ability. Of course, the bad kinetics during this regime could be compensated by very large masses in the carbonator, but it is unlikely that this approach would be economical feasible due to the increase of the utility size by several hundred times.

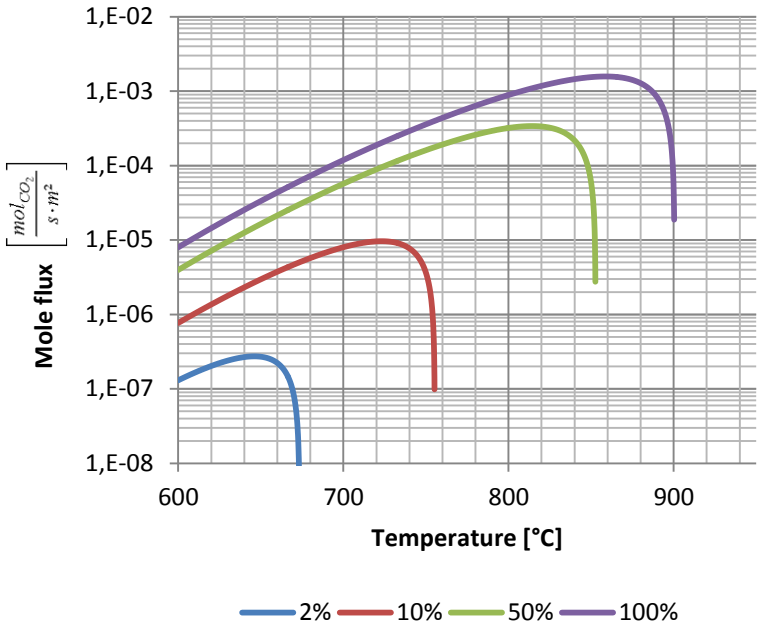

Fig. 6-5: Mole flux of CO_2 through a 100 nm thick layer of $CaCO_3$ versus temperature for different CO_2 partial pressures.

However, only the fast surface reaction regime should be considered for the design of the CL process carbonator.

These outcomes can also be used for the evaluation of reactivation steps by prolonged re-carbonation. Fig. 2-14 shows that the grains of lime with medium reactivity have a size between 0.5 and 1 µm while sintered lime shows grains between 2 and 5 µm. These grains would be fully recarbonated after 2 respectively 40 min at 850°C and 100% CO_2. However, "pore mouth blocking" or more likely the full blocking of the outer surface of the particle will occur because the particle shrinks slightly during an extended calcination or during a lot of successive calcination steps. By this, is would take roughly one month for a particle with a final grain size of 400 µm to be fully recarbonated if it would have been treated at 850°C and 100% CO_2. Consequently, reactivaiton of sorbents by long re-carbonation steps might only be useful for products with a very open internal pore structure that enables the diffusion of CO_2 to the CaO bone structure from the inside of the particle and not only from the outside. Such a clase of products might be agglomerates. Thus, it is not suprising that these sorbents react very sensible towards a change in the test conditions.

The comparison between the sorbent D-2009-009 and the limestones coming from La Blance, Havelock and Cadomine can be seen in Fig. 6-6.

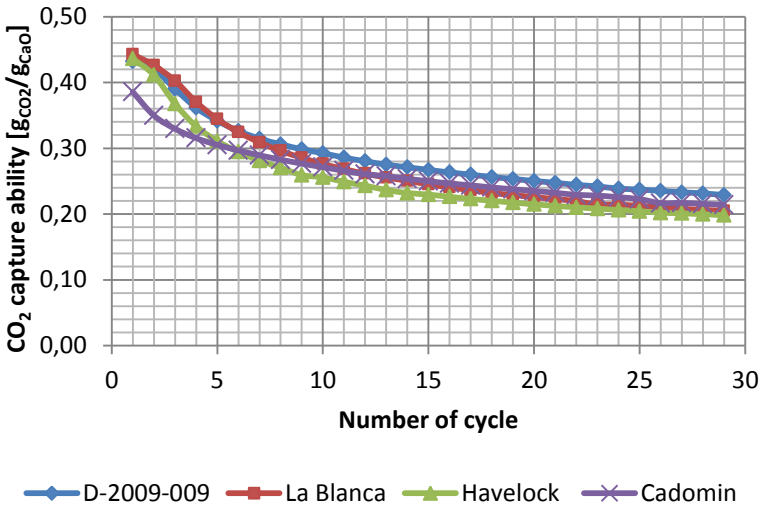

Fig. 6-6: CO_2 capture ability versus the number of cycles of D-2009-009 compared to other, often in the literature used sorbents.

It turned out that all products show a nearly equal and excellent CO_2 capture ability.

6.1.1.2 TGA Test with Special Conditions

Fig. 6-7 shows a comparisson of the CO_2 uptake of the sorbent D-2010-006, an industrial available agglomerate, that was tested under standard and under special TGA conditions.

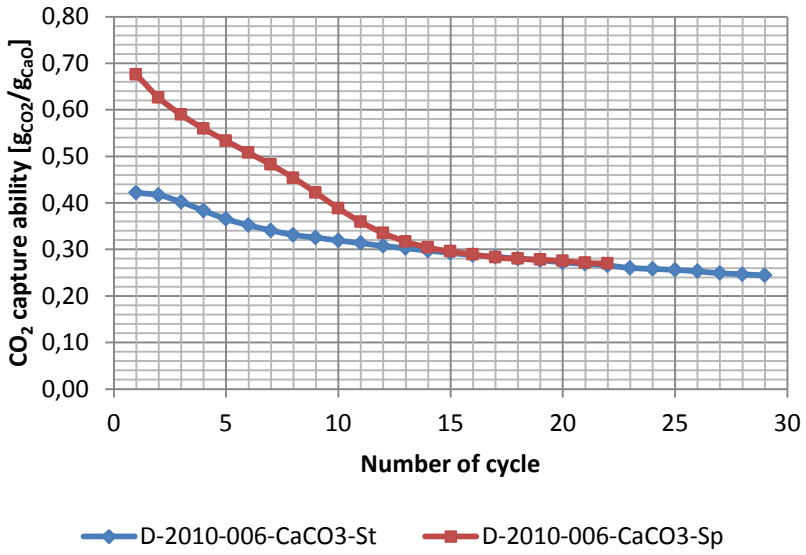

Fig. 6-7: CO_2 capture ability versus the numbers of cycles of the product D-2010-006 without any pre-treatment ($CaCO_3$) under standard (St) and special (Sp) TGA test conditions.

This product shows an improved CO_2 capture ability up to the 13th cycle under special TGA conditions. Afterwards the decay in the CO_2 capture ability is the same for both test protocols. This behaviour is believed to be linked with the milder special test conditions; calcination is done at a lower temperature and, for a shorter periode without CO_2. Therefore, the initial fast decrease of the CO_2 capture ability is significantly slowed down.

Fig. 6-8 shows the outcomes of the different test protocols, if the sorbent D-2010-006 was pre-calcined for 2.5 h at 1060°C under air.

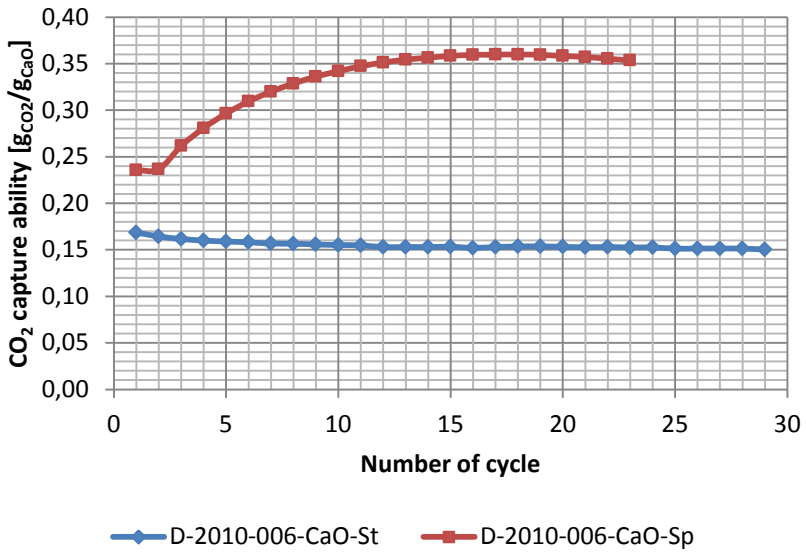

Fig. 6-8: CO_2 capture ability versus the numbers of cycles of the product D-2010-006 that was calcined at 1060°C for 2.5 h in air under standard (St) and special (Sp) TGA test conditions.

The standard test protocol delivered the expected outcome: Due to the intense pre-treatment, the CO_2 capture ability is nearly equal throughout all the cycles, indicating that this capture level is somehow the equilibrium between the creation and destruction of new surface area during the cycling. However, the special test procedure shows at the beginning of the cycling, just like in case of the untreated material, a better CO_2 capture ability. Somehow, this CO_2 capture ability is increasing up to the 17th cycle up to 35 g_{CO2}/g_{CaO}, an outstanding value for a material in the 17th cycle. Unfortunately, this good performance shows first indications of a decreasing CO_2 capture ability again, also this increasing CO_2 capture ability was never observed for any combination of material and pre-treatment conditions during the standard TGA test protocol.

Because the special test protocol was only experimental and far beyond of what is expected to happen in a large CL process, deeper investigations of this effect were not carried out.

6.1.2 Hardness Investigations

6.1.2.1 Delta Test

Carbonate and Once Calcined Materials

Fig. 6-9 shows a comparison between the hardness of the products as oxide and carbonate before cycling. The diagonal illustrates improvements (points above), worsenings (points below) and constants (points on the line) in the hardness of the products due to a single

calcination step at 900°C for one hour. Only six products show a significant improvement of the mechanical stability due to the calcination step, nine products remain their hardness as oxide as it was in the carbonate and 15 show a significant worsening.

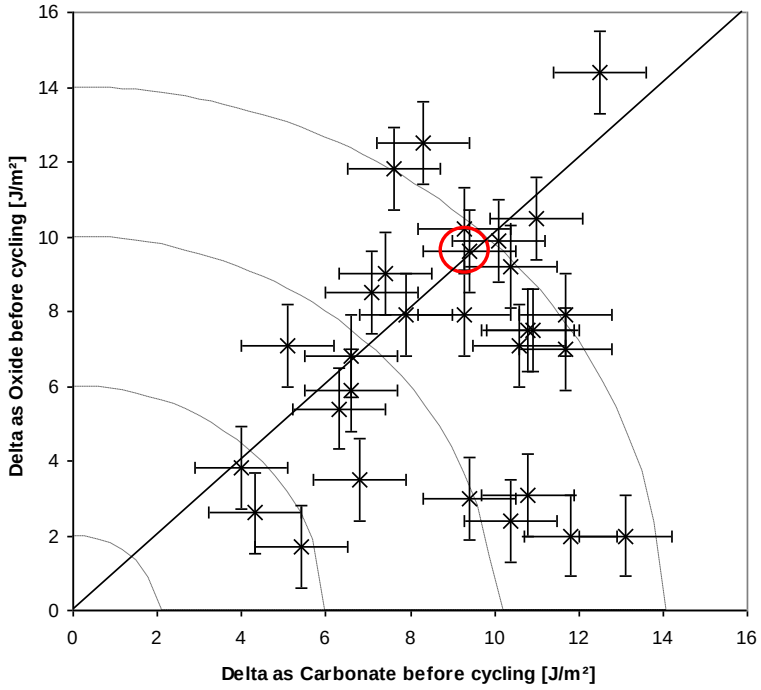

Fig. 6-9: Comparison of the hardness as carbonate and oxide. Material D-2009-009 is marked with a red circle. The error bars were calculated with a series of five delta measurements on quicklime received by calcination of limestone at 980°C for 2.5 h. The standard deviation was in the range of 0.48 J/m² while the error was 1.10 J/m² taking a confidence interval of 99%. The dashed circles in the Figure could be seen as general classification: Products in the smallest circle are completely unsuited for the process while samples in the larger circles may be suited.

A general classification could be done regarding Fig. 6-9: Samples in the lower left corner are unsuited for the process, samples in the lower right corner would be unsuited for low make-ups but the transportation of the raw material should be possible without any problems. Samples in the upper region of the graph are generally suited for a low make-up process but transportation problems for the raw products in the upper left could occur.

Links between Chemistry and Hardness

No link between the hardness as carbonate and the chemical composition could be identified. This finding is reasonable because the mechanical history (kind of crushing, sieving and transportation) and the formation must have led to different stress patterns in the particles. In special cases, this particle internal stress might be linked with a certain chemical composition but for the majority of the samples other parameters than the chemical composition itself determine the hardness as carbonate.

During calcination, chemical reactions are possible that lead to at least some indications (see Table 6-1).

Table 6-1: Chemical impacts on the hardness of the oxide of the tested sorbents. Correlations are based on 30 measurements on different samples.

Impurity	R^2	Effect (+ = increase of hardness)
S	0.4247	-
Cl	0.4897	-
CaO	0.3059	+
MgO	0,3081	-
Na_2O	0.2888	-

Even though that some impurities might form phases that are able to weaken the CaO structure, it is believed that the crystal size and arrangement (see Fig. 2-35) and the calcination conditions (see Fig. 2-14) have a much stronger impact on the mechanical properties of the oxide then the chemical composition. Of course, the occurrence of some impurities might be linked with the crystal size, shape and arrangement in the particle, but this link is too weak to draw conclusions from a given chemistry to the expected hardness.

Porosity and Hardness as Oxide

A link between the volume of pores from 0 up to 20 µm (see Fig. 6-10) and an even stronger link between the pore volume of pores between 0.5 and 5 µm (see Fig. 6-11) was identified.

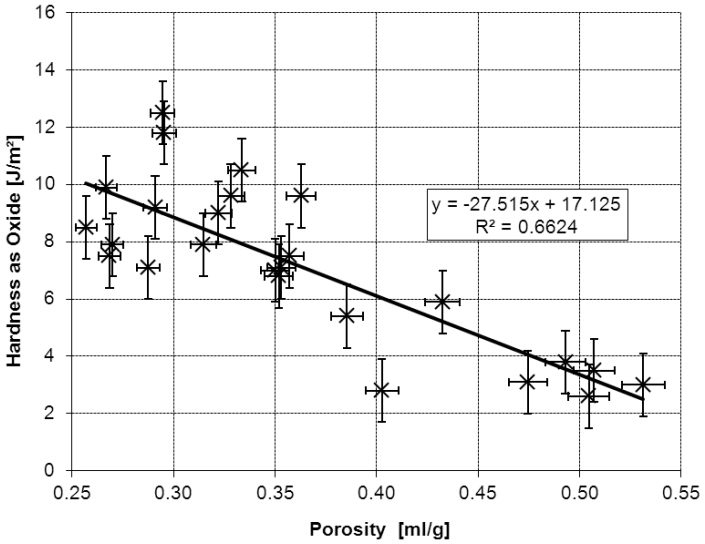

Fig. 6-10: Plot of the hardness versus the pore volume of the oxides of different sorbents. The error bars for the delta values and the individual members of the groups are explained in Fig. 6-9. The accuracy of the porosity measurement was assumed to be $\pm 2\%$. The overall porosity was determined with Mercury Intrusion Porosimetry with a maximum pore diameter of 20 µm.

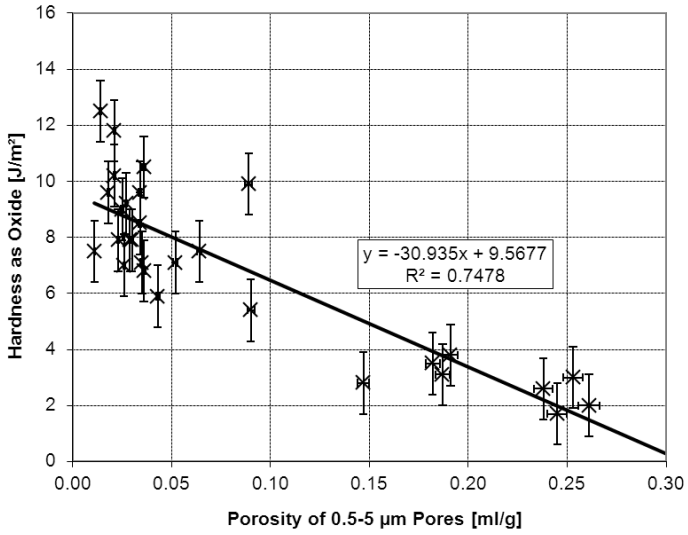

Fig. 6-11: Plot of the hardness versus the pore volume of the oxides of different sorbents. The error bars for the delta values are explain in Fig. 6-9. The accuracy of the porosity measurement was assumed to be $\pm 2\%$. The overall porosity was determined with Mercury Intrusion Porosimetry with a pore diameter between 0.5 and 20 µm.

From a general point of view (see Fig. 6-10) it seems that the overall porosity has a negative impact on the mechanical strength. In case that the porosity below 500 nm is subtracted from the total porosity, the correlation between hardness and volume of the pores between 0.5 and 5 µm becomes very good. This observation might be explained very well by the formation of cracks; pores larger than 500 nm cannot have formed during the calcination due to the decomposition of $CaCO_3$ but must have been present before or occurred during the heating of the carbonate. For sorbents that had a very poor mechanical strength as carbonate the first (fractured texture) might have happened, for those that were quite hard as carbonate and became very fragile during the calcination the second (formation of cracks upon heating) could have happened. Cracks appear often during the heating of carbonates with dense packed, large crystals due to the anisotropic thermal expansion coefficient of calcite. It could be speculated that real pores have no impact on the mechanical strength and that the measured porosity in dimensions above the real porosity (>500µm) simply shows secondary effects like cracks that effect the hardness of the particles.

Cycled Material

Ten samples were subjected to a pilot kiln in order to receive a sufficient quantity of material for the delta test and other characterisations. Light evidence that the hardness as partial carbonate and oxide after eight cycles are correlated can be seen in Fig. 6-12.

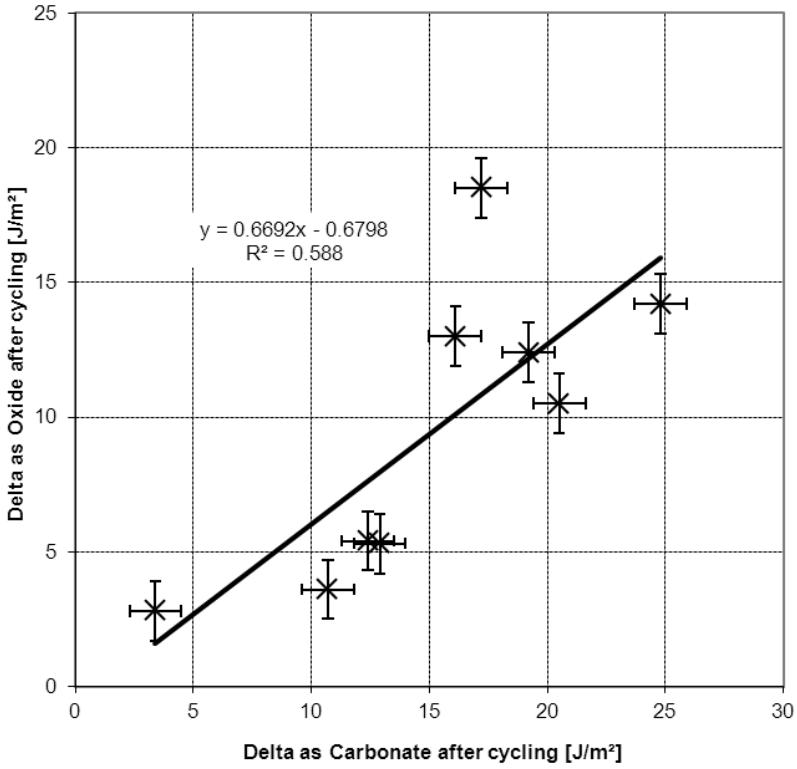

Fig. 6-12: Hardness of the oxide versus the hardness of carbonate after eight cycles in the pilot kiln. A weak correlation between the hardness as carbonate and oxide is noticed.

Comparing the hardness of freshly calcined material with the hardness of the material that had undergone cycling (Fig. 6-13) it can be stated that cycling improves the mechanical strength in eight out of ten cases. These improvements might be an effect of material annealing, i.e. small cracks that occurred after the first calcination are closed again by CaO or $CaCO_3$ due to diffusion and other effects like the product layer of $CaCO_3$ that is periodically formed and destroyed again. Of course, if the crack is too deep an annealing cannot take place.

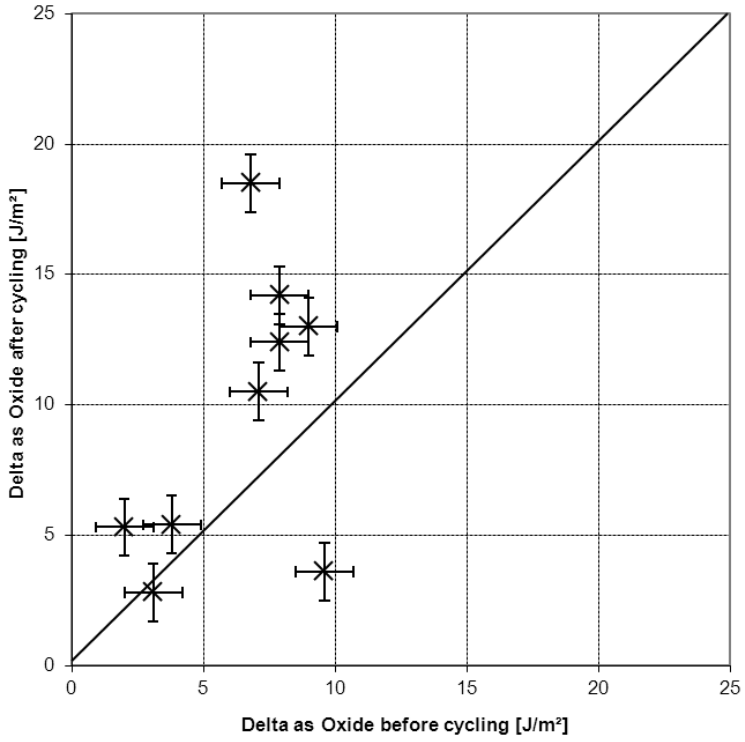

Fig. 6-13: Hardness of the oxide after cycling versus the hardness of the oxide before cycling.

Summary

The comparison between the hardness as raw and once calcined material illustrated that about 50% of the tested materials remain or increase their hardness due to the calcination while the other 50% lose their mechanical strength. A strong link between the chemical composition and the hardness was not obvious. Only slight indication for the sulphur and the chlorine content for the hardness of the once calcined material could be noticed. It is believed that the effect of the chemical composition on the hardness of the carbonate and the oxide is minor in comparison with the mechanical stress history the product has seen and the crystal size and arrangement, respectively. The first hypothesis is support by already conducted test with different grinding and sieving equipment: impact milling and additional sieving effect (improve) the hardness of the raw material. The second hypothesis is supported by porosity measurements: it seems that cracks in the particles with a width between 0.5 and 5 µm cause a weakening of the material. These cracks, maybe, have been caused by thermal stress that has its origin in the anisotropic thermal expansion coefficient of calcite.

The hardness determination on cycled material shows in eight out of test cases an increase of the mechanical stability. This could be caused by annealing processes that form bridges in the cracks that stabilise the particles. These bridges could be formed over distances of 100 nm or more ([10]).

6.1.2.2 Cold Fluidised Bed Tests

Evaluation of the Results

Cold CFB attrition tests were done with five different limestones and three different oxides according to the test procedure described in subsection 5.2.8. Fig. 6-14 shows three examples of attrition curves recorded during three different experiments.

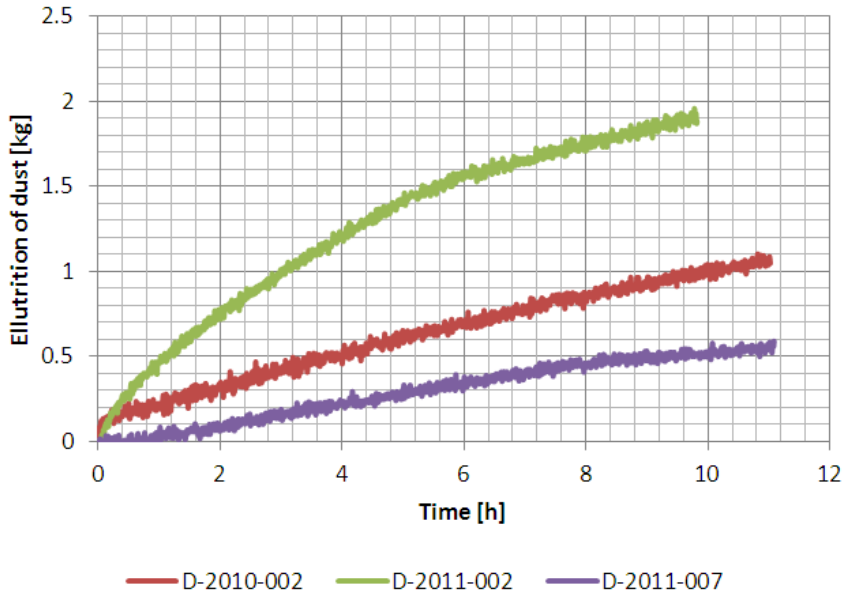

Fig. 6-14: Examples of attrition curves recorded during the cold CFB attrition experiments. The sorbent D-2011-002 was lime while the other two products have been $CaCO_3$.

Even though that these curves seem to enable a general classification of the products, they certainly do not display the full truth. The attrition one particle suffers depends on the number of interactions with other particles and the testing equipment. This number can be set equal to the virtual numbers of cycles one particle was moved between the ricer and the stand pipe. To derive this number two things have to be known: First the actual interior of sorbent in the system for each defined time and second the according circulating mass flow. The mass in the system at a given point $m_{Sorbent}(t)$ can be determined by the mass at the beginning m_0 minus the overall attrition up to the given time point $m_{Attrition}(t)$.

$$m_{Sorbent}(t) = m_0 - m_{Attrition}(t) \qquad \textbf{6-5}$$

The circulating mass flow depends on different operational parameter like the grain size and amount of fluidisation air into the loop seal. It was calculated using a calibration curve based on the difference in pressure between bottom (P_1) of the riser and the top (P_3). Following expressions have been found for the circulating mass flow of carbonate and oxide

$$m_{Ciruclating}^{CaCO_3}\left[\frac{kg}{\min}\right] = (P_1 - P_3)\cdot 1.3693 \qquad \textbf{6-6}$$

$$m_{Ciruclating}^{CaO}\left[\frac{kg}{\min}\right]=(P_1-P_3)\cdot 1.4616\,. \qquad \textbf{6-7}$$

It should be noted that the pressures in the open operation that were used for the calibration, were not the same like in the testes in the closed system. The reasons are the loop seal and the stand pipe, which acted as a short circuit for the fluidisation air from the riser. However, eq. 6-6 and 6-7 were already corrected.

Based on the circulation mass flow and the actual interior of the system, the circulation number can be defined by

$$N(t)=\int_{t=0}^{t}\frac{m_{Circulating}}{m_{Sorbent}(t)}dt\,. \qquad \textbf{6-8}$$

Outcomes on Carbonate

The reproducibility of the attrition curves for the dense material was very good (see Fig. 6-15). Unfortunately, high dust loadings, blockings and agglomeration caused instable operations conditions for porous and soft materials like D-2009-003.

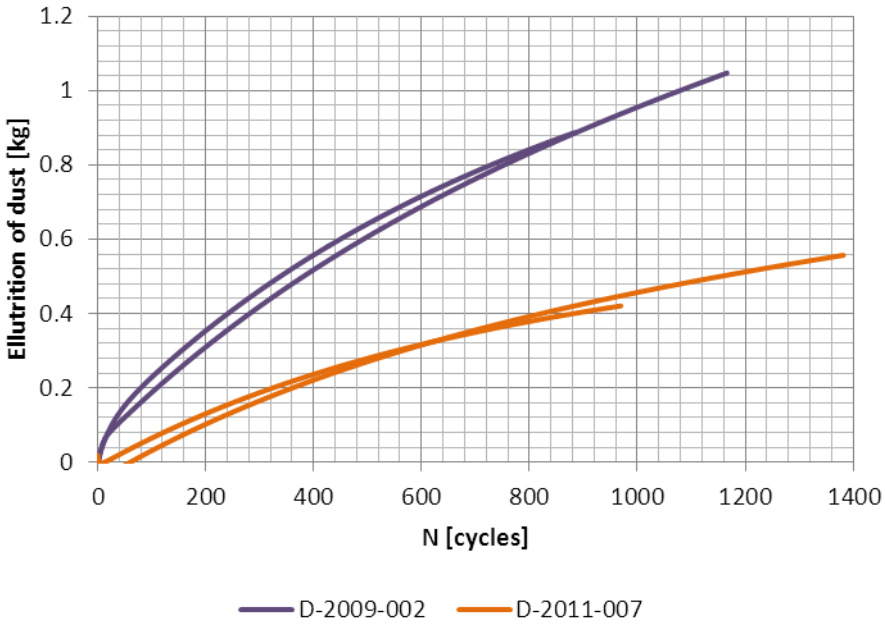

Fig. 6-15: Repeated measurements of the products D-2009-002 and D-2011-002. Good repeatability was achieved for carbonates.

The attrition curve of D-2009-002 shows a typical attrition shape: The slope at the beginning is very steep because dust is blown of and mechanical weak particles are broken and elutrited. As well, sharp edges are tossed of and driven out of the system. Top view microscopy pictures (see Fig. 6-16) show that the surfaces and the edges became notably smoother after CFB tests. This indicates that attrition by surface wear takes place during long term operation.

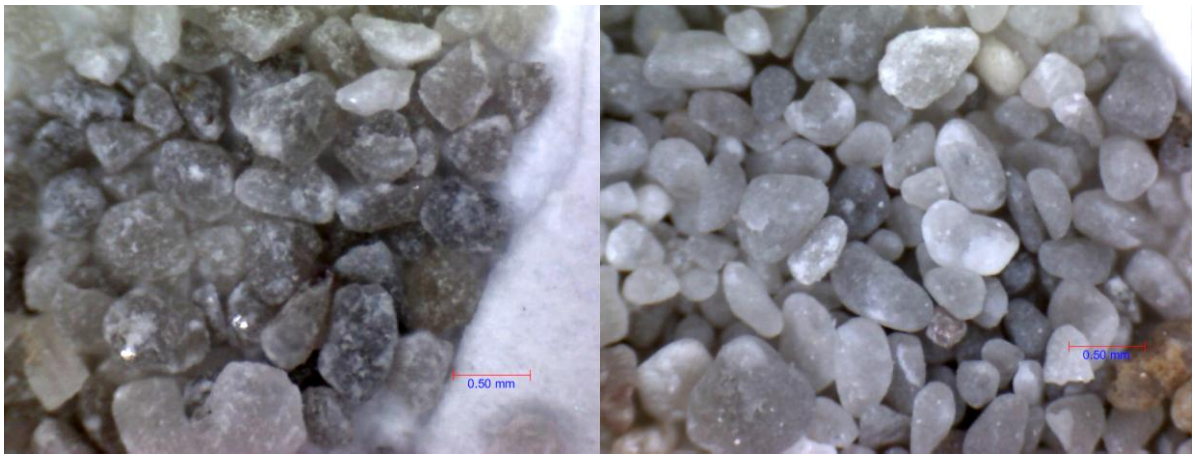

Fig. 6-16: Top view microscopy pictures of D-2009-002 before (left) and after (right) cold flow CFB testing. Smoother edges and surfaces can be noticed after the test.

In order to have a good measure of the stability of different sorbents, three points were chosen to describe the attrition behaviour:

- After 50 cycles (most of the dust should be blown of)
- After 200 cycles because (most of the weak particles and edges should have been gone)
- After 350 cycles (long term attrition behaviour)

The mass of elutriated material after those cycles was determined and the according attrition rate between those periods was calculated (see Table 6-2).

Table 6-2: Attrition in kg after a given number of cycles (left) and the according rates of attrition between those cycles in g/cycles (right) for carbonates and oxides. Experimental problems for the product D-2009-003, a very soft limestone, can be recognised.

	N [cycles]	50	200	350	800	0-50	50-200	200-350	350-800
Carbonat	D-2009-002	0.15	0.35	0.51	0.84	3.0	1.3	1.0	0.7
		0.12	0.31	0.47	0.83	2.4	1.3	1.1	0.8
	D-2009-003	0.39	1.37	2.47	n.a.	7.9	6.5	7.3	n.a.
		0.99	2.55	n.a	n.a.	19.8	10.4	n.a.	n.a.
		1.10	2.02	2.57	n.a.	22.0	6.1	3.7	n.a.
	D-2010-002	0.34	0.94	1.36	n.a.	6.9	4.0	2.8	n.a.
	D-2011-007	0.00	0.10	0.19	0.39	-	0.7	0.6	0.4
		0.03	0.13	0.21	0.38	0.6	0.7	0.5	0.4
	D-2011-008, original	0.30	0.72	0.99	n.a.	5.9	2.8	1.8	n.a.
	D-2011-008, 260-500	0.15	0.51	0.82	n.a.	3.1	2.4	2.1	n.a.
	D-2011-008, >500	0.20	0.67	n.a.	n.a.	4.0	3.1	n.a.	n.a.
		0.15	0.45	n.a.	n.a.	3.0	2.0	n.a.	n.a.
		0.16	n.a.	n.a.	n.a.	3.3	n.a.	n.a.	n.a.
	D-2011-008 syn	0.12	0.54	n.a.	n.a.	2.4	2.8	n.a.	n.a.
Oxide	D-2011-001	0.25	0.64	n.a.	n.a.	5.0	2.6	n.a.	n.a.
	D-2011-002	0.55	1.25	1.67	n.a.	11.0	4.7	2.8	n.a.
		0.84	1.44	1.94	n.a.	16.8	4.0	3.3	n.a.

Because a sorbent particle is very likely to be cycled several times in the carbonator or the calciner before it is exchanged between those reactors, the numbers of attrition relevant cycles will be more than ten times higher (five cycles in the carbonator and the calciner respectively) than the number of cycles referred to the CO_2 capture ability. Accordingly, one particle would have to withstand 400-800 reactor internal cycles (see Fig. 4-11 and 4-12) to reach the minimal efficiency penalty. Therefore, the hardness ranking shall be based on the long term attrition rate (200-350 cycles) which is given by:

D-2011-007 (0.5 g/cycle) < D-2009-002 (1.0 g/cycle) < D-2011-008, original (1.8 g/cycle) < D-2011-008, 260-500 (2.1 g/cycle) < D-2010-002 (2.8 g/cycle) < D-2009-003 (5.5 g/cycle)

One very important outcome is that a pre-sieving step can withdraw the fines from the original product but may not have any advantages for the long-term hardness. As well, very dense particles, with smooth surfaces show a high long-term attrition resistance.

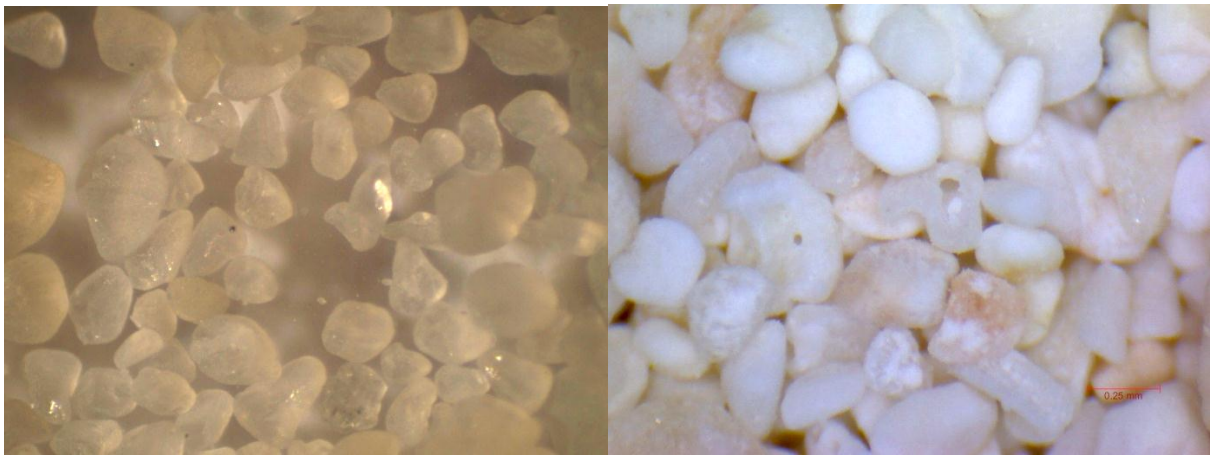

Fig. 6-17: Top view pictures of the products D-2011-007 (left) and D-2009-003 (right) after cold CFB tests.

One possible explanation could be that porous particles offer permanently a rough surface that is able to transport high friction forces between the particles themselves and the walls of the reactor and thus leading to a high overall loss of fines and dust (see Fig. 6-17). This hypothesis might explain the huge difficulties during the tests of different limes.

Considering the indications given by the delta test, the hardness ranking should have been D-2011-007 (29.8 J/m²) > D-2010-002 (11.7 J/m²) > D-2009-002 (7.7 J/m²) > D-2009-003 (6.3 J/m²). By this it is obvious that a differentiation between very hard and very soft material should be possible by the delta test. However, surface and other effects might cover intermediate particle strengths.

Outcomes on Oxides

Table 6-2 shows the attrition test results on the products D-2011-001 and D-2011-002. Both products revealed a completely different behaviour from each other; the first one causes the production of so many fines that were enriched in the system that the test had to be stopped

and restarted due to the breakdown of the transport in the loop seal and due to blockings in the test rig. The second showed clear signs of agglomeration that impacted the outcome significantly. Both cases are illustrated in Fig. 6-18.

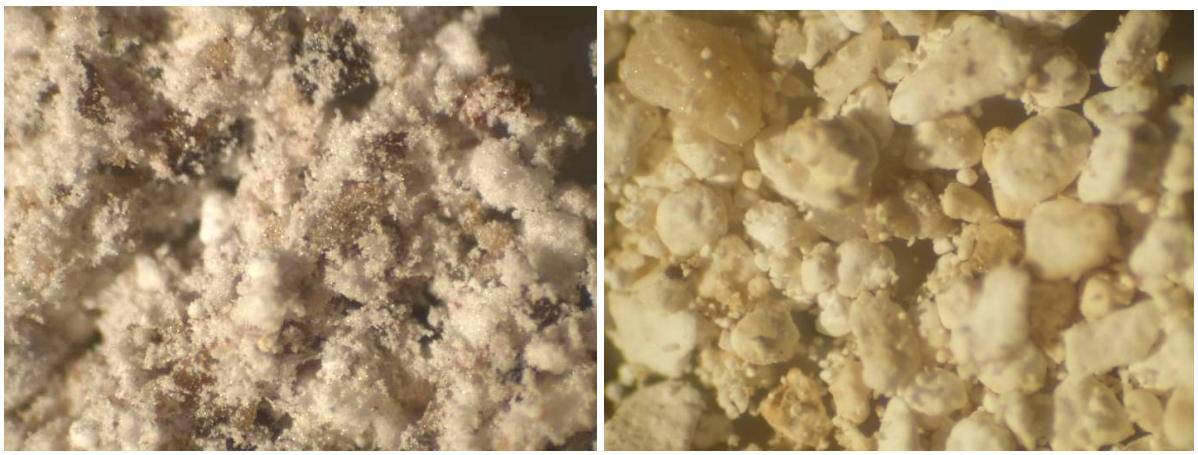

Fig. 6-18: Top view microscope pictures of D-2011-001 (left) and D-2011-002 (right) after cold CFB attrition tests. The fines that generated in case of D-2011-001 were very sticky and formed bridge like structures between the grains. Perfectly round small particles and extremely smooth, nearly slippery, surfaces indicated agglomeration in case of D-2011-002.

One potential explanation for the very different behaviours might be given by the chemistry (see Table 6-3). D-2011-001 was a very impure hard burned quicklime with significant elevated levels of SiO_2, Al_2O_3, SO_3 and K_2O. During the test roughly 2 wt% of impurities were discharged; even the hydration and the carbonation levels were decreased, which indicate that the particles did not react with the water vapour or the CO_2 content of the fluidisation air to hydroxide or carbonate. In case of D-2011-002, the situation looks completely different: The soft-burned nature enabled the reaction to hydroxide and carbonate to an extent of roughly 10 wt%. $Ca(OH)_2$ is often used industrially as a binder for agglomerates, while the re-carbonation reaction is used to harden the particles. Accordingly, the prerequisites for the formation of stable agglomerates were fulfilled in case of D-2011-002.

Table 6-3: Chemical composition before and after the cold CFB attrition tests of D-2011-001 and D-2011-002. Values are given in wt%

	D-2011-001		D-2011-002	
	Before	**After**	**Before**	**After**
CaO	90.92	92.80	96.11	94.29
MgO	1.39	0.99	0.55	0.54
SiO_2	3.48	2.38	0.75	1.02
SO_3	0.59	0.60	0.01	0.03
Fe_2O_3	0.43	0.54	0.21	0.23
Al_2O_3	1.38	1.01	0.26	0.26
Mn_2O_3	0.08	0.07	0.02	0.02
K_2O	0.27	0.24	0.03	0.04
LoI	1.45	1.18	1.40	3.37
CO_2	0.88	0.85	0.77	1.79
$CaCO_3$	2.00	1.93	1.75	4.07
$Ca(OH)_2$	2.34	1.36	2.59	6.50
CaO	88.03	90.69	93.17	87.10

However, attrition test results were achieved but could not be used for any hardness discussion. The third investigated product (D-2011-006) behaves very similar to D-2011-001 and was therefore not discussed. It became obvious that quicklimes can not be tested under cold CFB conditions due to effects of hydration, carbonation and agglomeration. As well, the sticky nature of fine CaO dust mixed with impurities caused major problems during the operation of the test rig. Hot CFB tests are mandatory for the assessment of the mechanical stability of quicklime.

6.1.2.3 Hot Fluidised Bed Tests

Hot BFB tests continued the cold CFB tests, which showed that the hardness of sorbents can only be investigated satisfactory under hot conditions. Table 6-4 summarises the outcomes.

Table 6-4: Compilation of hot BFB results and delta values.

	Carbonate		Calcine	
	BFB loss	Delta Value [J/m²]	BFB loss	Delta Value [J/m²]
D-2010-006	0.7%	6.2	0.5%	1.3
D-2011-007	2.1%	31.0	0.6%	1.4
D-2009-009	3.8%	8.1	1.1%	6.1
D-2009-002	1.7%	9.1	1.5%	9.4
D-2010-007	n.a.	9.4	n.a.	9.6
D-2009-010	n.a.	5.4	n.a.	1.7

Delta values and attrition values in the BFB show no correlation. This could be caused by:

- Dust created during the transportation and the first calcination,
- successive carbonation/calcination cycles that alter the overall particles properties and
- a hardening of the particles during the cycles due to annealing phenomena.

However, the last point might not be applicable in case of the sorbent D-2010-006 because the large spaces between the grains could prohibit annealing effects effectively leading to a very high overall attrition under nearly real conditions[18].

Due to a lack of a meaningful hardness tests and the fact that advanced and synthetic products were not available in a sufficient amount for hardness investigations, only TGA results will be taken into account in the next two sections.

6.2 Advanced Materials

As indicated in section 5.4, a lot of tests with different materials have been conducted to improve the CO_2 capture ability by special thermal pre-treatment steps. The best achieved outcome is shown in Fig. 6-19.

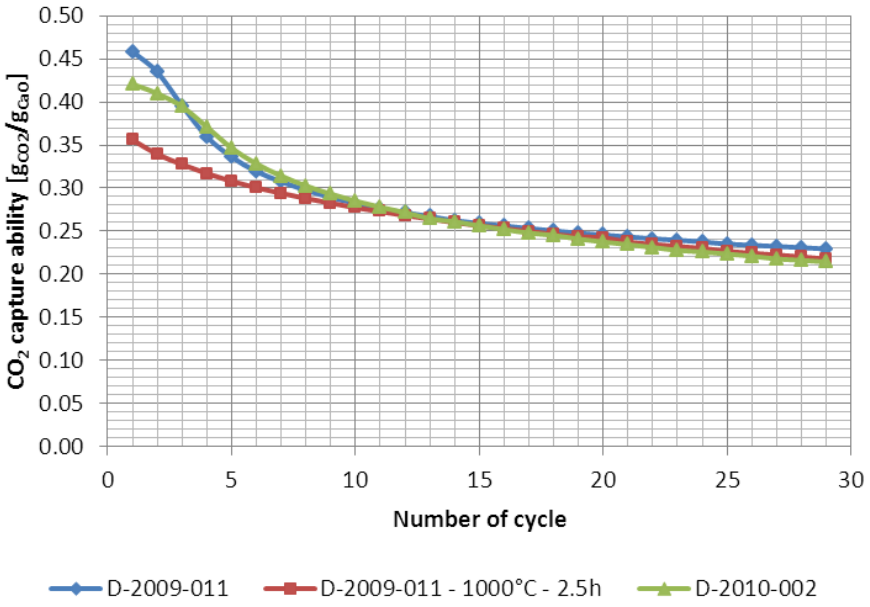

Fig. 6-19: CO_2 capture ability versus the number of cycles for the sorbent D-2009-011 and its treated species in comparison with D-2010-011.

The product D-2009-011 is a limestone, known to resist sintering very efficiently. As a pre-treatment measure, this product was subjected to 1000°C for 2.5 h.

However, it can be seen that a thermal pre-treatment does not cause any sorbent improvements. Even though, the opposite (a significant poorer CO_2 capture ability of the pre-treated sorbent) was observed for all other sorbents.

[18] Note that the product D-2010-006 was an industrial available agglomerate.

This finding might be interpreted in a way that a thermal pre-treatment equals the successive loss of specific surface area during the cycling in the calcination step. Accordingly, this kind of pre-treatment simply ages the sorbent so that the CO_2 capture ability is already lower at the beginning.

6.3 Synthetic Materials

Hydrolysis, co-precipitation, precursors and different kinds of dopants were tested for the production of synthetic sorbents. However, indications show that this sorbent class loses a great portion of its mechanical strength upon the first calcination. In addition, significant advantages in terms of CO_2 capture ability were only observed if special TGA conditions were applied; no synthetic product was able to outperform the best natural sorbents under harsh conditions.

The low advantages of synthetic products over natural sorbents and the high costs associated with the production of such materials make it hard to believe that synthetic sorbents might be employed in the CL process someday.

7 Summary

This thesis was considered with the Carbonate Looping (CL) process and in particular the impact of improved sorbents on the process performance.

A broad overview about solid state chemistry was given. Crystal systems of $CaCO_3$, CaO, $Ca(OH)_2$ and $CaSO_4$ have been presented. It was shown that CaO has the most dense package of all substances. However, CaO has the highest melting point in the group which indicates that sintering phenomena like loss of specific surface area and irreversible pore mouth blockage are much more likely to happen during the re-carbonation than during the calcination step.

Impurities of the coal appear to become a challenge for the operation of the CL process: On the one hand impurities might get enriched in the loop causing high circulating mass flows and on the other hand melting phases are very likely to occur. Special emphasis should be put on the usage of a fuel containing very low amounts of alkali metals. As well, reducing conditions should be avoided in the calciner to avoid any undesired effects resulting of the system $CaSO_4$-$CaSO_3$-CaO.

Theoretical investigations of the $CaCO_3$ decomposition showed that the majority of sorbent particles should be calcined within seconds in the calciner. Low residential times and rather low mass loadings in the calciner seem to be achievable.

The literature review on CL sorbents revealed a critical response of the CO_2 capture ability of sorbents on changed TGA test conditions. In this perspective a lot of promising approaches, like special thermal pre-treatments became less promising. It was speculated that the good reported outcomes on these materials, was only an effect of randomly beneficial chosen TGA test conditions. Own experiments under harsh TGA test conditions with improved and synthetic products did not indicate any benefits for the CL process in terms of CO_2 capture ability.

Mechanical and chemical reactivation routes were presented. The only process discussed within literature offering both reactivations at the same time is the SD process. Increased mechanical stability and refreshed CO_2 capture ability were reported by [86]. However, this process would have to be repeated after each third cycle leading to huge additional efforts for the sorbent reactivation.

The sophisticated CL process model showed that optimisations could be done with a variety of targets. Optimising the economics, for example, would only require large utilities that should be operated with a sorbent as hard as possible. In contrast, an optimal efficiency could only be reached with special sorbents offering an optimal compromise between CO_2 capture

ability and hardness. Minimal CO_2 capture costs were calculated to 20 €/t (including the compression of the CO_2 produced by the power plant and the CL process).

The calculations indicate that the handling of the huge amount of make-up and bleed might become a problem.

Sorbent research was categorised into basic, advanced and synthetic materials. Basic materials are common, now available limestones, advanced materials are thermally treated oxides and synthetic products are tailor-made lab samples. Based on TGA experiments it turned out that neither advanced nor synthetic materials had any long term advantages under harsh TGA conditions compared to good performing natural sorbents.

Hardness investigations with different experimental setups created a confusing picture in that no real correlations between the measurements of the individual test were achieved. Basically, two reasons were identified for this observation: First, depending on experimental conditions attrition by surface wear or impact stress was dominant. According to the nature of the products, the reaction on surface wear and impact might be completely different. Second, the cyclic change of sorbent properties that change from a carbonate shell to a soft CaO shell to a sintered particle. Additionally, the duration of the appearance of the different Ca-forms depends strongly on process conditions.

8 Outlook

Hardness Investigations

Static lab-based, cold CFB and cold and hot BFB tests were conducted in the scope of this work. It turned out that the correlation between those tests was not remarkable. It is speculated that this outcome is a result of the different appearances of the sorbent particles during the cycling; porous and fresh CaO will show higher attrition rates upon surface wear than dense $CaCO_3$ or re-carbonated CaO with a dense outer layer of $CaCO_3$.

Consequently, further approaches for the characterisation of the sorbent hardness could follow this route:

1. Determination of the FB operating conditions on the attrition in a cold state. Variation of:
    - Fluidisation velocities
    - Kind of fluidisation (different nozzles, sinter plaid,…) and
    - Kind of cyclone
2. Repetition of the first step at an elevated temperature level but below the calcination temperature of the used $CaCO_3$.
3. Repetition of the first step at an elevated temperature level above the calcination temperature with fresh CaO (highly porous).
4. Repetition of the first step at an elevated temperature level above the calcination temperature with sintered CaO.
5. Repetition of the fourth step at varying temperature.
6. Repetition of the fifth step with cycling.
7. Precise evaluation of all results and deduction of critical parameters.
8. Design of sophisticated lab tests.

The author of this work is convinced that the definition of one or more meaningful lab-based hardness tests can only be done through a precise description of the attrition and its dependencies under CFB conditions.

TGA Investigations

Fortunately, lab-based TGA tests seem to deliver slightly better, to CFB systems, correlated results than hardness tests. However, it was shown that products that could be clearly ranked in the TGA test after 30 cycles behaved the same way in the CFB environment after ten cycles. Additionally, a strong impact of the sorbent performance on changed test conditions was noticed for some products. The reason for this behaviour could not be clarified.

As well, it became obvious that there is a lack of information how critical high heating and cooling rates and constantly changing durations of carbonation and calcination are for the product performance. Accordingly, parameter studies with different kinds of materials and high cycle numbers should be conducted with high heating and cooling rates. Heating and cooling should be as close as possible to the real process conditions, say several 100°C per minute. Such a test cannot be done within a standard TGA. However, to the knowledge of the author, new kinds of TGA furnaces that enable heating and cooling rates of more than 100°C per second are in development. First commercially available products might be available in a couple of years.

Besides those parameter studies, investigations considering the CO_2 uptake in parallel to attrition should be done to get the full picture of the sorbent performance.

9 References

[1] 2000. *Versuch 5: Werkstoff Kalk - Thermische Carbonatzersetzung*.

[2] 2010. *Erneuerbare Energien - BIO-Gas. Demonstrationsprojekt zur Holzvergasung in Geislingen-Türkheim - Anlage steht vor der Genehmigung*.

[3] Abanades, C. J. *Calcium Sorbent Cycling for Simultaneous CO2 Capture and Clinker Production*.

[4] Abanades, C. J. 2002. The maximum capture efficiency of CO2 using a carbonation/calcination cycle of CaO/CaCO3. *Chemical Engineering Journal* 90, 303–306.

[5] Abanades, C. J., Alonso, M., Rodríguez, N., González, B., Fuentes, F., Grasa, G. S., and Murillo, R. 2008. *Capture of CO2 from flue gases with CaO. Results in a 30 kW Interconnected Fluidized Bed Facility*. 4 th International Workshop on In-Situ CO2 Removal, London.

[6] Abanades, C. J., Anthony, E. J., Lu, D. Y., Salvador, C., and Alvarez, D. 2004. Capture of CO2 from Combustion Gases in a Fluidized Bed of CaO. *Environmental and Energy Engineering* 50, 7, 1614–1622.

[7] Abanades, C. J., Grasa, G. S., Alonso, M., Rodríguez, N., Anthony, E. J., and Romeo, L. M. 2007. Cost Structure of a Postcombustion CO2 Capture System Using CaO. *Environ. Sci. Technol.* 41, 5523–5527.

[8] ACARP. 2008. *Hardgrove Grindability Index*, Riverside Centre, Australia.

[9] Akdolit GmbH & Co. KG. 2011. *Akdolit Hydro-Calcit C G*. http://www.akdolit.com/de/neutralisation/akdolit-hydro-calcit.html. Accessed 22 April 2011.

[10] Alvarez, D. and Abanades, C. J. 2005. Determination of the Critical Product Layer Thickness in the Reaction of CaO with CO2. *Industrial & Engineering Chemistry Research* 44, 5608–5615.

[11] Alvarez, D. and Abanades, C. J. 2005. Pore-Size and Shape Effects on the Recarbonation Performance of Calcium Oxide Submitted to Repeated Calcination/Recarbonation Cycles. *Energy & Fuels* 19, 270–278.

[12] Alvarez, D. and Diez, M. A. 2007. *CO2 CAPTURE IN A LIME CARBONATION/CALCINATION LOOP*.

[13] Alvarez, D., Pena, M., and Borrego, A. G. 2007. Behavior of Different Calcium-Based Sorbents in a Calcination/Carbonation Cycle for CO2 Capture. *Energy & Fuels* 21, 1534–1542.

[14] American Mineralogist Crystal Structure Database. 2011. http://rruff.geo.arizona.edu/AMS/amcsd.php.

[15] Antao, S. M. and Hassan, I. 2010. Temperature dependence of the structural parameters in the transformation of aragonite to calcite, as determined from in situ synchrotron powder x-ray-diffraction data. *Can Mineral*, 48, 1225–1236.

[16] Anthony, E. J. 2007. *SOLID LOOPING CYCLES: A NEW TECHNOLOGY FOR COAL CONVERSION*.

[17] Ar, I. and Dogu, G. 2001. Calcination kinetics of high purity limestones. *Chemical Engineering Journal* 83, 2, 131–137.

[18] Baerns, M., Behr, A., Brehm, A., Gmehling, J., Hofmann, H., Onken, U., and Renken, A. 2008. *Technische Chemie*. Wiley-VCH, Weinheim.

[19] Baker, E. H. 1962. The CaO-CO2 system in the pressure range 1-300 atm. *Journal of the Chemical Society*, 464–470.

[20] Benedix, R. 2006. *Bauchemie. Einführung in die Chemie für Bauingenieure*. Vieweg+Teubner Verlag / GWV Fachverlage GmbH Wiesbaden, Wiesbaden.

[21] Beruto, D., Botter, R., and Searcy, A. W. 1984. Thermodynamics and kinetics of carbon dioxide chemisorption on calcium oxide. *The Journal of Physical Chemistry* 88, 18, 4052–4055.

[22] Blamey, J., Anthony, E. J., Wang, J., and Fennell, P. S. 2009. The calcium looping cycle for large-scale CO2 capture. *Progress in Energy and Combustion Science*, 1–20.

[23] Blamey, J., Florin, N. H., Paterson, N., Dugwell, D. R., and Fennell, P. S. 2009. *Some Aspects of Calcium Looping Research at Imperial College, London*. 1st Meeting of the High Temperture Solid Looping Cycles Network, Oviedo.

[24] Borgwardt, R. H. 1989. Calcium Oxide Sintering in Atmospheres Containing Water and Carbon Dioxide. *Industrial & Engineering Chemistry Research* 28, 493–500.

[25] Borgwardt, R. H. 1989. Sintering of Nascent CaO. *Chem. Eng. Sci* 44, 53.

[26] Bosoaga, A. and Oakey, J. 2007. CO2 capture using lime as sorbent in a carbonation/calcination cycle.

[27] Bundesverband der Deutschen Kalkindustrie. 2011. *Willkommen!* www.kalk.de.

[28] Carniglia, S. C. and Barna, G. L. 1992. *Handbook of industrial refractories technology. Principles, types, properties and applications*. Noyes Publ., Park Ridge, N.J.

[29] Charitos, A., Hawthorne, C., Bidwe, A. R., Sivalingam, S., Schuster, A., and Scheffknecht, G. 2009. *Investigation of the Effect of Operational Parameters on the CO2 Capture Efficiency of a 10 kWth Calcium Looping Dual Fluidized Bed (DFB)*. 1st Meeting of the High Temperture Solid Looping Cycles Network, Oviedo.

[30] Chen, Z., Grace, J. R., and Lim, C. J. 2008. Limestone particle attrition and size distribution in a small circulating fluidized bed. *Fuel* 87, 1360–1371.

[31] Chen, Z., Song, H. S., Portillo, M., Lim, C. J., Grace, J. R., and Anthony, E. J. 2009. Long-Term Calcination/Carbonation Cycling and Thermal Pretreatment for CO2 Capture by Limestone and Dolomite. *Energy & Fuels* 23, 3 (Mar. 2009), 1437–1444.
[32] Cherniak, D. J. 1997. An experimental study of strontium and lead diffusion in calcite, and implications for carbonate diagenesis and metamorphism. *Geochimica et Cosmochimica Acta* 61, 19, 4173–4179.
[33] Chrissafis, K. and Paraskevopoulos, K. M. 2005. The effect of sintering on the maximum capture efficiency of COsub2/sub using a carbonation/calcination cycle of carbonate rocks. *Journal of Thermal Analysis and Calorimetry* 81, 463–468.
[34] Curran, G. P. and Gorin, E. 1968. *Preparation of Carbon Dioxide Acceptors by the Melt Process,* 3516808.
[35] Dennis, J. S. and Pacciani, R. 2008. *Synthetic, Calcium-Based Sorbents for the Capture of CO2. SUMMARY OF RESULTS AND MODELLING*. 4 th International Workshop on In-Situ CO2 Removal, London.
[36] Department of Energy Systems and Technology. 2010. *Carbon Capture by means of an Indirectly Heated Carbonate Looping Process*.
[37] Dreuscher, H., Epple, B., Priesmeier, U., and Tschaffon, H. 2010. *Verfahren zur Verbrennung eines kohlenstoffhaltigen Brennstoffs, insbesondere fossilen Brennstoffs,* EP 2 145 670.
[38] Ströhle, J., Galloy, A., and Epple, B. 2008. *Feasibility Study on the Carbonate Looping Process for Post-Combustion CO2 Capture from Coal-Fired Power Plants.* Energy Procedia, 1–8.
[39] Epple, B. and Ströhle, J. 2008. *CO_2 Capture Based on Chemical and Cabonate Looping.* VGB PowerTech 11, 85–89.
[40] Epple, B. 2008. *Einsparpotentiale beim Carbonate-Looping-Verfahren durch Verwendung optimierter Kalksteinprodukte,* Darmstadt.
[41] Epple, B. and Galloy, A. 2008. *Research at the Chair of Energy Systems and Technology*, Nivelles.
[42] Fennell, P. S., Davidson, J. F., Dennis, J. S., and Hayhurst, A. N. 2007. Regeneration of sintered limestone sorbents for the sequestration of CO2 from combustion and other systems. *Journal of the Energy Institute* 82, 2, 116–119.
[43] Fennell, P. S., Pacciani, R., Dennis, J. S., Davidson, J. F., and Hayhurst, A. N. 2007. The Effects of Repeared Cycles of Calcination and Carbonation on a Variety of Different Limestones, as Measured in a Hot Fluidized Bed of Sand. *Energy & Fuels* 21, 4, 2072–2081.
[44] Fierro, V., Adánez, J., and GarcIa-Labiano, F. 2004. Effect of pore geometry on the sintering of Ca-based sorbents during calcination at high temperatures. *Fuel* 83, 13, 1733–1742.
[45] Florin, N. H. W. Y. and Fennell, P. S. 2009. *Modified CaO-based sorbents for Ca-looping*. Chemical-looping and Calcium-looping Processes for Carbon Capture European workshop, Edinburgh.
[46] Fukui, H., Ohtaka, O., Nagai, T., Katsura, T., Funakoshi, K., and Utsumi, W. 2000. Melting of portlandite up to 6 GPa. *Physics and Chemistry of Minerals* 27, 367–370.
[47] Galwey, A. K. 2007. Melting and Thermal Decompositions of Solids. Anppraisal of mechanistic interpretations of thermal processes in crystals. *Journal of Thermal Analysis and Calorimetry* 87, 601–615.
[48] Galwey, A. K. 2008. What can we learn about the Mechanisms of Thermal Decompositions of Solids from Kinetic Measurements? *Journal of Thermal Analysis and Calorimetry* 92, 3, 967–983.
[49] Galwey, A. K. and Brown, M. E. 2000. Solid-state Decompositions - Stagnation or Progress? *Journal of Thermal Analysis and Calorimetry*, 60, 863–877.
[50] Gibbs, J. W. 1892. Thermodynamische Studien. *Leipzig*.
[51] Grasa, G. S. and Abanades, C. J. 2006. CO2 Capture Capacity of CaO in Long Series of Carbonation/Calcination Cycles. *Industrial & Engineering Chemistry Research* 45, 8846–8851.
[52] Grasa, G. S., Abanades, C. J., Alonso, M., and González, B. 2007. Reactivity of highly cycled particles of CaO in a carbonation/calcination loop. *Chemical Engineering Journal*.
[53] Grasa, G. S., Abanades, C. J., Alonso, M., and González, B. 2008. Reactivity of highly cycled particles of CaO in a carbonation/calcination loop. *Chemical Engineering Journal* 137, 561–567.
[54] Gupta, R. P., Wall, T. F., and Baxter, L., Eds. 2002. *Impact of Mineral Impurities in Solid Fuel Combustion*. Springer US.
[55] Hampel, R. 2010. *Beitrag zur Analyse von kinetischen Einflüssen auf die Wirbelschicht-Sprühagglomeration*. Dissertation, Otto-von-Guericke-Universität Magdeburg.
[56] Harris, A. T. and Florin, N. H. 2009. Reactivity of CaO derived from nano-sized CaCO3 particles throughmultipleCO2 capture-and-release cycles. *Chemical Engineering Science* 64, 187–191.
[57] Hogewoning, S. and Mehling, C. 2010. *Heutiger Stand zur Bestimmung der Reaktivität von Branntkalken mittels Nasslöschkurve*. http://www.nasslöschkurve.de/verbesserte-auswertung-der-nassloeschkurve. Accessed 6 January 2011.
[58] Hogewoning, S. and Wolter, A. 2008. *Vorhersage und Beeinflussung der Reaktivität von Branntkalk*, Clausthal.

[59] Jia, L., Hughes, R., Lu, D. Y., Anthony, E. J., and Lau, I. 2007. Attrition of Calcining Limestones in Circulating Fluidized-Bed Systems. *Industrial & Engineering Chemistry Research* 46, 5199–5209.
[60] Kainer, H. 1982. *Kopplung von Wärme- und Stoffaustausch mit chemischer Kinetik bei der Zersetzung von natürlichen Karbonaten*. PHD, Technische Universität Clausthal.
[61] Kang, S.-J. L. 2005. *Sintering*. *Densification, grain growth, and microstructure*. Elsevier Butterworth-Heinemann, Oxford.
[62] Kassing, R. 2005. *Festkorper*. Lehrbuch der experimentalphysik 6. De Gruyter, Berlin.
[63] Knacke, O. and Stranski, I. N. 1952. Die Theorie des Kristallwachstums. *Ergebn. der exakten Naturwiss.*, 26, 383–427.
[64] Knautz, personal communication.
[65] Kober, T. 2010. *Technische und ökonomische Aspekte des CO2-Transports.* Süddeutsche CCS-Symposium, Stuttgart.
[66] Kofstad, P. and Norby, T. 2004. *Defects and Transport in Crystalline Solids*. *Defect Chemistry and Reactions in Solids*. Compedium, University of Oslo.
[67] Krüger, R. 2005. *Herstellen von Weichbrannt im KDO Flandersbach*, Wülfrath.
[68] Lee, D. K. 2004. An apparent kinetic model for the carbonation of calcium oxide by carbon dioxide. *Chemical Engineering Journal* 100, 71–77.
[69] Leroy, A. 2008. *CCS: Best available technologies and application to the lime industry*, Nivelles.
[70] Levin, E. M., Robbins, C. R., and McMurdie, H. F. 1964. *Phase Diagrams for Ceramists*. Compiled at the National Bureau of Standards. The Americyn Ceramic Society, Columbus, Ohio.
[71] Li, Y.-j., Zhao, C.-s., Chen, H.-c., Liang, C., Duan, L.-b., and Zhou, W. 2008. Modified CaO-based sorbent looping cycle for CO2 mitigation. *Fuel*, 1–8.
[72] Li, Y.-j., Zhao, C.-s., Duan, L.-b., Liang, C., Li, Q.-z., Zhou, W., and Chen, H.-c. 2008. Cyclic calcination/carbonation looping of dolomite modified with acetic acid for CO2 capture. *Fuel Processing Technology* 89, 1461–1469.
[73] Lisbona, P., Martinez, A., Lara, Y., and Romeo, L. M. 2010. Integration of Carbonate CO2 Capture Cycle and Coal-Fired Power Plants. A Comparative Study for Different Sorbents. *Energy & Fuels* 24, 728–736.
[74] Lu, D. Y., Manovic, V., Hughes, R., and Anthony, E. J. 2007. *STUDY OF CO2 CAPTURE USING CO2 LOOPING COMBUSTION TECHNOLOGY*. CANMET Energy Technology Centre, Natural Resources Canada, Ottawa, Canada.
[75] Lucion, T. 2009. *LLCR Project*. *Hardgrove Results*, Nivelles.
[76] L'vov, B. V., Polzik, L. K., and Ugolkov, V. L. 2002. Decomposition kinetics of calcite: a new approach to the old problem. *Thermochinica Acta* 390, 5–19.
[77] Lysikov, A. I., Salanov, A. N., and Okunev, A. G. 2007. Change of CO2 Carrying Capacity of CaO in Isothermal Recarbonation - Decomposition Cycles. *Industrial & Engineering Chemistry Research* 46, 13 (Jun. 2007), 4633–4638. doi:10.1021/ie0702328 / http://dx.doi.org/10.1021/ie0702328.
[78] MacKenzie, A., Granatstein, D. L., Anthony, E. J., and Abanades, C. J. 2007. Economics of CO2 Capture Using the Calcium Cycle with a Pressurized Fluidized Bed Combustor. *Energy & Fuels* 21, 920–926.
[79] Manovic, V. and Anthony, E. J. 2007. Steam Reactivation of Spent CaO-Based Sorbent for Multiple CO2 Capture Cycles. *Environ. Sci. Technol.* 41, 1420–1425.
[80] Manovic, V. and Anthony, E. J. 2009. Long-Term Behavior of CaO-Based Pellets Supported by Calcium Aluminate Cements in a Long Series of CO2 Capture Cycles. *Industrial & Engineering Chemistry Research* 48, 19, 8906–8912.
[81] Manovic, V. and Anthony, E. J. 2009. Screening of Binders for Pelletization of CaO-Based Sorbents for CO2 Capture. *Energy & Fuels* 23, 10, 4797–4804. doi:10.1021/ef900266d / http://dx.doi.org/10.1021/ef900266d.
[82] Manovic, V., Anthony, E. J., Lon, and Loncarevic, D. 2009. CO2 looping cycles with CaO- based sorbent pretreated in CO2 at high temperature. *Chemical Engineering Science* 64, 3236–3245.
[83] Marquard-Möllenstedt, T. 2003. *Innovative Wasserstofferzeugung*. *Absorptionsunterstützte Dampfreformierung*. Absorption Enhanced Reforming (AER).
[84] Marquard-Möllenstedt, T., Sichler, P., Specht, M., Michel, M., Berger, R., Hein, K. R. G., Höftberger, E., Rauch, R., and Hofbauer, H. 2004. *NEW APPROACH FOR BIOMASS GASIFICATION TO HYDROGEN*.
[85] Materic, Edwards, Smedley and Holt, personal communication.
[86] Materic, V. and Holt, R. 2009. *Attrition Free Reactivation of Lime via Hydration*. 1st Meeting of the High Temperture Solid Looping Cycles Network, Oviedo.
[87] Moropoulou, A., Bakolas, A., and Aggelakopoulou, E. 2001. The effects of limestone characteristics and calcination temperature to the reactivity of the quicklime. *Cement and Concrete Research* 31, 4, 633–639.
[88] Muhammadieh, M. 2007. *Beitrag zur Ermittlung des Ansatzbildungspotenzials von Braunkohlen in Dampferzeugern*. Dissertation, TU Freiberg.
[89] Müller, personal communication.

[90] Murthy, M. S., Harish, B. R., Rajanandam, K. S., and K. Y. Ajoy Pavan Kumar. 1994. Investigation on the kinetics of thermal decomposition of calcium carbonate. *Chemical Engineering Science* 49, 13, 2198–2204.
[91] Neumann, M. 2008. *Synthese und Charakterisierung von Calciumcarbonat-Phasen und Calciumphosphat-basierter Knochenersatzmaterialien*. Dissertation.
[92] Okrusch, M. and Matthes, S. 2010. *Mineralogie. Eine Einführung in die spezielle Mineralogie, Petrologie und Lagerstättenkunde*. Springer, Berlin.
[93] Pacciani, R., Müller, C. R., Davidson, J. F., Dennis, J. S., and Hayhurst, A. N. 2008. Synthetic Ca-Based Solid Sorbents Suitable for Capturing CO2 in a Fluidized Bed. *The Canadian Journal of Chemical Engineering* 86, 356–366.
[94] Peglow, M. 2005. *Beitrag zur Modellbildung von eigenschaftsverteilten dispersen Systemen am Beispiel der Wirbelschicht-Sprühagglomeration*. Dissertation, Otto-von-Guericke-Universität Magdeburg.
[95] Perry, R. H., Green, D. W., and Maloney, J. O. 1997. *Perry's Chemical Engineers' Handbook*. McGraw-Hill, New York.
[96] Pfaff, I. and Kather, A. 2009. Comparative thermodynamic analysis and integration issues of CCS steam power plants based on oxy-combustion with cryogenic or membrane based air separation. Greenhouse Gas Control Technologies 9, Proceedings of the 9th International Conference on Greenhouse Gas Control Technologies (GHGT-9), 16-20 November 2008, Washington DC, USA. *Energy Procedia* 1, 1, 495–502.
[97] Roesch, A., Reddy, E. P., and Smirniotis, P. G. 2005. Parametric Study of Cs/CaO Sorbents with Respect to Simulated Flue Gas at High Temperatures. *Industrial & Engineering Chemistry Research* 44, 16, 6485–6490.
[98] Romeo, L. M., Abanades, C. J., Escosa, J. M., Pano, J., Gimenze, A., Sanchez-Biezma, A., and Ballesteros, J. C. 2008. Oxyfuel carbonation/calcination cycle for low cost CO2 capture in existing power plants. *Energy Conversion and Management* 49, 10, 2809–2814.
[99] Romeo, L. M., Lara, Y., Lisbona, P., and Escosa, J. M. 2009. Optimizing make-up flow in a CO2 capture system using CaO. *Chemical Engineering Journal* 147, 2-3, 252–258.
[100] Rosenbaum, S. H. and Turnbull, D. 1959. *Acta Met.*, 7, 467.
[101] RWE Power. *Kraftwerk Niederaußem*.
[102] Sahm, P. R. and Egry, I. 1999. *Schmelze, Erstarrung, Grenzflächen. Eine Einführung in die Physik und Technologie flüssiger und fester Metalle*. Vieweg, Braunschweig.
[103] Salatino, P. 2007. *A Survey of Particle Attrition Phenomena relevant to Fluidized Bed Combustion and Gesification of Solid Fuels*. 8th Particle Technology Forum, Cambridge.
[104] Salvador, C., Lu, D. Y., Anthony, E. J., and Abanades, C. J. 2003. Enhancement of CaO for CO2 capture in an FBC environment. *Chemical Engineering Journal* 96, 187–195.
[105] Sauer, H. D. 2011. CO2 noch nicht im Speicher und schon Zankapfel. *VDI nachrichten*, 8 (Feb. 2011), 7.
[106] Scheffknecht, G. and Poboß, N. 2008. *MACHBARKEITSSTUDIE FÜR DAS CARBONATE – LOOPING – VERFAHREN ZUR CO2 ABSCHEIDUNG AUS KRAFTWERKSABGASEN*, Stuttgart.
[107] Schiele, E. and Berens, L. W. 1972. *Kalk. Herstellung – Eigenschaften – Verwendung*. Stahleisen, Düsseldorf.
[108] Schmahl, W. W. *Geomaterialien. Teil 2*, München.
[109] Schreiner, M., Krzack, S., and Meyer, B. 2010. *Verhalten und mögliche Nutzung von Aschen aus Biomassen*. Ascheverwertung bei der energetischen Biomassenutzung zur Schließung von Stoffkreisläufen, Stuttgart.
[110] Schubert, H. 2003. *Handbuch der Mechanischen Verfahrenstechnik: herausgegeben von Heinrich Schubert*, Wiley VCH 2003.
[111] Schüppel, B. 2009. *Attrition in Fluidised Bed Systems*. 1st Meeting of the High Temperture Solid Looping Cycles Network, Oviedo.
[112] Schuster, A. 2008. *Calcium Looping activities at IVD*. 4 th International Workshop on In-Situ CO2 Removal, London.
[113] Schweinfurth, S. P. 2009. *The National Coal Resource Assessment Overview. An Introduction to Coal Quality*, Reston, Virginia.
[114] Schwertmann, personal communication.
[115] Sichler, P. 2003. *Materialentwicklung für den AER-Prozess. Simultane Thermische Analyse (STA)*.
[116] SLAC National Accelerator Laboratory. *PHYSICAL CONSTANTS OF INORGANIC COMPOUNDS*.
[117] Sun, P., Grace, J. R., Lim, C. J., and Anthony, E. J. 2007. Removal of CO2 by Calcium-Based Sorbents in the Presence of SO2. *Energy & Fuels* 21, 163–170.
[118] Sun, P., Grace, J. R., Lim, C. J., and Anthony, E. J. 2007. Sequential Capture of CO2 and SO2 in a Pressurized TGA Simulating FBC Conditions. *Environ. Sci. Technol.* 41, 41, 2943–2949.
[119] Sun, P., Grace, J. R., Lim, C. J., and Anthony, E. J. 2007. The Effect of CaO Sintering on Cyclic CO2 Capture in Energy Systems. *Environmental and Energy Engineering* 53, 9, 2432–2442.

[120] Sun, P., Grace, J. R., Lim, C. J., and Anthony, E. J. 2008. Investigation of Attempts to Improve Cyclic CO2 Capture by Sorbent Hydration and Modification. *Industrial & Engineering Chemistry Research* 47, 2024–2032.
[121] Sun, P., Lim, C. J., and Grace, J. R. 2008. Cyclic CO2 Capture by Limestone- Derived Sorbent During Prolonged Calcination/Carbonation Cycling. *American Institute of Chemical Engineers* 54, 1668–1677.
[122] Symonds, R. T. 2010. *The Effect of Steam on the Carbonation and Sulphation Environment and its Implications for Calcium Looping*. 2nd Meeting of the High Temperature Solid Looping Cycles Network, Alkmaar.
[123] Symonds, R. T., Lu, D. Y., and Anthony, E. J. 2008. Steam-Enhanced CO2 Capture using Partially Sulphated Sorbent.
[124] Toni, A. de. 2010. *CO-Oxidation an Au/TiO2 Aggregaten stabilisiert in einer mesoporösen MCM-48 Matrix: Studien zur Aktivität, Vergiftung und Träger/Metall-Wechselwirkung*. Dissertation, Ruhr-Universität Bochum.
[125] U.S. Geological Survey. 2011. *Coal Database*. http://energy.er.usgs.gov/coal_quality/coal_databases.html. Accessed 23 March 2011.
[126] Various. 2010. *Vaterit*. http://de.wikipedia.org/wiki/Vaterit. Accessed 6 January 2011.
[127] Various. 2011. *Coal*. http://en.wikipedia.org/wiki/Coal. Accessed 21 March 2011.
[128] Various. 2011. *Kornfeinung*. http://de.wikipedia.org/wiki/Kornfeinung. Accessed 18 April 2011.
[129] Various. 2011. *Kraftwerk Jänschwalde*. http://de.wikipedia.org/wiki/Kraftwerk_J%C3%A4nschwalde. Accessed 5 July 2011.
[130] Wang, Y., Lin, S., and Suzuki, Y. 2007. Study of Limestone Calcination with CO2 Capture: Decomposition Behavior in a CO2 Atmosphere. *Energy & Fuels*.
[131] Weiler, personal communication.
[132] Wheelock, T. D. and Iowa, A. 1976. *Simultaneous Reductive and Oxidative Decomposition of Calcium Sulfate in the Same Fluidised Bed*, 4102989.
[133] Wissel, S., Rath-Nagel, S., Blesl, M., Fahl, U., and Voß, A. 2008. *Stromerzeugungskosten im Vergleich*. http://www.ier.uni-stuttgart.de/publikationen/arbeitsberichte/Arbeitsbericht_04.pdf. Accessed 10 May 2011.
[134] Wu, T.-C., Shen, A. H., Weathers, M. S., and Bassett, W. A. 1995. Anisotropic thermal expansion of calcite at high pressures. An in situ X-ray diffraction study in a hydrothermal diamond-anvil cell. *American Mineralogist*, 80, 941–946.
[135] Wuhrer, J. and Radermacher, G. 1956. Mathematische Behandlung des Problems der Entsäuerung von stückigen Carbonaten, insbesondere von Kalkstein. *Chemie Ing. Techn* 28, 5, 328–336.
[136] Wulff, G. 1901. Zur Frage der Geschwindigkeit des Wachstums und der Auflösung der Kristallflächen. *Z. Kristallogr.*, 34, 449–530.
[137] Zeman, F. 2008. Effect of steam hydration on performance of lime sorbent for CO2 capture. *International Journal of Greenhouse Gas Control* 2, 203–209.
[138] Zuberbühler, U. 2008. *Informationsgespräch*, Stuttgart.
[139] Zuberbühler, U. 2008. *Supply and mechanical stability of mineral based CO2 sorbent*. 4 th International Workshop on In-Situ CO2 Removal, London.
[140] Zuberbühler, U. 2009. *Untersuchung von Kalkstein/Kalk mittels Thermogravimetrischer Analyse und der Abriebfestigkeit in der Kugelmühle*. *Untersuchungsbericht*, Stuttgart.
[141] Ströhle, J., Lasheras, A., Galloy, A., and Epple, B. 2009. *Simulation of the Carbonate Looping Process for Post-Combustion CO_2 Capture from a Coal-Fired Power Plant.* Chem. Eng. Technol. 32, 3, 435–442.